Nonperturbative aspects of supersymmetric quantum field theories in low dimensions

Habilitation Thesis

Urs Wenger

Albert Einstein Center for Fundamental Physics
Institute for Theoretical Physics
University of Bern
Switzerland

November 2014

Contents

Part I

Introduction, overview and summary

i Introduction

In particle physics nonperturbative phenomena are ubiquitous and play important or even crucial roles. Quantum Chromodynamics (QCD) at low energies for example exhibits colour confinement and spontaneous breaking of chiral symmetry. The former is responsible for the fact that only composite colour-neutral particles, so-called hadrons, can be observed in nature, but not the quarks and gluons themselves. The latter leads to the particular spectrum of the lightest hadrons observed in nature. The qualitative and quantitative understanding of such nonperturbative aspects of quantum field theories is of utmost importance for the justification of the underlying fundamental theories. In particular this also applies to QCD and its justification as the theory of the strong interactions and for the justification of the Standard Model (SM) in general.

In this spirit my research embraces two directions of research, both in the context of nonperturbative calculations in strongly interacting quantum field theories:

(a) The first direction concerns the quantitative determination of low-energy properties of QCD via computer simulations from first principles. Precise ab-initio calculations at the physical point enable a further reduction and control of the systematic errors present in such computations and provide a further confirmation of the theoretical framework. The main challenges for nonperturbative QCD calculations lie, e.g., in the accurate and reliable determination of hadronic matrix elements and form factors which in many cases constitute the main source of theoretical uncertainties in the direct confrontation of the theory with experiment. Furthermore, such results are being used as valuable input into nonperturbative effects in SM phenomenology, and beyond, via the reduction of theoretical uncertainties in the hadronic sector. This provides stringent tests of the SM and constitutes an invaluable contribution towards the potential discovery of new Beyond the Standard Model (BSM) physics at the Large Hadron Collider (LHC).

(b) The second direction concerns the nonperturbative study of strongly interacting supersymmetric (SUSY) quantum field theories in low dimensions on the lattice. While it is interesting per se to study various discretisation schemes for SUSY field theories regularised on the lattice, e.g., using twisted SUSY or orbifolding techniques, our recent developments in simulating SUSY field theories in low dimensions efficiently and without critical slowing down brings the nonperturbative study of these theories to a new, unprecedented level of accuracy. Such quantitative studies are for example relevant for establishing spontaneous supersymmetry breaking phase transitions, or for the understanding of certain aspects of the gauge/gravity duality, e.g., the relation between the thermodynamics of super Yang-Mills theory and the corresponding black hole string solutions in higher dimensions.

The present habilitation thesis concentrates on the latter part of my research, because the research described under (a) above can only be performed in large international collaborations which nowadays in some cases involve up to 30 or more people. Hence this part is less suited for a habilitation thesis, simply because many of the achievements constitute a collaborative effort which can rarely be assigned to a single researcher. Sometimes the involvement in a project concerns a crucial, but highly technical contribution which is rather distant from the overall physics goal, and, as a consequence, is only indirectly reflected in

the final publications. Therefore, in the present thesis we concentrate on the second main direction of my research which is outlined under (b) above.

Nevertheless, in order to judge the importance and relevance of this effort it is necessary to understand the overall main context within which the work in this thesis has to be seen. Therefore, I will start with a brief review of my recent research concerned with the precise determination of low-energy properties of QCD, before I then start with the main topic of the thesis, our effort to better understand – qualitatively and quantitatively – the nonperturbative properties of supersymmetric quantum field theories in low dimensions.

ii Overview

Until a few years ago it has been considered notoriously difficult – if not prohibitive – to simulate lattice QCD with dynamical quarks corresponding to pion-masses below 600 MeV [1, 2]. One of the difficulties in lattice QCD calculations with Hybrid Monte Carlo (HMC) algorithms [3] is the fact that the theory involves quantum fluctuations at all length scales, from the infrared to the ultraviolet, leading to an ill-conditioned Dirac fermion matrix and a severe critical slowing down of numerical calculations towards the chiral regime. However, in 2005 we have achieved a major breakthrough by developing new algorithms allowing simulations with very light quarks [4]. The range of low pion-masses that are now accessible through numerical simulations reaches down to below 200 MeV. It allows to make reliable contact with Chiral Perturbation Theory (χPT) and this ensures a reliable extrapolation, or even interpolation to the physical point with good control over the corresponding systematic errors.

Our own algorithmic breakthrough as well as other related developments [5, 6] combined with the usual increase of computing power has led to an increased activity, and astonishing progress in the field of numerical simulations of lattice QCD in the chiral regime has been achieved. Apart from our own effort within the European Twisted Mass (ETM) collaboration, cf. further below, there are several other collaborations in Europe (Alpha, BMW, CLS, QCDSF, UKQCD), the USA (HPQCD, FNAL, MILC, RBC) and Japan (JLQCD, PACS-CS) pursuing large scale simulations of QCD making this field of research very competitive at an international level. For a summary of results concerning low energy particle physics we refer to our review of lattice results by the FLAG working group [7] which has now evolved into the Flavour Lattice Averaging Group (FLAG) [8]. The FLAG project is described in more detail further below. The report makes it clear that for some quantities, in particular the quark masses, the effects of neglecting the charm quark start to become significant and hence need to be quantified. Moreover, at very fine lattice spacings $a \lesssim 0.05$fm it has been observed that simulations suffer from long autocorrelations in the topological charge [9]. It has therefore become a necessity to check whether and how much the simulations are affected by this. In fact, some of my main current involvement in the calculations of the ETM collaboration consists in keeping an eye on topological properties [10] as a function of the lattice spacing determined through various gluonic and hadronic scales [11].

Despite the tremendous progress in this field, it should be kept in mind that simulations of QCD with such light quarks continue to be extremely demanding and that typical calculations run on time scales of several years. There-

fore, it is necessary, and indeed absolutely essential, to work in large international collaborations. For this reason I have been involved in forming the European Twisted Mass Collaboration (ETMC) to combine both computational power and theoretical expertise in a European-wide effort. The collaboration includes research groups at DESY Zeuthen (Dr. K. Jansen, spokesperson) and Hamburg (Prof. I. Montvay), in Bonn (Prof. C. Urbach), Frankfurt a. M. (Prof. M. Wagner), Münster (Prof. G. Münster), Rome (Prof. G.C. Rossi, Dr. R. Frezzotti), Liverpool (Prof. C. Michael), Paris-Orsay (Prof. Ph. Boucaud), Groningen (Prof. E. Pallante), Valencia (Prof. V. Gimenez) and Cyprus (Prof. C. Alexandrou). Within the collaboration we have access to purpose-built, massively-parallel computers like JuQueen in Juelich, Fermi at Cineca and many others across Europe, and our code is optimised to run efficiently on these architectures [12, 13]. Over the last years we have been performing extensive QCD calculations with two mass degenerate quark flavours at several volumes and at four lattice spacings using the twisted mass (TM) discretisation of QCD [14, 15]. We have obtained many competitive results concerning for example quark masses, low-energy constants of chiral perturbation theory, the kaon bag parameter B_K, meson and baryon spectra and many more results [16, 17, 18, 19, 20, 21, 22]. Some of these results belong to the most reliable and accurate ones available, cf. the FLAG report [7] discussed further below.

In the last couple of years the ETM collaboration has extended these calculations to $N_f = 2 + 1 + 1$ flavour calculations in the chiral regime at several lattice spacings and on a range of physical volumes, with the aim to get the continuum, the thermodynamic and the chiral limit under control. We emphasise that apart from similar calculations by the FNAL/MILC and the HPQCD collaboration these are the only calculations that take the effect of the charm quark into account. The main results of our calculations have been made available in various publications [23, 24, 25, 26, 27, 28]. For our overview here, it is sufficient to emphasise just the latest highlights published in [29]. There we present the results of a calculation based on a unitary setup for the two light quarks and a mixed action approach for the strange and charm quarks. The analysis uses data at three values of the lattice spacing and pion masses in the range $210 - 450$ MeV, allowing for an accurate continuum limit and controlled chiral extrapolation. After an appropriate nonperturbative renormalisation, the results for the quark masses in the $\overline{\rm MS}$ scheme at the renormalisation scale $\mu = 2$ GeV are: $m_{ud} = 3.70(17)$ MeV, $m_s = 99.6(4.3)$ MeV while the charm quark mass at the scale of the charm is $m_c(m_c) = 1.348(46)$ GeV. In addition we also determine the quark mass ratios $m_s/m_{ud} = 26.66(32)$ and $m_c/m_s = 11.62(16)$. By studying the mass splitting between the neutral and charged kaons and using available lattice results for the electromagnetic contributions, we eventually also evaluate $m_u/m_d = 0.470(56)$, leading to $m_u = 2.36(24)$ MeV and $m_d = 5.03(26)$ MeV.

Another of our efforts worth mentioning concerns the implementation of new computational strategies for maximally twisted mass Wilson fermions, such as smearing or the use of the clover improvement term, in order to push the simulations to the physical point. In [30] we present the first results from such simulations with a physical pion mass using two mass-degenerate, clover improved, maximally twisted quark flavours at a single lattice spacing on large volumes. The results are extremely promising, also because the lattice artefacts seem to be very small, as indicated by the supressed pion mass splitting between

charged and neutral pions being around 20(20) MeV only [31]. The analysis of pseudoscalar meson masses and decay constants involving linear interpolations in the strange and charm quark masses yields the preliminary quark mass ratios $m_s/m_{ud} = 27.63(13)$, $m_c/m_{ud} = 339.6(2.2)$ and $m_c/m_s = 12.29(10)$ and preliminary results for $f_K = 153.9(7.5)$ MeV, $f_D = 219(11)$ MeV, $f_{D_s} = 255(12)$ MeV and $M_{D_s} = 1894(93)$ MeV with errors currently dominated by those from the determination of the lattice spacing.

The astonishing precision with which strong interaction effects can apparently be quantified from first principles using large-scale numerical simulations of lattice QCD is of course difficult to assess for non-lattice-experts. In particular, the simulations of different collaborations employ different lattice actions (discretisations of QCD) with a variety of lattice spacings and volumes, and with a range of masses for the u- and d-quarks. Not only are the systematic errors different, but also the methodology used to estimate these uncertainties varies between collaborations. Understandably, questions from the general particle physics community such as "What is currently the best lattice value for a particular quantity?" or "How reliable is the determination of a particular quantity?" are frequently asked and in fact appropriate. It is for this reason that in 2007 a working group – now named as the Flavour Lattice Averaging Group (FLAG) – has been set up in the framework of a European Network on Flavour Physics (Flavianet) with the aim to review the current status of lattice results for a variety of physical quantities in low-energy physics. The first edition of the FLAG review was published in 2011 [7] and was limited to lattice results related to pion and kaon physics: light-quark masses (u-, d- and s-flavours), the form factor $f_+(0)$ arising in semileptonic $K \to \pi$ transitions at zero momentum transfer and the decay constant ratio f_K/f_π, as well as their implications for the CKM matrix elements V_{us} and V_{ud}. Furthermore, results were reported for some of the low-energy constants of $SU(2)_L \otimes SU(2)_R$ and $SU(3)_L \otimes SU(3)_R$ Chiral Perturbation Theory (χPT) and the B_K parameter of neutral kaon mixing. The aim of this collaborative effort is to summarize the main features of each of the calculations and to provide a framework for judging and combining the different results. Sometimes it is a single result which provides the best value; more often it is a combination of results from different collaborations. The complete review article is complemented by a website `http://itpwiki.unibe.ch/flag`, where figures as well as pdf-files for the individual sections can be downloaded. The effort has been well taken by the particle physics community: by now the review has already almost 390 citations and the main entry webpage alone over 33'000 clicks.

In order for this venture to be successful it is crucial to have all major lattice QCD collaborations on board and to guarantee a smooth cooperation between the various working groups involved. Upon completion of the first review we therefore decided to concentrate these efforts here in Bern by forming an Editorial Board (EB) which coordinates the activities. The EB is supported by an Advisory Board (AB) which is available for general supervision and consultation. This new structure has proven to function well and allowed to extend FLAG both in terms of the geographical location of its members, the lattice collaborations to which they belong and the scope of the review. In the second edition of the review [8] lattice results related to B- and D-meson physics are included with a focus on B- and D-meson decay constants, form factors, and mixing parameters, which are most relevant for the determination of CKM ma-

trix elements and the global CKM unitarity-triangle fit. Last but not least, also the current status of lattice results on the QCD coupling α_s is reviewed. Despite the reorganisation, the workload for the EB is immense at times – in fact a large fraction of my research time over the last few years has been devoted to it – and for the third edition of the review the EB has hence been enlarged to contain six members. In addition, the diversity with respect to collaborations has been extended further and the new review will also include results for the bottom- and charm-quark masses, which are important parametric inputs to Standard Model (SM) calculations.

Before I now summarise the main topic of the present thesis, let me emphasise that despite the large collaborations necessary to advance lattice QCD calculations, new innovative ideas continue to be important, and these usually emerge from smaller projects. In this context I would like to point out just two achievements to which I contributed in recent years. The first one concerns the spectral properties of the Dirac operator which are known to be well described by Random Matrix Theory (RMT) in a specific parameter regime of QCD, the ϵ-regime. RMT allows in particular to establish a powerful link to the low-energy constants of χPT. In [32, 33] we demonstrated that Wilson fermions can also be used in connection with RMT despite their obstructed properties with respect to the topology of the underlying gauge fields. It turns out that it is indeed possible to extract low-energy constants from the spectral properties of the Wilson Dirac operator. The second project concerns the simulation of QCD at finite baryon density which constitutes one of the main challenges for lattice QCD calculations. In [34] we presented a possible new approach to lattice simulations of QCD in separate canonical sectors with fixed baryon number. It is based on a reduction method for Wilson Dirac fermions with non-zero chemical potential which generates a dimensionally reduced fermion matrix. The size of the reduced fermion matrix is independent of the temporal lattice extent and the dependence on the chemical potential is factored out. As a consequence the reduced matrix allows a simple evaluation of the Wilson fermion determinant for any value of the chemical potential and hence the exact projection to the canonical partition functions. Since the reduction method also plays a role for supersymmetric Yang-Mills quantum mechanics covered in this thesis, we have included the paper in the appendix of the thesis, even though it is not strictly concerned with supersymmetric field theories in low dimensions.

iii Summary

The activities overviewed in the previous section provide the background for our nonperturbative investigations in supersymmetric quantum field theories which go beyond the calculations of QCD in the SM. Supersymmetric field theories are one possible extension of the SM potentially capable of describing new physics beyond the SM. In addition, since they find applications in physical systems reaching far beyond quantum field theories, they are interesting per se, independent of whether or not they eventually turn out to be relevant for particle physics. So, while lattice calculations of supersymmetric field theories alone provide a rather narrow and highly specialised focus for nonperturbative investigations, they nevertheless provide a complementary view on elementary particle physics, specifically also concerning numerical simulations, far beyond

the context given above. In particular, this also applies to our investigations of supersymmetric theories in low dimensions for which the direct relevance for nature is not always apparent immediately. On the other hand, simple models in low dimensions can provide valuable insights into mechanisms, which are at work also in higher dimensions, such as, e.g., the ones related to the spontaneous breaking of supersymmetry. Moreover, new approaches to discretise quantum field theories and related algorithmic improvements can be thoroughly tested and understood in low dimensional models, such that their usefulness and practicability in higher dimensions can be better assessed. So, it is this reasoning which motivates our work covered in the present thesis.

Let me now outline and summarise the research described in the main part of the thesis. It is organised in five parts. After the introductory first part here, part II describes the algorithmic developments, which form the foundation of the subsequent analytic and numerical work. Part III is concerned with the models in one dimensions which I subsume under the title "Supersymmetric quantum mechanics". Part IV presents our results on two-dimensional supersymmetric models. In particular this concerns solid results on dynamical supersymmetry breaking in the $\mathcal{N} = 1$ Wess-Zumino model, as well as our our attempts at the supersymmetric nonlinear O(N) sigma model. Finally, part V contributes one more paper as an appendix.

The foundation of our activities in simulating supersymmetric field theories in low dimensions lies in our paper [35] – paper 1 of this thesis – where we develop an efficient simulation algorithm for strongly interacting relativistic fermions in two-dimensional field theories relying on the formulation of Majorana fermions as self-avoiding fermion loops. The approach is based on the work of Prokof'ev and Svistunov who developed so-called 'worm' algorithms for classical statistical models in [36]. Our work extends this algorithm to systems describing fermionic degrees of freedom, in particular ones in which the Majorana fermions are regularised using Wilson's discretisation scheme [37]. The fermion loop models describing the dynamics of the fermions can be mapped to statistical vertex models and our proposal is in fact an efficient simulation algorithm for generic vertex models in arbitrary dimensions. In that sense the proposal in [35] is far more general than indicated by the specific applications described in this thesis. What is important, however, is the fact that the algorithm essentially eliminates critical slowing down by sampling two-point correlation functions. In addition, it allows simulations directly in the massless limit. The absence of critical slowing down is easy to see once one understands the generic approach taken by the algorithm. By sampling directly the fermionic correlation function, close to a critical point where the correlation length grows large, the configurations are updated equally well on all length scales up to a scale of the order of the correlation length. In that sense, the algorithm works similar to cluster algorithms which are also know to eliminate critical slowing down in large parts. Another viewpoint is, that by enlarging the configuration space of closed fermion loops to contain also configurations with an open fermion string, the algorithm can probe the original configuration space much more efficiently. Essentially, a global update of a closed fermion loop configuration results from a sequence of local moves of the physical open fermion string. By enlarging the allowed moves by ones which are even unphysical, the efficiency of the algorithm can be enhanced even further. Moreover, the open fermion string generates loop configurations with fluctuating topological boundary conditions enabling the simulation of fermions

with arbitrary periodic or antiperiodic boundary conditions.

As illustrative examples, the algorithm is applied to the free Majorana Gross-Neveu model, and to the Schwinger model in the strong coupling limit in our original paper [35] mentioned above and in [38] – paper 2 of this thesis. In the context of the Schwinger model, there is an interesting aspect which, however, is not covered in this thesis. The bosonisation of the Schwinger model in the strong coupling limit, which is made explicit in the fermion loop formulation, can also be applied in three dimensions. There, one can show how the fermion sign problem is resolved using the fermion loop formulation, and the system can hence be simulated using the open fermion string algorithm. The application of the algorithm to the interacting O(N) Gross-Neveu model is further investigated in [39] – paper 3 of this thesis. For the case of two interacting Majorana fermions, the Thirring model, we demonstrate the efficiency of the algorithm by determining the critical mass as a function of the coupling to very high accuracy. This is a necessary prerequisite for any investigation of the non-perturbative properties of the Thirring model using Wilson fermions, and hence forms the basis for further research. Moreover, in that paper we also propose a simple modification of the open fermion string algorithm which can be used to measure the fermion bound state spectrum with very high accuracy.

The property of the open fermion string algorithm to generate loop configurations with fluctuating topological boundary conditions, together with the absence of critical slowing down, eventually forms the basis for the success of the algorithm in $\mathcal{N} = 2$ supersymmetric quantum mechanics and eventually also in the $\mathcal{N} = 1$ Wess-Zumino model. The two properties are crucial ingredients to enable a proper numerical treatment of supersymmetric theories with spontaneously broken supersymmetry. This is because simulations of supersymmetric models on the lattice with spontaneously broken supersymmetry generically suffer from a fermion sign problem related to the vanishing of the Witten index. In [40] – paper 4 of this thesis – we point this out and propose a novel approach which solves this problem in low dimensions by formulating the path integral on the lattice in terms of fermion loops. The formulation allows the explicit decomposition of the partition function into bosonic and fermionic contributions, which can be distinguished by the topological boundary conditions of the fermionic degrees of freedom. Of course this forms the perfect ground for the application of the open fermion string algorithm described in the first part of this thesis. The algorithm separately samples the fermionic and bosonic sectors, as well as the relative probabilities between them. The latter then allows a direct calculation of the Witten index and the corresponding Goldstino mode. Since the Goldstino mode is massless, the usual fermion simulation algorithms suffer from critical slowing down, apart from the fermion sign problem. The elimination of critical slowing down by the open fermion string algorithm is hence crucial to obtain reliable results in the supersymmetry broken phase. Hence, in [40] we discuss in detail the fermion sign problem due to the vanishing of the Witten index, describe the fermion loop formulation of the $\mathcal{N} = 1$ Wess-Zumino model, as well as that of $\mathcal{N} = 2$ supersymmetric quantum mechanics. For the latter we also present first simulation results for the Witten index and the mass gap spectrum, both for a standard discretisation employing standard Wilson fermions with an appropriate counterterm, and for a so-called Q-exact discretisation which maintains one of the two supersymmetries exactly on the lattice.

It turns out that in the case of $\mathcal{N} = 2$ supersymmetric quantum mechanics, the system can be formulated completely in terms of bosonic and fermionic bonds. While the fermion loop formulation allows the solution of the sign problem, its combination with the bosonic bond formulation enables the exact solution of the system at finite lattice spacing. The solution is based on the explicit construction of transfer matrices and allows for example to determine in detail how supersymmetry is restored in the mass gap spectrum towards the continuum. In addition, in the case of broken supersymmetry, the emergence of the goldstino mode can be observed and understood quantitatively. In [41] – paper 5 of this thesis – we introduce the transfer matrix approach and show some first, exact results concerning the Witten index and the mass gap spectrum of the theory.

Our research on $\mathcal{N} = 2$ supersymmetric quantum mechanics eventually culminates in a series of publications [42] – paper 6,7 and 8 of this thesis – in which we present a complete investigation of the nonperturbative properties of the $\mathcal{N} = 2$ supersymmetric quantum mechanics. Of course, as field theorists we put a special emphasis on the interplay between the cut-off artefacts due to the finite lattice spacing and the infrared effects due to the finite size of the system. In paper 6 we concentrate on the details of the reformulation of this model in terms of fermionic and bosonic bonds for various lattice discretisations including one which is Q-exact. We also discuss in detail the origin of the generic sign problem appearing in systems with broken supersymmetry. In paper 7 we then work out the full details of the transfer matrix approach and discuss a range of exact results for observables such as the Witten index, the mass spectra and Ward identities. Finally, in paper 8 we present the details of how the algorithms from [36] and [35] can be adapted to the present case, and demonstrate that the algorithm is indeed capable to solve the fermion sign problem. Since the system can be solved exactly, this work is rather a feasibility study and serves to test the practicability of the algorithmic approach.

After the successful excursion to the most simple supersymmetric quantum mechanics case, the obvious question is whether the fermion loop approach, in particular the exact solution employing transfer matrices, can be extended to more complicated systems. It turns out that this is indeed the case. In [43] – paper 9 of this thesis – we apply the fermion loop formulation to $\mathcal{N} = 4$ supersymmetric SU(N) Yang-Mills quantum mechanics. The system is interesting for several reasons. Firstly, the model stems from dimensionally reducing $\mathcal{N} = 1$ supersymmetric Yang-Mills (SYM) in $d = 4$ dimensions, but is expected to share many qualitative features with the 16 supercharge model which derives from $\mathcal{N} = 1$ SYM in $d = 10$ dimensions by dimensional reduction. The reduced theory is supposed to describe the dynamics of D0 branes which are the degrees of freedom of the underlying M-theory. The connection to so-called black p-branes allows to study the thermodynamics of black holes through the corresponding strongly coupled gauge theory. So, understanding the nonperturbative dynamics of the quantum mechanical system allows to probe the gauge/gravity duality conjecture. Secondly, because the system also contains a gauge degree of freedom, it is a prototype model for investigating the fermion loop formulation when gauge fields are involved. The loop formulation naturally separates the contributions to the partition function into its bosonic and fermionic parts with fixed fermion number. The separation into the canonical sectors of the theory is of particular interest because there are specific predictions for the various sec-

tors about the energy spectra [44]. It turns out that the transfer matrices can indeed be constructed in each sector separately, but since the bosonic degrees of freedom are still dynamical, the matrices depend on the bosonic background field and hence on the time coordinate. The gauge degree of freedom on the other hand can be expressed in terms of a single transfer matrix, if the temporal or the uniform gauge is employed. The insight into the structure of the transfer matrices yields a generic recipe which appears to be applicable far beyond the simple quantum mechanical model, and our construction opens the door to a new approach for simulating canonical fermion sectors in higher dimensional gauge theories. The relevance of our result becomes even clearer through the construction of a reduced fermion matrix determinant which we also present in [43]. It is simply the one-dimensional analogue of the reduced determinant for Wilson fermions derived some time ago in [34] for QCD with a finite chemical potential. In order to underline this connection in the present thesis we include the corresponding publication in the appendix – paper 14 of this thesis. Finally, in the one dimensional case we algebraically establish the equivalence between the reduced fermion matrix determinant and the transfer matrix approach [43], and this relation provides a useful tool for future numerical investigations of the canonical sectors in gauge theories.

Another obvious question is whether the fermion loop formulation and the open fermion string algorithm is also capable of solving the fermion sign problem in higher dimensional supersymmetric models with spontaneously broken supersymmetry. We already know from our investigations in [40] that the fermion sign in two dimensional systems containing Majorana degrees of freedom, such as the $\mathcal{N} = 1$ Wess-Zumino model, is encoded in the topological boundary conditions. Moreover, from [35, 38] it is also clear that the algorithm efficiently avoids critical slowing down. Therefore, in [45] – paper 10 of this thesis – we are able to present first results from numerical simulations of the Wess-Zumino model. In particular, we discuss the phase structure of the theory and identify the parameter regime, where supersymmetry is spontaneously broken and the additional $\mathbb{Z}_2$-chiral symmetry is restored, and vice versa. This can be done through appropriate order parameters, but in the the fermion loop formulation the ground state structure of the theory, as well as the symmetry breaking pattern, is directly indicated by the probability distribution of the topological fermion sectors. One important result of the paper is also a first preliminary, nonperturbative determination of a perturbatively improved critical coupling indicating the location of a supersymmetry breaking phase transition in the thermodynamic and continuum limit. This is then further elaborated in [46] – paper 11 of this thesis – where we outline the precise procedure to control the two limits. Furthermore, in that paper we also investigate the particle spectrum, both in the supersymmetric and the supersymmetry broken phase. Simulations in the latter are only possible due to the open fermion string algorithm with which the severe fermion sign problem can be avoided. Moreover, the algorithm allows extremely precise calculations of the fermion correlators, and as a consequence the emergence of the massless Goldstino in the supersymmetry broken phase can be observed in detail. These results are then finally corroborated in [47] – paper 12 of this thesis – where we perform careful infinite volume and continuum extrapolations of the spectra in both phases and thereby confirm the vanishing mass of the Goldstino accompanied by a massive boson in the supersymmetry broken phase. Interestingly, the degeneracy between the fermion and

boson in the supersymmetric phase is maintained to extremely high accuracy even at rather coarse lattice spacing. This is in contrast to the supersymmetric quantum mechanics case, where the degeneracy is maintained at finite lattice spacing only by using the complicated Q-exact discretisation. In addition, we present in [47] also a fully controlled determination of the critical coupling of the supersymmetry breaking phase transition with an accuracy of only 2%.

Another particularly interesting class of low-dimensional models enjoying supersymmetry are the supersymmetric nonlinear O(N) sigma models, because they share many nonperturbative properties with the corresponding four-dimensional strongly coupled SYM theories. However, it turns out that implementing a lattice discretisation which maintains the O(N) symmetry and at least one supersymmetry, guaranteeing the full supersymmetry in the continuum, is far from trivial [48, 49, 50]. Moreover, the model suffers from a severe fermion sign problem which renders simulations on large lattices ineffective. While the Wilson discretisation breaks both the supersymmetry and the chiral symmetry, there are indications that both are restored in the continuum limit. In all these approaches, however, the implementation of the O(N) constraints, particularly in the fermionic sector, causes difficulties in numerical simulations. It turns out that these constraints can be implemented rather straighforwardly in the fermion loop formulation, where they induce simple interactions between the bosonic and fermionic degrees of freedom. In [51] – paper 13 of this thesis – we hence derive the details of the fermion loop formulation for this model. We find that for $N = 2$ the fermion sign problem can be controlled in the same way as in the other two-dimensional fermion theories described earlier, but the bosonic contributions to the flavour changing interactions are unfortunately not guaranteed to be positive. Moreover, for $N \geq 3$, the fermion loops are no longer selfavoiding and the fermion loop formulation is hence not able to provide a solution to the fermion sign problem in those cases. Nevertheless, controlled simulations of the O(2) model are possible and in [51] we present a first determination of the critical mass for various values of the coupling, as well as the calculation of the lowest boson and fermion masses. The results indicate that the mass degeneracy between the boson and fermion masses at the critical point emerges in the continuum limit where the model becomes chirally invariant, but it remains to be seen whether or not the supersymmetry is fully restored in the continuum limit.

Acknowledgements

First of all I would like to thank my family for their continuing support and in particular for their bearing with my recurrent absences, sometimes even during vacation.

In addition I would like to thank my former PhD students David Baumgartner, Vidushi Maillart and Kyle Steinhauer who helped me working out the details of my ideas. They worked hard to generate the data which lead to the plethora of results summarised in this thesis. It has been a pleasure to work with you!

Bibliography

[1] CP-PACS and JLQCD, A. Ukawa, Nucl. Phys. Proc. Suppl. **106**, 195 (2002).

[2] K. Jansen, Nucl. Phys. Proc. Suppl. **129**, 3 (2004), [hep-lat/0311039].

[3] S. Duane, A. D. Kennedy, B. J. Pendleton and D. Roweth, Phys. Lett. **B195**, 216 (1987).

[4] C. Urbach, K. Jansen, A. Shindler and U. Wenger, Comput. Phys. Commun. **174**, 87 (2006), [hep-lat/0506011].

[5] M. Luscher, Comput. Phys. Commun. **165**, 199 (2005), [hep-lat/0409106].

[6] M. Clark and A. Kennedy, Phys.Rev.Lett. **98**, 051601 (2007), [hep-lat/0608015].

[7] G. Colangelo *et al.*, Eur.Phys.J. **C71**, 1695 (2011), [1011.4408].

[8] S. Aoki *et al.*, Eur.Phys.J. **C74**, 2890 (2014), [1310.8555].

[9] S. Schaefer, PoS **LATTICE2012**, 001 (2012), [1211.5069].

[10] K. Cichy *et al.*, PoS **LATTICE2014**, 075 (2014), [1411.1205].

[11] A. Deuzeman and U. Wenger, PoS **LATTICE2012**, 162 (2012).

[12] K. Jansen and C. Urbach, Comput.Phys.Commun. **180**, 2717 (2009), [0905.3331].

[13] A. Deuzeman, S. Reker and C. Urbach, Comput.Phys.Commun. **183**, 1321 (2012), [1106.4177].

[14] R. Frezzotti and G. C. Rossi, JHEP **08**, 007 (2004), [hep-lat/0306014].

[15] R. Frezzotti and G. C. Rossi, JHEP **10**, 070 (2004), [hep-lat/0407002].

[16] ETM Collaboration, P. Boucaud *et al.*, Phys.Lett. **B650**, 304 (2007), [hep-lat/0701012].

[17] ETM Collaboration, B. Blossier *et al.*, JHEP **0804**, 020 (2008), [0709.4574].

[18] ETM Collaboration, P. Dimopoulos, R. Frezzotti, G. Herdoiza, C. Urbach and U. Wenger, PoS **LAT2007**, 102 (2007), [0710.2498].

[19] ETM collaboration, P. Boucaud *et al.*, Comput.Phys.Commun. **179**, 695 (2008), [0803.0224].

[20] ETM Collaboration, C. Alexandrou *et al.*, Phys.Rev. **D78**, 014509 (2008), [0803.3190].

[21] ETM Collaboration, B. Blossier *et al.*, JHEP **0907**, 043 (2009), [0904.0954].

[22] ETM Collaboration, R. Baron *et al.*, JHEP **1008**, 097 (2010), [0911.5061].

[23] ETM Collaboration, R. Baron *et al.*, PoS **LATTICE2008**, 094 (2008), [0810.3807].

[24] ETM Collaboration, R. Baron *et al.*, PoS **LAT2009**, 104 (2009), [0911.5244].

[25] R. Baron *et al.*, JHEP **1006**, 111 (2010), [1004.5284].

[26] ETM Collaboration, R. Baron *et al.*, Comput.Phys.Commun. **182**, 299 (2011), [1005.2042].

[27] ETM Collaboration, R. Baron *et al.*, PoS **Lattice2010**, 119 (2014), [1009.2074].

[28] ETM Collaboration, R. Baron *et al.*, PoS **LATTICE2010**, 123 (2010), [1101.0518].

[29] The European Twisted Mass Collaboration, N. Carrasco *et al.*, Nucl.Phys. **B887**, 19 (2014), [1403.4504].

[30] A. Abdel-Rehim *et al.*, PoS **LATTICE2013**, 264 (2014), [1311.4522].

[31] The European Twisted Mass Collaboration, B. Kostrzewa *et al.*, PoS **LATTICE2014**, 119 (2014).

[32] A. Deuzeman, U. Wenger and J. Wuilloud, JHEP **1112**, 109 (2011), [1110.4002].

[33] A. Deuzeman, U. Wenger and J. Wuilloud, PoS **LATTICE2011**, 241 (2011), [1112.5160].

[34] A. Alexandru and U. Wenger, Phys.Rev. **D83**, 034502 (2011), [1009.2197].

[35] U. Wenger, Phys. Rev. **D80**, 071503 (2009), [arXiv:0812.3565].

[36] N. V. Prokof'ev and B. V. Svistunov, Phys.Rev.Lett. **87**, 160601 (2001), [cond-mat/0103146].

[37] K. G. Wilson, Phys. Rev. **D10**, 2445 (1974).

[38] U. Wenger, PoS **LAT2009**, 022 (2009), [0911.4099].

[39] V. Maillart and U. Wenger, PoS **LAT2010**, 257 (2010), [1104.0569].

[40] D. Baumgartner and U. Wenger, PoS **LATTICE2011**, 245 (2011), [1104.0213].

[41] D. Baumgartner and U. Wenger, PoS **LATTICE2011**, 239 (2011), [1201.1485].

[42] D. Baumgartner and U. Wenger, submitted to Nucl.Phys. **B** (2014).

[43] K. Steinhauer and U. Wenger, accepted for publication in JHEP (2014), [1410.0235].

[44] J. Wosiek, Nucl.Phys. **B644**, 85 (2002), [hep-th/0203116].

[45] D. Baumgartner, K. Steinhauer and U. Wenger, PoS **LATTICE2011**, 253 (2011), [1111.6042].

[46] D. Baumgartner, K. Steinhauer and U. Wenger, PoS **LATTICE2012**, 043 (2012), [1311.5089].

[47] K. Steinhauer and U. Wenger, accepted for publication in PRL (2014), [1410.6665].

[48] S. Catterall and S. Ghadab, JHEP **0405**, 044 (2004), [hep-lat/0311042].

[49] S. Catterall and S. Ghadab, JHEP **0610**, 063 (2006), [hep-lat/0607010].

[50] R. Flore, D. Korner, A. Wipf and C. Wozar, JHEP **1211**, 159 (2012), [1207.6947].

[51] K. Steinhauer and U. Wenger, PoS **LATTICE2013**, 092 (2013), [1311.5403].

Part II

Fermion loop algorithm

Paper 1

Efficient simulation of relativistic fermions via vertex models

Urs Wenger, Physical Review D **80**, 071503(R) (2009).

PHYSICAL REVIEW D **80,** 071503(R) (2009)

Efficient simulation of relativistic fermions via vertex models

Urs Wenger

Institute for Theoretical Physics, University of Bern, Sidlerstrasse 5, CH-3012 Bern, Switzerland

(Received 1 June 2009; published 29 October 2009)

We have developed an efficient simulation algorithm for strongly interacting relativistic fermions in two-dimensional field theories based on a formulation as a loop gas. It essentially eliminates critical slowing down by sampling two-point correlation functions and allows simulations directly in the massless limit at the critical point. It generates loop configurations with fluctuating topological boundary conditions enabling one to simulate fermions with arbitrary periodic or antiperiodic boundary conditions. As illustrative examples, the algorithm is applied to the Gross-Neveu model and to the Schwinger model in the strong coupling limit.

DOI: 10.1103/PhysRevD.80.071503 PACS numbers: 11.15.Ha, 02.70.−c, 05.50.+q

Simulating strongly interacting fermions, like in quantum chromodynamics (QCD) or in Nambu-Jona–Lasinio models, is considered to be rather difficult and continues to be a challenge due to the nonlocality of the determinant obtained upon integrating out the fermionic fields. Moreover, simulations of fermions are usually hampered by critical slowing down towards the chiral limit where the fermions become massless and the correlation length of the fermionic two-point function diverges. The established standard method to perform such calculations on the lattice is to use the hybrid Monte Carlo algorithm [1] which deals with the nonlocality of the determinant by rewriting it as an integral over bosonic ''pseudofermion'' fields. The algorithm then requires one to deal with the inverse of the fermion Dirac operator, however, the operator becomes ill-conditioned towards the massless limit and the simulations slow down dramatically. In this paper we propose a novel approach which circumvents the above mentioned problems. It is based on a (high-temperature) expansion of the fermion actions which reformulates the fermionic systems as q-state vertex models, i.e., statistical closed loop models. In particular, the method is directly applicable to the Gross-Neveu (GN) model and to the Schwinger model in the strong coupling limit. These models can be shown to be equivalent to specific vertex models [2–5] and our simulation method, based on a proposal by Prokof'ev and Svistunov [6], is effectively a very efficient updating algorithm for generic vertex models (in arbitrary dimensions). In fact, the algorithm essentially eliminates critical slowing down and is able to simulate the fermionic systems at the critical point and directly in the massless limit.

We start with illustrating the reformulation in terms of closed loops in the GN model. The model is most naturally formulated by employing Majorana fermions [7,8]. Here we are using Wilson's Euclidean lattice discretization for which the action density of the model is

$$\mathcal{L}_{\mathrm{GN}} = \frac{1}{2}\xi^T\mathcal{C}\Big(\gamma_\mu\tilde{\partial}_\mu - \frac{1}{2}\partial^*\partial + m\Big)\xi - \frac{g^2}{4}(\xi^T\mathcal{C}\xi)^2, \quad (1)$$

where ξ is a real, two component Grassmann field describing a Majorana fermion with mass m, $\mathcal{C} = -\mathcal{C}^T$ is the charge conjugation matrix, and ∂, ∂^*, $\tilde{\partial}$ denote the forward, backward and symmetric lattice derivative, respectively. The Wilson term $\frac{1}{2}\partial^*\partial$, responsible for removing the fermion doublers, explicitly breaks the discrete chiral symmetry $\xi \to \gamma_5\xi$, $\xi^T\mathcal{C} \to \xi^T\mathcal{C}\gamma_5$ and requires a fine-tuning of $m \to m_c$ towards the continuum limit in order to restore the symmetry. A pair ξ_1, ξ_2 of Majorana fermions may be considered as one Dirac fermion using the identification $\psi = \frac{1}{\sqrt{2}}(\xi_1 + i\xi_2)$, $\bar{\psi} = \frac{1}{\sqrt{2}}(\xi_1^T - i\xi_2^T)\mathcal{C}$ and the corresponding GN model with N Dirac fermions has an $O(2N)$ flavor symmetry. At $g = 0$, integrating out the Grassmann variables yields the partition function in terms of the Pfaffian

$$Z_{\mathrm{GN}} = \mathrm{Pf}\Big[\mathcal{C}\Big(\gamma_\mu\tilde{\partial}_\mu + m - \frac{1}{2}\partial^*\partial\Big)\Big]^{2N}. \quad (2)$$

For $g \neq 0$ one usually performs a Hubbard-Stratonovich transformation and introduces a scalar field σ conjugate to $\xi^T\mathcal{C}\xi$ together with an additional Gaussian Boltzmann factor $\exp\{-1/(2g^2)\sum_x\sigma(x)^2\}$ for the scalar field.

In order to reformulate the model in terms of closed loops (or equivalently dimers and monomers) we follow the recent derivation of Wolff [8] (see [4,5] for alternative, but more complicated derivations). One simply expands the Boltzmann factor for the fermionic fields and makes use of the nil-potency of the Grassmann variables upon integration. Introducing $\varphi(x) = 2 + m + \sigma(x)$ and the projectors $P(\pm\mu) = (1 \mp \gamma_\mu)/2$ we can write the fermionic part of the GN path integral (up to an overall sign) as

$$\int\mathcal{D}\xi\prod_x(\varphi(x)\xi^T(x)\mathcal{C}\xi(x))^{m(x)} \times\prod_{x,\mu}(\xi^T(x)\mathcal{C}P(\mu)\xi(x+\hat{\mu}))^{b_\mu(x)} \quad (3)$$

where $m(x) = 0, 1$ and $b_\mu(x) = 0, 1$ are the monomer and bond (or dimer) occupation numbers, respectively. Integration over the fermion fields yields the constraint that at each site $m(x) + \frac{1}{2}\sum_\mu b_\mu(x) = 1$. Here the sum

runs over positive and negative directions and $b_{-\mu}(x) = b_{\mu}(x - \hat{\mu})$. The constraint ensures that only closed and nonintersecting loops of occupied bonds contribute to the partition function and also accounts for the fact that the loops are nonbacktracking, a consequence of the orthogonal projectors $P(\pm\mu)$. The weight $\omega(\ell)$ of each loop ℓ can be calculated analytically [9] and yields $|\omega(\ell)| = 2^{-n_c/2}$ where n_c is the number of corners along the loop. The sign of ω will generically depend on the geometrical shape of the loop [9] prohibiting a straightforward probabilistic interpretation of the loop weights in dimensions $d > 2$.

In two dimensions, however, the sign of the loop only depends on the topology of the loop and is determined by the fermionic boundary conditions (BC). This has been well known for a long time [10] but has recently been clarified by Wolff [8] in the context of the GN model. It is therefore useful to classify all loop configurations into the four equivalence classes $\mathcal{L}_{00}$, $\mathcal{L}_{10}$, $\mathcal{L}_{01}$, $\mathcal{L}_{11}$ where the index denotes the total winding (modulo two) of the loops in the two directions. The weights of all configurations in $\mathcal{L}_{10}$ and $\mathcal{L}_{11}$ for example will pick up an overall minus sign if we change the fermionic boundary condition in the first direction from periodic to antiperiodic, while the weights of the configurations in $\mathcal{L}_{00}$ and $\mathcal{L}_{01}$ remain unaffected. As a consequence, if we sum over all the topological equivalence classes with positive weights, i.e., $Z \equiv Z_{\mathcal{L}_{00}} + Z_{\mathcal{L}_{10}} + Z_{\mathcal{L}_{01}} + Z_{\mathcal{L}_{11}}$ we effectively describe a system with unspecified fermionic boundary conditions. Vice versa, the partition function $Z_{\xi}^{10} \equiv Z_{\mathcal{L}_{00}} + Z_{\mathcal{L}_{10}} - Z_{\mathcal{L}_{01}} + Z_{\mathcal{L}_{11}}$, e.g., describes a system with fermionic BC antiperiodic in the first and periodic in the second direction.

It is useful to point out the equivalence of the loop gas formulation to the 8-vertex model [11,12] which is formulated in terms of the eight vertex configurations shown in the top row of Fig. 1 with weights ω_i, $i = 1, \ldots, 8$. The partition function is defined as the sum over all possible tilings of the square lattice with the eight vertices such that only closed (but possibly intersecting) paths occur. To be precise, one has

$$Z_{8\text{-vertex}} = \sum_{\mathrm{CP}} \prod_{x} \omega_i(x), \tag{4}$$

where the sum is over all closed path configurations (CP) and the weight of each configuration is given by the product of all vertex weights in the configuration. For the GN model we have the following weights

$$\omega_1 = \varphi(x), \qquad \omega_2 = 0, \qquad \omega_3 = \omega_4 = 1, \qquad \omega_5 = \omega_6 = \omega_7 = \omega_8 = \frac{1}{\sqrt{2}}, \tag{5}$$

i.e. each corner contributes a factor $1/\sqrt{2}$, while crossings of two lines are forbidden ($\omega_2 = 0$) and each empty site carries the monomer weight $\omega_1 = \varphi(x)$.

The GN model with a single Majorana fermion is effectively a free fermion system and we use it as a benchmark to compare the results of our algorithm with analytic results. Instances of the 8-vertex model for which no analytic solutions are known include the Ising model with additional next-to-nearest-neighbor and quartic interactions [13]. The one-flavor Schwinger model with Wilson fermions in the strong coupling limit is an 8-vertex model with a fermionic interpretation [2,14]. The vertex weights are given by

$$\omega_1 = (m + 2)^2, \qquad \omega_2 = 0, \qquad \omega_3 = \omega_4 = 1, \qquad \omega_5 = \omega_6 = \omega_7 = \omega_8 = \frac{1}{2}, \tag{6}$$

where the monomer weight and the corner weights are squared due to the fact that we are dealing with a pair of Majorana fermions glued together [15].

Let us now turn to the description of the new method to efficiently simulate any vertex model in arbitrary dimensions with generic (positive) weights ω_i, including the fermionic models discussed above. For illustrative purpose we restrict the discussion to the 8-vertex model. The method is an extension of the so-called worm algorithm by Prokof'ev and Svistunov [6]. The configuration space of closed loops is enlarged to also contain open strings. For the GN model such an open string with ends at x and y corresponds to the insertion of two Majorana fields at positions x and y which is simply the Majorana fermion propagator

$$G(x, y) = \int \mathcal{D}\xi e^{-S_{\mathrm{GN}}} \xi(x)\xi(y)^T \mathcal{C}. \tag{7}$$

Similar interpretations of the open string can be obtained for other vertex models. The open string is now the basis for a Monte Carlo algorithm which samples directly the space of 2-point correlation functions instead of the standard configuration space. This is the reason why the algorithm is capable of beating critical slowing down as demonstrated below: at a critical point where the correlation length grows large, the configurations are updated equally well on all length scales up to a scale of the order of the correlation length.

In the vertex language the insertions correspond to the new vertex configurations depicted in the bottom row of

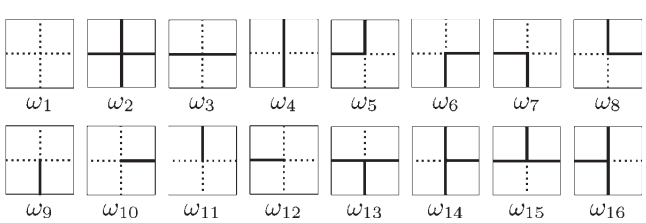

FIG. 1. The vertex configurations and weights of the eight-vertex model (top row) and the extended model (bottom row).

Fig. 1. A configuration containing a single open string corresponds to a loop configuration with two instances of vertex 9–16 which are connected by a string. Note that vertices 13–16, while present in the generic extended vertex model, do not have a physical interpretation in terms of fermionic fields since they are explicitly forbidden by Pauli's exclusion principle (fermionic lines are not allowed to intersect). Nevertheless they can also be included in the fermionic models, simply for algorithmic efficiency, and we do so in our implementation.

The algorithm now proceeds by locally updating the ends of the open string using a simple Metropolis or heat bath step according to the weights of the corresponding 2-point function. When one end is shifted from, say, x to one of its neighboring points y, a dimer on the corresponding bond is destroyed or created depending on whether the bond is occupied or not. In the process, the two vertices at x and y are changed from v_x, v_y to v'_x, v'_y and the move is accepted with probability

$$P(x \to y) = \min\left[1, \frac{\omega_{v'_x}}{\omega_{v_x}} \frac{\omega_{v'_y}}{\omega_{v_y}}\right] \tag{8}$$

in order to satisfy detailed balance. So a global update results from a sequence of local moves, and in this sense it is similar in spirit to the loop cluster update [16], the directed loop algorithm [17] or the directed path algorithm for constrained monomer-dimer systems [18].

Whenever the two ends of the open string meet, a new closed loop is formed and the new configuration contributes to the original partition function Z in one of the classes $\mathcal{L}_{00}, \mathcal{L}_{10}, \mathcal{L}_{01}, \mathcal{L}_{11}$. In this way the overall normalization is ensured, and expectation values can be calculated as usual. The algorithm switches between the topological sectors with ease: as the string evolves it can grow or shrink in any direction and wrap around the torus. Effectively, the algorithm simulates a system with fluctuating topological boundary conditions.

In principle, the weight of the open string can be chosen arbitrarily, but the physical interpretation in Eq. (7) suggests to choose the weights ω_9 to ω_{16} such that the open string configurations sample directly the 2-point correlation function, hence providing an improved estimator. During the simulation one simply updates a table for $G(x, y)$ as the string end points move around and the expectation value is obtained by forming $\langle G(x, y)\rangle_Z = G(x, y)/Z$.

For the fermionic models we also need to keep track of the Dirac structure associated with $G(x, y)$. This is most easily done by adding the product of the Dirac projectors along the string ℓ, i.e. $\prod_{\mu\in\ell} P(\mu)$, as a contribution at each step. Care has to be taken when the open string winds an odd times around a boundary on which we want to impose antiperiodic boundary conditions for the fermions. In that case we need to account for an additional minus sign in the contribution to $G(x, y)$. For the fermionic models where vertices 13–16 have no physical meaning, the weights ω_{13} to ω_{16} can be tuned for algorithmic efficiency and do not follow any physically inspired rule. A good choice is to use the geometric mean of the weights ω_i of those vertices that can be reached in one further update step, e.g. $\omega_{13} = (\omega_4\omega_6\omega_7)^{1/3}$. Finally, let us emphasize again that the algorithm described here is applicable to any vertex model, also in higher dimensions, as long as the weights are positive definite in well-defined configuration classes.

We have performed extensive tests of our algorithm by comparing to exact results known from Pfaffians (for the Majorana GN model) or from explicit calculations on small lattices. Simple observables are linear combinations of partition functions and ratios thereof, e.g. $Z_{\mathcal{L}_{ij}}/Z$ with $i, j = 0, 1$. In Fig. 2 we show the results for the ratios $Z_{\mathcal{L}_{ij}}/Z$ in the Majorana GN model on a 128^2 lattice as a function of the bare mass m. Dashed lines are the exact results calculated from the Pfaffians. Note that all partition function ratios are obtained in the same simulation. In the inset we also show the ratio Z^{00}_ξ/Z where $Z^{00}_\xi \equiv Z_{\mathcal{L}_{00}} - Z_{\mathcal{L}_{01}} - Z_{\mathcal{L}_{10}} - Z_{\mathcal{L}_{11}}$ is the partition function with fermionic BC periodic in space and time direction. In that situation the Majorana Dirac operator has a zero mode at $m = 0$ (and at $m = -2$) and the system is critical. The inset in Fig. 2 illustrates that the algorithm can reproduce this zero mode without problems and that we can in fact simulate directly at the critical point. Conversely, we can use $Z^{00}_\xi/Z = 0$ as a definition of the critical point $m = m_c$. In Fig. 3 we show our results for Z^{00}_ξ/Z as a function of the bare mass m in the Schwinger model in the strong coupling limit for various volumes. The critical point can be determined accurately with very little computational effort and we obtain $m_c = -0.686\,506(27)$ (cf. inset in Fig. 3) from

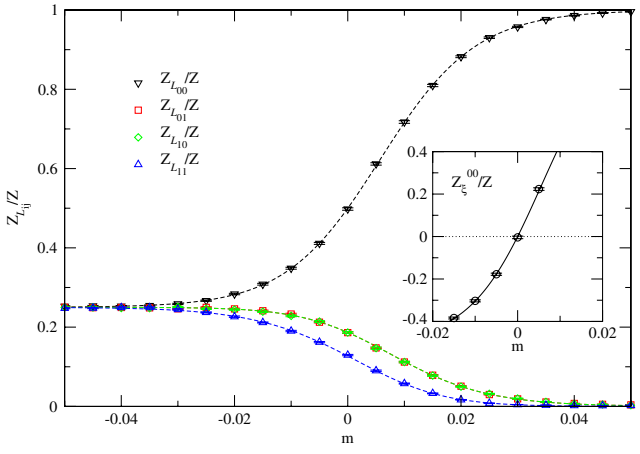

FIG. 2 (color online). Results for the ratios $Z_{\mathcal{L}_{ij}}/Z$ for the Majorana GN model on a 128^2 lattice as a function of the bare mass m. Dashed lines are the exact results. The inset shows Z^{00}_ξ/Z and illustrates how the zero mode at $m = 0$ is reproduced.

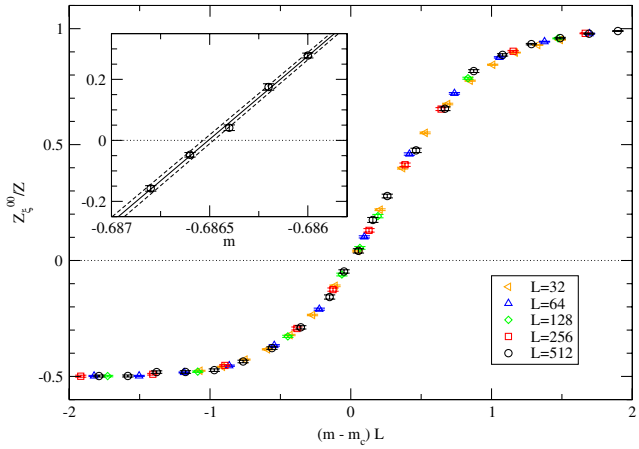

FIG. 3 (color online). Finite size scaling data collapse of Z_ξ^{00}/Z in the Schwinger model at strong coupling consistent with a second order phase transition with critical exponent $\nu = 1$). The inset shows the determination of the critical mass $m_c = -0.686\,506(27)$ from a linear interpolation of the data on the largest lattice with $L = 512$.

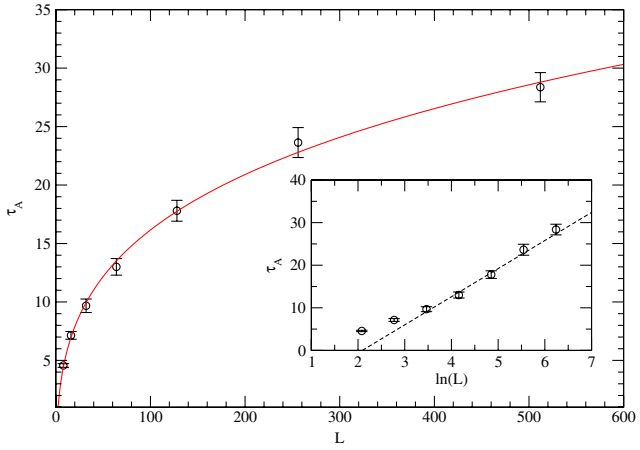

FIG. 4 (color online). Integrated autocorrelation time τ_A of the energy for the Schwinger model in the strong coupling limit at the critical point $m = m_c$. The line is a fit $\tau_A \propto L^z$ yielding $z = 0.25(2)$. The inset shows the logarithmic dependence $-18(3) + 7.5(6)\ln(L)$ from fitting to $L \geq 64$.

our simulations on the largest lattice with $L = 512$. Further improvement could be achieved by employing standard reweighting techniques as done in [19] where they obtained $m_c = -0.6859(4)$. These calculations indicated a second order phase transition in the universality class of the Ising model (with critical exponent $\nu \simeq 1$). Our results in Fig. 3 now confirm this by demonstrating that the partition function ratios Z_ξ^{00}/Z as a function of the rescaled mass $(m - m_c)L^\nu$ with $\nu = 1$ beautifully collapse onto a universal scaling curve.

The efficiency of the algorithm and the fact that critical slowing down is essentially absent is demonstrated in Fig. 4 where we show the integrated autocorrelation time τ_A of the energy as a function of the linear system size L at the critical point $m = m_c$. (Similar plots can be obtained for the Majorana GN model.) The functional dependence on L can be well fitted (χ^2/d.o.f. $= 1.28$) by $\tau_A \propto L^z$ all the way down to our smallest system size $L = 8$. We obtain $z = 0.25(2)$ which is consistent with just using the largest two system sizes. It is an amazing result that our local Metropolis-type update appears to have a dynamical critical exponent close to zero. The autocorrelation time may also depend logarithmically on L and a fit to $L \geq 64$ yields $-13.8(1.9) + 6.6(4)\ln(L)$ with χ^2/d.o.f. $= 1.00$.

In conclusion, we have presented a new type of algorithm for generic vertex models. It relies on sampling directly 2-point correlation functions and essentially eliminates critical slowing down. We have successfully tested our algorithm on the Majorana GN model and on the Schwinger model in the strong coupling limit and found remarkably small dynamical critical exponents. The algorithm definitely opens the way to simulate efficiently generic vertex models (with positive weights) in arbitrary dimensions, in particular the GN model with any number of flavors, the Thirring model, the Schwinger model and QED_3 in the strong coupling limit, as well as fermionic models with Yukawa-type scalar interactions, all with Wilson fermions.

I would like to thank Philippe de Forcrand and Michael Fromm for useful and sometimes crucial discussions. This work is supported by SNF Grant No. PP002-_119015.

Note added.—The technical details of our proposal have also been worked out independently in [20] which appeared while we finalized this paper.

[1] S. Duane, A. D. Kennedy, B. J. Pendleton, and D. Roweth, Phys. Lett. B **195**, 216 (1987).
[2] M. Salmhofer, Nucl. Phys. **B362**, 641 (1991).
[3] K. Scharnhorst, Nucl. Phys. **B479**, 727 (1996).
[4] K. Scharnhorst, Nucl. Phys. **B503**, 479 (1997).
[5] C. Gattringer, Nucl. Phys. **B543**, 533 (1999).
[6] N. Prokof'ev and B. Svistunov, Phys. Rev. Lett. **87**, 160601 (2001).
[7] C. Itzykson and J. M. Drouffe, *Statistical Field Theory* (Cambridge University Press, Cambridge, England, 1989), Vol. 2.
[8] U. Wolff, Nucl. Phys.**B789**, 258 (2008).

[9] I. O. Stamatescu, Phys. Rev. D **25**, 1130 (1982).
[10] P. W. Kasteleyn, Physica (Amsterdam) **27**, 1209 (1961).
[11] B. Sutherland, J. Math. Phys. (N.Y.) **11**, 3183 (1970).
[12] C. Fan and F. Y. Wu, Phys. Rev. B **2**, 723 (1970).
[13] R. J. Baxter, *Exactly Solved Models in Statisticals Mechanics* (Academic, London, 1982).
[14] C. Gattringer, Nucl. Phys. **B559**, 539 (1999).
[15] One can in fact derive these weights also for $d = 3$ and show that all loop contributions are positive, hence allowing simulations of QED_3 in the strong coupling limit.
[16] H. G. Evertz, G. Lana, and M. Marcu, Phys. Rev. Lett. **70**, 875 (1993).
[17] O. F. Syljuasen and A. W. Sandvik, Phys. Rev. E **66**, 046701 (2002).
[18] D. H. Adams and S. Chandrasekharan, Nucl. Phys. **B662**, 220 (2003).
[19] H. Gausterer and C. B. Lang, Nucl. Phys. **B455**, 785 (1995).
[20] U. Wolff, Nucl. Phys. **B814**, 549 (2009).

Paper 2

Simulating Wilson fermions without critical slowing down

Urs Wenger, Proceedings of Science (Lattice 2009) 022.

PROCEEDINGS OF SCIENCE

Simulating Wilson fermions without critical slowing down

Urs Wenger*
Albert Einstein Center for Fundamental Physics
Institute for Theoretical Physics
University of Bern, Sidlerstr. 5, CH-3012 Bern, Switzerland
E-mail: wenger@itp.unibe.ch

We present a simulation algorithm for Wilson fermions based on the exact hopping expansion of the fermion action. The algorithm essentially eliminates critical slowing down by sampling the fermionic two-point correlation function and it allows simulations directly in the massless limit. As illustrative examples, the algorithm is applied to the Gross-Neveu and the Schwinger model, the latter in the strong coupling limit.

The XXVII International Symposium on Lattice Field Theory - LAT2009
July 26-31 2009
Peking University, Beijing, China

*Speaker.

PoS(LAT2009)022

1. Introduction

Simulating strongly interacting fermions continues to be a major challenge in computational physics. The standard procedure to deal with fermionic degrees of freedom is to integrate out the fermionic fields in order to obtain the fermion determinant $\det D$, where D denotes the Dirac operator. However, this procedure is not unproblematic. Consider for example a fermion interacting with a bosonic field U. After integrating out the fermion fields one obtains $\det D(U)$ which yields an effective action non-local in the bosonic field. The standard method is now to re-express the determinant using bosonic 'pseudo-fermions' and use the Hybrid Monte Carlo algorithm [1] which in essence encodes the non-locality of the fermion determinant in the inverse $D(U)^{-1}$. Another problem is that the standard approach suffers from critical slowing down (CSD) towards the chiral limit. In that limit the correlation length of the fermionic two-point function diverges. As a consequence the Dirac operator $D(U)$ develops very small modes and eventually the inverse $D(U)^{-1}$ becomes ill-conditioned. Yet another problem concerns the phase of $\det D$ which for Wilson fermions is in general non-zero. Hence a probabilistic interpretation of the integration measure, necessary for any Monte Carlo simulation, is not possible and leads to a sign problem when an odd number of Wilson fermion flavours is simulated.

Here we propose a novel approach [2] circumventing the above mentioned problems. It is based on the exact hopping expansion of the fermion action, i.e. a reformulation of the fermion system as a statistical closed loop model. We develop a simulation algorithm which samples directly the fermionic two-point function and in this way eliminates CSD. Moreover, it allows to specify the fermionic boundary conditions a posteriori, i.e. after the simulation, and allows simulations directly in the massless limit. The approach is applicable to the Gross-Neveu (GN) model in $D = 2$ dimensions, to the Schwinger model in the strong coupling limit in $D = 2$ and $D = 3$ dimensions, to supersymmetric quantum mechanics and the $N = 1$ and 2 supersymmetric Wess-Zumino model in $D = 2$ dimensions. In the present proceedings we concentrate on the application to the GN and the Schwinger model.

Finally, we would like to emphasise that the reformulation based on the hopping expansion is not new [3, 4, 5, 6]. Mostly, however, it has been applied to staggered fermions in the strong coupling limit where a reformulation in terms of monomers and dimers [7] allows efficient algorithms [8, 9] that were subsequently applied to many interesting systems [10, 11, 12], see also the recent review by Chandrasekharan [13]. For Wilson fermions on the other hand the loop formulation has been developed for the Schwinger model in the strong coupling limit [14] and the GN model [5, 6, 15] and what we propose in [2] is just a very efficient algorithm for these loop formulations.

2. Loop formulation of Wilson fermions

We start with the reformulation of $D = 2$ fermionic systems involving Wilson fermions in terms of a statistical loop gas model. We use the GN model, a prototype for strongly interacting fermions, as an illustrative example. The model is most naturally formulated in terms of Majorana fermions. Employing the Wilson lattice discretisation for a Majorana fermion the Euclidean Lagrange density reads

$$\mathscr{L} = \frac{1}{2}\xi^T\mathscr{C}(\gamma_\mu\tilde{\partial}_\mu - \frac{1}{2}\partial^*\partial + m)\xi - \frac{g^2}{4}\left(\xi^T\mathscr{C}\xi\right)^2 \tag{2.1}$$

where ξ is a real 2-component Grassmann field, $\mathscr{C} = -\mathscr{C}^T$ is the charge conjugation matrix and ∂, ∂^* and $\tilde{\partial}$ are the forward, backward and the symmetric lattice derivative, respectively. In the continuum, the massless model enjoys a discrete chiral symmetry $\xi \to \gamma_5 \xi$ which on the lattice is broken explicitly by the Wilson term $\frac{1}{2}\partial^*\partial$. The symmetry can be restored in the continuum by fine tuning $m \to m_c$. Further we note that a pair of Majorana fermions may be considered as one Dirac fermion, i.e. $\psi = 1/\sqrt{2}(\xi_1 + i\xi_2), \quad \overline{\psi} = 1/\sqrt{2}(\xi_1^T - i\xi_2^T)\mathscr{C}$, exposing the $O(2N)$ flavour symmetry explicitly. Since integrating out Majorana fermions yields the Pfaffian of the antisymmetric Dirac operator, the model with $2N$ Majorana fermions is equivalent to N Dirac fermions through the identity $(\mathrm{Pf}D)^{2N} = (\det D)^N$.

At non-vanishing coupling $g \neq 0$ one usually employs a Hubbard-Stratonovich transformation and introduces the scalar field $\sigma \propto \xi^T \mathscr{C} \xi$. With $M(x) = 2 + m + \sigma(x)$ and $P(\pm\mu) = \frac{1}{2}(1 \mp \gamma_\mu)$ the action then becomes the sum of monomer and hopping terms

$$S_{\mathrm{GN}} = \frac{1}{2}\sum_x \xi^T(x)\mathscr{C}M(x)\xi(x) - \sum_{x,\mu} \xi^T(x)\mathscr{C}P(\mu)\xi(x+\hat{\mu}). \tag{2.2}$$

Using the nil-potency of Grassmann elements one can now expand the Boltzmann factor and perform an exact hopping expansion for the Majorana Wilson fermions [15]. We emphasise that this can be done for any fermionic theory (bilinear in the fermionic fields). At each site, the fields $\xi^T\mathscr{C}$ and ξ must be exactly paired in order to give a non-vanishing contribution to the path integral,

$$\int \mathscr{D}\xi \prod_x \left(M(x)/2\,\xi^T(x)\mathscr{C}\xi(x)\right)^{m(x)} \prod_{x,\mu} \left(\xi^T(x)\mathscr{C}P(\mu)\xi(x+\hat{\mu})\right)^{b_\mu(x)} \tag{2.3}$$

where the occupation numbers $m(x) = 0,1$ for monomers and $b_\mu(x) = 0,1$ for bonds (or dimers) satisfy the constraint

$$m(x) + \frac{1}{2}\sum_\mu b_\mu(x) = 1. \tag{2.4}$$

This constraint encodes that only closed, non-intersecting paths survive the integration and we end up with a closed loop representation of the partition function in terms of monomers and dimers, i.e. $Z = \sum_\ell \omega(\ell)$. The weight ω of each loop ℓ can be calculated analytically [5, 6, 15, 16] yielding $|\omega(\ell)| = 2^{-c/2}$ where c is the number of corners in the loop, while the phase of $\omega(\ell)$ depends on the geometrical shape of ℓ. In $D = 2$ dimensions and for a torus geometry of the lattice, $\mathrm{sign}[\omega(\ell)] \in \{-1,1\}$ depends on the boundary conditions (BC) $\varepsilon_\mu \in \{0,1\}$ and on the number n_μ of loop windings in direction μ,

$$\mathrm{sign}[\omega(\ell)] = (-1)^{n_\mu(\varepsilon_\mu + n_\mu)}. \tag{2.5}$$

As a consequence the overall sign of a given configuration depends only on the fermionic BC and the total winding number $l = \{l_\mu\}$ (modulo 2).

If we separate all configurations into the equivalence classes $\mathscr{L}_{ij}$ where the subscripts i, j specify the total winding numbers l_μ (modulo 2) in the two directions, then the partition function summing over all non-oriented, self-avoiding loops with positive weight,

$$Z = \sum_{\{\ell\}\in\mathscr{L}} |\omega[\ell]| \prod_{x\notin\ell} M(x), \quad \mathscr{L} \in \mathscr{L}_{00} \cup \mathscr{L}_{10} \cup \mathscr{L}_{01} \cup \mathscr{L}_{11}, \tag{2.6}$$

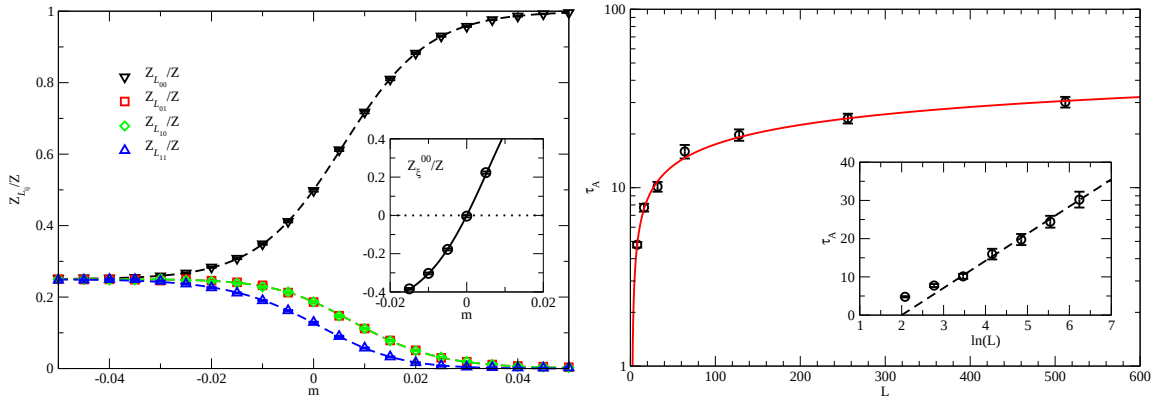

Figure 1: $N = 1$ Majorana GN model on a 128^2 lattice. Left: Comparison of simulation results (symbols) and analytic calculations (dashed lines) for the partition function ratios $Z_{\mathscr{L}_{ij}}/Z$. The inset shows the reproduction of the zero mode of Z_ξ^{00} at $m_c = 0$. Right: Integrated autocorrelation time of the condensate at the critical point $m_c = 0$ fitted by $\tau_A \sim L^z$ with $z = 0.31(4)$. The inset shows a fit to a logarithmic dependence on L.

represents a system with unspecified fermionic BC while systems with specific fermionic BC can be constructed a posteriori by taking the signs of each class according to

$$Z_\xi^\varepsilon = 2Z_{\mathscr{L}_{00}} - \sum_{i,j=0}^{1} (-1)^{\varepsilon_\mu l_\mu} Z_{\mathscr{L}_{ij}} \,. \tag{2.7}$$

Finally we note that if one considers $N > 1$ Majorana flavours the occupation numbers m, b_μ are decorated by the flavour index α and one considers N different loop flavours. The monomer weight $M(x)$ depends on the local fermion density $\sum_\alpha m^\alpha(x)$ only and one ends up with a model of locally coupled loops.

In the Schwinger model the hopping term contains a $U(1)$ phase coming from the gauge field $\phi_\mu(x)$, and the non-oriented (Majorana) bonds carry an additional factor $\propto \cosh(\phi_\mu(x))$. Moreover the gauge field introduces an interaction between the two Majorana flavours proportional to $\pm\sinh(\phi_\mu(x))$, These additional factors introduce a sign problem since each loop can now have an arbitrary sign. However, in the strong coupling limit, the two flavours are bound together. In the present formulation it means that two different Majorana loops lay on top of each other and the resulting double loop describes the world line of the bosonic bound state. It also turns out that all the signs cancel in a non-trivial way and so the bosonisation is realised explicitly. Eventually we end up with a model of non-oriented loops [14] in which all the loop and monomer weights are squared compared to the GN model. Note further that eq.(2.7) no longer applies because the fermionic BC have no impact on the BC of the corresponding bosonic bound state – instead the relevant partition function is the one where all topological classes contribute positively, i.e. Z.

3. Simulation algorithm for loops and strings

A standard procedure to simulate loop gas models as the one described above is to perform local loop updates involving plaquette moves only [17, 18]. One problem with such an algorithm

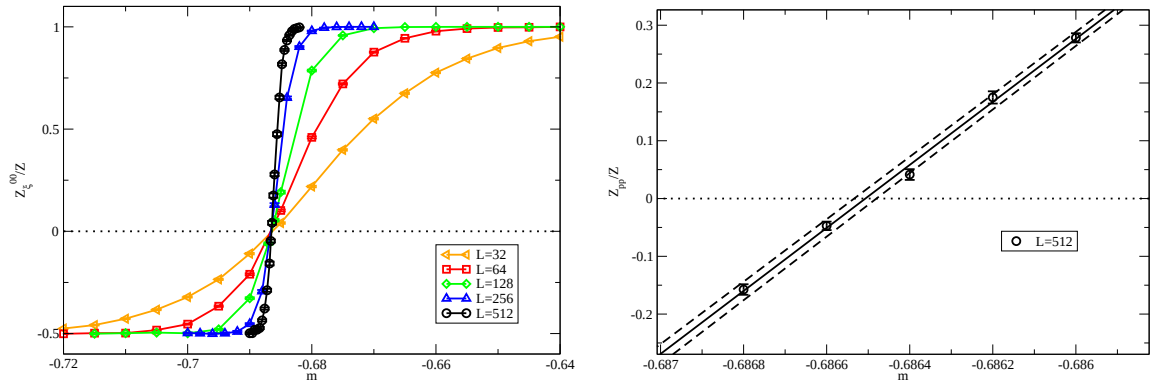

Figure 2: The Schwinger model in the strong coupling limit. Left: Partition function ratio Z_ξ^{00}/Z on various lattices. Right: Determination of the critical point $m_c = -0.686506(27)$ on the largest lattice with $L = 512$.

is that it can not change between the topological classes $\mathscr{L}_{00}, \mathscr{L}_{10}, \mathscr{L}_{01}, \mathscr{L}_{11}$. Moreover, if the correlation length of the system grows large these algorithms become highly inefficient and suffer from CSD. Our proposal [2] (subsequently worked out in [19]) follows the one of Prokof'ev and Svistunov [20] and enlarges the configuration space by open fermionic strings. In the GN model an open string corresponds to the insertion of a Majorana fermion pair $\{\xi(x), \xi^T(y)\mathscr{C}\}$ at position x and y into the path integral, and the open string samples directly the correlation function

$$G(x,y) = \int \mathscr{D}\xi e^{-S_{\rm GN}} \xi(x)\xi(y)^T\mathscr{C} \,. \tag{3.1}$$

This is the reason why CSD is eliminated: configurations are updated on all length scales up to $O(\zeta)$ where ζ is the correlation length corresponding to the fermionic two point function. As a consequence the update remains efficient even at a critical point where the correlation length diverges. Contact with the partition functions $Z_{\mathscr{L}_{ij}}$ is made each time the open string closes and this provides the proper normalisation for the expectation value of the 2-pt. function, $\langle \xi(x)\xi(y)^T\mathscr{C}\rangle_Z = G(x,y)/Z$, or any other observables. In practice, the ends of the open string are updated with a standard local Metropolis or heat bath procedure [2]. Similar ideas have been around for a long time in various other contexts [20, 21, 22] – what is new here is the practical application to Wilson fermions and the demonstration that CSD is essentially eliminated.

4. Absence of critical slowing down

Before investigating the efficiency of the algorithm, we demonstrate its correctness by comparing simulation results with analytically know expressions. For this purpose we use the $N = 1$ Majorana GN model. This model is essentially a free fermion model and can be solved exactly by calculating Pfaffians in momentum space. In the left plot of Figure 1 we show the results for the partition function ratios $Z_{\mathscr{L}_{ij}}/Z$ on a 128^2 lattice from 2M closed path configurations (symbols) compared to the exact results (dashed lines). The inset shows the combination $Z_\xi^{00} = Z_{\mathscr{L}_{00}} - Z_{\mathscr{L}_{10}} - Z_{\mathscr{L}_{01}} - Z_{\mathscr{L}_{11}}$ which has a zero mode at the critical point $m_c = 0$. The algorithm is indeed able to reproduce the zero mode without problems. In order to investigate the efficiency of the algorithm at the critical point we measure the condensate $\langle \xi^T\mathscr{C}\xi\rangle_{Z_\xi}$. The right plot of Figure 1 shows the integrated

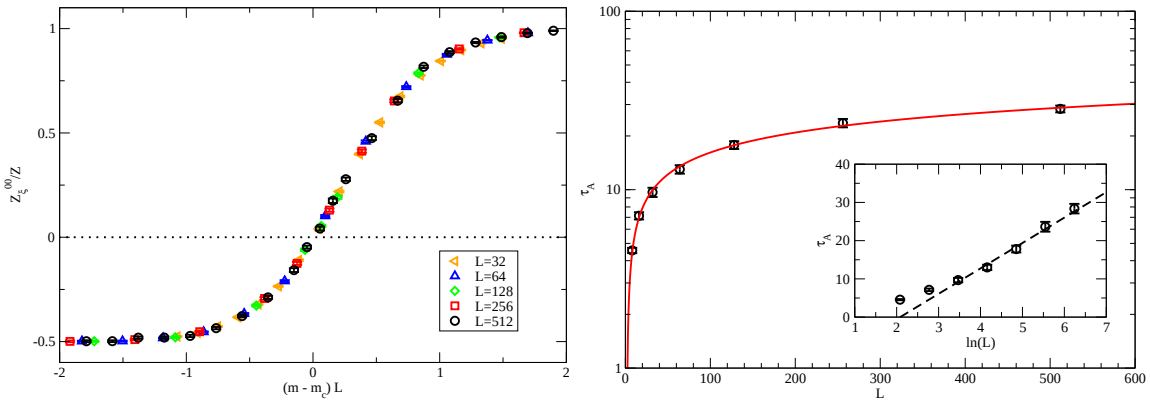

Figure 3: The Schwinger model in the strong coupling limit. Left: Finite size scaling of Z_ξ^{00}/Z for a second order phase transition in the universality class of the Ising model. Right: Integrated autocorrelation time of the condensate at the critical point m_c fitted by $\tau_A \sim L^z$ with $z = 0.25(2)$. The inset shows a fit to a logarithmic dependence on L.

autocorrelation time τ_A of the condensate as a function of the linear system size L. The dynamic exponent z relevant for CSD, i.e. $\tau_A \sim L^z$, turns out to be $z \simeq 0.31(4)$. A dependence logarithmically on L can also be fitted to $L \geq 32$ yielding $-14.2(2.5) + 7.1(6)\ln(L)$ with $\chi^2/\mathrm{dof} = 0.18$.

Next we consider the Schwinger model in the strong coupling limit $g \to \infty$ as a non-trivial example for strongly interacting fermions. In the left plot of Figure 2 we show the partition function ratio Z_ξ^{00}/Z on various lattices up to $L = 512$. As in the Majorana GN model we find a zero of the partition function which depends only very little on the extent of the lattice. We can use $Z_\xi^{00}(m_c) = 0$ as a definition for the critical point m_c. It can be determined by a linear fit and we obtain $m_c = -0.686506(27)$ (cf. right plot in Figure 2) from our simulations on the largest lattice with $L = 512$. Further improvement could be achieved by employing standard reweighting techniques as done in [23] where they obtained $m_c = -0.6859(4)$. These calculations indicated a second order phase transition in the universality class of the Ising model (with critical exponent $\nu \simeq 1$). Our results in the left plot of Figure 3 now confirm this by demonstrating that the partition function ratios Z_ξ^{00}/Z as a function of the rescaled mass $(m - m_c)L^\nu$ with $\nu = 1$ beautifully collapse onto a universal scaling curve. The efficiency of the algorithm and the fact that CSD is essentially absent is demonstrated in the right plot of Fig. 3 where we show the integrated autocorrelation time τ_A of the energy as a function of the linear system size L at the critical point $m = m_c$. The functional dependence on L can be well fitted ($\chi^2/\mathrm{dof} = 1.28$) by $\tau_A \sim L^z$ all the way down to our smallest system size $L = 8$. We obtain $z = 0.25(2)$ which is consistent with just using the largest two system sizes. The autocorrelation time may also depend logarithmically on L and a fit to $L \geq 32$ yields $-13.8(1.9) + 6.6(4)\ln(L)$ with $\chi^2/\mathrm{dof} = 1.00$. In any case it is an amazing result that our local Metropolis-type update appears to have a dynamical critical exponent close to zero.

5. Conclusions

In conclusion, we have presented a new type of algorithm for Wilson fermions in two dimensions. It relies on sampling directly 2-point correlation functions and essentially eliminates

critical slowing down. We have successfully tested our algorithm on the Majorana GN model and on the Schwinger model in the strong coupling limit and found remarkably small dynamical critical exponents. The algorithm definitely opens the way to simulate efficiently generic loop models (with positive weights) in arbitrary dimensions, in particular the GN model with any number of flavours, the Thirring model, the Schwinger model and QED_3 in the strong coupling limit, as well as fermionic models with Yukawa-type scalar interactions like the $N = 1$ and 2 Wess-Zumino models, all with Wilson fermions.

References

[1] S. Duane, A. D. Kennedy, B. J. Pendleton and D. Roweth, Phys. Lett. **B195**, 216 (1987).

[2] U. Wenger, Phys. Rev. **D80**, 071503 (2009), [arXiv:0812.3565].

[3] M. Karowski, R. Schrader and H. J. Thun, Commun. Math. Phys. **97**, 5 (1985).

[4] I. Montvay, Phys. Lett. **B227**, 260 (1989).

[5] C. Gattringer, Int. J. Mod. Phys. **A14**, 4853 (1999), [cond-mat/9811139].

[6] C. Gattringer, Nucl. Phys. **B543**, 533 (1999), [hep-lat/9811014].

[7] P. Rossi and U. Wolff, Nucl. Phys. **B248**, 105 (1984).

[8] F. Karsch and K. H. Mutter, Nucl. Phys. **B313**, 541 (1989).

[9] D. H. Adams and S. Chandrasekharan, Nucl. Phys. **B662**, 220 (2003), [hep-lat/0303003].

[10] S. Chandrasekharan and F.-J. Jiang, Phys. Rev. **D68**, 091501 (2003), [hep-lat/0309025].

[11] S. Chandrasekharan and F.-J. Jiang, Phys. Rev. **D74**, 014506 (2006), [hep-lat/0602031].

[12] Ph. de Forcrand and M. Fromm, arXiv:0907.1915.

[13] S. Chandrasekharan, PoS **LATTICE2008**, 003 (2008), [arXiv:0810.2419].

[14] M. Salmhofer, Nucl. Phys. **B362**, 641 (1991).

[15] U. Wolff, Nucl. Phys. **B789**, 258 (2008), [arXiv:0707.2872].

[16] I. O. Stamatescu, Phys. Rev. **D25**, 1130 (1982).

[17] H. Gausterer, C. B. Lang and M. Salmhofer, Nucl. Phys. **B388**, 275 (1992).

[18] C. Gattringer, V. Hermann and M. Limmer, Phys. Rev. **D76**, 014503 (2007), [arXiv:0704.2277].

[19] U. Wolff, Nucl. Phys. **B814**, 549 (2009), [arXiv:0812.0677].

[20] N. Prokof'ev and B. Svistunov, Phys. Rev. Lett. **87**, 160601 (2001).

[21] H. G. Evertz, G. Lana and M. Marcu, Phys. Rev. Lett. **70**, 875 (1993), [cond-mat/9211006].

[22] O. F. Syljuasen and A. W. Sandvik, Phys. Rev. **E66**, 046701 (2002).

[23] H. Gausterer and C. B. Lang, Nucl. Phys. **B455**, 785 (1995), [hep-lat/9506028].

Paper 3

Worm algorithm for the O($2N$) Gross-Neveu model

Vidushi Maillart and Urs Wenger, Proceedings of Science (Lattice 2010) 257.

PROCEEDINGS OF SCIENCE

Worm algorithm for the $O(2N)$ Gross-Neveu model

Vidushi Maillart*
Albert Einstein Center for Fundamental Physics, Institute for Theoretical Physics, Sidlerstrasse 5, CH-3012 Bern, Switzerland
Institute for Theoretical Physics, University of Regensburg, 93040 Regensburg, Germany
E-mail: vidushi.maillart@itp.unibe.ch

Urs Wenger
Albert Einstein Center for Fundamental Physics, Institute for Theoretical Physics, Sidlerstrasse 5, CH-3012 Bern, Switzerland
E-mail: wenger@itp.unibe.ch

We study the lattice $O(2N)$ Gross-Neveu model with Wilson fermions in the fermion loop formulation. Employing a worm algorithm for an open fermionic string, we simulate fluctuating topological boundary conditions and use them to tune the system to the critical point. We show how the worm algorithm can be extended to sample correlation functions of bound states involving an arbitrary number of Majorana fermions and present first results.

The XXVIII International Symposium on Lattice Field Theory, Lattice2010
June 14-19, 2010
Villasimius, Italy

*Speaker.

PoS(Lattice 2010)257

1. Introduction

It is well known that fermionic degrees of freedom are difficult to simulate on the lattice due to their Grassmannian nature. The fermion matrix determinant, obtained after integrating out the fermion fields, remains the major bottleneck of Monte-Carlo simulations, since it is highly non-local and connects all the degrees of freedom. Each Monte-Carlo update step changes the fermion matrix and requires a new calculation of the determinant. On the other hand, if an algorithm can update the determinant by a local procedure, then a significant gain in efficiency might be achievable. However, simulations of fermions usually suffer from critical slowing down when the fermion correlation length diverges, i.e. when the fermions become massless, and it is by no means obvious whether a local algorithm can be constructed to circumvent this problem.

An interesting attempt to deal with the problems related to simulating fermions on the lattice has recently been suggested in [1, 2] in the context of the $O(2N)$ Gross-Neveu (GN) model. It is based on reformulating the model in terms of closed fermion loops [3, 4, 5]. Introducing an open fermionic string, an algorithm can be devised for which critical slowing is essentially absent. It follows the spirit of Prokof'ev and Svistunov's worm algorithm [6] and makes use of the fact that a global update of the closed fermion loops can be obtained by locally updating the open fermionic string. The open string corresponds to the insertion of a Majorana fermion pair and directly samples the two-point correlation function. In this way the configurations are updated on all length scales up to the correlation length, and this eventually guarantees the absence of critical slowing down. Moreover, the algorithm also allows simulations directly in the massless limit [1, 2] and provides direct access to the critical point via ratios of partition functions [7].

The algorithm has been successfully applied to simulate free fermions in two dimensions, but it has proven equally successfull also in its application to strongly interacting fermions, e.g. in the Schwinger model in the strong coupling limit [1, 2] and in supersymmetric quantum mechanics [8]. Here we report on the application of the worm algorithm to another two-dimensional system of interacting fermions - the $O(2N)$ Gross-Neveu model. We demonstrate how a simple modification of the worm algorithm can be used to measure the fermion bound state spectrum and we present preliminary results for $N = 1$, in which case the GN model corresponds to the Thirring model.

2. Fermion loop formulation of the Gross Neveu model

We consider the two-dimensional $O(2N)$-symmetric GN model [9] described by the Lagrangian

$$\mathscr{L} = \sum_{i=1}^{N} \overline{\psi}_i(\gamma_\mu \partial_\mu + m)\psi_i - \frac{g^2}{2}(\sum_{i=1}^{N} \overline{\psi}_i \psi_i)^2 \,. \tag{2.1}$$

This is a relativistic quantum field theory of N self-interacting Dirac fermion fields. For $N = 1$ the $O(2)$ GN model is equivalent to the massive Thirring model as $(\overline{\psi}\psi)^2 = \frac{1}{4}(\overline{\psi}\gamma_\mu\psi)(\overline{\psi}\gamma_\mu\psi)$. It has a pseudoscalar bosonic fermion-antifermion bound state [10] and is especially interesting due to its equivalence to the sine-Gordon model [11], in which the boson is the fundamental particle and the fermion emerges as a soliton solution.

To make the model amenable for the fermion loop algorithm in [1], we decompose the complex Dirac fermion fields ψ_j and $\overline{\psi}_j$ into real Majorana fields ξ_{2j} and ξ_{2j+1} according to $\psi_j =$

$(\xi_{2j}+i\xi_{2j+1})/\sqrt{2}$ and $\overline{\psi}_j=(\overline{\xi}_{2j}-i\overline{\xi}_{2j+1})\sqrt{2}$. The Lagrangian density can then be written as

$$\mathscr{L}=\frac{1}{2}\sum_{i=1}^{2N}\overline{\xi}_i(\gamma_\mu\partial_\mu+m)\xi_i-\frac{g^2}{8}\left(\sum_{i=1}^{2}\overline{\xi}_i\xi_i\right)^2. \tag{2.2}$$

Note that the $O(2N)$ symmetry is now obvious, as (2.2) is invariant under rotations of the Majorana fields in flavour space. Discretising the action with Wilson fermions gives

$$\mathrm{S}=\frac{1}{2}\sum_x\sum_{i=1}^{2N}\varphi\overline{\xi}_i(x)\xi_i(x)-\frac{g^2}{8}\sum_x\left(\sum_{i=1}^{2N}\overline{\xi}_i(x)\xi_i(x)\right)^2-\sum_{i=1}^{2N}\sum_{x,\mu}(\overline{\xi}_i(x)P(\mu)\xi_i(x+\hat{\mu}))\,, \tag{2.3}$$

where $\varphi=(2+m)$ and $P(\pm\mu)=\frac{1}{2}(1\mp\gamma_\mu)$. When expanding the Boltzmann factor in the partition function to all orders, terms quadratic or higher order in each field component vanish due to the nilpotency of the Grassmann fields. Restricting now to $N=1$ for simplicity and keeping only non-trivial terms, the partition function can be written as

$$\begin{aligned}\mathrm{Z}=\int\mathscr{D}\xi\prod_x\left(1-\frac{\varphi}{2}\left(\sum_{i=1}^{2}\overline{\xi}_i(x)\xi_i(x)\right)+\frac{(\varphi^2+g^2)}{4}\overline{\xi}_1(x)\xi_1(x)\overline{\xi}_2(x)\xi_2(x)\right)\\ \times\prod_{x,\mu}\prod_{i=1}^{2}\left(1+\overline{\xi}_i(x)P(\hat{\mu})\xi_i(x+\hat{\mu})\right)\end{aligned} \tag{2.4}$$

The integration measure is saturated site by site by combinations $\overline{\xi}_i\xi_i$, and it is straightforward to identify the non-vanishing contributions to the partition function. They are characterised by the fact that for a particular Majorana flavour either two adjacent hopping terms and no monomer terms, or one of the monomer terms, but no hopping terms are present at a given site. This results in the constraint that for each flavour only closed, non-intersecting fermion loops survive the Grassmann integration. Furthermore, the loops are non-backtracking due to the orthogonality of the projectors, viz. $P(+\mu)P(-\mu)=0$. Thus, the partition function is a sum over all possible combinations of two different species of loops (corresponding to the two Majorana flavours). The generalisation to an arbitrary number of N Dirac fields is straightforward – the number of species of loops involved is simply equal to $2N$, the number of Majorana fermions.

3. Worm algorithm for Majorana fermions

In order to generate configurations of closed loops we employ a variant of the algorithm of Prokof'ev and Svistunov [6]. Here we explain the main ideas of the open fermionic string ("worm") algorithm in a few schematic steps and point out the modifications we have introduced to increase efficiency. Further details can be found in [6, 1].

A peculiar feature of the worm algorithm is that the fermion correlation function is measured during the update procedure. This is due to the fact that the insertion of the open fermionic string, which is used to update the loop configuration, corresponds to the insertion of a pair of Majorana fermions $\xi_i(x)\overline{\xi}_i(y)$ of flavour i at positions x and y, respectively. In the path integral formalism this is equivalent to the correlation function

$$G_i(x,y)=\langle\xi_i(x)\overline{\xi}_i(y)\rangle=\frac{1}{Z}\int\mathscr{D}\xi\;\xi_i(x)\overline{\xi}_i(y)\,e^{-S}\,. \tag{3.1}$$

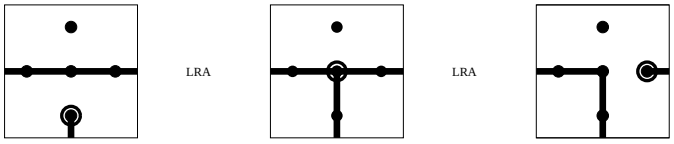

Figure 1: Update moves for the break-up/reconnect step. Note that the configuration in the middle has no physical interpretation and hence gives no contribution to the correlation function.

The algorithm now proceeds by locally updating the ends of the open string using a simple Metropolis procedure according to the weights of the corresponding two-point function. The main steps are as follows:

- *Relocation step:* Given a closed loop configuration, choose a fermion flavour i and a lattice site x at random and place the head ξ_i and the tail $\overline{\xi_i}$ of the worm on this site with a probability given by the weight ratio of the loop configurations before and after the step. If accepted, it gives a contribution to $G_i(x,x)$ unless a loop of species i passes through x in the original closed loop configuration, in which case the new configuration has no physical interpretation and gives no contribution to $G_i(x,x)$.

- *Move step:* Choose a direction μ at random, and move the head of the worm to site $y = x+\hat{\mu}$. Add or delete a fermion bond between x and $x+\hat{\mu}$ depending on whether the bond is empty or occupied. The resulting configuration gives a contribution to $G_i(x,x+\mu)$.

- *Break-up/reconnect step:* In case the new site $x+\hat{\mu}$ is already occupied by a fermion loop of flavour i, we still allow the move, although the corresponding configuration (cf. middle plot in figure 1) is forbidden by the Pauli exclusion principle. Consequently, it does not contribute to the correlation function, but induces transitions between allowed configurations as indicated in the figure.

- *Removal step:* Once the head of the worm reaches its starting position, i.e. head and tail meet again at site x, we may propose to remove head and tail. If accepted, we have a closed loop configuration contributing to the partition function.

We emphasise that the break-up/reconnect step is crucial for the algorithm to work efficiently, since it allows the loops to be opened and restructured. Especially close to the critical point, where loops proliferate, this step gives the worm much more freedom to update the configurations.

4. Topological and fermionic boundary conditions

On a finite lattice with a periodic torus geometry, fermion loops can wind around the lattice and the loop configurations can hence be categorised into different homotopy classes depending on the number of loop windings. For each Majorana fermion ξ_i a two dimensional vector $\vec{l}_i = (l_x, l_t)_i$ is assigned to each configuration to account for the windings in space and time direction, respectively. The components of $\vec{l}_i$ are either 0 or 1 corresponding to an overall even or odd number of loop windings, respectively, in the corresponding direction. Configurations with different $\vec{l}_i$

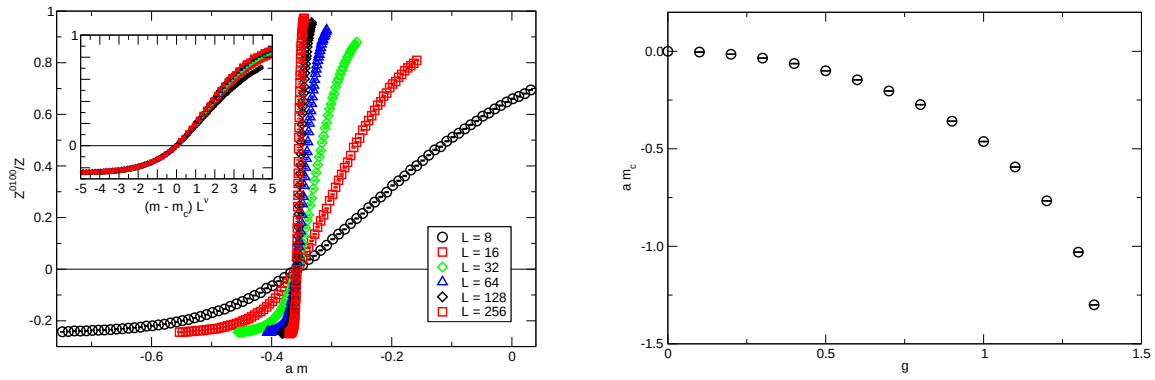

Figure 2: The figure on the left shows the ratio Z^{0100}/Z for the Thirring model at $g = 0.9$ as a function of the bare mass am on square lattices of size $L = 8, 16, 32, 64, 128$ and 256. The inset shows the finite size scaling. The right plot summarises our results for the critical mass am_c as a function of the coupling g.

contribute to separate partition functions $Z_{\vec{l}_1,\vec{l}_2,\ldots}$ with fixed topological boundary conditions (b.c.). Since the open fermion string of the worm algorithm tunnels between the configurations in the various homotopy classes, it samples all the partition functions $Z_{\vec{l}_1,\vec{l}_2,\ldots}$. More importantly, the configurations in all homotopy classes are sampled with positive weights relative to each other, i.e. the partition function $Z \equiv \sum_{\vec{l}_1,\vec{l}_2,\ldots} Z_{\vec{l}_1,\vec{l}_2,\ldots}$ corresponds to one with fluctuating topological b.c., but unspecified fermionic b.c. As a consequence, the b.c. for the fermions can be chosen at the end of the simulation and all possible fermionic b.c. can be studied *a posteriori*.

In order to encode the fermionic b.c. we introduce a two dimensional vector $\vec{\varepsilon}_i$ in analogy to $\vec{l}_i$. The components of $\vec{\varepsilon}_i$ are 0 or 1, and correspond to periodic or anti-periodic b.c., respectively. The partition function $Z^{\vec{\varepsilon}_1,\vec{\varepsilon}_2,\cdots}$ for fixed $\vec{\varepsilon}_1, \vec{\varepsilon}_2, \ldots$ can now be written as a linear combination of the partition functions $Z_{\vec{l}_1,\vec{l}_2,\ldots}$, e.g. for $N = 1$,

$$Z^{\vec{\varepsilon}_1,\vec{\varepsilon}_2} = 4Z_{\vec{0},\vec{0}} - 2\sum_{\vec{l}_1}(-1)^{\vec{\varepsilon}_1\vec{l}_1} Z_{\vec{l}_1,\vec{0}} - 2\sum_{\vec{l}_2}(-1)^{\vec{\varepsilon}_2\vec{l}_2} Z_{\vec{0},\vec{l}_2} + \sum_{\vec{l}_1,\vec{l}_2}(-1)^{(\vec{\varepsilon}_1\vec{l}_1+\vec{\varepsilon}_2\vec{l}_2)} Z_{\vec{l}_1,\vec{l}_2}\,. \tag{4.1}$$

As shown in [7], choosing periodic b.c. for all fermions in all directions, except antiperiodic in one direction for one single fermion, e.g. $\vec{\varepsilon}_1 = (0,1)$ and $\vec{\varepsilon}_{i>1} = (0,0)$, the corresponding partition function $Z^{0100\cdots}$ vanishes at the massless, critical point, i.e. when the bare mass m is equal to the critical mass m_c. Hence, the criterion can be used to determine m_c for various couplings by tuning the bare mass m to the point where $Z^{0100\cdots} = 0$.

In figure 2 we show the results of such a determination for the Thirring model. The plot on the left shows the partition function ratio Z^{0100}/Z as a function of the bare mass am for square lattices with $L = 8, \ldots, 256$ at the coupling $g = 0.9$. As the lattice size increases the jump from $Z^{0100}/Z \sim 1$ to $Z^{0100}/Z \sim -0.25$ is more and more pronounced, so that the critical point $Z^{0100} = 0$ can be determined very precisely. Since the critical point corresponds to a second order phase transition where the correlation length diverges, one should find a corresponding universal finite size scaling (FSS) behaviour. The inset in the left plot of figure 2 illustrates that this is indeed the case. There we show the partition function ratios as a function of $(m - m_c)L^{\nu}$, and from the FSS we can determine the critical exponent ν and the critical mass am_c in the thermodynamic

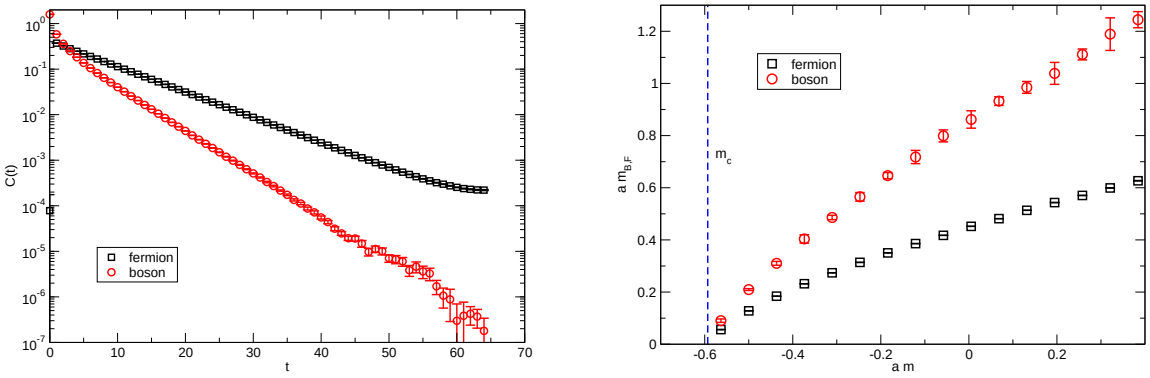

Figure 3: In the left plot the single fermion and bound state correlation functions are plotted. The right plot shows the fermion and boson masses as a function of the bare mass *am* for the Thirring model at $g = 1.1$.

limit $L \to \infty$ to a very high precision with a rather modest computational effort. The right plot in figure 2 summarises our results for the critical mass in the thermodynamic limit as a function of the coupling g.

5. Bound states of fermions

It can easily be worked out that the correlation function of the pseudoscalar bound state $\overline{\psi}\gamma_5\psi$ in the Thirring model is given by

$$\langle \mathcal{O}(x)\mathcal{O}(y)\rangle = \langle \overline{\xi}_1(x)\,\gamma_5\,\xi_2(x)\overline{\xi}_1(y)\,\gamma_5\,\xi_2(y)\rangle\,. \tag{5.1}$$

In the loop formulation, this corresponds to two open fermion strings, one for each Majorana fermion flavour, with common endpoints at positions x and y. In complete analogy to the single fermion update using the fermionic 2-point correlation function, we can update the configurations using the bosonic bound state correlation function in eq.(5.1). In practice, we insert two instances of the bound state wave function $\mathcal{O}(x) = \overline{\xi}_1(x)\,\gamma_5\,\xi_2(x)$ into the system and let them move around by employing again a local Metropolis update. This procedure samples the bound state correlation function, and at the same time updates the loop configuration of both fermion flavours. In order for this to work efficiently, the break-up and reconnection step described in section 3 is the crucial ingredient, since otherwise the algorithm would be restricted to move the bound state wave function only to sites where no fermion loop is present. Obviously, this would become increasingly difficult towards the critical point, where the fermion loops proliferate.

The efficiency of the algorithm is illustrated in figure 3. In the left plot we show the single fermion and the bosonic bound state correlation functions at zero momentum obtained from a simulation of the Thirring model on a $L = 128$ lattice at coupling $g = 1.1$. It is remarkable that in both cases the signal can be followed over several orders of magnitude. Consequently, the corresponding masses can be reliably determined towards the continuum limit. This is illustrated in the right plot of figure 3 where we show the fermion and boson masses versus the bare mass *am*.

6. Conclusions and outlook

Using Wilson's fermion discretisation, the path integral for the $O(2N)$ Gross-Neveu (GN) model can be described on the lattice in terms of interacting fermion loops. We discussed how the loop system can efficiently be simulated using open fermion strings. Single fermion and bound state correlation functions are measured while updating the system. In addition, the algorithm allows the direct calculation of ratios of partition functions with arbitrary fermion boundary conditions. We have successfully implemented the fermion loop algorithm for $N = 1$, in which case the GN model is equivalent to the Thirring model, and presented first preliminary results for the determination of the critical point from the partition function ratios. Moreover, we also presented first promising results for the single fermion and the bound state masses. Currently we are working on measuring these quantities for the massive Thirring model in the continuum limit at various values of the couplings, in order to compare the results to predictions based on the equivalence of the model to the Sine-Gordon model. The extension of the algorithm to a larger number of fermions is interesting and rather straightforward.

An obvious question to ask is whether and how the idea of updating an open fermionic string can be put to use in the context of gauged fermions or in higher dimensions. Successfull attempts were so far reported only in the strong coupling limit [1, 2, 12], but there are many other interesting and promising extensions [13] using worm-type algorithms, even in connection with pure gauge theories [14].

Acknowledgements

This work has partly been supported by the European Union under grant 238353 (ITN STRONGnet).

References

[1] U. Wenger, *Phys. Rev.* **D80** (2009) 071503, [arXiv:0812.3565].

[2] U. Wenger, *PoS* **LAT2009** (2009) 022, [arXiv:0911.4099].

[3] I. O. Stamatescu, *Phys. Rev.* **D25** (1982) 1130.

[4] C. Gattringer, *Nucl. Phys.* **B543** (1999) 533–542, [hep-lat/9811014].

[5] U. Wolff, *Nucl. Phys.* **B789** (2008) 258–276, [arXiv:0707.2872].

[6] N. Prokof'ev and B. Svistunov, *Phys. Rev. Lett.* **87** (2001) 160601.

[7] O. Bär, W. Rath, and U. Wolff, *Nucl. Phys.* **B822** (2009) 408–423, [arXiv:0905.4417].

[8] D. Baumgartner and U. Wenger, *PoS* **LATTICE2010** (2010).

[9] D. J. Gross and A. Neveu, *Phys. Rev.* **D10** (1974) 3235.

[10] R. F. Dashen, B. Hasslacher, and A. Neveu, *Phys. Rev.* **D11** (1975) 3424.

[11] S. R. Coleman, *Phys. Rev.* **D11** (1975) 2088.

[12] S. Chandrasekharan and A. Li, *JHEP* **12** (2010) 021, [arXiv:1009.2774].

[13] S. Chandrasekharan, *Phys. Rev.* **D82** (2010) 025007, [arXiv:0910.5736].

[14] T. Korzec and U. Wolff, *PoS* **LATTICE2010** (2010) 029, [arXiv:1011.1359].

Part III

Supersymmetric quantum mechanics

Paper 4

Simulation of supersymmetric models on the lattice without a sign problem

David Baumgartner and Urs Wenger, Proceedings of Science (Lattice 2010) 245.

PROCEEDINGS OF SCIENCE

Simulation of supersymmetric models on the lattice without a sign problem

David Baumgartner* **and Urs Wenger***
Albert Einstein Center for Fundamental Physics
Institute for Theoretical Physics
University of Bern
Sidlerstrasse 5
CH–3012 Bern
Switzerland
E-mail: baumgart@itp.unibe.ch, wenger@itp.unibe.ch

Simulations of supersymmetric models on the lattice with (spontaneously) broken supersymmetry suffer from a fermion sign problem related to the vanishing of the Witten index. We propose a novel approach which solves this problem in low dimensions by formulating the path integral on the lattice in terms of fermion loops. The formulation is based on the exact hopping expansion of the fermionic action and allows the explicit decomposition of the partition function into bosonic and fermionic contributions. We devise a simulation algorithm which separately samples the fermionic and bosonic sectors, as well as the relative probabilities between them. The latter then allows a direct calculation of the Witten index and the corresponding Goldstino mode. Finally, we present results from simulations on the lattice for the spectrum and the Witten index for $\mathcal{N} = 2$ supersymmetric quantum mechanics.

The XXVIII International Symposium on Lattice Field Theory
June 14-19,2010
Villasimius, Sardinia Italy

*Speaker.

 http://pos.sissa.it/

PoS(Lattice 2010)245

1. Introduction

Supersymmetry (SUSY) is thought to be a crucial ingredient in the unification of the Standard Model interactions as well as in the solution of the hierarchy problem. On the other hand, we know that the low energy physics is not supersymmetric, and consequently the SUSY must be broken at low energies, either explicitly or spontaneously. Since the origin and mechanism of spontaneous SUSY breaking is a non-perturbative effect, it can not be understood in perturbation theory – instead, non-perturbative methods are required. One way to study non-perturbative effects in quantum field theories is provided by the lattice regularisation. However, the lattice discretisation comes with various problems, for example the explicit breaking of Poincaré symmetry, or the absence of Leibniz' rule, and it is therefore not clear at all whether and how SUSY can be realised within the lattice regularisation.

If the lattice discretisation, for example, enjoys some exact symmetries that allow only irrelevant symmetry breaking operators, which become unimportant in the infrared regime, so-called 'accidental' symmetries may emerge from a non-symmetric lattice action and the full symmetry develops in the continuum limit. This is for example the case for (Euclidean) Poincaré symmetry in lattice QCD or SUSY in $\mathcal{N} = 1$ SU(N) Super-Yang-Mills theory. In the latter case, the only relevant symmetry breaking operator is the gaugino mass term which violates the Z_{2N} chiral symmetry. Therefore, a chirally invariant lattice action forbids such a term and SUSY is automatically recovered in the continuum limit. For SUSY theories involving scalar fields, however, such a way out is not available: the scalar mass term $m^2|\phi|^2$ breaks SUSY, and there is no other symmetry available to forbid that term. In principle, even in such cases, some symmetries can be obtained in the continuum by fine tuning the theory with counterterms. The restoration of chiral symmetry for Wilson fermions is one such example. For SUSY, such an approach is in general not practical, but in lower dimensions, when theories are superrenormalisable, it sometimes is [1]. Yet another approach to SUSY on the lattice is to look for an exact lattice realisation of a subalgebra of the full SUSY algebra, e.g. by combining the Poincaré and flavour symmetry group, so-called twisted SUSY (cf. [2] and references therein). This approach is applicable to systems with extended SUSY and leads to so-called Q-exact discretisations.

Yet another difficulty, and maybe the most severe for supersymmetry on the lattice, is the fact that supersymmetric models with broken supersymmetry inherently suffer from a fermion sign problem that hinders Monte Carlo simulations of such models on the lattice. This can easily be seen as follows. The vanishing of the Witten index

$$W \equiv \lim_{\beta\to\infty} \mathrm{Tr}(-1)^F \exp(-\beta H),$$

where F is the fermion number and H the Hamiltonian of the system, provides a necessary (but not sufficient) condition for spontaneous supersymmetry breaking. On the other hand, the index is equivalent to the partition function with periodic boundary conditions,

$$W = \int_{-\infty}^{\infty} \mathscr{D}\phi \ \det[\not{D}(\phi)]\, e^{-S_B[\phi]} = Z_p\,,$$

and the only way for the path integral to vanish is through the fermionic determinant (or Pfaffian) being indefinite, independent of the fermion discretisation. Indeed, this has been seen in many

studies of supersymmetric models on the lattice that allow spontaneous supersymmetry breaking, e.g. SUSY quantum mechanics with a supersymmetry breaking superpotential[1] [3, 4, 5], $\mathscr{N} = 16$ Yang-Mills quantum mechanics [6, 7, 8, 9], $\mathscr{N} = 1$ Wess-Zumino model in 2D [10], or $\mathscr{N} = (2,2)$ Super-Yang-Mills in 2D [11] (see, however, also [12, 13]).

Here we propose a novel approach based on [14, 15] that circumvents the fermionic sign problem by formulating the path integral on the lattice in terms of fermion loops. The formulation is based on the exact hopping expansion of the fermionic action and allows the explicit decomposition of the partition function into bosonic and fermionic contributions. Consequently, one can then devise a simulation algorithm that separately samples the fermionic and bosonic sectors, as well as the relative probabilities between them. This then allows a precise calculation of the Witten index and a direct determination of the presence or absence of a Goldstino mode. Furthermore, although this is less relevant in the present context, the approach eliminates critical slowing down and also allows simulations directly in the massless limit or at negative bare mass values [14].

2. Fermion sign problem from spontaneous SUSY breaking

Let us briefly elaborate further on the issue of spontaneous SUSY breaking (SSB), the vanishing of the Witten index and the connection to the fermion sign problem.

It is well known that the Witten index provides a necessary, but not sufficient, condition for SSB [16]. One has

$$W \equiv \lim_{\beta\to\infty} \mathrm{Tr}(-1)^F \exp(-\beta H) \quad \Rightarrow \begin{cases} = 0 & \text{SSB may occur,} \\ \neq 0 & \text{no SSB.} \end{cases}$$

From the definition it is clear that the index counts the difference between the number of n_B bosonic and n_F fermionic zero energy states:

$$W \equiv \lim_{\beta\to\infty} \left[\mathrm{Tr}_B \exp(-\beta H) - \mathrm{Tr}_F \exp(-\beta H)\right] = n_B - n_F \,.$$

In a field theoretic language the index is equivalent to the partition function of the system with periodic boundary conditions imposed on both the bosonic and fermionic degrees of freedom,

$$W = \int_{-\infty}^{\infty} \mathscr{D}\phi \;\det\left[\not{D}(\phi)\right] e^{-S_B(\phi)} = Z_p \,.$$

Here the determinant has been obtained by integrating out the complex valued Dirac fermion fields[2], while $S_B(\phi)$ is the action for the bosonic degrees of freedom, collectively denoted by ϕ. It is now clear that in order to obtain a vanishing Witten index, we need both positive and negative contributions to the path integral, and this can only be achieved by the fermion determinant being indefinite. This is the source of the fermion sign problem in the context of spontaneous SUSY breaking, and we argue that such a sign problem must occur in any model aspiring to accommodate spontaneous SUSY breaking.

[1] Note that in the context of SUSY quantum mechanics it is misleading to speak of spontaneous or dynamical SUSY breaking; it is rather a static breaking determined by the form of the superpotential.

[2] In case one is dealing with real-valued Majorana fermion fields, one obtains the Pfaffian $\mathrm{Pf}\left[\not{D}(\phi)\right]$ instead of the determinant.

It is instructive to illustrate the argument in the explicit example of SUSY quantum mechanics. The continuum action of $\mathcal{N}=2$ supersymmetric quantum mechanics reads

$$S = \int dt\, \frac{1}{2}\left(\frac{d\phi(t)}{dt}\right)^2 + \frac{1}{2}P'(\phi(t))^2 + \bar{\psi}(t)\left(\frac{d}{dt} + P''(\phi(t))\right)\psi(t)\,, \tag{2.1}$$

where the real field ϕ denotes the bosonic coordinate, while $\bar{\psi}$ and ψ denote the two fermionic coordinates. $P(\phi)$ is the superpotential and the derivatives P' and P'' are taken with respect to ϕ. The (regulated) fermion determinant with periodic boundary conditions can be calculated analytically [17, 18],

$$\det\left[\frac{\partial_t + P''(\phi)}{\partial_t + m}\right]_p = \sinh\int_0^T \frac{P''(\phi)}{2}dt\,,$$

and by rewriting the sinh-function in terms of two exponentials, one can separate the positive and negative, or rather, the bosonic and fermionic contributions to the partition function,

$$\det\left[\frac{\partial_t + P''(\phi)}{\partial_t + m}\right]_p = \frac{1}{2}\exp\left(+\int_0^T \frac{P''(\phi)}{2}dt\right) - \frac{1}{2}\exp\left(-\int_0^T \frac{P''(\phi)}{2}dt\right) \quad\Longrightarrow\quad Z_0 - Z_1\,.$$

As an example, consider the superpotential $P_e(\phi) = \frac{1}{2}m\phi^2 + \frac{1}{4}g\phi^4$, which is even under the parity transformation $\phi \to \tilde{\phi} = -\phi$. In this case one finds $P_e''(\phi) \geq 0$ and hence $Z_0 \neq Z_1$, i.e. no SUSY breaking. On the other hand, for the superpotential $P_o(\phi) = -\frac{\mu^2}{4\lambda}\phi + \frac{1}{3}\lambda\phi^3$, which is odd under parity, one has $P_o''(\tilde{\phi}) = -P_o''(\phi)$ and, since $S_B(\tilde{\phi}) = S_B(\phi)$, one finds $Z_0 = Z_1$, i.e. a vanishing Witten index and the corresponding SUSY breaking. Here, the vanishing of the Witten index is guaranteed by the fact that to each configuration ϕ there exists another configuration $\tilde{\phi}$ (the parity transformed one) that contributes to the path integral with the same weight, but with opposite sign stemming from the fermion determinant. Furthermore, $Z_0 = Z_1$ means that (in the limit of zero temperature, i.e. $\beta \to \infty$) the free energies of the bosonic and fermionic vacua are equal, and that proves the existence of a massless, fermionic mode connecting the two vacua, i.e. the Goldstino mode.

Turning now to SUSY quantum mechanics on the lattice one obtains with a Wilson type discretisation (cf. next section for further details)

$$\det\left[\nabla^* + P''(\phi)\right]_p = \prod_t \left[1 + P''(\phi_t)\right] - 1\,, \tag{2.2}$$

where t now denotes a discrete lattice site index and ∇^* is the backward derivative. Also in this case one can identify the bosonic and fermionic contributions (i.e. the first and second term of the difference in eq.(2.2)), and we will show below that this separation is always explicit in the fermion loop formulation. As a side remark, let us note that in the limit of zero lattice spacing one finds

$$\lim_{a\to 0}\det\left[\nabla^* + P''\right] \quad\longrightarrow\quad \exp\left(+\int_0^T \frac{P''(\phi)}{2}dt\right)\,\det\left[\partial_t + P''(\phi)\right]\,,$$

where the exponential term can be understood as coming from radiative contributions that need to be corrected by 'fine-tuning' a corresponding counterterm [19, 18]. Reconsidering the two examples for the superpotential mentioned above, we find for P_e with $m > 0$ and $g \geq 0$ that

$$\det\left[\nabla^* + P_e''\right] = \prod_t \left[1 + m + 3g\phi_t^2\right] - 1 > 0\,,$$

while for P_o one finds

$$\det\left[\nabla^* + P_o''\right] = \prod_t \left[1 + 2\lambda\phi_t\right] - 1\,, \tag{2.3}$$

which turns out to be indefinite, even when $\lambda > 0$. While this is necessary in order to enable a vanishing Witten index, it imposes a serious problem on any Monte Carlo simulation, for which positive weights are strictly required. Moreover, the sign problem is severe in the sense that towards the continuum limit (i.e. when the lattice volume goes to infinity), the fluctuations of the first summand in eq.(2.3) around 1 tend to zero, such that $W \to 0$ is exactly realised in that limit. Hence, the source of the fermionic sign problem lies in the exact cancellation of the first and the second summand in eq.(2.3), i.e. of the bosonic and fermionic contribution to the partition function, and this observation also holds more generally in higher dimensions.

In the loop formulation, to be discussed in the next section, the separation of the partition function into the various fermionic and bosonic sectors is made explicit and allows the construction of a simulation algorithm that samples these sectors separately, and more importantly also samples the relative weights between them. In this way, the loop formulation eventually provides a solution to the fermion sign problem.

3. Loop formulation and separation of fermionic and bosonic sectors

In this section we illustrate the loop formulation and the separation of the partition function into its fermionic and bosonic sectors by means of the $\mathscr{N} = 1$ Wess-Zumino model in two dimensions and $\mathscr{N} = 2$ supersymmetric quantum mechanics in one dimension.

3.1 $\mathscr{N} = 1$ Wess-Zumino model in two dimensions

The Lagrangian of the $\mathscr{N} = 1$ Wess-Zumino model in two dimensions is given by

$$\mathscr{L} = \frac{1}{2}\left(\partial_\mu\phi\right)^2 + \frac{1}{2}P'(\phi)^2 + \frac{1}{2}\bar{\psi}\left(\partial\!\!\!/ \; + P''(\phi)\right)\psi\,, \tag{3.1}$$

where ψ is a real, two-component Majorana field, ϕ a real bosonic field and $P(\phi)$ an arbitrary superpotential. Integrating out the fermionic Majorana fields yields a Pfaffian which in general, as discussed above, is not positive definite.

On the lattice, one can use the exact reformulation of the fermionic Majorana degrees of freedom in terms of non-intersecting, self-avoiding loops, in order to separate the contributions of the Pfaffian to the various bosonic and fermionic sectors of the partition function. A similar exact reformulation of the bosonic degrees of freedom in terms of bonds, can also be accomplished [20]. While this is not necessary for the solution of the sign problem, it provides a convenient way to simulate also those degrees of freedom without critical slowing down, and hence we will discuss this construction below.

Employing the Wilson lattice discretisation for the fermionic part of the Lagrangian in eq.(3.1) yields

$$\mathscr{L}_F = \frac{1}{2}\xi^T\mathscr{C}(\gamma_\mu\tilde{\nabla}_\mu - \frac{1}{2}\nabla_\mu^*\nabla_\mu + P''(\phi))\xi\,,$$

where ξ now represents the real, 2-component Grassmann field, while $\mathscr{C} = -\mathscr{C}^T$ is the charge conjugation matrix and $\nabla_\mu^* \nabla_\mu$ the Wilson term. Using the nilpotency of Grassmann elements one can expand the Boltzmann factor leading to

$$\int \mathscr{D}\xi \prod_x \left(1 - \frac{1}{2} M(\phi_x) \xi_x^T \mathscr{C} \xi_x\right) \prod_{x,\mu} \left(1 + \xi_x^T \mathscr{C} \Gamma(\mu) \xi_{x+\hat{\mu}}\right) ,$$

where $M(\phi_x) = 2 + P''(\phi_x)$, $\Gamma(\pm\mu) = \frac{1}{2}(1 \mp \gamma_\mu)$ and x denotes the discrete lattice site index. Performing now the integration over the fermion field, at each site x the fields $\xi_x^T \mathscr{C}$ and ξ_x must be exactly paired in order to give a contribution to the path integral, so one finds

$$\int \mathscr{D}\xi \prod_x \left(-M(\phi_x) \xi_x^T \mathscr{C} \xi_x\right)^{m(x)} \prod_{x,\mu} \left(\xi_x^T \mathscr{C} \Gamma(\mu) \xi_{x+\hat{\mu}}\right)^{b_\mu(x)} ,$$

where the occupation numbers $m(x) = 0, 1$ for the monomer terms and $b_\mu(x) = 0, 1$ for the fermionic bonds (or dimers), satisfy the constraint

$$m(x) + \frac{1}{2} \sum_\mu \left(b_\mu(x) + b_\mu(x - \hat{\mu})\right) = 1 \quad \forall x . \tag{3.2}$$

This constraint is equivalent to the fact that only closed, self-avoiding paths survive the Grassmann integration. When integrating out the fermion fields, the projectors $\Gamma(\mu)$ eventually yield a weight ω, which only depends on the geometric structure of the specific constrained path (CP) configuration $\ell \in \mathscr{L}$. In particular, one has

$$|\omega(\ell)| = 2^{-n_c/2} ,$$

where n_c denotes the number of corners in the loop configuration, while the sign depends on the topology of the loop configuration and will be discussed below.

As mentioned above, the bosonic fields can be treated analogously [20]. On the lattice, the kinetic term $(\partial_\mu \phi)^2$ yields $\phi_x \phi_{x-\hat{\mu}}$, and expanding this hopping term to all orders gives

$$\int \mathscr{D}\phi \prod_{x,\mu} \sum_{n_\mu(x)} \frac{1}{n_\mu(x)!} \left(\phi_x \phi_{x-\hat{\mu}}\right)^{n_\mu(x)} \prod_x \exp\left(-\frac{1}{2} V(\phi_x)\right) M(\phi_x)^{m(x)} \tag{3.3}$$

with bosonic bond occupation numbers $n_\mu(x) = 0, 1, 2, \ldots$ and $V(\phi_x) = 4 + P'(\phi_x)^2$. In contrast to the fermionic case, the exact reformulation requires one to include an infinite number of terms in the hopping expansion, and hence occupation numbers up to infinity, instead of just 0 and 1 as for the fermionic bonds. Integrating out the bosonic fields ϕ_x yields the site weights

$$Q(n_\mu(x), m(x)) = \int d\phi_x \, \exp\left(-\frac{1}{2} V(\phi_x)\right) \phi_x^{N(x)} M(\phi_x)^{m(x)} ,$$

where $N(x) = \sum_\mu \left(n_\mu(x) + n_\mu(x - \hat{\mu})\right)$ counts the number of bosonic bonds attached to a given site, while $M(\phi_x)^{m(x)}$ may contribute additional powers of ϕ_x. So the bosonic contribution to the weight of a given configuration factorises into a product of local weights,

$$W(n_\mu(x), m(x)) = \prod_{x,\mu} \frac{1}{n_\mu(x)!} \prod_x Q(n_\mu(x), m(x)) .$$

In summary, the fermionic and bosonic degrees of freedom in our original partition function are now expressed in terms of fermionic monomers and dimers and bosonic bonds, and the integration over the fields has been replaced by a constrained sum over all allowed monomer-dimer-bond configurations, yielding

$$Z = \sum_{\{\ell\}\in\mathscr{L}} \sum_{\{n_\mu\}\in CP} |W(n_\mu(x), m(x)) \cdot \omega(\ell)| \,.$$

In particular, the partition function for the fermionic degrees of freedom is represented by a sum over all non-oriented, self-avoiding fermion loops

$$Z_{\mathscr{L}} = \sum_{\{\ell\}\in\mathscr{L}} |W(n_\mu(x), m(x)) \cdot \omega(\ell)|, \quad \mathscr{L} \in \mathscr{L}_{00} \cup \mathscr{L}_{10} \cup \mathscr{L}_{01} \cup \mathscr{L}_{11} \,, \tag{3.4}$$

where ℓ represents a fermion loop configuration in one of the four topological classes $\mathscr{L}_{l_1,l_2}$, with $l_1, l_2 = 0,1$ denoting the total number of loop windings (modulo 2) along the first and second direction, respectively, on the periodic lattice torus. ω denotes the weight of the specific loop configuration and depends on the geometry of the loop configuration, as discussed above. The sign of the weight is solely determined by the topological class and the fermionic boundary conditions ε_μ, where $\varepsilon_\mu = 0,1$ stands for periodic and anti-periodic boundary conditions, respectively. Configurations in $\mathscr{L}_{00}$ have positive weights independent of the boundary conditions, while the sign of the weights for configurations in $\mathscr{L}_{01}, \mathscr{L}_{10}$ and $\mathscr{L}_{11}$ is given by $(-1)^{l_\mu \cdot \varepsilon_\mu + 1}$. So the partition function $Z_{\mathscr{L}}$ in eq.(3.4), where all sectors contribute positively, represents a system with unspecified fermionic boundary conditions [21], while a partition function with fermionic b.c. periodic in the spatial and anti-periodic in the temporal direction, respectively, is described by the combination

$$Z_{pa} = Z_{\mathscr{L}_{00}} - Z_{\mathscr{L}_{10}} + Z_{\mathscr{L}_{01}} + Z_{\mathscr{L}_{11}} \,.$$

This combination represents the system at finite temperature. Analogously, the partition function with fermionic b.c. periodic in all directions – the Witten index – is given by

$$Z_{pp} = Z_{\mathscr{L}_{00}} - Z_{\mathscr{L}_{10}} - Z_{\mathscr{L}_{01}} - Z_{\mathscr{L}_{11}} \,.$$

The interpretation of the Witten index in terms of the partition functions $Z_{\mathscr{L}_{ij}}$ is straightforward. Any fermion loop winding non-trivially around the lattice carries fermion number $F = 1$, hence configurations with an odd number of windings, i.e. configurations in $Z_{\mathscr{L}_{10}}, Z_{\mathscr{L}_{01}}$ and $Z_{\mathscr{L}_{11}}$, also carry fermion number $F = 1$, while configurations with no, or an even number of windings, i.e. in $Z_{\mathscr{L}_{00}}$, have $F = 0$. The partition function $Z_{\mathscr{L}_{00}}$ may therefore be interpreted as representing the bosonic vacuum, while the combination $Z_{\mathscr{L}_{10}} + Z_{\mathscr{L}_{01}} + Z_{\mathscr{L}_{11}}$ corresponds to the fermionic vacuum. Consequently, the latter contributes to the Witten index $W \equiv Z_{pp}$ with opposite sign relative to the bosonic vacuum. Since each of the four partition functions is positive, vanishing of the Witten index implies $Z_{\mathscr{L}_{00}} = Z_{\mathscr{L}_{10}} + Z_{\mathscr{L}_{01}} + Z_{\mathscr{L}_{11}}$.

3.2 $\mathscr{N} = 2$ supersymmetric quantum mechanics

The loop formulation for the $\mathscr{N} = 2$ supersymmetric quantum mechanics on the lattice is obtained in a completely analogous manner. Using again the Wilson lattice discretisation for the

fermionic part, the continuum action in eq.(2.1) reads

$$S_L = \sum_x \frac{1}{2}(P'(\phi_x)^2 + 2\phi_x^2) - \phi_x\phi_{x-1} + (1+P''(\phi_x))\bar{\psi}_x\psi_x - \bar{\psi}_x\psi_{x-1}\,,$$

where x now denotes the one-dimensional, discrete lattice site index. Note that in one dimension the fermionic lattice derivative, including the contribution from the Wilson term with Wilson parameter $r=1$, becomes a simple, directed hop $\bar{\psi}_x\psi_{x-1}$ which, in the loop formulation, can be described by the (directed) bond occupation number $b(x)=0,1$. Integrating out the fermionic degrees of freedom yields a constraint for the fermion monomer and bond occupation numbers, analogous to eq.(3.2), namely

$$m(x) + \frac{1}{2}\,(b(x)+b(x-1)) = 1 \quad \forall x.$$

So for $\mathscr{N}=2$ supersymmetric quantum mechanics the loop formulation becomes particularly simple: there are just two different loop configurations, namely a bosonic one, where $m(x)=1, b(x)=0$ for all x, and a fermionic one where $m(x)=0, b(x)=1$ for all x. Since the latter corresponds to a closed fermion loop, it will pick up a minus sign from the Grassmann integration, relative to the bosonic contribution.

On top of the two fermion loop configurations one may treat the bosonic fields in the same way as before and employ a hopping expansion to all orders. After rearranging the bosonic fields the integration can eventually be performed separately at each site and one ends up with the weight

$$W(n(x),m(x)) = \prod_x \frac{1}{n(x)!}\int d\phi_x\ \phi_x^{n(x)+n(x-1)}\ \mathrm{e}^{-\frac{1}{2}V(\phi_x)}(1+P''(\phi_x))^{m(x)} \tag{3.5}$$

for a given bosonic and fermionic bond configuration, with $V(\phi_x) = 2+P'(\phi)^2$. In terms of these weights the partition function can now be written as

$$Z_{\mathscr{L}} = \int \mathscr{D}\phi\mathscr{D}\bar{\psi}\mathscr{D}\psi\ \mathrm{e}^{-S_L} = \sum_{\{\ell\}\in\mathscr{L}}\sum_{\{n\}\in\mathrm{CP}} |W(n(x),m(x))|, \quad \mathscr{L}\in\mathscr{L}_0\cup\mathscr{L}_1\,, \tag{3.6}$$

where the second sum is over all allowed bosonic bond configurations $\{n\}\in\mathrm{CP}$, and ℓ represents one of the two fermion loop configurations in the topological classes $\mathscr{L}_0$ or $\mathscr{L}_1$, respectively. As before, the sign of the weight is solely determined by the topological class and the fermionic boundary condition. If $l=0,1$ denotes the fermion loop winding number and, as before, $\varepsilon=0,1$ the periodic and anti-periodic fermionic boundary condition, respectively, the sign is given by $(-1)^{l\cdot(\varepsilon+1)}$.

Choosing anti-periodic fermionic boundary conditions $\varepsilon=1$ we find

$$Z_a = Z_{\mathscr{L}_0} + Z_{\mathscr{L}_1}\,,$$

which is simply the partition function for the system at finite temperature, while choosing periodic fermionic boundary conditions $\varepsilon=0$ yields

$$Z_p = Z_{\mathscr{L}_0} - Z_{\mathscr{L}_1}$$

representing the Witten index. Here, the interpretation is particularly intuitive: the two fermion loop configurations simply represent the bosonic and fermionic vacuum, while $Z_{\mathscr{L}_0}$ and $Z_{\mathscr{L}_1}$ represent the bosonic and fermionic partition function in the corresponding sectors. The Witten index

vanishes whenever $Z_{\mathscr{L}_0} = Z_{\mathscr{L}_1}$, i.e. when the contributions from the bosonic and fermionic sectors cancel. In this case, the free energy of the bosonic and fermionic vacuum is equal, and this is equivalent to saying that there exists a gapless, fermionic excitation which oscillates between the two vacua, i.e. the Goldstino mode.

4. Solution of the fermion sign problem

In this section we briefly describe the simulation algorithm and explain how it eventually solves the fermion sign problem. The loop system can most efficiently be simulated by enlarging the configuration space by open strings. Following [20] the bosonic bonds are updated by inserting two bosonic sources, which sample directly the bosonic 2-point correlation function. Similarly, the fermion bonds are most efficiently updated by simulating a fermionic string [14] that samples the configuration space of the fermionic 2-point correlation function, instead of the standard configuration space of loops.

For the $\mathscr{N} = 1$ Wess-Zumino model in two dimensions, where the fermionic degrees of freedom are Majorana, the open fermionic string is non-oriented and corresponds to the insertion of a Majorana fermion pair $\{\xi_x^T \mathscr{C}, \xi_y\}$ at position x and y, while for $\mathscr{N} = 2$ supersymmetric quantum mechanics, where the fermionic degrees of freedom are Dirac, the string is oriented and corresponds to the insertion of a Dirac fermion pair $\{\bar{\psi}_x, \psi_y\}$.

The algorithm proceeds by locally updating the endpoints of the open fermionic string using a simple Metropolis or heat bath step according to the weights of the corresponding 2-point function (cf. [14] for details). When one end is shifted from, say, x to one of its neighbouring sites y, a fermionic dimer on the corresponding bond is destroyed or created depending on whether the bond is occupied or not. Contact with the partition functions $Z_{\mathscr{L}_{ij}}$ and $Z_{\mathscr{L}_i}$, respectively, is made each time the open string closes. This then provides the proper normalisation for the expectation value of the 2-point function.

The solution of the fermion sign problem discussed above relies on the correct determination of the relative weights between the bosonic and fermionic sectors, and the simulation algorithm described in [14] achieves this in a most efficient way. The open fermionic string tunnels between loop configurations in the various topological homotopy classes $\mathscr{L}_{00}, \mathscr{L}_{10}, \mathscr{L}_{01}, \mathscr{L}_{11}$ in two, and $\mathscr{L}_0, \mathscr{L}_1$ in one dimension, thereby determining the relative weights between the partition functions $Z_{\mathscr{L}_{00}}, Z_{\mathscr{L}_{10}}, Z_{\mathscr{L}_{01}}, Z_{\mathscr{L}_{11}}$, or $Z_{\mathscr{L}_0}, Z_{\mathscr{L}_1}$, respectively. From the relative weights, the Witten index (or any other partition function of interest) can be reconstructed a posteriori.

Let us emphasise that the open string algorithm and the corresponding absence of critical slowing down at the critical point as reported in [14] is crucial for the solution of the sign problem. Since the algorithm updates the configurations according to the fermionic 2-point correlation function, they are updated equally well on all length scales up to a scale of the order of the largest fermionic correlation length. This is in fact the reason why critical slowing down is essentially absent even at a critical point when the correlation length becomes infinite. Now, in order to have $W = 0$ in the continuum ($L \to \infty$) the Goldstino mode has to become massless. Since the algorithm ensures an efficient update of that mode, the tunneling between the bosonic and fermionic vacua is guaranteed and the Witten index indeed vanishes in practice.

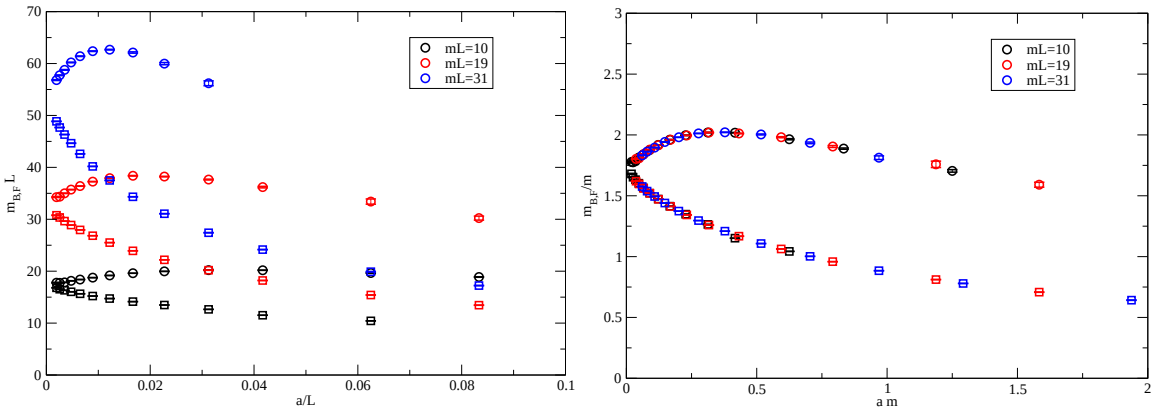

Figure 1: Spectrum for the perturbatively improved standard discretisation at $g/m^2 = 1.0$. In the left plot the excitation energies m_B (circles) and m_F (squares) and the lattice spacing are expressed in units of the lattice extent L, while in the right plot they are expressed in units of the bare mass parameter m.

5. Results for $\mathcal{N} = 2$ supersymmetric quantum mechanics

We are now ready to present some results for the spectrum and the Witten index for the case of $\mathcal{N} = 2$ supersymmetric quantum mechanics.

5.1 Spectrum for the perturbatively improved standard discretisation

Here we present our results for the spectrum using the standard discretisation including a counterterm. As discussed in [19], for the standard discretisation described above, the correct continuum limit is spoiled by radiative corrections[3]. This can be corrected by adding a counterterm of the form $\frac{1}{2}\sum_x P'(\phi_x)$ [19]. By doing so, one ensures that all observables reach the correct continuum limit and that the full supersymmetry is eventually restored.

As an example we consider a superpotential with unbroken supersymmetry, i.e. $P_e(\phi) = \frac{1}{2}m\phi^2 + \frac{1}{4}g\phi^4$, and choose the coupling $g/m^2 = 1.0$. The results are presented in figure 1 where we show the lowest lying excitation energies for the boson (circles) and the fermion (squares) as a function of the lattice spacing a for various values of fixed mL. In the left plot, the quantities are expressed in units of the lattice extent L, while in the right plot, they are expressed in units of the bare mass parameter m in order to illustrate the common scaling behaviour. The leading lattice artifacts turn out to be $\mathcal{O}(a)$ for both the fermion and boson masses. At finite lattice spacing the supersymmetry is explicitly broken by the discretisation, and hence the boson and fermion masses are not degenerate. In the continuum limit, however, the supersymmetry is restored and the masses become degenerate.

5.2 Spectrum for the Q-exact discretisation

As briefly discussed in the introduction, for models with extended supersymmetry it is sometimes possible to preserve some of the supersymmetries exactly at finite lattice spacing [22]. The so-called Q-exact discretisations preserve a suitable sub-algebra of the full supersymmetry algebra,

[3]Note, however, that in one dimension these corrections are finite.

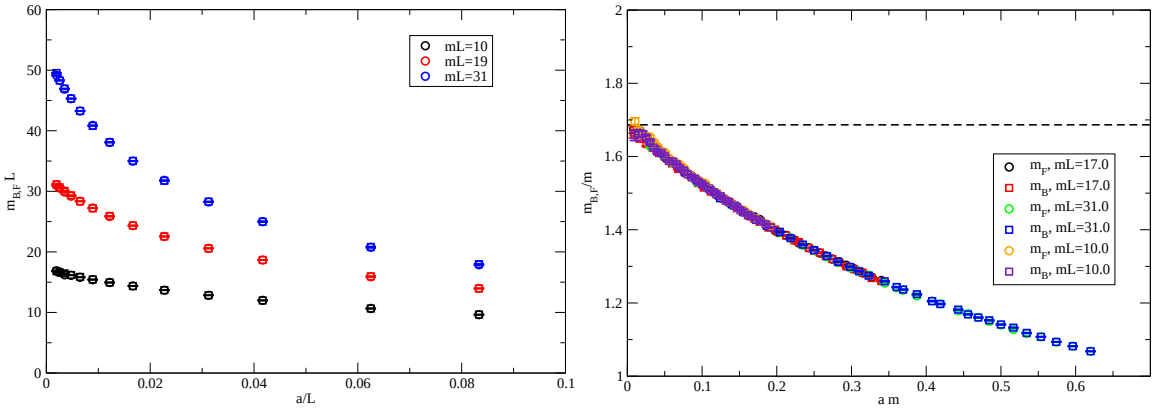

Figure 2: Spectrum for the Q-exact discretisation at $g/m^2 = 1.0$. In the left plot the excitation energies m_B (circles) and m_F (squares) and the lattice spacing are expressed in units of the lattice extent L, while in the right plot they are expressed in units of the bare mass parameter m. The dashed line denotes the exact value obtained with Numerov's method.

i.e. a linear combination of the available supersymmetries. In the context of $\mathcal{N} = 2$ supersymmetric quantum mechanics the Q-exact action is obtained from the standard action by adding, e.g., the term $\sum_x P'(\phi_x)\nabla^*\phi_x$, but other forms are also possible [23, 18]. Since the term contains a derivative, there are additional hopping terms that need to be considered in the hopping expansion [24].

In the following we concentrate again on the superpotential P_e with unbroken supersymmetry. Using the Q-exact discretisation one expects degenerate fermion and boson masses even at finite lattice spacing [22] and this is beautifully confirmed by our results at $g/m^2 = 1.0$ presented in figure 2. Note that the leading lattice artifacts are again $\mathcal{O}(a)$ for both the fermion and boson masses.

Finally, in the right plot we show the results of a high precision simulation that serves the purpose of checking the correctness of the new simulation algorithm, as well as our procedures for the extraction of the fermion and boson masses. Indeed, we can confirm the mass degeneracy to a precision better than a few per mill at all lattice spacings, and the continuum value of the mass gap agrees with the exact result in the continuum obtained with Numerov's method (dashed line) also within a few per mill. Due to the loop formulation and the efficiency of the new simulation algorithm, these results can be obtained with a very modest computational effort.

5.3 Witten index

Let us turn to the Witten index $W \propto Z_p/Z_a$, i.e. the partition function with periodic boundary conditions Z_p, normalised to the finite temperature partition function Z_a. We start with the superpotential $P_e(\phi) = \frac{1}{2}m\phi^2 + \frac{1}{4}g\phi^4$ for which supersymmetry is unbroken and $W \neq 0$. The results are presented in figure 3, where we show Z_p/Z_a in the left plot as a function of the bare mass parameter am for the coupling $g/m^2 = 1.0$ using the Q-exact discretisation. The continuum limit is reached as $am \to 0$, and we indeed find that $Z_p/Z_a \to 1$, i.e. $W \neq 0$ in that limit on a sufficiently large lattice. The fact that at fixed lattice extent L the partition function ratio goes to zero with $am \to 0$ can be interpreted as a 'finite size', or rather finite temperature effect, since the temperature T is inversely proportional to the extent of the lattice L. So if we plot the data as a function of $m/T = mL$, $mL = 0$ corresponds to infinitely high temperature, while the limit $mL \to \infty$ corresponds to $T \to 0$. This is

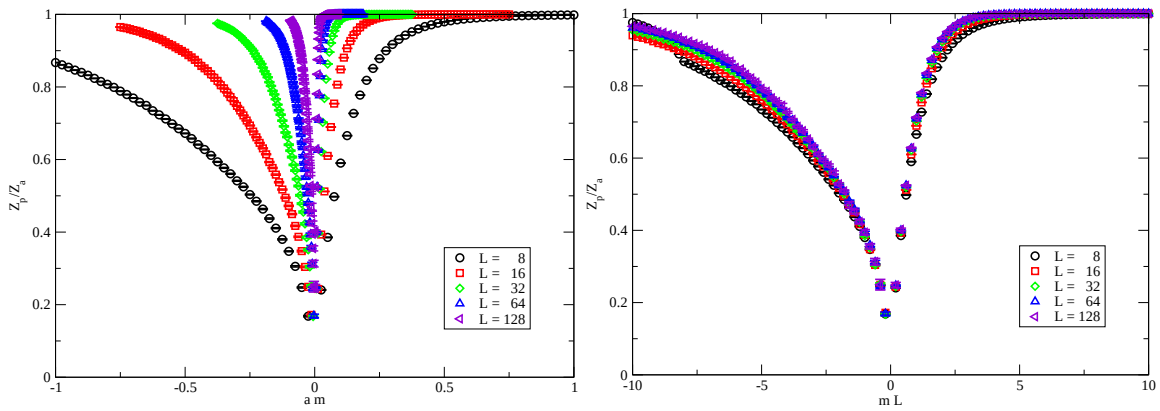

Figure 3: Simulation results for the Witten index $W \propto Z_p/Z_a$ as a function of the bare mass parameter am (left plot), and as a function of the inverse temperature mL (right plot), for a system with *unbroken* supersymmetry using the Q-exact discretisation at $g/m^2 = 1.0$.

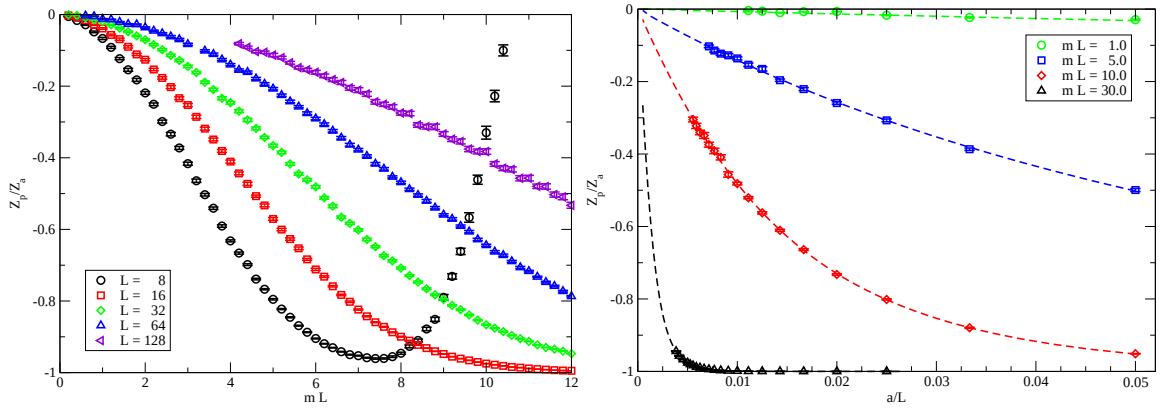

Figure 4: Simulation results for the Witten index $W \propto Z_p/Z_a$ as a function of the inverse temperature mL (left plot), and as a function of the lattice spacing a/L at fixed temperature (right plot), for a system with *broken* supersymmetry using the standard, perturbatively improved discretisation at $\lambda^2/m^3 = 1.0$.

illustrated in the right plot of figure 3, from where we find $Z_p/Z_a \to 1$ in the continuum limit for temperatures $mL \gtrsim 5$. The data shows a rather good scaling behaviour towards the continuum limit ($L \to \infty$ at fixed mL). In the continuum, the value $Z_p/Z_a = 1$ is approached exponentially fast with mL, i.e. towards zero temperature $mL \to \infty$.

Note that with the formulation and algorithm presented here, it is also possible to simulate at negative bare mass $m < 0$. In this case, we still find $Z_p/Z_a \to 1$ in the continuum limit towards zero temperature, albeit at a slower rate.

When repeating this exercise for the superpotential $P_o(\phi) = -\frac{m^2}{4\lambda}\phi + \frac{1}{3}\lambda\phi^3$, for which supersymmetry is broken, we should expect a vanishing Witten index. Our results for this case are presented in figure 4, where we show the Witten index $W \propto Z_p/Z_a$ as a function of mL in the left plot, and as a function of the lattice spacing a/L at fixed values of mL in the right plot using the standard, perturbatively improved discretisation at $\lambda^2/m^3 = 1.0$. In this case we find that while the Witten index $W \propto Z_p/Z_a$ approaches zero at 'infinite temperature' $mL \to 0$ as in the unbroken case, it also does so at any value of mL in the continuum limit, even though for large values of mL the

scaling towards the continuum limit is reached only at very fine lattice spacings. In fact, for large mL the approach $W \to 0$ is exponentially slow in the lattice spacing. This is exemplified in the right plot of figure 4, where the dashed lines are the results of an analytic calculation which will be reported elsewhere [24]. The absence of critical slowing down for our update algorithm guarantees that reliable results can be obtained despite the exponentially slow approach to the continuum.

6. Summary and outlook

We have discussed the occurrence of a fermion sign problem in the context of spontaneous supersymmetry breaking on the lattice and its relevance for the vanishing of the Witten index, regulated as a path integral on the lattice. We then argued that with the help of the fermion loop expansion one can achieve an explicit separation of the bosonic and fermionic contributions to the path integral in such a way that the source of the sign problem, namely the cancellation between the bosonic and fermionic contributions to the partition function with periodic boundary conditions, is isolated. The solution of the fermion sign problem is then achieved by devising an algorithm which separately samples the bosonic and fermionic contributions to the partition functions and, in addition, also samples the relative weights between them, essentially without any critical slowing down. In such a way one is able to calculate the Witten index on the lattice without suffering from the fermion sign problem even when the index vanishes. The absence of critical slowing down is essentially due to the fact that the algorithm directly samples the massless Goldstino mode which mediates the tunnelings between the bosonic and fermionic vacua.

As examples we described in some detail the exact reformulation of the lattice path integral in terms of fermionic bonds and monomers, and bosonic bonds for the $\mathscr{N} = 1$ supersymmetric Wess-Zumino model in 2 dimensions and $\mathscr{N} = 2$ supersymmetric quantum mechanics. For the latter we presented some results from lattice simulations. For a superpotential with unbroken supersymmetry, we calculate the energy gap of the lowest bosonic and fermionic excitation using both the standard discretisation with a fine-tuned counterterm, as well as a Q-exact discretisation which preserves a linear combination of the two supersymmetries. In the latter case the boson and fermion spectra are degenerate even at finite lattice spacing, while in the former case they become degenerate only in the continuum limit. Finally, we also present lattice calculations of the Witten index for broken and unbroken supersymmetry using the standard discretisation with a counterterm. For both cases we are able to reproduce the correct Witten index in the continuum limit. For broken supersymmetry the approach to the continuum limit is exponentially slow in the lattice spacing. Using the loop formulation and the fermion worm algorithm [14] the exponentially slow approach as well as the sign problem is no obstacle in practice.

Obviously, the approach presented here is particularly interesting for the $\mathscr{N} = 1$ supersymmetric Wess-Zumino model in 2 dimensions, where so far simulations on the lattice have suffered from the fermion sign problem [10]. Work in this direction is in progress.

References

[1] M. F. L. Golterman and D. N. Petcher, *Nucl. Phys.* **B319** (1989) 307–341.

[2] S. Catterall, *PoS* **LATTICE2010** (2010) 002, [arXiv:1010.6224].

[3] I. Kanamori, H. Suzuki, and F. Sugino, *Phys. Rev.* **D77** (2008) 091502, [arXiv:0711.2099].

[4] I. Kanamori, *Nucl. Phys.* **B841** (2010) 426–447, [arXiv:1006.2468].

[5] I. Kanamori, *PoS* **LATTICE2010** (2010) 254, [arXiv:1011.0940].

[6] S. Catterall and T. Wiseman, *JHEP* **12** (2007) 104, [arXiv:0706.3518].

[7] K. N. Anagnostopoulos, M. Hanada, J. Nishimura, and S. Takeuchi, *Phys. Rev. Lett.* **100** (2008) 021601, [arXiv:0707.4454].

[8] M. Hanada, A. Miwa, J. Nishimura, and S. Takeuchi, *Phys. Rev. Lett.* **102** (2009) 181602, [arXiv:0811.2081].

[9] M. Hanada, arXiv:1011.1284.

[10] S. Catterall and S. Karamov, *Phys. Rev.* **D68** (2003) 014503, [hep-lat/0305002].

[11] J. Giedt, *Nucl. Phys.* **B668** (2003) 138–150, [hep-lat/0304006].

[12] I. Kanamori and H. Suzuki, *Nucl. Phys.* **B811** (2009) 420–437, [arXiv:0809.2856].

[13] M. Hanada and I. Kanamori, *JHEP* **01** (2011) 058, [arXiv:1010.2948].

[14] U. Wenger, *Phys. Rev.* **D80** (2009) 071503, [arXiv:0812.3565].

[15] U. Wenger, *PoS* **LAT2009** (2009) 022, [arXiv:0911.4099].

[16] E. Witten, *Nucl. Phys.* **B202** (1982) 253.

[17] F. Cooper, A. Khare, and U. Sukhatme, *Phys. Rept.* **251** (1995) 267–385, [hep-th/9405029].

[18] G. Bergner, T. Kaestner, S. Uhlmann, and A. Wipf, *Annals Phys.* **323** (2008) 946–988, [arXiv:0705.2212].

[19] J. Giedt, R. Koniuk, E. Poppitz, and T. Yavin, *JHEP* **12** (2004) 033, [hep-lat/0410041].

[20] N. Prokof'ev and B. Svistunov, *Phys. Rev. Lett.* **87** (2001) 160601.

[21] U. Wolff, *Nucl. Phys.* **B789** (2008) 258–276, [arXiv:0707.2872].

[22] S. Catterall and E. Gregory, *Phys. Lett.* **B487** (2000) 349–356, [hep-lat/0006013].

[23] S. Catterall, *Nucl. Phys. Proc. Suppl.* **129** (2004) 871–873, [hep-lat/0309040].

[24] D. Baumgartner and U. Wenger, *in progress*.

Paper 5

Exact results for supersymmetric quantum mechanics on the lattice

David Baumgartner and Urs Wenger, Proceedings of Science (Lattice 2011) 239.

PROCEEDINGS OF SCIENCE

Exact results for supersymmetric quantum mechanics on the lattice

David Baumgartner* **and Urs Wenger**
Albert Einstein Center for Fundamental Physics
Institute for Theoretical Physics
University of Bern
Sidlerstrasse 5
CH-3012 Bern
Switzerland
E-mail: baumgart@itp.unibe.ch, wenger@itp.unibe.ch

We discuss $\mathcal{N} = 2$ supersymmetric quantum mechanics on the lattice using the fermion loop formulation. In this approach the system naturally decomposes into a bosonic and fermionic sector. This allows us to deal with the sign problem arising in the context of broken supersymmetry due to the vanishing of the Witten index. Employing transfer matrix techniques we obtain exact results at finite lattice spacing and are hence able to study how the continuum limit is approached. In particular, we determine how supersymmetry is restored and how, in the case of broken supersymmetry, the goldstino mode emerges.

The XXIX International Symposium on Lattice Field Theory
July 11-16, 2011
Squaw Valley, California, USA

*Speaker.

 http://pos.sissa.it/

PoS(Lattice 2011)239

1. Introduction

Calculating nonperturbative properties of supersymmetric theories on the lattice encounters various difficulties related to the fact that the discretisation of space-time explicitly breaks supersymmetry and violates Leibniz' rule. Moreover, the vanishing of the Witten index in the context of spontaneous supersymmetry breaking leads to a fermion sign problem which makes straightforward numerical simulations impossible. While the restoration of supersymmetry can sometimes be achieved in the continuum limit of the lattice theory, e.g. by fine tuning or by constructing Q-exact discretisations [1], a solution to the sign problem is not easy to find. A possible way out has been proposed in [2, 3, 4]. It is based on the fermion loop formulation which can be simulated without critical slowing down even when a massless goldstino mode is present.

In this work, we apply the fermion loop formulation to $\mathscr{N} = 2$ supersymmetric quantum mechanics for superpotentials yielding broken or unbroken supersymmetry. Using transfer matrix techniques we are able to obtain exact results for partition functions and various observables at finite lattice spacing. We investigate how the supersymmetric spectrum is recovered in the continuum limit and how the goldstino mode emerges in the case of broken supersymmetry. In these proceedings we confine ourselves to the presentation of results obtained using a Wilson type discretisation together with the appropriate fine tuning of counterterms, although results using a Q-exact discretisation have been derived as well.

2. Supersymmetric quantum mechanics on the lattice

The continuum action of $\mathscr{N} = 2$ supersymmetric quantum mechanics can be written as

$$S = \int dt \left[\frac{1}{2} \left(\frac{d\phi(t)}{dt} \right)^2 + \frac{1}{2} P'(\phi(t))^2 + \overline{\psi}(t) \left(\frac{d}{dt} + P''(\phi(t)) \right) \psi(t) \right] \tag{2.1}$$

with one real bosonic coordinate ϕ, two anticommuting fermionic coordinates $\overline{\psi}$ and ψ, and a generic superpotential $P(\phi)$. The derivative of the superpotential $P'(\phi)$ is taken with respect to ϕ, $P'(\phi) \doteq \frac{\partial P(\phi)}{\partial \phi}$. For periodic boundary conditions (*PBC*) the action is invariant under two supersymmetry transformations $\delta_{1,2}$:

$$\begin{aligned} \delta_1 \phi &= \psi \overline{\varepsilon}, & \delta_2 \phi &= \overline{\psi} \varepsilon, \\ \delta_1 \psi &= 0, & \delta_2 \psi &= (\tfrac{d\phi}{dt} - P') \varepsilon, \\ \delta_1 \overline{\psi} &= (\tfrac{d\phi}{dt} + P') \overline{\varepsilon}, & \delta_2 \overline{\psi} &= 0, \end{aligned}$$

with two Grassmann valued parameters ε and $\overline{\varepsilon}$. Note that for supersymmetric quantum mechanics it is the form of the superpotential $P(\phi)$ which determines the supersymmetry breaking pattern. If the highest power of $P(\phi)$ is even (odd), supersymmetry is unbroken (broken). A main feature of supersymmetry is the degeneracy between the energy levels in the bosonic and the fermionic sector. For unbroken supersymmetry, however, there is one single unpaired energy level at zero energy, i.e., a unique ground state, either in the bosonic or in the fermionic sector. This is in contrast to the case of broken supersymmetry, where the lowest energy levels in both sectors are degenerate and lifted above zero. In addition, there is a zero energy goldstino mode which mediates between the two degenerate ground states.

The supersymmetry breaking pattern can also be partly infered from the Witten index. It is formally defined as

$$W \equiv \lim_{\beta\to\infty} \mathrm{Tr}\left[(-1)^F \exp(-\beta H)\right],$$

where F denotes the fermion number operator and H is the Hamiltonian of the system. Essentially, W counts the difference between the number of bosonic and fermionic zero energy states and its vanishing provides a neccessary but not sufficient condition for supersymmetry breaking. W can also be written more explicitely as

$$W = \lim_{\beta\to\infty} [\mathrm{Tr}_b \exp(-\beta H) - \mathrm{Tr}_f \exp(-\beta H)] = \lim_{\beta\to\infty} [Z_0 - Z_1] = \lim_{\beta\to\infty} Z_{PBC}\,, \tag{2.2}$$

where $\mathrm{Tr}_{b,f}$ denote the traces over the bosonic and fermionic states. $Z_{0,1}$ are the partition functions in the $F = 0,1$ sectors and Z_{PBC} is the one with periodic boundary conditions. In the language of field theory, the latter can be calculated via

$$Z_{PBC} = \int \mathscr{D}\phi \mathscr{D}\overline{\psi}\mathscr{D}\psi \exp(-S) = \int_{-\infty}^{\infty} \mathscr{D}\phi \det D(\phi) \exp(-S_\phi).$$

In the last step, the fermions have been integrated out yielding the fermion matrix determinant $\det D$ and the bosonic part of the action S_ϕ. In this representation, the origin of a fermion sign problem becomes evident when supersymmetry is broken: a vanishing Witten index requires the determinant $\det D$ to be indefinite.

2.1 Lattice formulation

For the construction of a lattice version of the model, we follow Golterman and Petcher [5] and employ the same lattice derivative for the bosons as for the fermions. To avoid fermion doublers, we use the Wilson lattice derivative with Wilson parameter $r = 1$. In one dimension this simplifies to the backward derivative $(\Delta^- f)_x = f_x - f_{x-1}$ and the discretised action explicitly reads

$$S_L = \sum_x \left[\frac{1}{2}(P'(\phi_x)^2 + 2\phi_x^2) - \phi_x\phi_{x-1} + (1 + P''(\phi_x))\overline{\psi}_x\psi_x - \overline{\psi}_x\psi_{x-1}\right]. \tag{2.3}$$

Due to radiative corrections the lattice theory is, however, not guaranteed to yield a supersymmetric theory in the continuum limit. The corrections can be accounted for either by adding a suitable counterterm $\frac{1}{2}\sum P''$ to the action [5, 6], which restores the supersymmetries in the continuum limit, or by adding the surface term $\sum P'(\Delta^-\phi)$ [7, 8, 9] resulting in a Q-exact action. The latter construction preserves a particular combination of the supersymmetries $\delta_{1,2}$ exactly even at finite lattice spacing and hence guarantees the correct continuum limit without any fine tuning.

To circumvent the sign problem discussed above, we make use of the fermion loop formulation [2, 3, 4]. The basic idea here is to exactly rewrite the exponential of the fermion degrees of freedom as a power series to all orders. Upon integration of the fermion fields, the nilpotency of the Grassman variables yields a constraint on the oriented fermionic bond occupation numbers $n_x^f = 0,1$ between the sites x and $x-1$ related to the fermion hopping term $\overline{\psi}_x\psi_{x-1}$, and on the monomer occupation numbers $m_x^f = 0,1$ stemming from the term $(1 + P''(\phi_x))\overline{\psi}_x\psi_x$. The constraint is given by

$$m_x^f + \frac{1}{2}(n_x^f + n_{x+1}^f) = 1 \quad \forall x,$$

and allows only two fermion configurations: $\{m_x^f = 1, n_x^f = 0, \forall x\}$ with fermion number $F = 0$, and $\{m_x^f = 0, n_x^f = 1, \forall x\}$ with fermion number $F = 1$. For PBC the latter receives an additional minus sign relative to the former due to the fermion loop. As a consequence, the partition function naturally decomposes into a bosonic and fermionic contribution Z_0 and Z_1, in accordance with eq.(2.2). It is this decomposition which eventually allows to take care of the fermion sign problem.

In addition to the fermion bonds and monomers we also introduce non-oriented bonds for the bosonic degrees of freedom, with the corresponding bosonic bond occupation numbers $n_x^b \in \mathbb{N}^0$ [4]. Depending on the symmetries of the action, these bosonic bond configurations may obey certain constraints. By summing over these constrained configurations $\{n_x^b\}$ we obtain the locally factorised partition functions with fixed fermion number $F = 0, 1$,

$$Z_F = \sum_{\{n_x^b\}} \prod_x \frac{1}{n_x^b!} Q_F(N_x)$$

where the local weights Q_F are defined as

$$Q_F(N) = \int d\phi \; \phi^N \mathrm{e}^{-\frac{1}{2}(P'(\phi)^2 + 2\phi^2)} (1 + P''(\phi))^{1-F}$$

with the bosonic site occupation number $N_x = n_x^b + n_{x+1}^b$. The Q-exact discretisation requires additional types of bosonic bonds, but still leads to a locally factorised partition function.

2.2 Transfer matrix

The dimensionality of the system allows a further reformulation in terms of a transfer matrix between states defined on the dual lattice. Each state is characterised by the fermion bond occupation number number n^f and the boson bond occupation number n^b, i.e. $|n^f, n^b\rangle$. Since the fermion number is conserved the transfer matrix has a block structure consisting of the two matrices $T^{F=0,1}_{m^b,n^b}$ which take the system from state $|F, n^b\rangle$ to $|F, m^b\rangle$. To be specific, the transfer matrix elements are given by

$$T^F_{m^b,n^b} = \frac{1}{\sqrt{m^b!}} \frac{1}{\sqrt{n^b!}} Q_F(m^b + n^b) \,.$$

In order to keep the size of the matrices finite, we introduce a cutoff on the maximal bosonic bond occupation number. Keeping it of the order $\mathcal{O}(10^2)$ turns out to be sufficient to render all results independent of the cutoff.

In terms of these transfer matrices, the partition function for a system with L_t lattice sites is calculated in each sector F according to

$$Z_F = \mathrm{Tr}[(T^F)^{L_t}].$$

These partition functions can then be combined to $Z_{PBC} = Z_0 - Z_1$ and $Z_{aPBC} = Z_0 + Z_1$ for *PBC* and antiperiodic boundary conditions (*aPBC*), respectively. The construction via the transfer matrices allows the straightforward calculation of various observables, such as correlation functions, Ward identities and mass gaps. The latter are directly associated with the eigenvalues of the transfer matrices. If we denote the eigenvalues of T^F by $\lambda_0^F > \lambda_1^F > \ldots$, the k-th bosonic mass gap in the sector F can be calculated as

$$m_b^{F,k} = -L_t \cdot \log\left(\lambda_k^F / \lambda_0^F\right), \quad k = 1, 2, \ldots,$$

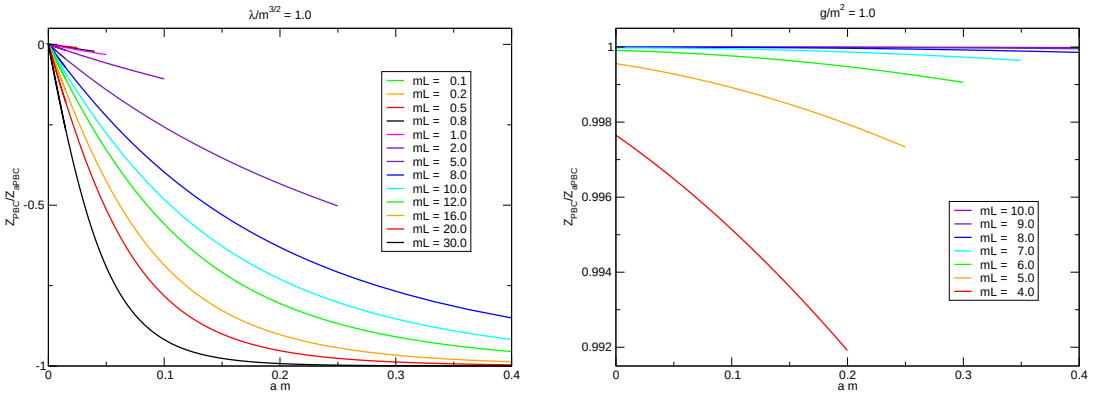

Figure 1: The Witten index $W = Z_{PBC}/Z_{aPBC}$ versus the lattice spacing for broken (left plot) and unbroken supersymmetry (right plot) at various values of the inverse temperature mL. The continuum limit corresponds to $am \to 0$.

whereas the k-th fermionic energy gap is given by

$$m_f^{F,k} = -L_t \cdot \log\left(\lambda_k^{1-F}/\lambda_0^F\right), \quad k = 0,1,\ldots.$$

The transfer matrix approach can, of course, be generalised straightforwardly to any kind of discretisation of the action eq.(2.1), in particular also to the Q-exact discretisation.

3. Results

We now present the results for the action (2.3) with the counterterm using the techniques introduced above. For our calculations, we use the superpotential $P_u(\phi) = \frac{1}{2}m\phi^2 + \frac{1}{4}g\phi^4$ as an example with unbroken supersymmetry and $P_b(\phi) = -\frac{m^2}{4\lambda}\phi + \frac{1}{3}\lambda\phi^3$ as an example for which the supersymmetry is broken. The calculations are performed at coupling strengths $g/m^2 = 1.0$ and $\lambda/m^{3/2} = 1.0$, respectively, thus we are clearly in a regime where perturbation theory is not applicable. For a system with aPBC for the fermion the temporal extent of the lattice is inversely related to the temperature T of the system, such that $mL \to \infty$ corresponds to the zero temperature limit. Finally, the continuum limit is reached by taking $L_t \to \infty$.

3.1 Witten index

The Witten index is determined by the quantity $Z_{PBC}/Z_{aPBC} = (Z_0 - Z_1)/(Z_0 + Z_1)$. It measures the relative weight between the bosonic and fermionic sectors Z_0 and Z_1, respectively. In the system with broken supersymmetry both ground states are equally favourable, yielding $Z_{PBC}/Z_{aPBC} = 0$ in the zero temperature limit. Of course, the degeneracy between the two ground states is broken at finite lattice spacing, so one expects a Witten index $W = \pm 1$ in the limit $T \to 0$ at fixed a. It turns out that for our choice of parameters, the fermionic ground state has a slightly lower energy at finite a leading to $W = -1$ in the $T \to 0$ limit, *cf.* left plot in figure 1. This is true for any finite a, so the order of the limits $\lim_{T\to 0}\lim_{a\to 0}$ is crucial to obtain $W = 0$. Note also that for $T \gg 1$ the

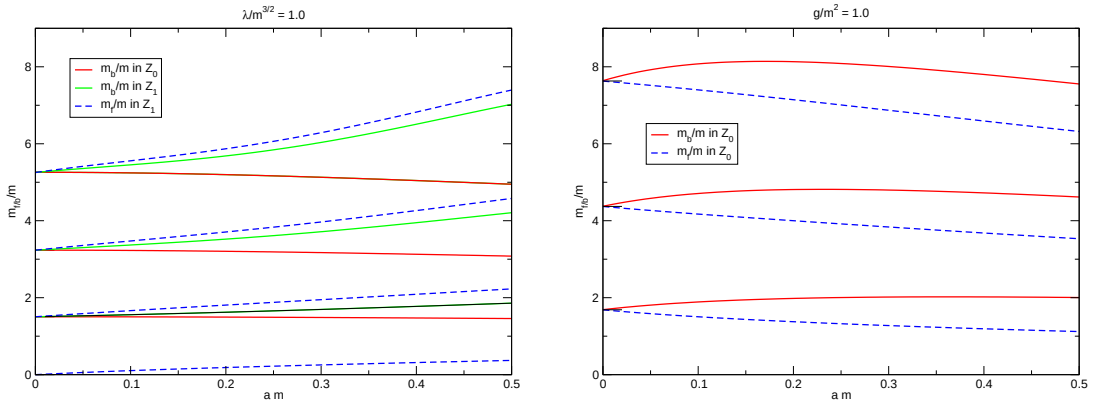

Figure 2: Bosonic and fermionic mass gaps m_b and m_f versus the lattice spacing a, all expressed in units of the bare mass m. Results for broken and unbroken supersymmetry are displayed in the left and right panel, respectively. Note that for broken supersymmetry the zero energy Goldstino mode emerges in the continuum limit.

Witten index tends to zero at any finite a, in accordance with the counting of the states in eq.(2.2) at finite temperature.

In the situation with unbroken supersymmetry the system is forced to occupy the single unique ground state in the zero temperature limit, yielding $Z_{PBC}/Z_{aPBC} = +1$ or -1. Note that for our specific choice of parameters the ground state is bosonic, hence $W = +1$. However, while one finds that the index is pushed away from 0 for $T \gg 1$ as before, in the limit $T \to 0$ it will always go to 1 at any finite a, *cf.* right plot in figure 1. So it turns out that for unbroken symmetry, the order of the two limits $\lim_{T\to 0}$ and $\lim_{a\to 0}$ is not relevant.

3.2 Mass gaps

It is also interesting to study how the energy or mass gaps approach the continuum limit. In figure 2 we show the results for the lowest few masses as a function of the lattice spacing a, everything expressed in units of the bare mass m, for broken (left plot) and for unbroken supersymmetry (right plot). Since we extract the mass gaps from the eigenvalues of the transfer matrices, the results are obtained directly in the limit $T \to 0$. As a consequence, for broken supersymmetry, where there are two degenerate ground states in the continuum, it makes sense to calculate bosonic excitations m_b both in the $F = 0$ and $F = 1$ sector. The plots illustrate nicely how the supersymmetry in the spectrum, i.e. the degeneracies between the bosonic and fermionic excitations, are restored in the continuum limit. Furthermore, when the supersymmetry is broken one expects a zero energy fermionic excitation, the goldstino mode, which is responsible for the fact that $Z_{PBC} = 0$. From the plot it becomes clear how the lattice acts as a regulator for the goldstino mode and, as a consequence, also for the vanishing Witten index W, hence allowing to give meaning to (finite) observables even in the system with PBC. Finally, we make the observation that the leading lattice artefacts of the spectral mass gaps are all $\mathcal{O}(a)$ except for m_b in the $F = 0$ sector when the supersymmetry is broken. In that case they are $\mathcal{O}(a^2)$.

4. Conclusions

We have presented exact results for $\mathcal{N} = 2$ supersymmetric quantum mechanics on the lattice using the fermion loop formulation and corresponding transfer matrices. With these techniques we are able to study in detail how the supersymmetric spectrum is recovered in the continuum limit and how the Witten index is regularised on the lattice.

In the loop formulation the partition function naturally separates into bosonic and fermionic contributions and this is crucial for containing the fermion sign problem in supersymmetric systems with broken supersymmetry. The transitions between the bosonic and fermionic sectors are controlled by the (would-be) goldstino mode which becomes massless only in the continuum limit. Since massless fermion modes can be efficiently simulated with the fermion loop algorithm proposed in [2, 3] our approach provides a way to circumvent the sign problem. Indeed, results from Monte Carlo simulations of $\mathcal{N} = 2$ supersymmetric quantum mechanics have already been presented in [4] and in this work we have provided the corresponding exact results using transfer matrices.

It is also interesting to apply our approach to higher dimensions where it allows to investigate the spontaneous breaking of supersymmetry nonperturbatively and from first principles. In particular, the approach can be applied to supersymmetric Wess-Zumino models [4] in $d = 2$ dimensions and first results from simulations of the $\mathcal{N} = 1$ model including one Majorana fermion and one scalar field have been presented at this conference [10].

References

[1] S. Catterall, *Twisted lattice supersymmetry and applications to AdS/CFT*, *PoS* **LATTICE2010** (2010) 002, [arXiv:1010.6224].

[2] U. Wenger, *Efficient simulation of relativistic fermions via vertex models*, *Phys. Rev.* **D80** (2009) 071503, [arXiv:0812.3565].

[3] U. Wenger, *Simulating Wilson fermions without critical slowing down*, *PoS* **LAT2009** (2009) 022, [arXiv:0911.4099].

[4] D. Baumgartner and U. Wenger, *Simulation of supersymmetric models on the lattice without a sign problem*, *PoS* **LATTICE2010** (2010) 245, [arXiv:1104.0213].

[5] M. F. L. Golterman and D. N. Petcher, *A local interactive lattice model with supersymmetry*, *Nucl. Phys.* **B319** (1989) 307–341.

[6] J. Giedt, R. Koniuk, E. Poppitz, and T. Yavin, *Less naive about supersymmetric lattice quantum mechanics*, *JHEP* **12** (2004) 033, [hep-lat/0410041].

[7] S. Catterall and E. Gregory, *A lattice path integral for supersymmetric quantum mechanics*, *Phys. Lett.* **B487** (2000) 349–356, [hep-lat/0006013].

[8] S. Catterall, *Lattice supersymmetry and topological field theory*, *JHEP* **0305** (2003) 038, [hep-lat/0301028].

[9] G. Bergner, T. Kaestner, S. Uhlmann, and A. Wipf, *Low-dimensional supersymmetric lattice models*, *Annals Phys.* **323** (2008) 946–988, [arXiv:0705.2212].

[10] D. Baumgartner, K. Steinhauer, and U. Wenger, *Supersymmetry breaking on the lattice: the N=1 Wess-Zumino model*, *PoS* **LATTICE2011** (2011) 253, [arXiv:1111.6042].

Paper 6

Supersymmetric quantum mechanics on the lattice: I. Loop formulation

David Baumgartner and Urs Wenger, accepted for publication in Nucl. Phys. **B**

Supersymmetric quantum mechanics on the lattice: I. Loop formulation

David Baumgartner and Urs Wenger

Albert Einstein Center for Fundamental Physics,
Institute for Theoretical Physics, University of Bern,
Sidlerstrasse 5, CH–3012 Bern, Switzerland

Abstract

Simulations of supersymmetric field theories on the lattice with (spontaneously) broken supersymmetry suffer from a fermion sign problem related to the vanishing of the Witten index. We propose a novel approach which solves this problem in low dimensions by formulating the path integral on the lattice in terms of fermion loops. For $\mathcal{N} = 2$ supersymmetric quantum mechanics the loop formulation becomes particularly simple and in this paper - the first in a series of three - we discuss in detail the reformulation of this model in terms of fermionic and bosonic bonds for various lattice discretisations including one which is Q-exact.

1 Introduction

Independent of whether or not supersymmetry is realised in high energy particle physics, supersymmetric quantum field theories remain to be interesting and fascinating on their own. One intriguing feature of supersymmetric theories is for example the emergence of a Goldstino mode when the supersymmetry is broken, or the appearance of mass degenerate multiplets of fermionic and bosonic particles if the ground state of the theory is invariant under the supersymmetry transformation. In nature though, such degeneracies among elementary particles have so far not been observed, and as a consequence the supersymmetry must be spontaneously broken at some scale [1] if supersymmetry is indeed a true symmetry of nature. In fact, the spontaneous breaking of supersymmetry is a generic phenomena which is relevant for many physical systems beyond particle physics and quantum field theories. The question of spontaneous supersymmetry breaking however cannot be addressed in perturbation theory and nonperturbative methods are therefore desirable and even crucial. In the past, numerical simulations of quantum field theories on Euclidean lattices have proven to be a very successful tool for studying nonperturbative phenomena. Consequently, a lot of effort has been put into the lattice formulation of supersymmetric field theories, e.g. [2, 3, 4, 5, 6, 7, 8], see [9] for a comprehensive review. Finding an appropriate formulation, however, turns out to be far from trivial due to the explicit breaking of symmetries in connection with the discretisation. The Poincaré group for example is broken down to the subgroups of discrete rotations and finite translations by multiples of the lattice spacing. Since supersymmetry is an extension of

the Poincaré algebra, a complete realisation of the continuum supersymmetry algebra on the lattice is therefore not possible. For lattice regularised theories which are composed of local lattice operators, however, the remnant subgroups guarantee that the Poincaré symmetry is fully restored in the continuum. Unfortunately, in contrast to the Poincaré symmetry, for supersymmetry there is in general no subgroup left on the lattice which could play the role of the discrete subgroups above. It is therefore a priori not clear at all how a lattice formulation can be found for which supersymmetry is restored in the continuum [10], a problem which can eventually be traced back to the failure of the Leibniz rule on the lattice [11, 12, 13].

Apart from the explicit breaking of supersymmetry by the finite lattice spacing, additional complications for the investigation of supersymmetric theories on the lattice arise from the finite extent of the lattice. One problem concerns for example supersymmetry breaking due to finite temperature, or the tunneling between separate ground states on finite volumes. While the former problem can be circumvented by assigning periodic boundary conditions to the fermionic variables in (imaginary-)time direction (at the price of losing the concept of temperature), the latter problem requires an explicit extrapolation to the thermodynamic infinite volume limit. Whether and how such an extrapolation interferes with the extrapolation to the continuum limit, where the lattice spacing goes to zero, is obviously an interesting question. It is hence important to understand all the systematics of the lattice regularisation in detail, in particular the interplay between the infrared and ultraviolet regulators, and a thorough comprehension of these problems and the corresponding solutions is crucial for any investigation of spontanoues supersymmetry breaking.

It turns out that even a simple system such as $\mathcal{N} = 2$ supersymmetric quantum mechanics subsumes all the complications discussed above [14, 15]. In addition, it also provides a testing ground for any new approach to regularise, and possibly simulate, supersymmetric field theories on the lattice [16, 17, 18]. Therefore, besides being worth studying in its own right, supersymmetric quantum mechanics provides an ideal set up for nonperturbative investigations of supersymmetric field theories on the lattice. Consequently, supersymmetric quantum mechanics on the lattice has been the subject of intensive studies. Over time, different discretisation schemes have been developed in order to meet the requirement of the correct continuum limit of the theory [9, 19, 20]. In the context of unbroken supersymmetry, these schemes have well established numerical support [21, 22, 23, 24]. For broken supersymmetry, however, the model reveals a severe fermion sign problem affecting simulations with standard Monte Carlo methods [25, 26]. Because of this additional obstruction, first results in the context of broken supersymmetry were published only very recently [27].

In a series of three papers we introduce and exploit a novel approach with which it is possible to study, and in fact solve, supersymmetric quantum mechanics on the lattice for both broken and unbroken supersymmetry. In particular, we reformulate the system and its degrees of freedom in terms of fermionic and bosonic bond variables. This reformulation – the subject matter of the present paper – is based on the exact hopping expansion of the bosonic and fermionic actions on the lattice and allows the explicit decomposition of the partition function into bosonic and fermionic contributions. This explicit separation of the system paves the way for circumventing the fermion sign problem which appears for broken supersymmetry due to the vanishing of the Witten index. Furthermore, the formulation in terms of bond variables enables the construction of explicit transfer matrices which in turn allow to solve the lattice system exactly. As a consequence we are then able to study in extenso the continuum and infinite volume limit of systems both with broken or unbroken

supersymmetry. In particular, by means of Ward identities one can precisely illustrate how supersymmetry is restored. Furthermore, in the context of broken supersymmetry the emergence of the Goldstino mode in the thermodynamic limit and at zero temperature can be studied in detail. In summary, all the problems and issues appearing in the context of realising supersymmetry on the lattice can be addressed and studied by means of the exact results from the loop formulation. This investigation will be the subject matter of the second paper in the series. Finally, the formulation also forms the basis for a highly efficient fermion string algorithm [28, 29] which may be employed in numerical Monte Carlo simulations. Thus in the third paper of the series we eventually describe the details and properties of the algorithm which can be validated using the exact results from the transfer matrices. While the exact solution of the lattice system is specific to the low dimensionality and the subsequent simplicity of the supersymmetric quantum mechanics system, the bond formulation and the fermion string algorithm is applicable also to more complicated systems, e.g. in higher dimensions, or involving gauge fields. In particular it can be applied to supersymmetric Yang-Mills quantum mechanics [30] and certain two-dimensional supersymmetric field theories, such as the $\mathcal{N} = 1$ Wess-Zumino model [31, 32, 33, 34] and the supersymmetric nonlinear O(N) sigma model [35].

The present paper concerns the reformulation of supersymmetric quantum mechanics on the lattice in terms of bosonic and fermionic bonds. Starting from the formulation of supersymmetric quantum mechanics as an Euclidean quantum field theory, we discuss its lattice formulation using different variants of Wilson fermions including a Q-exact discretisation in section 2. There we also emphasise the generic fermion sign problem which arises for numerical simulations of systems with broken supersymmetry due to the vanishing of the Witten index. In section 3 we derive the loop formulation for both the fermionic and the bosonic degrees of freedom, while in section 4 we discuss in detail how observables such as the fermionic and bosonic two-point functions are calculated for generic boundary conditions in the loop formulation. Finally, in appendix A we summarise the explicit actions emerging for the various discretisations from the different superpotentials which we employ throughout this and the following papers of the series.

2 Supersymmetric quantum mechanics on the lattice

We start our discussion with the partition function of a zero dimensional supersymmetric quantum mechanical system with temporal extent L in the path integral formalism [36],

$$Z = \int \mathcal{D}\phi\mathcal{D}\overline{\psi}\mathcal{D}\psi \ \mathrm{e}^{-S(\phi,\overline{\psi},\psi)} \tag{1}$$

with the Euclidean action

$$S(\phi,\overline{\psi},\psi) = \int_0^\beta dt \Big\{ \frac{1}{2}\left(\frac{d\phi(t)}{dt}\right)^2 + \frac{1}{2}P'(\phi(t))^2 + \overline{\psi}(t)\left(\partial_t + P''(\phi(t))\right)\psi(t) \Big\}. \tag{2}$$

Here, $\phi(t)$ is a commuting bosonic coordinate while the two (independent) anticommuting fermionic coordinates are denoted by $\overline{\psi}(t)$ and $\psi(t)$. The derivative of the arbitrary superpotential $P(\phi(t))$ is taken with respect to ϕ, i.e. $P' = \frac{\partial P}{\partial \phi}$ and $P'' = \frac{\partial^2 P}{\partial \phi^2}$. For infinite temporal

extent and fields vanishing at infinity, the action is invariant under the $\mathcal{N} = 2$ supersymmetry transformations $\delta_{1,2}$,

$$\begin{aligned} \delta_1\phi &= \overline{\epsilon}\psi, & \delta_2\phi &= \overline{\psi}\epsilon, \\ \delta_1\psi &= 0, & \delta_2\psi &= \left(\dot{\phi} - P'\right)\epsilon, \\ \delta_1\overline{\psi} &= -\overline{\epsilon}\left(\dot{\phi} + P'\right), & \delta_2\overline{\psi} &= 0, \end{aligned} \tag{3}$$

where $\overline{\epsilon}$ and ϵ are Grassmann parameters and $\dot{\phi} = \frac{d\phi}{dt}$. For finite extent, however, the variation of the action under the supersymmetry transformations $\delta_{1,2}$ yields the nonvanishing terms

$$\delta_1 S = \int_0^\beta dt \left(-\overline{\epsilon}\left(\psi P''\dot{\phi} + \dot{\psi}P'\right)\right) = \overline{\epsilon}\psi P' \Big|_0^\beta, \tag{4}$$

$$\delta_2 S = \int_0^\beta dt \left(\dot{\overline{\psi}}\dot{\phi} + \overline{\psi}\ddot{\phi}\right)\epsilon = \overline{\psi}\dot{\phi}\epsilon \Big|_0^\beta \tag{5}$$

which can only be brought to zero by imposing periodic boundary conditions for the fermionic degrees of freedom, i.e.,

$$\psi(\beta) = \psi(0), \qquad \overline{\psi}(\beta) = \overline{\psi}(0). \tag{6}$$

Thus, choosing thermal, i.e., antiperiodic boundary conditions for the fermionic degrees of freedom breaks supersymmetry explicitly.

For specific choices of the superpotential $P(\phi)$ the supersymmetric system may enjoy additional symmetries. With the superpotential

$$P_u(\phi) = \frac{1}{2}\mu\phi^2 + \frac{1}{4}g\phi^4 \tag{7}$$

the resulting action is for example invariant under a parity transformation $\phi \to -\phi$, since

$$\left(P_u'(-\phi)\right)^2 = \left(P_u'(\phi)\right)^2, \qquad P_u''(-\phi) = P_u''(\phi), \tag{8}$$

and thus has an additional $\mathbb{Z}_2$-symmetry. This is the potential we will use in the following as an illustrating example for a quantum mechanical system with unbroken supersymmetry, hence the subscript u. Using the superpotential

$$P_b(\phi) = -\frac{\mu^2}{4\lambda}\phi + \frac{1}{3}\lambda\phi^3 \tag{9}$$

which we will use as an illustrating example for a system with broken supersymmetry, one finds that the action is invariant under a combined CP symmetry,

$$\phi(t) \to -\phi(t), \tag{10}$$

$$\psi(t) \to \overline{\psi}(t), \tag{11}$$

$$\overline{\psi}(t) \to \psi(t). \tag{12}$$

In the Schroedinger formalism, the partner potentials $\frac{1}{2}P_b'^2 \pm P_b''$ of a system with broken supersymmetry are connected through a mirror symmetry, and it turns out that the combined CP symmetry is just a manifestation of this mirror symmetry in the field theory language.

We now formulate the theory on a discrete lattice Λ by replacing the continuous (Euclidean) time variable $t \in [0, L]$ by a finite set of L_t lattice sites $x_n = an$, $n = 0, \ldots, L_t - 1$ separated by the lattice spacing $a = \frac{L}{L_t}$,

$$\Lambda = \{x \in a\mathbb{Z} \mid 0 \leq x \leq a(L_t - 1)\}. \tag{13}$$

Then, in order to formulate the path integral of supersymmetric quantum mechanics as a one-dimensional lattice field theory, we define the path integral measure on the lattice as

$$\int \mathcal{D}\phi\mathcal{D}\overline{\psi}\mathcal{D}\psi \equiv \prod_{x=0}^{L_t-1} \int_{-\infty}^{\infty} d\phi_x \int d\overline{\psi}_x \int d\psi_x, \tag{14}$$

such that the lattice partition function is given by

$$Z = \int \mathcal{D}\phi\mathcal{D}\overline{\psi}\mathcal{D}\psi \ \mathrm{e}^{-S_\Lambda(\phi,\overline{\psi},\psi)}, \tag{15}$$

where S_Λ is a suitable discretisation of the action. It requires the replacement of the temporal integration in the action by a discrete sum over all lattice sites,

$$\int_0^L dt \ \longrightarrow \ a \sum_{x=0}^{L_t-1}, \tag{16}$$

and the replacement of the continuous derivatives by suitable lattice derivatives. In the following two subsections 2.1 and 2.2 we discuss in detail two suitable lattice actions.

In principle, it is now straightforward to evaluate the partition function (15), for example numerically using Monte Carlo algorithms. However, for a system with broken supersymmetry one encounters a severe fermion sign problem when standard Metropolis update algorithms are employed. We will address this issue in more detail in subsection 2.3.

Finally, we note that the continuum limit of the lattice theory is taken by fixing the dimensionful parameters μ, g, λ and L while taking the lattice spacing $a \to 0$. In practice, the dimensionless ratios $f_u = g/\mu^2, f_b = \lambda/\mu^{3/2}$ fix the couplings and μL the extent of the system in units of μ, while $a\mu$ and a/L are subsequently sent to zero. Then, by attaching a physical scale to L for example, the physical values for all other dimensionful quantities follow immediately. Employing antiperiodic boundary conditions for the fermion, the extent L corresponds to the inverse temperature, hence the system at finite μL represents a system at finite temperature and the limit $\mu L \to \infty$ implies a system at zero temperature.

2.1 Standard discretisation

The most obvious choice for discretising the continuous derivatives in the action is to use the discrete symmetric derivative

$$\widetilde{\nabla} = \frac{1}{2}(\nabla^+ + \nabla^-) \tag{17}$$

where

$$\nabla^- f_x = \frac{1}{a}(f_x - f_{x-a}), \tag{18}$$

$$\nabla^+ f_x = \frac{1}{a}(f_{x+a} - f_x) \tag{19}$$

are the backward and forward derivatives, respectively. However, it is well known that the symmetric derivative leads to the infamous fermion doubling which, for the sake of maintaining supersymmetry, should be avoided. This can be achieved by introducing an additional Wilson term which removes all fermion doublers from the system,

$$\nabla^W(r) = \widetilde{\nabla} - \frac{ra}{2}\Delta,$$

where $\Delta = \nabla^+\nabla^-$ is the Laplace operator and the Wilson parameter takes values $r \in [-1,1]\backslash\{0\}$. It turns out that for one-dimensional derivatives the standard choice $r = \pm 1$ yields $\nabla^W(\pm 1) = \nabla^{\mp}$, hence for $r = 1$ the discretised action reads

$$S_\Lambda = a\sum_x \left\{\frac{1}{2}(\nabla^-\phi_x)^2 + \frac{1}{2}P'(\phi_x)^2 + \overline{\psi}_x(\nabla^- + P''(\phi_x))\psi_x\right\} \tag{20}$$

and setting the lattice spacing $a = 1$ we obtain

$$S_\Lambda = \sum_x \left\{\frac{1}{2}(P'(\phi_x)^2 + 2\phi_x^2) - \phi_x\phi_{x-1} + (1 + P''(\phi_x))\overline{\psi}_x\psi_x - \overline{\psi}_x\psi_{x-1}\right\}. \tag{21}$$

This is the standard discretisation for the action of supersymmetric quantum mechanics on the lattice. Correspondingly, the supersymmetry transformations eq.(3) discretised on the lattice Λ read

$$\begin{array}{rclcrcl} \delta_1\phi &=& \overline{\epsilon}\psi, & & \delta_2\phi &=& \overline{\psi}\epsilon, \\ \delta_1\psi &=& 0, & & \delta_2\psi &=& (\nabla^-\phi - P')\,\epsilon, \\ \delta_1\overline{\psi} &=& -\overline{\epsilon}\,(\nabla^-\phi + P')\,, & & \delta_2\overline{\psi} &=& 0, \end{array} \tag{22}$$

and the variation of the action under δ_1 yields

$$\delta_1 S_\Lambda = -\overline{\epsilon}\sum_x \left\{\psi_x P''(\phi_x)(\nabla^-\phi_x) + P'(\phi_x)(\nabla^-\psi_x)\right\}\,, \tag{23}$$

and similarly for δ_2. Note, that (23) is the lattice version of the surface term in the continuum, eq.(4). Since the Leibniz rule does not apply on the lattice, it is not possible to integrate this term by parts and S_Λ is therefore not invariant under the supersymmetry transformations δ_1 and δ_2. This is the explicit supersymmetry breaking by the lattice discretisation which we already pointed out in the introduction. In addition, the Wilson term also breaks the time reversal symmetry, or equivalently the charge conjugation for the fermion in our quantum mechanical system. This can be seen from the fact that the oriented hopping term $\overline{\psi}_x\psi_{x-1}$ is directed only in forward direction $x-1 \to x$, while the backward hopping is completely suppressed[1]. As a matter of fact, the discretised system only describes a fermion propagating forward in time, but not the corresponding antifermion propagating backward in time. As we will see later, this has an important consequence for the fermion bond formulation. In the continuum the symmetry is restored and this comes about by the relative contributions of the fermion and antifermion approaching each other in this limit.

At this point, it is necessary to stress that the action in eq.(20) does not correctly reproduce the continuum limit of the theory [15, 19, 22]. In figure 1, we illustrate this failure by extrapolating the lowest mass gaps of the fermion and the boson for the system with superpotential P_u (unbroken supersymmetry) to the continuum $a\mu \to 0$. The exact calculation is

[1]For an arbitrary choice of the Wilson parameter $0 < |r| < 1$ both directions would be present.

based on the extraction of the mass gaps via transfer matrix techniques which will be discussed in detail in the second paper of this series [37]. Note, that the extrapolation of the masses does not yield the known continuum values indicated by the horizontal dotted lines. In fact the bosonic and fermionic mass gaps are not even degenerate in the continuum and supersymmetry is not restored for this discretisation. It turns out that the mismatch is due

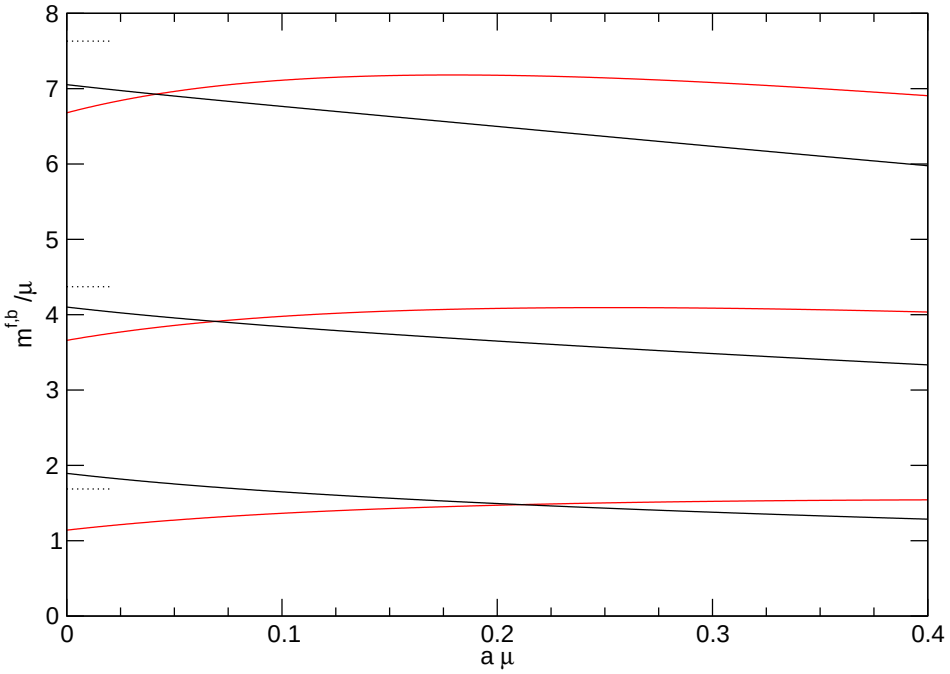

Figure 1: Continuum extrapolation $a\mu \to 0$ of the bosonic (red lines) and fermionic (black lines) mass gaps expressed in units of μ for unbroken supersymmetry at the coupling $f_u = 1$ using the standard discretisation. The expected continuum values are indicated by dotted lines.

to perturbative corrections and a careful analysis of those in the lattice theory is therefore mandatory [15]. However, since this quantum mechanics model is superrenormalisable, there are only a finite number of terms which do not converge to the correct continuum limit, and it is therefore sufficient to add a finite number of counterterms to the lattice action. Note that as opposed to a quantum field theory in higher dimensions, the counterterms do not diverge in quantum mechanics, but remain finite as $a \to 0$. As explicitly shown in [15], in order to restore supersymmetry in the continuum, it is necessary and sufficient to add the term $P''/2$ to the lattice action, i.e.,

$$S_\Lambda \longrightarrow S_\Lambda^c = S_\Lambda + \frac{1}{2}\sum_x P''(\phi_x)\,. \tag{24}$$

The term can be understood as a radiative correction and we will see in section 2.3 how the term arises in the explicit calculation of the determinant of the Wilson Dirac matrix. Finally, it is important to note that the resulting lattice theory is not supersymmetric at finite lattice spacing, but in the continuum limit it will nevertheless flow to the correct supersymmetric theory without any further fine tuning.

2.2 Q-exact discretisation

A discretisation of supersymmetric quantum mechanics which avoids the fine tuning of counterterms is based on the idea that it might be sufficient to preserve only a subset of the full supersymmetry at finite lattice spacing in order to reach the correct continuum limit. This approach, known under the name of twisted supersymmetry, was first applied to supersymmetric quantum mechanics in [19] and can be established in the context of topological field theory [38], or from a lattice superfield formalism [14]. For $\mathcal{N} = 2$ supersymmetric quantum mechanics it relies on the observation that the lattice variation $\delta_1 S_\Lambda$ of the standard discretised action in (23) can be written – up to a minus sign – as the variation of the lattice operator

$$O = \sum_x P'(\phi_x)(\nabla^- \phi_x) \tag{25}$$

under the same supersymmetry transformation δ_1, such that we have

$$\delta_1 S_\Lambda = -\delta_1 O. \tag{26}$$

It is then clear that the invariance of the action under the supersymmetry transformation δ_1 can be restored by simply adding the term O to the action. The bosonic part of the so constructed action can be written as

$$S^Q_{\Lambda,\text{bosonic}} = \sum_x \left\{ \frac{1}{2}(\nabla^- \phi_x)^2 + \frac{1}{2} P'(\phi_x)^2 + P'(\phi_x)(\nabla^- \phi_x) \right\}, \tag{27}$$

and the total action in more compact form as

$$S^Q_\Lambda = \sum_x \left\{ \frac{1}{2} \left((\nabla^- \phi_x) + P'(\phi_x) \right)^2 + \overline{\psi}_x (\nabla^- + P''(\phi_x)) \psi_x \right\}. \tag{28}$$

This is the Q-exact lattice action which preserves the supersymmetry δ_1 exactly (but not δ_2) for finite lattice spacing. The Q-exactness can be best seen in the off-shell formulation of the total action. Using an auxiliary field and defining the fermionic variation by $\delta_1 = \bar{\epsilon} Q$, where Q is the generator of the supersymmetry transformation [38], one can write the total action off-shell as the Q-variation of a particular function F, i.e. $S_\Lambda = QF$. This makes the Q-exact invariance of the action explicit via the nilpotency property $Q^2 = 0$ [9]. Maintaining this single supersymmetry on the lattice is sufficient to protect the theory from radiative contributions which would otherwise spoil the continuum limit. Note, that this action corresponds to the Ito prescription in [22]. In complete analogy, one can also construct a Q-exact action invariant under δ_2 but not δ_1, or in fact a Q-exact action invariant under any linear combination of δ_1 and δ_2, but not invariant under the corresponding orthogonal linear combination. This property is related to the fact that the improved lattice field theory is topological and hence the improvement term O can be added to the action with any prefactor different from zero to obtain a Q-exact action [38]. Each variant leads to a different discretisation of the bosonic part of the action. For the loop formulation we will concentrate on the form given in eq.(27) and (28), but of course the reformulation can be achieved for any Q-exact action. Before getting more specific, we will now discuss the fermion sign problem emerging in simulations of systems with broken supersymmetry.

2.3 Fermion sign problem from broken supersymmetry

In this section we discuss the fermion sign problem which affects standard Monte Carlo simulations of supersymmetric systems with broken supersymmetry. The problem is generic and affects all supersymmetric systems with (spontaneously) broken supersymmetry since it is related to the vanishing of the Witten index accompanying any spontaneous supersymmetry breaking. In the particularly simple supersymmetric quantum mechanics case we consider here in this paper, the problem can be illustrated very explicitly.

In order to evaluate the partition function in eq.(15), in a first step one usually integrates out the fermionic degrees of freedom in the path integral which then yields the determinant of the fermion Dirac operator $D(\phi)$, i.e.,

$$Z = \int \mathcal{D}\phi \ \det(D(\phi)) \ \mathrm{e}^{-S^B_\Lambda(\phi)}, \tag{29}$$

with $S^B_\Lambda(\phi)$ being the purely bosonic part of the lattice action. In the following we will concentrate on the Wilson Dirac operator $D(\phi) = \nabla^- + P''(\phi)$, but the considerations apply equally to any fermion discretisation. It turns out that depending on the specific choice of the superpotential $P(\phi)$ the determinant is not positive definite. In that case the effective Boltzmann weight $\det(D(\phi))\exp\{-S^B_\Lambda(\phi)\}$ can not be interpreted as a probability distribution and the standard Monte Carlo approach breaks down. In fact, since the partition function with periodic boundary conditions is proportional to the Witten index, which vanishes in systems with (spontaneously) broken supersymmetry, the partition function itself must be zero. From eq.(29) it then becomes clear that this can only be achieved by the determinant being indefinite and in fact zero on average. The cancellations between positive and negative contributions of the determinant to the partition function are hence maximal and constitute a severe fermion sign problem. Since the fermion determinant $\det(D(\phi))$ can be calculated analytically both in the continuum [22, 39, 40] and on the lattice, one can illustrate this explicitly and we will do so in the next two subsections. Moreover, the considerations will also be useful for the interpretation of the reformulation in terms of fermion loops.

2.3.1 The fermion determinant in the continuum

For the evaluation of the fermion determinant in the continuum, some regularisation is necessary. A suitable choice is given by dividing the determinant by the fermion determinant of the free theory, $\det(\partial_t + \mu)$. Moreover, the computation of the fermion determinant depends essentially on the choice of the boundary conditions for the fermionic degrees of freedom.

For antiperiodic boundary conditions $\psi(L) = -\psi(0)$, the regularised determinant yields

$$\det\left(D(\phi)\right) \doteq \det\left(\frac{\partial_t + P''(\phi)}{\partial_t + \mu}\right) = \frac{\cosh\left(\frac{1}{2}\int_0^L dt \ P''(\phi)\right)}{\cosh\left(\frac{1}{2}\mu L\right)} \tag{30}$$

and we observe that this is always positive. Furthermore, writing the cosh function in terms of exponentials, we find that

$$\det\left(D(\phi)\right) \propto \exp\left(+\frac{1}{2}\int_0^L dt \ P''(\phi)\right) + \exp\left(-\frac{1}{2}\int_0^L dt \ P''(\phi)\right) \tag{31}$$

and hence the partition function eq.(29) decomposes into two parts which just correspond to the bosonic and the fermionic sector, respectively. To be specific, one has

$$\int \mathcal{D}\phi \ \det\left(D(\phi)\right) \ \mathrm{e}^{-S^B(\phi)} = \int \mathcal{D}\phi \ \mathrm{e}^{-S^B_-(\phi)} + \int \mathcal{D}\phi \ \mathrm{e}^{-S^B_+(\phi)} \equiv Z_0 + Z_1 \,, \tag{32}$$

where the actions

$$S^B_\pm(\phi) = \int_0^L dt \Big\{ \frac{1}{2} \left(\frac{d\phi(t)}{dt} \right)^2 + \frac{1}{2} P'(\phi(t))^2 \pm \frac{1}{2} P''(\phi(t)) \Big\} \tag{33}$$

remind us of the partner potentials in the usual Hamilton formulation of supersymmetric quantum mechanics, and Z_0 and Z_1 are the partition functions in the bosonic and fermionic sector, respectively. Since we have calculated the determinant for antiperiodic boundary conditions, we have

$$Z_0 + Z_1 = Z_a \tag{34}$$

and we note that Z_a is positive since both Z_0 and Z_1 are positive.

For periodic boundary conditions $\psi(L) = \psi(0)$, the analogous calculation of the regularised fermion determinant yields

$$\det\left(D(\phi)\right) = \frac{\sinh\left(\frac{1}{2}\int_0^L dt \ P''(\phi)\right)}{\sinh\left(\frac{1}{2}\mu L\right)} \tag{35}$$

and writing out the sinh function as a sum of exponentials, we find

$$\int \mathcal{D}\phi \ \det\left(D(\phi)\right) \ \mathrm{e}^{-S^B(\phi)} = \int \mathcal{D}\phi \ \mathrm{e}^{-S^B_-(\phi)} - \int \mathcal{D}\phi \ \mathrm{e}^{-S^B_+(\phi)} = Z_0 - Z_1 \equiv Z_p \,. \tag{36}$$

More importantly, we note that for this choice of boundary conditions the partition function is indefinite and the fermion determinant is hence not necessarily positive.

We now recalling the definition of the Witten index W from quantum mechanics [41],

$$W = \mathrm{Tr}\left[(-1)^F e^{-\beta H}\right] = \mathrm{Tr}_B\left[e^{-\beta H}\right] - \mathrm{Tr}_F\left[e^{-\beta H}\right] \tag{37}$$

where H is the Hamilton operator and F the fermion number, while $\mathrm{Tr}_{B,F}$ denotes the trace over the bosonic and fermionic states, respectively. Identifying β with L we realise that the Witten index is in fact proportional to the expectation value of the fermion determinant, i.e., the partition function with fully periodic boundary conditions,

$$W \propto Z_p \,. \tag{38}$$

The relation is given as a proportionality because the path integral measure is only defined up to a constant multiplicative factor as compared to the traces in eq.(37).

In order to see the implications of these results, we consider the two superpotentials P_u and P_b defined in the introduction of section 2. Recall that the superpotential P_u in eq.(7) is invariant under the parity transformation $\phi \to -\phi$. Furthermore, for $\mu > 0$ and $g \geq 0$, $P''_u(\phi) > 0$, and eq.(35) and (36) then imply that $Z_p \neq 0$ and hence the Witten index is nonzero, $W \neq 0$. Thus, we conclude that for this superpotential supersymmetry is indeed unbroken, in agreement with the generic expectation from supersymmetric quantum

mechanics. Next, we consider the superpotential P_b in eq.(9) which we recall is odd under the parity transformation $\phi \to -\phi$, and so is its second derivative, $P_b''(-\phi) \to -P_b''(\phi)$. On the other hand, the bosonic action $S^B(\phi)$ for this superpotential,

$$S^B(\phi) = \int dt \, \left\{ \frac{1}{2} \left(\frac{d\phi}{dt} \right)^2 - \frac{1}{2} \left(\frac{\mu^2}{2} \phi^2 - \lambda^2 \phi^4 \right) \right\}, \tag{39}$$

is invariant under the parity transformation, $S^B(-\phi) \to S^B(\phi)$. Therefore, eq.(35) and (36) imply that with periodic b.c. for each configuration contributing to the partition function, there is the parity transformed one with exactly the same weight but opposite sign coming from the fermion determinant. Consequently, the partition function Z_p vanishes and the Witten index is $W = 0$. Indeed, for the superpotential P_b one expects on general grounds that supersymmetry is broken.

Obviously, the argument can be reversed leading to the conclusion discussed at the beginning of this section: since the Witten index is zero for a supersymmetric system with broken supersymmetry, the partition function with periodic boundary conditions Z_p, and hence the expectation value of $\det(D)$, vanishes, and this then leads to the fermion sign problem for numerical simulations.

2.3.2 The fermion determinant on the lattice

Next, we calculate the fermion determinant on the lattice. The lattice provides a regularisation, such that we can calculate the determinant directly without division by the determinant of the free theory. Using the lattice discretisation introduced in section 2.1, the determinant of the fermion matrix can easily be seen to be

$$\det \left(\nabla^- + P''(\phi_x) \right) = \prod_x (1 + P''(\phi_x)) \mp 1, \tag{40}$$

where the -1 $(+1)$ in the last term is associated with periodic (antiperiodic) boundary conditions. Note that this result is consistent with the expression derived for supersymmetric Yang-Mills quantum mechanics in [30]. As in the continuum the fermion determinant decomposes into a bosonic part, the product over all lattice sites x, and a fermionic part, the term ∓ 1. We will see later in section 3 from the fermion loop formulation that this interpretation is indeed correct.

At this point it is interesting to discuss the continuum limit of the lattice determinant. In principle, one would expect to recover the expressions in eq.(30) and eq.(35) when dividing the lattice determinant by the determinant of the free lattice theory and then taking the lattice spacing to zero, $a \to 0$. However, one finds

$$\lim_{a \to 0} \det \left(\frac{\nabla^- + P''(\phi_x)}{\nabla^- + \mu \cdot \mathbb{1}} \right) = \frac{\exp \left(\frac{1}{2} \int_0^L dt \; P''(\phi) \right)}{\exp \left(\frac{1}{2} \mu L \right)} \det \left(\frac{\partial_t + P''(\phi)}{\partial_t + \mu} \right), \tag{41}$$

i.e., taking the naive continuum limit apparently yields an additional factor in front of the continuum determinant. This factor can be understood as the remnants of the radiative corrections from the Wilson discretisation which survive the naive continuum limit [15]. The term is in fact responsible for the wrong continuum limit of the fermion and boson masses discussed in section 2.1 and illustrated in figure 1.

Let us now proceed by discussing the determinant of the Wilson Dirac matrix for both superpotentials P_u and P_b explicitly. Using the superpotential for unbroken supersymmetry P_u, the determinant yields

$$\det(\nabla^- + P_u''(\phi_x)) = \prod_x (1 + \mu + 3g\phi_x^2) \mp 1 \tag{42}$$

which for $\mu > 0$ and $g \geq 0$ is strictly positive, independent of the boundary conditions. Using the superpotential for broken supersymmetry P_b, the determinant yields

$$\det(\nabla^- + P_b''(\phi_x)) = \prod_x (1 + 2\lambda\phi_x) \mp 1 \tag{43}$$

which is indefinite even for $\lambda > 0$. While this is necessary in order to accommodate a vanishing Witten index, it imposes a serious problem on any Monte Carlo simulation, for which positive weights, and hence positive determinants, are strictly required. Moreover, the sign problem is severe in the sense that towards the continuum limit (i.e., when the lattice volume goes to infinity), the fluctuations of the first summand in eq.(43) around 1 tend to zero, such that $W \to 0$ is exactly realised in that limit. Hence, the source of the fermion sign problem lies in the exact cancellation between the first and the second summand in eq.(43), i.e., of the bosonic and fermionic contributions to the partition function, and this observation also holds more generally in higher dimensions [31, 32, 33]. In the loop formulation, to be discussed in the next section, the separation of the partition function into the various fermionic and bosonic sectors is made explicit and allows the construction of a simulation algorithm that samples these sectors separately, and more importantly also samples the relative weights between them. In this way, the loop formulation eventually provides a solution to the fermion sign problem.

3 Loop formulation of supersymmetric quantum mechanics

We will now discuss in detail the reformulation of supersymmetric quantum mechanics in terms of bosonic and fermionic bonds, eventually leading to the so-called loop formulation. The bond formulation is based on the hopping expansion for the bosonic and fermionic degrees of freedom. For the latter, the hopping expansion becomes particularly simple due to the nilpotent character of the fermionic variables and in addition reveals the decomposition of the configuration space into the bosonic and fermionic subspaces.

3.1 Loop formulation of the fermionic degrees of freedom

We start by splitting the action into a bosonic and fermionic part

$$S_\Lambda = S_\Lambda^B(\phi) + S_\Lambda^F(\phi, \overline{\psi}, \psi) \tag{44}$$

with

$$S_\Lambda^B(\phi) = \sum_x \left\{ \frac{1}{2}(\nabla^-\phi_x)^2 + \frac{1}{2}P'(\phi_x)^2 \right\}, \tag{45}$$

$$S_\Lambda^F(\phi, \overline{\psi}, \psi) = \sum_x \left\{ \overline{\psi}_x(\nabla^- + P''(\phi_x))\psi_x \right\}, \tag{46}$$

so that the partition function can be written as

$$Z = \int \mathcal{D}\phi \; \mathrm{e}^{-S_\Lambda^B(\phi)} \int \mathcal{D}\overline{\psi}\mathcal{D}\psi \; \mathrm{e}^{-S_\Lambda^F(\phi,\overline{\psi},\psi)} \,. \tag{47}$$

Rewriting the fermionic action as in eq.(21) and introducing $M(\phi) = 1 + P''(\phi)$ for the monomer term we have

$$S_\Lambda^F(\phi,\overline{\psi},\psi) = \sum_x \Big\{ M(\phi_x)\overline{\psi}_x\psi_x - \overline{\psi}_x\psi_{x-1} \Big\}, \tag{48}$$

and expanding separately the two terms in the Boltzmann factor yields

$$\mathrm{e}^{-S_\Lambda^F} = \prod_x (1 - M(\phi_x))\overline{\psi}_x\psi_x \prod_x \left(1 + \overline{\psi}_x\psi_{x-1}\right) \,. \tag{49}$$

Due to the nilpotency of the Grassmann variables, all terms of second or higher order in $\overline{\psi}_x\psi_x$ or $\overline{\psi}_x\psi_{x-1}$ vanish in the expansion. Introducing fermionic monomer occupation numbers $m(x) \in \{0,1\}$ as well as the fermionic bond occupation numbers $n^f(x) \in \{0,1\}$, we can further rewrite the expansion as

$$\mathrm{e}^{-S_\Lambda^F} = \prod_x \left(\sum_{m(x)=0}^{1} \left(-M(\phi_x)\overline{\psi}_x\psi_x\right)^{m(x)} \right) \prod_x \left(\sum_{n^f(x)=0}^{1} \left(\overline{\psi}_x\psi_{x-1}\right)^{n^f(x)} \right). \tag{50}$$

The fact that the fermionic occupation numbers can only take the values 0 or 1 can be seen as a realisation of the Pauli exclusion principle and follows naturally from the nilpotency property of the fermion fields. Obviously, it is natural to assign the bond occupation number $n^f(x)$ to the link connecting the sites $x-1$ and x, while the monomer occupation number $m(x)$ lives on the lattice site. The directed fermionic bond can be represented as illustrated in figure 2 by an arrow associated to the hopping term $\overline{\psi}_x\psi_{x-1}$ which is either occupied or not.

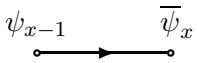

Figure 2: Graphical representation of the directed fermionic bond b^F.

In a next step we can now integrate out the fermionic variables. The Grassmann integration rule

$$\int d\overline{\psi}d\psi \; \overline{\psi}\psi = -1 \tag{51}$$

tells us that each site x must be occupied by exactly one variable ψ_x and one variable $\overline{\psi}_x$ in order to obtain a nonzero contribution to the path integral. The Grassmann integration at a given site x is either saturated by the monomer term $\propto \overline{\psi}_x\psi_x$, yielding the contribution $M(\phi_x)$ after the integration, or by exactly one ingoing and one outgoing fermionic bond $\propto \overline{\psi}_{x+1}\psi_x \cdot \overline{\psi}_x\psi_{x-1}$, yielding the contribution 1 for each bond after the Grassmann integration. The fact that these two possibilities are exclusive at each site leads to a local constraint on the monomer and bond occupation numbers $m(x)$ and $n^f(x)$ given by

$$m(x) + \frac{1}{2}\Big(n^f(x) + n^f(x-1)\Big) = 1, \qquad \forall x \,. \tag{52}$$

As a consequence, the integration over the Grassmann degrees of freedom ψ and $\overline{\psi}$ is replaced by a sum over all possible configurations of monomer and bond occupation numbers satisfying the local constraint eq.(52). The constraint implies that there are only two possible fermionic bond configurations with nonzero weight. On the one hand, eq.(52) is satisfied if $m(x) = 1$ and $n^f(x) = 0\ \forall x$. In this case, there are no fermionic bonds, i.e. the fermion number is $F = 0$, and such a configuration hence contributes to the bosonic sector. Each site is then saturated with the monomer term and by applying the Grassmann integration rules we identify the total fermionic contribution to the weight of a configuration to be the product of monomer weights $M(\phi_x)$ at each site x, i.e., $\prod_x (1 + P''(\phi_x))$. On the other hand, eq.(52) can also be satisfied by $n^f(x) = 1$ and $m(x) = 0\ \forall x$. For such a configuration the fermion number is $F = 1$, since all sites x are connected by fermionic bonds forming a fermionic loop which winds around the lattice. The fermionic bonds contribute with weight 1, hence the total fermionic contribution to the weight of such a configuration is just a factor (-1) where the minus sign follows from integrating out the cyclic loop of hopping terms and is the usual, characteristic fermion sign associated with closed fermion loops. In addition, the fermion loop receives an additional minus sign if antiperiodic boundary conditions for the fermion field are employed. We will discuss this in more detail in section 3.3.

Summarising the two contributions to the path integral from the integration of the fermionic variables, we have

$$\prod_x \Big(1 + P''(\phi_x)\Big) \mp 1 \tag{53}$$

for periodic and antiperiodic b.c., respectively, and we recognise this as the determinant of the lattice Dirac operator, cf. eq.(40). The first term from the configuration without any fermionic bonds is identified as the bosonic contribution to the path integral, while the second term from the fermion loop configuration is identified as the fermionic contribution. The partition function can hence be written as

$$Z_{p,a} = Z_0 \mp Z_1 \tag{54}$$

with

$$Z_0 = \int \mathcal{D}\phi\ \mathrm{e}^{-S^B_\Lambda(\phi)} \prod_x \Big(1 + P''(\phi_x)\Big), \tag{55}$$

$$Z_1 = \int \mathcal{D}\phi\ \mathrm{e}^{-S^B_\Lambda(\phi)} \tag{56}$$

where the subscript 0 and 1 denotes the fermion winding number of the underlying fermionic bond configuration, or equivalently the fermion number F. We have thus confirmed the interpretation of the bosonic and fermionic parts contributing to the fermion determinant alluded to in section 2.3.2.

3.2 Loop formulation of the bosonic degrees of freedom

In complete analogy to the previous section we can also replace the continuous bosonic variables ϕ by integer bosonic bond occupation numbers. To keep the discussion simple we first consider the standard discretisation. The bosonic action S^B_Λ in eq.(21) can be written in the form

$$S^B_\Lambda = \sum_x \{-w \cdot \phi_x \phi_{x-1} + V(\phi_x)\} \tag{57}$$

where we have separated the (nonoriented) hopping term $w \cdot \phi_x \phi_{x-1}$ with the hopping weight $w = 1$ from the local potential term $V(\phi_x) = \frac{1}{2}(P'(\phi_x)^2 + 2\phi_x^2)$. Expanding now the exponential of the hopping term in the Boltzmann factor we obtain

$$\mathrm{e}^{-S_\Lambda^B} = \prod_x \left(\sum_{n^b(x)=0}^{\infty} \frac{(w \cdot \phi_{x-1}\phi_x)^{n^b(x)}}{n^b(x)!} \right) \prod_x \mathrm{e}^{-V(\phi_x)}. \tag{58}$$

The summation indices $n^b(x)$ can be interpreted as bosonic bond occupation numbers, but in contrast to the fermionic case there is no Pauli exclusion principle which truncates the expansion, and hence the summation runs from 0 to infinity.

To make further progress we now need to combine this with the result from the expansion in the fermionic variables, and so we obtain for the full partition function

$$Z = \int \mathcal{D}\phi \prod_x \left(\sum_{n^b(x)=0}^{\infty} \frac{(w \cdot \phi_{x-1}\phi_x)^{n^b(x)}}{n^b(x)!} \right) \prod_x \mathrm{e}^{-V(\phi_x)} \prod_x \left(\sum_{m(x)=0}^{1} M(\phi_x)^{m(x)} \right). \tag{59}$$

In order to integrate over the variable ϕ_x locally at each site we select a particular entry in each of the sums. This is equivalent to choosing a particular bond configuration $\{n^b(x)\}$ and fermionic monomer configuration $\{m(x)\}$. The rearrangement of the bosonic fields, essentially collecting locally all powers of ϕ_x, yields local integrals of the form

$$Q(N(x), m(x)) = \int_{-\infty}^{\infty} d\phi_x \; \phi_x^{N(x)} \mathrm{e}^{-V(\phi_x)} M(\phi_x)^{m(x)} \tag{60}$$

where the site occupation number

$$N(x) = n^b(x) + n^b(x-1) \tag{61}$$

counts the total number of bosonic bonds attached to the site x. This can be visualised by a graphical representation of the bond as a (dashed) line connecting the sites $x-1$ and x as in figure 3. The site occupation number is then just the number of bonds connected to a site from the left and the right.

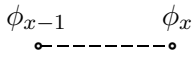

Figure 3: Graphical representation of the bosonic bond $b^B_{1\to 1}$.

As a consequence of the reordering, the weight of the chosen bond and monomer configuration factorises as

$$W\left(\{n^b(x)\}, \{m(x)\}\right) = \prod_x \frac{w^{n^b(x)}}{n^b(x)!} Q(N(x), m(x)) \,. \tag{62}$$

Depending on the specific form of the superpotential $P(\phi)$ the site weight Q might vanish for certain values of N and m. This essentially induces a local contraint on the number of bosonic bonds attached to a site, e.g. $N \bmod 2 = 0$ for potentials even in ϕ, similar to the constraint on the fermionic bond occupation numbers. The constraint simply reflects the

symmetry property of the underlying bosonic field and has important consequences e.g. for the observables as discussed in section 4.

Let us now consider how the bosonic hopping expansion is modified when the action with a counterterm, eq.(24), or the Q-exact action in eq.(27) is employed. While the counterterm simply changes $V(\phi) \to V(\phi) + P''(\phi)/2$ and hence the site weight Q, the Q-exact discretisation has a more severe impact on the hopping expansion. To be more specific, the Q-exact actions demand for additional kinds of bosonic bonds as can be seen by explicitly calculating the term O in eq.(25). Using for example the superpotential P_u we have

$$O = \sum_x P_u'(\phi_x)(\nabla^- \phi_x) = \sum_x \left\{ \mu\phi_x^2 + g\phi_x^4 - \mu\phi_x\phi_{x-1} - g\phi_x^3\phi_{x-1} \right\}. \tag{63}$$

While the first two terms $\mu\phi_x^2$ and $g\phi_x^4$ just modify the potential $V(\phi)$ describing the local bosonic self-interaction, the third term $-\mu\phi_x\phi_{x-1}$ matches the standard hopping term and modifies the hopping weight $w = 1 \to w = 1 + \mu$. The fourth term $-g\phi_x^3\phi_{x-1}$ however introduces a new kind of bosonic hopping and hence a new bosonic bond with weight g. Since the hopping carries one power of the bosonic variable ϕ at the left ending and three powers ϕ^3 at the right ending the new bosonic bond is directed. In order to distinguish the two different types of bosonic bonds, we label them by indicating the number of bosonic variables they carry at each ending, i.e. $b^B \to b^B_{1\to1}$ and $b^B_{1\to3}$ for the new bond. Of course the new bosonic bond also contributes to the site occupation number,

$$N(x) = n^b_{1\to1}(x) + n^b_{1\to1}(x-1) + n^b_{1\to3}(x) + 3 \cdot n^b_{1\to3}(x-1)\,, \tag{64}$$

and the total weight of a bond configuration becomes

$$W = \prod_x \frac{(1+\mu)^{n^b_{1\to1}(x)}}{n^b_{1\to1}(x)!} \frac{g^{n^b_{1\to3}(x)}}{n^b_{1\to3}(x)!} Q\left(N(x), m(x)\right). \tag{65}$$

For the superpotential P_b, the explicit expression for the surface term reads

$$O = \sum_x P_b'(\phi_x)(\nabla^- \phi_x) = \sum_x \left\{ \lambda\phi_x^3 - \lambda\phi_x^2\phi_{x-1} \right\}. \tag{66}$$

The first term $\lambda\phi_x^3$ modifies the local potential $V(\phi)$ and therefore just changes the site weight Q. In contrast to the previous case there is no additional term $\propto \phi_x\phi_{x-1}$, hence the corresponding hopping weight $w = 1$ is unchanged. The hopping term $-\lambda\phi_x^2\phi_{x-1}$ generates a new type of bosonic bond $b^B_{1\to2}$ with weight λ. This directed bond carries one power of the bosonic variable ϕ at the left ending and two powers ϕ^2 at the right ending, so the site occupation number is therefore modified as

$$N(x) = n^b_{1\to1}(x) + n^b_{1\to1}(x-1) + n^b_{1\to2}(x) + 2 \cdot n^b_{1\to2}(x-1)\,. \tag{67}$$

Eventually, the total weight of a bond configuration is then found to be

$$W = \prod_x \frac{w^{n^b_{1\to1}(x)}}{n^b_{1\to1}(x)!} \frac{\lambda^{n^b_{1\to2}(x)}}{n^b_{1\to2}(x)!} Q\left(N(x), m(x)\right) \tag{68}$$

with $w = 1$. In analogy to the illustration for the $b^B_{1\to1}$ bond in figure 3, we give a graphical representation of the new bonds $b^B_{1\to3}$ and $b^B_{1\to2}$ in figure 4 illustrating their contributions to

Figure 4: Graphical representation of the bosonic bonds $b^B_{1\to 3}$ and $b^B_{1\to 2}$ appearing in the bond formulation for the Q-exact action with the superpotentials P_u and P_b, respectively.

the site weights at each ends. As a side remark we note that it is in fact not too surprising to find directed bosonic hopping terms for the Q-exact actions: since these preserve part of the supersymmetry the oriented fermion hopping needs to be matched in some way by corresponding oriented boson hopping terms.

It is straightforward to generalise the above construction to even more complicated discretisations. For example, we mentioned before that the addition of the surface term in eq.(25) to the original action with any weight different from zero yields a whole class of Q-exact actions [38]. Another example is the discretisation of the action using the Stratanovich prescription [21, 22, 42]. In general, in addition to the bonds of type $(1 \to 1)$ and $(1 \to 2)$ or $(1 \to 3)$, these actions will also generate bonds of type $(2 \to 1)$ or $(3 \to 1)$ for the superpotentials P_b and P_u. Superpotentials of higher order produce bonds of correspondingly higher order. All these bonds can be treated in exactly the same way as discussed above. Each new hopping of type $(i \to j)$ induces a new bond $b^B_{i\to j}$ carrying weight $w_{i\to j} \equiv w$ and a corresponding bond occupation number $n^b_{i\to j} \equiv n$, contributing a factor $w^n/n!$ to the local weight and eventually also modifies the site occupation number N.

3.3 Partition functions in the loop formulation

After having integrated out the fermionic and bosonic fields $\overline{\psi}, \psi$ and ϕ, respectively, we are left with discrete fermionic and bosonic bond occupation numbers as the degrees of freedom. The path integral has eventually been replaced by a sum over all allowed bond configurations, possibly restricted by local constraints, and hence represents a discrete statistical system. By itself this is already a huge reduction in complexity. Any bond configuration contributing to the partition function consists of the superposition of a generic bosonic bond configuration with one of the two allowed fermionic bond configurations, namely the one representing a closed fermion loop winding around the lattice or the one without any fermionic bonds. Therefore, each bond configuration is either associated with the fermionic sector with fermion number $F = 1$, or with the bosonic sector with $F = 0$. In figure 5 we illustrate two such possible configurations in the fermionic and bosonic sectors on a $L_t = 8$ lattice. Collecting our results from the previous two sections we can now write down the contribution of a generic bond configuration $\mathcal{C} = \{n^b_i(x), m(x)\}$ to the partition function. It depends on the fermion number and reads

$$W_F(\mathcal{C}) = \prod_x \left(\prod_i \frac{w_i^{n_i^b(x)}}{n_i^b(x)!} \right) \prod_x Q_F(N(x)) \tag{69}$$

where the index i runs over all the types of bosonic bonds appearing for the specific discretisation under consideration, i.e. $i \in \{1 \to 1, 1 \to 2, 1 \to 3\}$. In appendix A we summarise the various bond types and corresponding weights for the discretisations and superpotentials

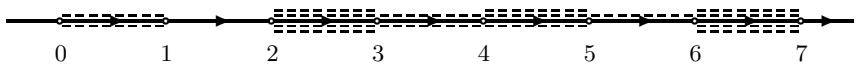

(a) $F = 1$

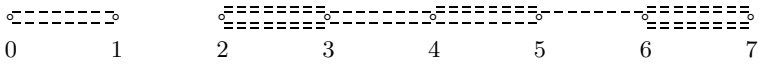

(b) $F = 0$

Figure 5: Illustration of a possible bosonic bond configuration in the fermionic sector $F = 1$ and the same configuration in the bosonic sector $F = 0$ on a $L_t = 8$ lattice.

discussed in the previous two sections. The site weights are given by

$$Q_F(N(x)) = \int_{-\infty}^{\infty} d\phi \; \phi^{N(x)} \mathrm{e}^{-V(\phi)} M(\phi)^{1-F} \,, \tag{70}$$

where the site occupation number $N(x)$ counts all the bosonic bonds connected to the site x,

$$N(x) = \sum_{j,k} \Big(j \cdot n^b_{j\to k}(x) + k \cdot n^b_{j\to k}(x-1) \Big) \,. \tag{71}$$

The potential $V(\phi)$ depends on the first derivative of the superpotential, $P'(\phi)$, while the monomer term $M(\phi)$ depends on second derivative $P''(\phi)$ and is present if the fermion is not ($F = 0$) and vice versa ($F = 1$). For superpotentials of polynomial form they can be written as

$$V(\phi) = \sum_n k_n \phi^n \,, \quad M(\phi) = \sum_n m_n \phi^n \,. \tag{72}$$

The values of the various coefficients for the superpotentials discussed in this paper are compiled in the tables in appendix A, where we summarise the details of the various discretisations. Finally, the full partition functions in the two sectors can be written as the sum over all configurations $\mathcal{C}$ in the corresponding configuration space $\mathcal{Z}_F$,

$$Z_F = \sum_{\mathcal{C}\subset\mathcal{Z}_F} W_F(\mathcal{C}) \,. \tag{73}$$

The separation of the bond configuration space into the bosonic and fermionic sectors comes about naturally in the loop formulation, since the bond configurations fall into separate equivalence classes $\mathcal{Z}_F$ specified by the fermion number F. In principle one can consider each sector separately and the partition functions simply describe canonical quantum mechanical systems with fixed fermion number $F = 0$ or 1. In terms of a winding fermion this corresponds to boundary conditions which fix the topology of the winding fermion string, i.e., topological boundary conditions. In order to specify the usual fermion boundary conditions,

$$\overline{\psi}_{x+L_t} = (-1)^{\varepsilon} \overline{\psi}_x, \qquad \psi_{x+L_t} = (-1)^{\varepsilon} \psi_x \tag{74}$$

with $\varepsilon = 0$ and 1 for periodic and antiperiodic boundary conditions, respectively, the two partition functions need to be combined. From our discussion in section 3.1 we know that the

configurations in the fermion sector, apart from having different weights, pick up a relative sign (-1) coming from the closed fermion loop. An additional sign stems from the fermion loop crossing the boundary if antiperiodic boundary conditions are employed. The relative sign between the contributions of the two sectors can therefore be summarised as $(-1)^{\varepsilon \cdot F}$, and the partition functions for the systems with periodic or antiperiodic fermionic boundary conditions can be written as

$$Z_{p,a} = Z_0 \mp Z_1 \,. \tag{75}$$

Depending on the relative size of Z_0 and Z_1 the combination for Z_p vanishes or can even be negative. This has important consequences for the Witten index W which is proportional to Z_p. The index vanishes whenever $Z_0 = Z_1$, i.e., when the contributions from the bosonic and fermionic sectors cancel each other exactly. In this case, the free energies of the bosonic and fermionic vacuum must be equal and hence there exists a gapless, fermionic excitation which oscillates between the two vacua, namely the Goldstino mode. As discussed before, the Witten index is regulated at finite lattice spacing, essentially through the fact that Z_0 and Z_1 have different lattice artefacts and therefore do not cancel exactly. More precisely, the finite lattice spacing breaks the degeneracy between the vacuum states by inducing a small free energy difference between the bosonic and fermionic vacua. Consequently, the Goldstino mode receives a small mass, which only disappears in the continuum limit, and is hence also regulated. From that point of view standard Monte Carlo simulations seem to be safe in the sense that there is no need to simulate at vanishing fermion mass. Nevertheless, sufficiently close to the massless limit in a supersymmetry broken system, standard simulation algorithms will almost certainly suffer from critical slowing down and from fluctuating signs of the determinant due to the sign problem discussed before.

The separation of the partition function into a bosonic and fermionic part offers several ways to approach and in fact solve the sign problem when the supersymmetry is broken. Firstly, one can in principle perform simulations in each sector separately, but of course one then misses the physics of the Goldstino mode. Secondly, one can devise an algorithm which efficiently estimates the relative weights of the sectors and hence directly probes the signal on top of the potentially huge cancellations between Z_0 and Z_1. Fortunately, such an algorithm is available [29, 43]. Since this so called open fermion string algorithm directly samples the Goldstino mode, there is no critical slowing down and the physics of the Goldstino is properly captured. The application of the algorithm to the quantum mechanical system is the topic of our third paper in the series [44].

Finally, we note that the equivalence classes $\mathcal{Z}_F$ of the bond configurations specified by the fermion number F can also be characterised by the winding of the fermion around the lattice. In our quantum mechanical system the two characterisations are equivalent, but in more complicated systems the classification in terms of the topology of the fermion winding is more appropriate. It turns out that the discussion of the topological sectors with fixed fermion winding number is in fact crucial for the successful operational application of the fermion loop formulation in more complicated quantum mechanical systems [30], or in higher dimensions [29, 45]. As a matter of fact, the separation of the bond configurations into topological classes provides the basis for the solution of the fermion sign problem in the $\mathcal{N} = 1$ Wess-Zumino model [31, 32, 33, 34] in complete analogy to how it is illustrated here in the quantum mechanical system.

4 Observables in the loop formulation

We now discuss how bosonic and fermionic observables are expressed in the loop formulation and how the calculation of vacuum expectation values is affected by the decomposition of the partition function into its bosonic and fermionic parts. In general, the expectation value of an observable $\langle \mathcal{O} \rangle$ is given by

$$\langle \mathcal{O} \rangle = \frac{1}{Z} \int \mathcal{D}\phi \mathcal{D}\overline{\psi} \mathcal{D}\psi \; \mathcal{O}(\phi, \overline{\psi}, \psi) \; \mathrm{e}^{-S(\phi,\overline{\psi},\psi)} \tag{76}$$

and the explicit expression for periodic and antiperiodic boundary conditions is

$$\langle \mathcal{O} \rangle_{p,a} = \frac{\langle\!\langle \mathcal{O} \rangle\!\rangle_0 \mp \langle\!\langle \mathcal{O} \rangle\!\rangle_1}{Z_0 \mp Z_1} \,. \tag{77}$$

Here, we have denoted the non-normalised expectation value of the observable in the sector F by $\langle\!\langle \mathcal{O} \rangle\!\rangle_F \equiv \langle \mathcal{O} \rangle_F \cdot Z_F$. According to our discussion at the end of the previous section, it is important that in order to calculate the expectation values it is not sufficient to determine $\langle \mathcal{O} \rangle$ in each sector separately, but it is mandatory to calculate the ratio Z_0/Z_1, or similar ratios which contain the same information such as $Z_F/(Z_0 + Z_1)$.

Recalling that for broken supersymmetry the Witten index is $W = 0$, and hence $Z_p = Z_0 - Z_1 = 0$, it is obvious from eq.(77) that the vacuum expectation values for periodic boundary conditions $\langle \mathcal{O} \rangle_p$ require a division by zero. Of course this is simply a manifestation of the fermion sign problem discussed earlier in section 2.3. One might then wonder whether vacuum expectation values of observables are well defined at all when the supersymmetry is broken. It turns out, however, that the finite lattice spacing in fact provides a regularisation for this problem. For the standard discretisation, supersymmetry is explicitly broken, such that $Z_p \neq 0$ for $a \neq 0$. It is therefore possible to calculate expectation values for periodic b.c. at finite lattice spacing, when they are well defined, and then take the continuum limit. Whether or not eq.(77) with periodic b.c. remains finite or diverges in that limit depends on the observable under consideration. For sensible observables, both the numerator and the denominator go to zero such that their ratio remains finite It is then possible to give continuum values for periodic b.c. even when the supersymmetry is broken in the continuum and $Z_0 - Z_1 \to 0$. Sensible observables are those which couple to the Goldstino mode in the same way as $Z_0 - Z_1$ does, i.e., observables for which the expectation values in both the bosonic and fermionic sector converge to the same value towards the continuum limit. For Q-exact discretisations, the situation is more complicated since in systems with broken supersymmetry $Z_0 - Z_1 = 0$ even at finite lattice spacing. In that case, the physics of the Goldstino mode is realised exactly at $a \neq 0$. It is then more useful to calculate observables separately in the fermionic and bosonic sectors and to verify that they agree.

Important examples for observables are the moments of the bosonic field and two-point functions. The latter are typically used to measure the mass gaps in the particle spectrum by extracting the energy difference between the excited states and the vacuum state, but they also play important roles in the determination of Ward identities. In the following subsections, we will derive the representation of these observables in the loop formulation. This will turn out to be very useful also for the exact calculation of two-point functions and other observables using transfer matrices in the second paper of this series [37], where we discuss a plethora of results, and for the discussion of the simulation algorithm in the third paper of this series [44].

4.1 Moments of ϕ

The expectation value of the n-th moment of the field variable ϕ is defined as

$$\langle \phi^n \rangle = \langle \phi_x^n \rangle = \frac{1}{Z} \int \mathcal{D}\phi \mathcal{D}\overline{\psi} \mathcal{D}\psi \ \phi_x^n \ \mathrm{e}^{-S}. \tag{78}$$

When repeating the reformulation in terms of bosonic and fermionic bonds for this case, it is easy to see that the bond configurations contributing to the partition functions Z_F also contribute to $\langle \phi^n \rangle$. The only difference lies in the weight of each configuration which is modified due to the additional fields ϕ_x^n present at site x. The additional fields only change the local weight $Q_F(N(x))$ through a change of the local bosonic site occupation number at site x,

$$N(x) \to N(x) + n \,. \tag{79}$$

Hence, the non-normalised expectation value reads

$$\langle\!\langle \phi^n \rangle\!\rangle_F = \sum_{\mathcal{C} \subset \mathcal{Z}_F} \frac{Q_F(N(x)+n)}{Q_F(N(x))} W_F(\mathcal{C}) \tag{80}$$

$$= \langle\!\langle \frac{Q_F(N(x)+n)}{Q_F(N(x))} \rangle\!\rangle_F \tag{81}$$

and $\langle \phi^n \rangle$ then follows directly from eq.(77).

We noted earlier that the symmetry properties of the underlying fields are reflected in local constraints on the bond occupation numbers which in turn express themselves in the values of the site weights Q_F. As a consequence, the symmetry properties are then also promoted to the observables through the weights in eq.(80). Considering for example potentials $V(\phi)$ even in ϕ, such as the one following from P_u, one finds the constraint $N \bmod 2 = 0$ which is realised by all site weights with an odd occupation number being identically zero, i.e. $Q_F(N \bmod 2 = 1) = 0$. Consequently, the contributions to odd moments vanish for all bond configurations, $\langle \phi^n \rangle = 0, n \,\text{odd}$, because $Q_F(N(x)+n) = 0$.

4.2 The bosonic n-point correlation function

The bosonic two-point function is defined as

$$C^b(x_1 - x_2) \equiv \langle \phi_{x_1} \phi_{x_2} \rangle = \frac{g^b(x_1 - x_2)}{Z}, \tag{82}$$

where

$$g^b(x_1 - x_2) = \int \mathcal{D}\phi \mathcal{D}\overline{\psi} \mathcal{D}\psi \ \phi_{x_1} \phi_{x_2} \ \mathrm{e}^{-S} \equiv \langle\!\langle \phi_{x_1} \phi_{x_2} \rangle\!\rangle. \tag{83}$$

In the following we will abbreviate the configuration space of the bosonic two-point function g^b with $\mathcal{G}^b$. It is again straighforward to rederive the loop formulation in terms of fermionic and bosonic bond occupation numbers also for this case. In general one finds that the bond configurations contributing to $\mathcal{G}^b$ and $\mathcal{Z}$ are the same, but their weights differ due to the insertion of the additional bosonic field variables ϕ at site x_1 and x_2 in the configurations contributing to g^b. The additional sources only change the local bosonic site occupation numbers at site x_1 and x_2,

$$N(x) \to N(x) + \delta_{x,x_1} + \delta_{x,x_2} \,. \tag{84}$$

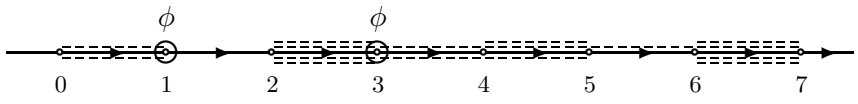

(a) $F = 1$

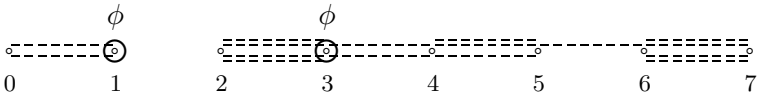

(b) $F = 0$

Figure 6: Graphical representation of possible configurations similar to the closed path configurations in figure 5, contributing to the bosonic two-point function (a) in the fermionic sector $F = 1$ and (b) the same configuration in the bosonic sector $F = 0$ on a $L_t = 8$ lattice. The additional bosonic variables are marked with a ○.

For $x_1 = x_2$ the situation reduces to the one for the second moment discussed in the previous section. The fermion number F is not affected by these sources. Thus, analogously to the configuration space $\mathcal{Z}$, the configuration space $\mathcal{G}^b$ decomposes into the bosonic part with $F = 0$ and the fermionic part with $F = 1$. We denote the separated configuration spaces by adding the subscript F, i.e. $\mathcal{G}^b \equiv \mathcal{G}^b_F$. In figure 6 we show two possible configurations with $F = 0$ and $F = 1$ contributing to the bosonic two-point function in the corresponding sectors. The weight of a configuration where bosonic sources are inserted at the sites $x_1 \neq x_2$ is then given by

$$W_{\mathcal{G}^b_F} = \prod_x \left(\prod_i \frac{w_i^{n_i^b(x)}}{n_i^b(x)!} \right) \left[\prod_{x \neq x_1, x_2} Q_F(N(x)) \right] Q_F(N(x_1)+1) \cdot Q_F(N(x_2)+1) \tag{85}$$

and the non-normalised expectation value reads

$$\langle\!\langle \phi_{x_1} \phi_{x_2} \rangle\!\rangle_F = \sum_{\mathcal{C} \subset \mathcal{G}^b_F} \frac{Q_F(N(x_1)+1)}{Q_F(N(x_1))} \cdot \frac{Q_F(N(x_2)+1)}{Q_F(N(x_2))} \cdot W_F(\mathcal{C}) \tag{86}$$

$$= \langle\!\langle \frac{Q_F(N(x_1)+1)}{Q_F(N(x_1))} \cdot \frac{Q_F(N(x_2)+1)}{Q_F(N(x_2))} \rangle\!\rangle_F \,. \tag{87}$$

It is straighforward to generalise the construction to arbitrary bosonic n-point functions. One simply adds n bosonic sources $\phi^{p_k}_{x_k}, k = 1, \ldots, n$ to a given configuration. The additional sources then contribute to the bosonic site occupation numbers with additional terms $p_k \cdot \delta_{x,x_k}$ modifying the site weights at positions x_k in analogy to eq.(84). Eventually one gets

$$\langle\!\langle \phi^{p_1}_{x_1} \ldots \phi^{p_n}_{x_n} \rangle\!\rangle_F = \langle\!\langle \prod_{k=1}^{n} \frac{Q_F(N(x_k)+p_k)}{Q_F(N(x_k))} \rangle\!\rangle_F \,. \tag{88}$$

As discussed before, for some actions there are constraints imposed on the bond configurations reflecting the symmetry properties of the bosonic field. In such a case, the bond configurations in the configuration spaces $\mathcal{Z}_F$ and $\mathcal{G}^b_F$ need no longer be the same. Considering again the example of a potential $V(\phi)$ even in ϕ such that the parity transformation

$\phi \to -\phi$ is a symmetry of the action, the constraint $N \bmod 2 = 0$ requires an odd number of bosonic bonds connected to a site containing an odd power of ϕ as a source term, but the corresponding underlying bond configuration contributes with weight zero to $\mathcal{Z}_F$. Hence the sets of configurations with nonvanishing weights contributing to Z_F and g_F^b have no overlap. In addition, from the symmetry it follows that operators with different quantum numbers, in this case the parity, do not mix, i.e. their correlation is exactly zero, e.g. $\langle \phi_{x_1}^2 \phi_{x_2} \rangle = 0$. It is easy to see that this property is strictly enforced in the loop formulation, since there exist no bond configurations which can accommodate the sources and fulfill the constraints $N(x) \bmod 2 = 0$ at the same time.

4.3 The fermionic correlation function

The fermionic two-point correlation function is defined as

$$C^f(x_1 - x_2) \equiv \langle \psi_{x_1} \overline{\psi}_{x_2} \rangle = \frac{g^f(x_1 - x_2)}{Z}, \tag{89}$$

where

$$g^f(x_1 - x_2) = \int \mathcal{D}\phi \mathcal{D}\overline{\psi} \mathcal{D}\psi \; \psi_{x_1} \overline{\psi}_{x_2} \; \mathrm{e}^{-S} \equiv \langle\langle \psi_{x_1} \overline{\psi}_{x_2} \rangle\rangle \,. \tag{90}$$

Similarly to the bosonic correlation function, configurations contributing to the fermionic correlation function have additional fermionic variables $\overline{\psi}$ and ψ inserted in the path integral at positions x_1 and x_2. We will refer to these variables as the source and the sink, respectively. To derive the weight of a configuration in the configuration space $\mathcal{G}^f$ of the fermionic two-point functions, we repeat the expansion of the fermionic Boltzmann factor in eq.(50) while including the additional fermionic variables. The expansion yields

$$\begin{aligned} &\psi_{x_1} \overline{\psi}_{x_2} \mathrm{e}^{-S_\Lambda^F} = \\ &\quad \psi_{x_1} \overline{\psi}_{x_2} \prod_x \left(\sum_{m(x)=0}^{1} \Big(- M(\phi_x) \overline{\psi}_x \psi_x \Big)^{m(x)} \right) \prod_x \left(\sum_{n^f(x)=0}^{1} \Big(\overline{\psi}_x \psi_{x-1} \Big)^{n^f(x)} \right) \end{aligned} \tag{91}$$

and the subsequent Grassmann integration, still requiring exactly one pair of variables $\overline{\psi}$ and ψ at each site x, yields an adjustment of the fermionic occupation numbers $m(x)$ and $n^f(x)$ in order to obtain a nonvanishing contribution to the two-point function.

We first consider the case where $x_1 = x_2 \equiv y$. It is easy to see that the only possibility to saturate each site is given by the choice

$$n^f(x) = 0 \qquad \forall x, \tag{92}$$

$$m(x) = \begin{cases} 0 & \text{if } x = y, \\ 1 & \text{else.} \end{cases} \tag{93}$$

For such a configuration, the site y is saturated through the source and the sink, yielding a factor 1 as the fermionic contribution to the bosonic integration. All other sites are saturated via the monomer terms which have to be accounted for by including the corresponding factors

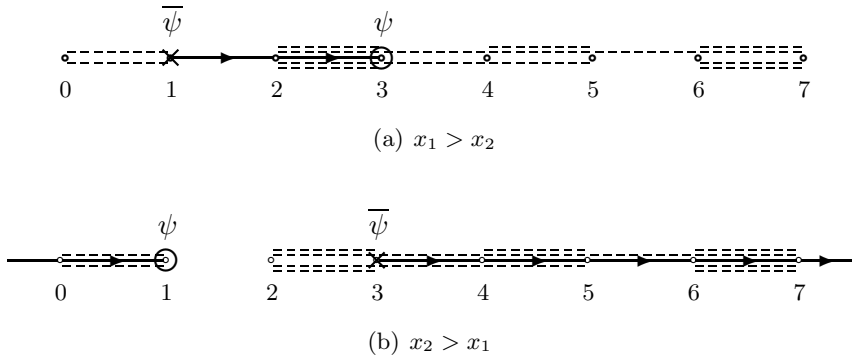

(a) $x_1 > x_2$

(b) $x_2 > x_1$

Figure 7: Graphical representation of possible configurations similar to the constrained path configurations in figure 5, contributing to the fermionic two-point function (a) for $x_1 > x_2$ and (b) the same configuration for $x_2 > x_1$ on a $L_t = 8$ lattice. The additional variables are marked with a $\bigcirc$ for ψ_{x_1} and a $\times$ for $\overline{\psi}_{x_2}$.

$M(\phi)$ into the bosonic integration for each of these sites, so one eventually obtains

$$\langle\!\langle \psi_y \overline{\psi}_y \rangle\!\rangle_0 = \sum_{\mathcal{C}\subset\mathcal{G}^f} \prod_x \left(\prod_i \frac{w_i^{n_i^b(x)}}{n_i^b(x)!} \right) \left[\prod_{x\neq y} Q_0(N(x)) \right] \cdot Q_1(N(y)) \tag{94}$$

$$= \sum_{\mathcal{C}\subset\mathcal{G}^f} \frac{Q_1(N(y))}{Q_0(N(y))} W_0(\mathcal{C}) \tag{95}$$

$$= \langle\!\langle \frac{Q_1(N(y))}{Q_0(N(y))} \rangle\!\rangle_0 \,. \tag{96}$$

If the additional fermionic variables are not at the same site, $x_1 \neq x_2$, source and sink can only be paired with the ending of a fermionic bond. Keeping in mind that the fermionic bonds are directed, it is straightforward to see that one needs $(x_1 - x_2) \bmod L_t$ of these bonds to connect the source with the sink, thus forming an open fermionic string. This is illustrated in figure 7 where we show two typical bond configurations using the symbols $\bigcirc$ and $\times$ to denote the sink ψ_{x_1} and the source $\overline{\psi}_{x_2}$, respectively. It is clear that each site along the open fermion string is automatically saturated by the variables of one ingoing and one outgoing fermionic bond. Those sites and the ones which are saturated with either the source or the sink and a fermionic bond attached to it yield a factor 1 as the fermion contribution to the bosonic integration, while all other sites contribute with the monomer weight $M(\phi)$.

Because the fermionic bonds are directed, the order of the source and the sink matters and we need to distinguish between the cases $x_2 > x_1$ and $x_1 > x_2$. For $x_2 > x_1$, the open string connects source and sink without crossing the boundary and each configuration is characterised by the numbers

$$n^f(x) = \begin{cases} 1 & \text{if } x_2 \leq x < x_1, \\ 0 & \text{else,} \end{cases} \tag{97}$$

$$m(x) = \begin{cases} 0 & \text{if } x_2 \leq x \leq x_1, \\ 1 & \text{else,} \end{cases} \tag{98}$$

while for $x_1 < x_2$, the fermionic string crosses the boundary and the numbers to characterise

the configuration are given by

$$n^f(x) = \begin{cases} 0 & \text{if } x_1 \le x < x_2, \\ 1 & \text{else,} \end{cases} \tag{99}$$

$$m(x) = \begin{cases} 1 & \text{if } x_1 < x < x_2, \\ 0 & \text{else.} \end{cases} \tag{100}$$

Whether or not the open fermionic string crosses the boundary of the lattice is relevant for the overall sign of the configuration. Namely, the crossing yields one extra factor of (-1) for antiperiodic boundary conditions, and this has to be taken into account in the overall book keeping for the 2-point function.

We are now able to give an explicit expression for the weight of an open fermion string configuration in $\mathcal{G}^f$ contributing to $C^f(x_1 - x_2)$. Each site x_i contributing a factor 1 to the bosonic integration amounts to a site weight $Q_1(N(x_i))$, while a site x_j contributing the monomer weight $M(\phi_{x_j})$ to the bosonic integration yields a site weight $Q_0(N(x_j))$. To simplify the notation we define the set $\mathcal{F}$ of lattice sites belonging to the open fermion string as

$$\mathcal{F}(x_1, x_2) = \begin{cases} \{x \in \Lambda \mid x_2 \le x \le x_1\} & \text{if } x_2 \le x_1, \\ \{x \in \Lambda \mid x \le x_1 \cup x \ge x_2\} & \text{if } x_1 < x_2. \end{cases} \tag{101}$$

The weight of a configuration contributing to $\mathcal{G}^f$ can then be written as

$$W_{\mathcal{G}^f} = \prod_x \left(\prod_i \frac{w_i^{n_i^b(x)}}{n_i^b(x)!} \right) \left[\prod_{x \in \mathcal{F}} Q_1(N(x)) \right] \left[\prod_{x \notin \mathcal{F}} Q_0(N(x)) \right], \tag{102}$$

and the non-normalised expectation value of the fermionic two-point function is

$$\langle\!\langle \psi_{x_1} \overline{\psi}_{x_2} \rangle\!\rangle_0 = \sum_{\mathcal{C} \subset \mathcal{G}^f} W_{\mathcal{G}^f}(\mathcal{C}) \tag{103}$$

$$= \sum_{\mathcal{C} \subset \mathcal{G}^f} \left[\prod_{x \in \mathcal{F}} \frac{Q_1(N(x))}{Q_0(N(x))} \right] \cdot W_0(\mathcal{C}) \tag{104}$$

$$= \langle\!\langle \prod_{x \in \mathcal{F}} \frac{Q_1(N(x))}{Q_0(N(x))} \rangle\!\rangle_0 . \tag{105}$$

This result implies that the configuration space $\mathcal{G}^f$ does not decompose into the bosonic and fermionic sector $F = 0$ and $F = 1$. Rather, all configurations in the configuration space of fermionic two point functions are associated with the bosonic sector. In a way, the configuration space $\mathcal{G}^f$ mediates between the bosonic and the fermionic sectors $\mathcal{Z}_0$ and $\mathcal{Z}_1$. The transition from one configuration space to another is induced by adding or removing the additional field variables $\overline{\psi}\psi$. The relation between the various bond configuration spaces is schematically illustrated in figure 8. The picture suggests to interpret the fermionic correlation function $C^f(x-y)$ as an open fermion string on the background of bosonic bond configurations in sector $\mathcal{Z}_0$, or as an open antifermion string on the background of bond configurations in sector $\mathcal{Z}_1$, i.e., as a antifermionic correlation function $-C^{\overline{f}}(y-x)$. It is this property which forms the basis for an efficient simulation algorithm which will be discussed in detail in the third paper of this series [44].

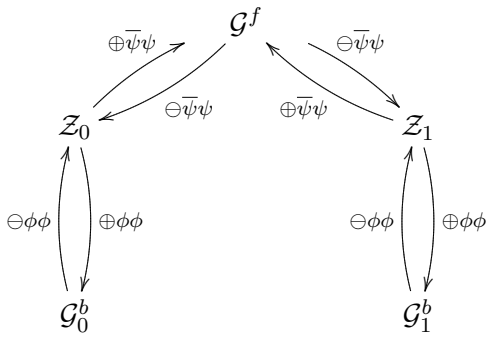

Figure 8: Schematic representation of the configuration spaces. The configuration space $\mathcal{G}^f \equiv \mathcal{G}_0^f = \mathcal{G}_1^{\overline{f}}$ mediates between the bosonic and the fermionic sector. By the symbols $\oplus$ and $\ominus$, we denote the addition and removal of the source and sink field variables, respectively.

Finally, the reformulation of the fermionic correlation functions in terms of bond variables can be generalised to include more complicated fermionic source and sink operators such as $\psi_x\phi_x^k$ or $\overline{\psi}_x\phi_x^k$. The construction is rather straightforward and yields

$$\langle\!\langle \psi_{x_1}\phi_{x_1}^k \cdot \overline{\psi}_{x_2}\phi_{x_2}^l \rangle\!\rangle_0 = \sum_{\mathcal{C}\subset\mathcal{G}^f} \left[\prod_{x\in\mathcal{F}} \frac{Q_1(N(x) + k\cdot\delta_{x,x_1} + l\cdot\delta_{x,x_2})}{Q_0(N(x))} \right] \cdot W_0(\mathcal{C}) \tag{106}$$

$$= \langle\!\langle \prod_{x\in\mathcal{F}} \frac{Q_1(N(x))}{Q_0(N(x))} \rangle\!\rangle_0 \,, \tag{107}$$

i.e., only the site occupation numbers at site x_1 and x_2 are modified accordingly. Similarly to the discussion concerning the bosonic n-point correlation function, operators with different quantum numbers, for example the parity for actions symmetric under $\phi \to -\phi$, do not mix if the symmetry is intact, e.g. $\langle \psi_{x_1}\phi_{x_1}^2 \cdot \overline{\psi}_{x_2}\phi_{x_2}\rangle = 0$. It is again easy to see that this property is strictly enforced through the constraints $N(x) \bmod 2 = 0$ for parity symmetric actions.

5 Conclusions

Simulations of supersymmetric models on the lattice with (spontaneously) broken supersymmetry suffer from a fermion sign problem related to the vanishing of the Witten index. This problem is a generic one and must occur whenever a massless Goldstino mode is present in the system. In this paper we discussed a novel approach which solves this problem for $\mathcal{N} = 2$ supersymmetric quantum mechanics by formulating its Euclidean path integral on the lattice in terms of fermion loops. The formulation is based on the exact hopping expansion of the fermionic action and allows the explicit decomposition of the partition function into a bosonic and a fermionic sector associated with the corresponding vacua. Since the two vacua contribute with opposite signs, the separation isolates the cause of the sign problem and opens the way for its solution. In fact, the explicit separation of the sectors in the fermion loop formulation allows the construction of a simulation algorithm which samples these sectors separately, and more importantly also samples the relative weights between them. We demonstrate in the third paper of this series [44] that in this way, the loop formulation indeed provides a solution to the fermion sign problem. The solution is not resctricted to the

quantum mechanics case, but it is in fact also applicable in higher dimensions. In particular, it also applies to the supersymmetric $\mathcal{N} = 1$ Wess-Zumino model [34], where the formulation has proven to sucessfully solve the fermion sign problem.

In addition to the sign problem, in this paper we have discussed various discretisation schemes for regularising $\mathcal{N} = 2$ supersymmetric quantum mechanics on the lattice using Wilson fermions. Because the lattice formulations break supersymmetry explicitly, special care has to be taken to guarantee the restoration of the supersymmetries in the continuum limit. A very straightforward discretisation for example requires the addition of a single counterterm which compensates certain perturbative loop corrections. We demonstrate explicitly by means of the boson and fermion mass spectra how the absence of such a term spoils the correct continuum limit. Another discretisation is based on the insertion of the Wilson term directly in the superpotential. This construction leads to the Q-exact discretisation which maintains one of the two supersymmetries exactly at finite lattice spacing. This eventually guarantees the automatic restoration of the full supersymmetries in the continuum.

For both discretisation schemes, in addition to the fermion loop reformulation, we have reformulated the quantum mechanics system on the lattice in terms of bosonic bonds. As in the fermionic case, the formulation is based on the exact hopping expansion of the bosonic actions. The bosonic bond formulation is not a necessary ingredient in the solution of the fermion sign problem, but completes the description of the quantum mechanical system in terms of solely discrete variables. In fact, while the fermion loop formulation is not affected by the choice of discretisation, the bond formulation is and in general requires arbitrary types of bonds beyond the simple one. We have discussed in detail how the simple bosonic bond formulation needs to be adapted in order to accommodate more complicated discretisations, such as the Q-exact one, as well as arbitrary superpotentials.

Furthermore, we also derived explicit expressions for various observables in the bond formulation, such as moments of the bosonic field, bosonic n-point correlation functions, and fermionic 2-point functions with arbitrary fermionic operators. For the latter we emphasised its interpretation as an open fermion string. In addition, we argued that the fermion correlator in the bosonic vacuum can equally well be interpreted as the antifermion correlator in the fermionic vacuum. More importantly, however, is the fact that the configurations including the open fermion string represent the configuration space mediating between the bosonic and fermionic configuration spaces. This eventually forms the basis for the efficient simulation algorithm discussed in paper three of this series [44].

Finally, as an outlook, we point out that using the bond formulation it is straightforward to construct transfer matrices separately for the bosonic and fermionic sector. They allow in turn to solve the lattice system exactly. This construction and the subsequent solution will be the subject of the second paper in this series [37].

A Summary of the discretisations

In this appendix, we write out explicitly the actions for which we discussed in detail the derivation of the loop formulation. The generic lattice actions are given by eqs.(20), (24) and

(27),

$$S_L = \sum_x \left\{ \frac{1}{2}(\nabla^- \phi_x)^2 + \frac{1}{2} P'(\phi_x)^2 + \overline{\psi}_x (\nabla^- + P''(\phi_x))\psi_x \right\}, \tag{108}$$

$$S_L^c = S_L + \frac{1}{2}\sum_x P''(\phi_x)\,, \tag{109}$$

$$S_L^Q = S_L + \sum_x P'(\phi_x)(\nabla^- \phi_x)\,. \tag{110}$$

For the polynomial superpotentials discussed in this paper the resulting bosonic self-interaction $V(\phi)$ and the fermionic monomer term $M(\phi)$ can be described by

$$V(\phi) = \sum_{n=1}^{6} k_n \phi^n, \qquad M(\phi) = \sum_{n=0}^{2} m_n \phi^n. \tag{111}$$

The weights of the directed bosonic bonds are given by $w_{1\to n}$, where n indicates the number of bosonic sources carried at the right ending of the specific bond. In the following we explicitly write out the actions and tabulate the coefficients k_n and m_n as well as the bond weights $w_{1\to n}$ for the two superpotentials

$$P_u(\phi) = \frac{1}{2}\mu\phi^2 + \frac{1}{4} g\phi^4, \tag{112}$$

$$P_b(\phi) = -\frac{\mu^2}{4\lambda}\phi + \frac{1}{3}\lambda\phi^3, \tag{113}$$

which yield systems with unbroken and broken supersymmetry, respectively.

A.1 The actions for the superpotential P_u

Writing out explicitly the actions for the superpotential P_u, we have

$$\begin{aligned} S_L = \sum_x \Big\{ & \frac{1}{2}\left(2+\mu^2\right)\phi_x^2 + \mu g \phi_x^4 + \frac{1}{2} g^2 \phi_x^6 - \phi_x \phi_{x-1} \\ & + \left(1+\mu+3g\phi_x^2\right)\overline{\psi}_x\psi_x - \overline{\psi}_x\psi_{x-1} \Big\}, \end{aligned} \tag{114}$$

$$\begin{aligned} S_L^c = \sum_x \Big\{ & \frac{1}{2}\left(2+\mu^2+3g\right)\phi_x^2 + \mu g \phi_x^4 + \frac{1}{2} g^2 \phi_x^6 - \phi_x \phi_{x-1} \\ & + \left(1+\mu+3g\phi_x^2\right)\overline{\psi}_x\psi_x - \overline{\psi}_x\psi_{x-1} \Big\}, \end{aligned} \tag{115}$$

$$\begin{aligned} S_L^Q = \sum_x \Big\{ & \frac{1}{2}\left(2+2\mu+\mu^2\right)\phi_x^2 + g(\mu+1)\phi_x^4 + \frac{1}{2} g^2 \phi_x^6 - g\phi_x^3\phi_{x-1} \\ & - (1+\mu)\,\phi_x\phi_{x-1} + \left(1+\mu+3g\phi_x^2\right)\overline{\psi}_x\psi_x - \overline{\psi}_x\psi_{x-1} \Big\}, \end{aligned} \tag{116}$$

and the coefficients and hopping weights can directly be read off. They are compiled in table 1.

	S_L	S_L^c	S_L^Q
k_1	0	0	0
k_2	$1+\frac{1}{2}\mu^2$	$1+\frac{1}{2}\mu^2+\frac{3}{2}g$	$1+\mu+\frac{1}{2}\mu^2$
k_3	0	0	0
k_4	μg	μg	$g(1+\mu)$
k_5	0	0	0
k_6	$\frac{1}{2}g^2$	$\frac{1}{2}g^2$	$\frac{1}{2}g^2$
$w_{1\to 1}$	1	1	$1+\mu$
$w_{1\to 3}$	0	0	g
m_0	$1+\mu$	$1+\mu$	$1+\mu$
m_1	0	0	0
m_2	$3g$	$3g$	$3g$

Table 1: Unbroken supersymmetric quantum mechanics: coefficients and hopping weights for the superpotential $P_u(\phi)=\frac{1}{2}\mu\phi^2+\frac{1}{4}g\phi^4$.

A.2 The actions for the superpotential P_b

So far we have concentrated on the superpotential with broken supersymmetry of the form

$$P_b(\phi)=-\frac{\mu^2}{4\lambda}\phi+\frac{1}{3}\lambda\phi^3, \tag{117}$$

yielding a potential for the bosonic field which is symmetric under the parity transformation $\phi\to-\phi$. Writing out explicitly the actions for this superpotential we obtain

$$\begin{aligned} S_L &= \sum_x \Big\{\frac{1}{2}\left(2-\frac{\mu^2}{2}\right)\phi_x^2+\frac{1}{2}\lambda^2\phi_x^4-\phi_x\phi_{x-1} \\ &\qquad +\left(1+2\lambda\phi_x^2\right)\overline{\psi}_x\psi_x-\overline{\psi}_x\psi_{x-1}\Big\}, \qquad (118)\\ S_L^c &= \sum_x \Big\{\lambda\phi_x+\frac{1}{2}\left(2-\frac{\mu^2}{2}\right)\phi_x^2+\frac{1}{2}\lambda^2\phi_x^4-\phi_x\phi_{x-1} \\ &\qquad +\left(1+2\lambda\phi_x^2\right)\overline{\psi}_x\psi_x-\overline{\psi}_x\psi_{x-1}\Big\}, \qquad (119)\\ S_L^Q &= \sum_x \Big\{\frac{1}{2}\left(2-\frac{\mu^2}{2}\right)\phi_x^2+\lambda\phi_x^3+\frac{1}{2}\lambda^2\phi_x^4-\lambda\phi_x^2\phi_{x-1} \\ &\qquad -\phi_x\phi_{x-1}+\left(1+2\lambda\phi_x^2\right)\overline{\psi}_x\psi_x-\overline{\psi}_x\psi_{x-1}\Big\}, \qquad (120) \end{aligned}$$

and the corresponding coefficients and hopping weights are given in table 2.

	S_L	S_L^c	S_L^Q
k_1	0	λ	0
k_2	$\frac{1}{4}(4-\mu^2)$	$\frac{1}{4}(4-\mu^2)$	$\frac{1}{4}(4-\mu^2)$
k_3	0	0	λ
k_4	$\frac{1}{2}\lambda^2$	$\frac{1}{2}\lambda^2$	$\frac{1}{2}\lambda^2$
k_5	0	0	0
k_6	0	0	0
$w_{1\to1}$	1	1	1
$w_{1\to2}$	0	0	λ
m_0	1	1	1
m_1	2λ	2λ	2λ
m_2	0	0	0

Table 2: Broken supersymmetric quantum mechanics: coefficients and hopping weights for the superpotential $P_b(\phi) = -\frac{\mu^2}{4\lambda}\phi + \frac{1}{3}\lambda\phi^3$.

In order to apply perturbation theory it is more useful to consider the shifted superpotential

$$P_b(\phi) = \frac{1}{2}\mu\phi^2 + \frac{1}{3}\lambda\phi^3 \tag{121}$$

which is obtained from eq.(117) by applying the shift $\phi \to \phi + \mu/2\lambda$ and neglecting any constant terms. The potential for the bosonic field then has a minimum at $\phi = 0$, but the parity symmetry is no longer manifest. Writing out explicitly the actions for this form of the superpotential P_b, we have

$$\begin{aligned} S_L &= \sum_x \Big\{ \frac{1}{2}\left(2+\mu^2\right)\phi_x^2 + \mu\lambda\phi_x^3 + \frac{1}{2}\lambda^2\phi_x^4 - \phi_x\phi_{x-1} \\ &\qquad + \left(1+\mu+2\lambda\phi_x^2\right)\overline{\psi}_x\psi_x - \overline{\psi}_x\psi_{x-1}\Big\}, \end{aligned} \tag{122}$$

$$\begin{aligned} S_L^c &= \sum_x \Big\{ \lambda\phi_x + \frac{1}{2}\left(2+\mu^2\right)\phi_x^2 + \mu\lambda\phi_x^3 + \frac{1}{2}\lambda^2\phi_x^4 - \phi_x\phi_{x-1} \\ &\qquad + \left(1+\mu+2\lambda\phi_x^2\right)\overline{\psi}_x\psi_x - \overline{\psi}_x\psi_{x-1}\Big\}, \end{aligned} \tag{123}$$

$$\begin{aligned} S_L^Q &= \sum_x \Big\{ \frac{1}{2}\left(2+2\mu+\mu^2\right)\phi_x^2 + \lambda(\mu+1)\phi_x^3 + \frac{1}{2}\lambda^2\phi_x^4 - \lambda\phi_x^2\phi_{x-1} \\ &\qquad - (1+\mu)\,\phi_x\phi_{x-1} + \left(1+\mu+2\lambda\phi_x^2\right)\overline{\psi}_x\psi_x - \overline{\psi}_x\psi_{x-1}\Big\}, \end{aligned} \tag{124}$$

and the corresponding coefficients and hopping weights are given in table 3.

References

[1] L. O'Raifeartaigh, *Spontaneous symmetry breaking for chirals scalar superfields*, *Nuclear Physics* **B96** (1975), no. 2 331 – 352.

[2] I. Montvay, *Supersymmetric gauge theories on the lattice*, *Nucl.Phys.Proc.Suppl.* **53** (1997) 853–855, [hep-lat/9607035].

	S_L	S_L^c	S_L^Q
k_1	0	λ	0
k_2	$\frac{1}{2}(2+\mu^2)$	$\frac{1}{2}(2+\mu^2)$	$\frac{1}{2}(2+2\mu+\mu^2)$
k_3	$\mu\lambda$	$\mu\lambda$	$(1+\mu)\lambda$
k_4	$\frac{1}{2}\lambda^2$	$\frac{1}{2}\lambda^2$	$\frac{1}{2}\lambda^2$
k_5	0	0	0
k_6	0	0	0
$w_{1\to 1}$	1	1	$1+\mu$
$w_{1\to 2}$	0	0	λ
m_0	$1+\mu$	$1+\mu$	$1+\mu$
m_1	2λ	2λ	2λ
m_2	0	0	0

Table 3: Broken supersymmetric quantum mechanics: coefficients and hopping weights for the superpotential $P_b(\phi) = \frac{1}{2}\mu\phi^2 + \frac{1}{3}\lambda\phi^3$.

[3] A. Feo, *Predictions and recent results in SUSY on the lattice*, *Mod.Phys.Lett.* **A19** (2004) 2387–2402, [hep-lat/0410012].

[4] J. Giedt, *Deconstruction and other approaches to supersymmetric lattice field theories*, *Int.J.Mod.Phys.* **A21** (2006) 3039–3094, [hep-lat/0602007].

[5] D. B. Kaplan, E. Katz, and M. Unsal, *Supersymmetry on a spatial lattice*, *JHEP* **0305** (2003) 037, [hep-lat/0206019].

[6] T. Takimi, *Relationship between various supersymmetric lattice models*, *JHEP* **0707** (2007) 010, [arXiv:0705.3831].

[7] P. H. Damgaard and S. Matsuura, *Lattice Supersymmetry: Equivalence between the Link Approach and Orbifolding*, *JHEP* **0709** (2007) 097, [arXiv:0708.4129].

[8] S. Catterall, *From Twisted Supersymmetry to Orbifold Lattices*, *JHEP* **0801** (2008) 048, [arXiv:0712.2532].

[9] S. Catterall, D. B. Kaplan, and M. Unsal, *Exact lattice supersymmetry*, *Phys.Rept.* **484** (2009) 71–130, [arXiv:0903.4881].

[10] J. Bartels and G. Kramer, *A lattice version of the Wess-Zumino model*, *Zeitschrift für Physik C Particles and Fields* **20** (1983) 159–170.

[11] P. H. Dondi and H. Nicolai, *Lattice supersymmetry*, *Nuovo Cim* **A41** (1977) 1.

[12] K. Fujikawa, *Supersymmetry on the lattice and the Leibniz rule*, *Nucl.Phys.* **B636** (2002) 80–98, [hep-th/0205095].

[13] F. Bruckmann and M. de Kok, *Noncommutativity approach to supersymmetry on the lattice: SUSY quantum mechanics and an inconsistency*, *Phys.Rev.* **D73** (2006) 074511, [hep-lat/0603003].

[14] J. Giedt and E. Poppitz, *Lattice supersymmetry, superfields and renormalization*, *JHEP* **0409** (2004) 029, [hep-th/0407135].

[15] J. Giedt, R. Koniuk, E. Poppitz, and T. Yavin, *Less naive about supersymmetric lattice quantum mechanics*, *JHEP* **0412** (2004) 033, [hep-lat/0410041].

[16] J. Wosiek, *Spectra of supersymmetric Yang-Mills quantum mechanics*, *Nucl.Phys.* **B644** (2002) 85–112, [hep-th/0203116].

[17] J. Wosiek, *Supersymmetric Yang-Mills quantum mechanics in various dimensions*, *Int.J.Mod.Phys.* **A20** (2005) 4484–4491, [hep-th/0410066].

[18] M. Campostrini and J. Wosiek, *Exact Witten index in $D = 2$ supersymmetric Yang-Mills quantum mechanics*, *Phys.Lett.* **B550** (2002) 121–127, [hep-th/0209140].

[19] S. Catterall and E. Gregory, *A Lattice path integral for supersymmetric quantum mechanics*, *Phys.Lett.* **B487** (2000) 349–356, [hep-lat/0006013].

[20] S. Catterall, *Twisted lattice supersymmetry and applications to AdS/CFT*, *PoS* **LATTICE2010** (2010) 002, [arXiv:1010.6224].

[21] M. Beccaria, G. Curci, and E. D'Ambrosio, *Simulation of supersymmetric models with a local Nicolai map*, *Phys.Rev.* **D58** (1998) 065009, [hep-lat/9804010].

[22] G. Bergner, T. Kaestner, S. Uhlmann, and A. Wipf, *Low-dimensional Supersymmetric Lattice Models*, *Annals Phys.* **323** (2008) 946–988, [arXiv:0705.2212].

[23] T. Kaestner, G. Bergner, S. Uhlmann, A. Wipf, and C. Wozar, *Supersymmetric lattice models in one and two dimensions*, *PoS* **LAT2007** (2007) 265, [arXiv:0709.0822].

[24] G. Bergner, *Complete supersymmetry on the lattice and a No-Go theorem*, *JHEP* **1001** (2010) 024, [arXiv:0909.4791].

[25] I. Kanamori, F. Sugino, and H. Suzuki, *Observing dynamical supersymmetry breaking with Euclidean lattice simulations*, *Prog.Theor.Phys.* **119** (2008) 797–827, [arXiv:0711.2132].

[26] I. Kanamori, H. Suzuki, and F. Sugino, *Euclidean lattice simulation for dynamical supersymmetry breaking*, *Phys.Rev.* **D77** (2008) 091502, [arXiv:0711.2099].

[27] C. Wozar and A. Wipf, *Supersymmetry breaking in low dimensional models*, *Annals Phys.* **327** (2012) 774–807, [arXiv:1107.3324].

[28] N. V. Prokof'ev and B. V. Svistunov, *Worm algorithms for classical statistical models*, *Phys.Rev.Lett.* **87** (2001) 160601, [cond-mat/0103146].

[29] U. Wenger, *Efficient simulation of relativistic fermions via vertex models*, *Phys.Rev.* **D80** (2009) 071503, [arXiv:0812.3565].

[30] K. Steinhauer and U. Wenger, *Loop formulation of supersymmetric Yang-Mills quantum mechanics*, *JHEP* **1412** (2014) 044, [arXiv:1410.0235].

[31] D. Baumgartner and U. Wenger, *Simulation of supersymmetric models on the lattice without a sign problem*, *PoS* **LAT2010** (2011) [arXiv:1104.0213].

[32] D. Baumgartner, K. Steinhauer, and U. Wenger, *Supersymmetry breaking on the lattice: the N=1 Wess-Zumino model*, *PoS* **LATTICE2011** (2011) 253, [arXiv:1111.6042].

[33] D. Baumgartner, K. Steinhauer, and U. Wenger, *Spontaneous supersymmetry breaking in the 2d N=1 Wess-Zumino model*, *PoS* **LATTICE2012** (2012) 043, [arXiv:1311.5089].

[34] K. Steinhauer and U. Wenger, *Spontaneous supersymmetry breaking in the two-dimensional N=1 Wess-Zumino model*, *Phys.Rev.Lett.* **113** (2014) 231601, [arXiv:1410.6665].

[35] K. Steinhauer and U. Wenger, *Loop formulation of the supersymmetric nonlinear O(N) sigma model*, *PoS* **LATTICE2013** (2013) 092, [arXiv:1311.5403].

[36] M. Creutz and B. Freedman, *A statistical approach to quantum mechanics*, *Annals of Physics* **132** (1981), no. 2 427 – 462.

[37] D. Baumgartner and U. Wenger, *Supersymmetric quantum mechanics on the lattice: II. Exact results*.

[38] S. Catterall, *Lattice supersymmetry and topological field theory*, *JHEP* **0305** (2003) 038, [hep-lat/0301028].

[39] E. Gozzi, *Functional-integral approach to Parisi-Wu stochastic quantization: Scalar theory*, *Phys.Rev.* **D28** (Oct, 1983) 1922–1930.

[40] F. Cooper, A. Khare, and U. Sukhatme, *Supersymmetry and quantum mechanics*, *Phys.Rept.* **251** (1995) 267–385, [hep-th/9405029].

[41] E. Witten, *Constraints on Supersymmetry Breaking*, *Nucl.Phys.* **B202** (1982) 253.

[42] H. Ezawa and J. R. Klauder, *Fermions without fermions*, *Progress of Theoretical Physics* **74** (1985), no. 4 904–915.

[43] U. Wenger, *Simulating Wilson fermions without critical slowing down*, *PoS* **LAT2009** (2009) 022, [arXiv:0911.4099].

[44] D. Baumgartner and U. Wenger, *Supersymmetric quantum mechanics on the lattice: III. Algorithms and simulations*.

[45] U. Wolff, *Cluster simulation of relativistic fermions in two space-time dimensions*, *Nucl.Phys.* **B789** (2008) 258–276, [arXiv:0707.2872].

Paper 7

Supersymmetric quantum mechanics on the lattice: II. Exact results

David Baumgartner and Urs Wenger, to be submitted to Nucl. Phys. **B**

Supersymmetric quantum mechanics on the lattice: II. Exact results

David Baumgartner and Urs Wenger

Albert Einstein Center for Fundamental Physics,
Institute for Theoretical Physics, University of Bern,
Sidlerstrasse 5, CH–3012 Bern, Switzerland

Abstract

Simulations of supersymmetric field theories with spontaneously broken supersymmetry require in addition to the ultraviolet regularisation also an infrared one, due to the emergence of the massless Goldstino. The intricate interplay between ultraviolet and infrared effects towards the continuum and infinite volume limit demands careful investigations to avoid potential problems. In this paper – the second in a series of three – we present such an investigation for $\mathcal{N} = 2$ supersymmetric quantum mechanics formulated on the lattice in terms of bosonic and fermionic bonds. In one dimension, the bond formulation allows to solve the system exactly, even at finite lattice spacing, through the construction and analysis of transfer matrices. In the present paper we elaborate on this approach and discuss a range of exact results for observables such as the Witten index, the mass spectra and Ward identities.

1 Introduction

Regularising supersymmetric quantum field theories on a lattice in order to investigate their nonperturbative properties remains to be a challenging and demanding task. Besides the fact that the discreteness of the space-time lattice explicitly breaks the Poincaré symmetry, and hence supersymmetry itself, it can also be broken by specific choices of the boundary conditions, in particular also by the finite temperature. As a consequence, the effects from the ultraviolet and infrared lattice regularisation are sometimes difficult to separate from each other. In addition, the restoration of supersymmetry in the continuum and infinite volume limit is in general a delicate process which requires careful finetuning or highly involved discretisation schemes, both of which are sometimes difficult to control. For these reasons a complete and thorough understanding of the intricate interplay between infrared and ultraviolet effects, when removing the corresponding lattice regulators, is a crucial prerequisite for any investigation of supersymmetric field theories on the lattice.

Supersymmetric quantum mechanics is a simple system which nevertheless contains many of the important ingredients characterising supersymmetric field theories. Moreover, in the path integral formalism the system differs little from field theories in higher dimensions and it is sufficiently involved to show similar complexity and complications. Hence, supersymmetric

quantum mechanics provides an adequate playground to address all the delicate questions and issues mentioned above. In this paper – the second in a series of three – we present exact results for $\mathcal{N} = 2$ supersymmetric quantum mechanics discretised on the lattice using the bond formulation. This formulation is based on the hopping expansion of the original bosonic and fermionic degrees of freedom and is described in detail in the first paper of our series [1]. For the fermions the bond formulation is more appropriately termed fermion loop formulation since the fermionic bond configurations turn out to be closed fermionic loops. In the case of $\mathcal{N} = 2$ supersymmetric quantum mechanics the fermion loop formulation is particularly simple, since there are only two different fermion loop configurations, namely one containing exactly one fermion loop winding around the lattice in temporal direction, and one without any fermion loop. The latter corresponds to the bosonic sector with fermion number $F = 0$ and the former to the fermionic sector with $F = 1$. This separation into the canonical sectors with fixed fermion number forms the basis for the solution of the fermion sign problem emerging in numerical Monte Carlo simulations of the quantum mechanical system with broken supersymmetry. For a detailed discussion of this issue we refer to our first paper in our series [1].

In the present paper we make use of the fact that in the bond formulation the weights of the bond configurations are completely localised and the local bond configuration states can be enumerated locally due to the discreteness of the new degrees of freedom. It is hence straightforward to construct a transfer matrix which in turn can be used to express the sum over all bond configurations, i.e., the partition function, as the trace over an appropriate product of the transfer matrix. As a consequence of the natural separation into bosonic and fermionic contributions the transfer matrix block diagonalises naturally into blocks with fixed fermion number, and this simplifies the calculations considerably. Since the transfer matrices do not depend on the imaginary time coordinate, they contain all the physics of the system. It is therefore sufficient to understand the spectral properties of the transfer matrices and calculate physical observables such as the mass gaps directly from the eigenvalues of the transfer matrices. More complicated observables such as correlation functions and Ward identities can be calculated exactly using modified transfer matrices.

As discussed above, the exact results at finite lattice spacing are most useful to gain a better understanding of the interplay between the various limits required in any lattice calculation, not restricted to supersymmetric quantum mechanics, in order to remove the infrared and ultraviolet regulators. In particular, we can study in detail how and under which circumstances supersymmetry is restored in the continuum and thermodynamic limit, and how, in the case of broken supersymmetry, the Goldstino mode emerges.

The outline of the paper is as follows. In section 2, we derive explicitly the construction of the transfer matrices for supersymmetric quantum mechanics starting from the bond formulation of the lattice system. We then work out the calculation of various observables such as correlation functions in 2.2, the mass gaps from the eigenvalues of the transfer matrices in 2.3, and discuss some Ward identities which may be used to investigate the restoration of supersymmetry in the continuum in 2.4. After these technical considerations, we present our exact results in section 3 for various observables of interest, such as the Witten index in 3.1 and correlation functions in 3.2. In addition, we demonstrate in detail how the supersymmetry is recovered in the continuum by means of energy spectra in 3.3 and Ward identities in 3.4, and finally present an exact calculation of the ground state energy in 3.5. For each quantity we discuss in turn the results using the standard discretisation including the counterterm

[2, 3] and the results for the Q-exact action [4]. We do so as far as possible for systems with unbroken and broken supersymmetry. Finally, in section 4 we summarise our results and close with some conclusions, while in appendix A we provide some technical details concerning the numerical calculation of the transfer matrices.

2 The transfer matrix approach

In order to introduce the notation we briefly recall the Euclidean action for supersymmetric quantum mechanics involving the bosonic field ϕ and the fermionic fields $\overline{\psi}$ and ψ,

$$S(\phi,\overline{\psi},\psi)=\int_0^\beta dt\left\{\frac{1}{2}\left(\frac{d\phi(t)}{dt}\right)^2+\frac{1}{2}P'(\phi(t))^2+\overline{\psi}(t)\left(\partial_t+P''(\phi(t))\right)\psi(t)\right\}. \tag{1}$$

The action depends on the superpotential $P(\phi)$ and is invariant under the two supersymmetry transformations

$$\begin{array}{lcllcl}\delta_1\phi &=& \overline{\epsilon}\psi, & \delta_2\phi &=& \overline{\psi}\epsilon,\\ \delta_1\psi &=& 0, & \delta_2\psi &=& \left(\dot{\phi}-P'\right)\epsilon,\\ \delta_1\overline{\psi} &=& -\overline{\epsilon}\left(\dot{\phi}+P'\right), & \delta_2\overline{\psi} &=& 0.\end{array} \tag{2}$$

In our series of papers we use throughout the superpotential

$$P_u(\phi)=\frac{1}{2}\mu\phi^2+\frac{1}{4}g\phi^4 \tag{3}$$

as an example for unbroken supersymmetry with additional parity symmetry $\phi\to-\phi$ and

$$P_b(\phi)=-\frac{\mu^2}{4\lambda}\phi+\frac{1}{3}\lambda\phi^3 \tag{4}$$

for broken supersymmetry with additional combined parity and charge conjugation symmetry $\phi\to-\phi,\psi\to\overline{\psi},\overline{\psi}\to\psi$.

After choosing a suitable discretisation of the derivatives, supersymmetric quantum mechanics can be formulated on the lattice in terms of bosonic and fermionic bond occupation numbers $n_i^b(x)\in\mathbb{N}_0$ and $n^f(x)=0,1$, respectively, connecting sites x and $x+1$. We refer to our first paper [1] for further details and explanations. In particular, the partition function can be written as a sum over all allowed, possibly constrained, bond configurations $\mathcal{C}=\{n_i^b(x),n^f(x)\}$ in the configuration space $\mathcal{Z}$,

$$Z=\sum_{\mathcal{C}\subset\mathcal{Z}}W_F(\mathcal{C}) \tag{5}$$

where the weight $W_F(\mathcal{C})$ of a configuration is given by

$$W_F(\mathcal{C})=\prod_x\left(\prod_i\frac{w_i^{n_i^b(x)}}{n_i^b(x)!}\right)\prod_x Q_F(N(x))\,. \tag{6}$$

Here, w_i is the weight of a bosonic bond b_i with $i\in\{j\to k\,|\,j,k\in\mathbb{N}\}$, while $F=0,1$ is the fermion number determined by the fermionic bond configuration $\{n^f(x)\}$. The site weight Q_F is given by

$$Q_F(N(x))=\int_{-\infty}^{\infty}d\phi\;\phi^N(x)\mathrm{e}^{-V(\phi)}M(\phi)^{1-F} \tag{7}$$

where

$$N(x) = \sum_{j,k} \Big(j \cdot n^b_{j\to k}(x) + k \cdot n^b_{j\to k}(x-1) \Big) \tag{8}$$

is the site occupation number, i.e. the total number of bosonic bonds connected to site x. Finally, the potential $V(\phi)$ and the monomer term $M(\phi)$ in eq.(7) depend on the superpotential $P(\phi)$ and the specifics of the chosen discretisation.

2.1 Transfer matrices and partition functions

We now express the bond formulation of supersymmetric quantum mechanics on the lattice in terms of transfer matrices. For the construction we start by considering a bond configuration $\mathcal{C}$ in the configuration space $\mathcal{Z}$ contributing to the partition function Z. The degrees of freedom are now expressed by means of bond occupation numbers $\{n^b_i(x), n^f(x)\}$ for the bosonic and fermionic bonds. These bonds connect nearest neighbouring lattice sites and it is hence natural to define bond states associated with the bonds of the lattice. The states are characterised by the fermionic and bosonic bond occupation numbers and are hence written as $|n^f(x), \{n^b_i(x)\}\rangle$, where the coordinate x refers to the bond connecting the sites x and $x+1$. The transfer matrix $T(x)$ then describes the transition of the bond state at $x-1$ to the bond state at x. Since the fermionic occupation number n^f, and hence the fermion number F, is conserved at each site, the transfer matrix decomposes into block diagonal form, each block representing separately the bosonic and fermionic sector. So the separation of bond configurations in the bond formulation into the bosonic and fermionic sectors $\mathcal{Z}_0$ and $\mathcal{Z}_1$, respectively, reflects itself in the block structure of the transfer matrix, and from now on it is sufficient to discuss separately the submatrices $T^F(x)$ with fixed fermionic bond occupation number $n^f = F$.

In figure 1 we give two examples for the characterisation of the transfer matrix for a system with only one type of bosonic bond $b_{1\to 1}$ with corresponding occupation numbers $n^b_{1\to 1}$ (dashed lines) in each of the sectors $F = 0, 1$. The occupation of the fermionic bond is

(a) (b)

Figure 1: Graphical representation of the transfer matrix for a system with only one type of bosonic bond $b_{1\to 1}$ with occupation numbers $n^b_{1\to 1}$ (dashed lines). Figure (a) represents the entry $T^0_{2,4}$ of the transfer matrix in the bosonic sector and figure (b) shows the entry $T^1_{0,4}$ of the transfer matrix in the fermionic sector. The occupation of the fermionic bond is represented by the directed full line.

represented by the directed full line, cf. the first paper of our series [1] for further explanations on the graphical notation. In fact, since the characterisation of the set of states is independent of the coordinate x, it is sufficient to characterise the states just by $|n^f, \{n^b_i\}\rangle$ and hence the transfer matrix does not depend on x. As a consequence, the complete system for fixed fermion number F is characterised by just one transfer matrix and all the physical information on the system can be extracted from it. This is a rather remarkable property of the bond formulation and stems from the fact that the reformulation of the continuous degrees of freedom into discrete ones allows a complete and explicit enumeration of all states. However,

since there are no upper limits on the bosonic bond occupation numbers, the two matrices $T^F, F = 0, 1$ are infinitely large.

For a lattice consisting of L_t lattice points the partition function for both the fermionic and the bosonic sector can be calculated independently in terms of T^F as

$$Z_F = \mathrm{Tr}\left[\left(T^F\right)^{L_t}\right] \tag{9}$$

where the transfer matrix multiplications now sum over all possible bond configurations and the matching of the bond configurations at the boundary is ensured by taking the trace. After diagonalisation of the transfer matrices one can calculate the partition functions equivalently via the eigenvalues λ_k^F of T^F,

$$Z_F = \sum_k \left(\lambda_k^F\right)^{L_t}. \tag{10}$$

Eventually, the partition functions in the two sectors can then be combined as usual into partition functions with periodic and antiperiodic boundary conditions for the fermion as

$$Z_p = Z_0 - Z_1, \qquad Z_a = Z_0 + Z_1. \tag{11}$$

Let us now write down the transfer matrix elements connecting the incoming state $|F, \{m_i^b\}\rangle$ with the outgoing state $|F, \{n_i^b\}\rangle$. This is straightforwardly done by comparing eq.(9) with eq.(5) and (6). Explicitly, we have

$$T^F_{\{m_i^b\},\{n_i^b\}} = \sqrt{\prod_i \frac{w_i^{m_i^b}}{m_i^b!}\frac{w_i^{n_i^b}}{n_i^b!}}\; Q_F\left(N\right) \tag{12}$$

where the site occupation number is given by $N = \sum_{j,k}\left(j \cdot n^b_{j\to k} + k \cdot m^b_{j\to k}\right)$. Here we choose to distribute the contributions $w^n/n!$ from the incoming and outgoing bonds symmetrically, but in principle one could choose any distribution, e.g. taking into account only contributions from the forward bonds.

To be more concrete, we now specify the general expression for the transfer matrices in detail for the two discretisations discussed in detail in the first paper of our series [1] and for which we present exact results in this paper. The standard discretisation including the counterterm involves only one type of bosonic bond $b_{1\to1}$ carrying weight $w_{1\to1} = 1$ and the bond states can simply be labeled by the occupation number $n \equiv n^b_{1\to1}$. Explicitly, denoting the incoming state by $m \equiv m^b_{1\to1}$ and the outgoing by $n \equiv n^b_{1\to1}$ the transfer matrix can be written as

$$T^F_{m,n} = \sqrt{\frac{1}{m!\cdot n!}}\; Q_F\left(m+n\right). \tag{13}$$

For the Q-exact discretisation in addition to the bond $b_{1\to1}$ with weight $w_{1\to1}$ we have the new type of bond $b_{1\to\nu}$ with weight $w_{1\to\nu}$ where $\nu = 3$ for the superpotential P_u and $\nu = 2$ for the superpotential P_b. The explicit expressions for the weights are given in our first paper [1]. Labelling the incoming state by $m \equiv \{m^b_{1\to1}, m^b_{1\to\nu}\}$ and the outgoing by $n \equiv \{n^b_{1\to1}, n^b_{1\to\nu}\}$ we have

$$T^F_{m,n} = \sqrt{\frac{(w_{1\to1})^{m^b_{1\to1}+n^b_{1\to1}}}{(m^b_{1\to1}!)(n^b_{1\to1}!)}}\sqrt{\frac{(w_{1\to\nu})^{m^b_{1\to\nu}+n^b_{1\to\nu}}}{(m^b_{1\to\nu}!)(n^b_{1\to\nu}!)}}\; Q_F(N) \tag{14}$$

(a) (b)

Figure 2: Graphical representation of the bosonic transfer matrix at a site with additional bosonic sources. Figure (a) represents the matrix element $T^0_{2,4}(1)$ and figure (b) the matrix element $T^0_{2,4}(2)$ of a site with one and two additional sources, respectively.

where $N = n^b_{1\to 1} + n^b_{1\to\nu} + m^b_{1\to 1} + \nu \cdot m^b_{1\to\nu}$.

Before discussing how various observables can be expressed in terms of the transfer matrices or their eigenvalues, we need to emphasise that one faces several numerical challenges when constructing and evaluating the transfer matrices. Firstly, as already mentioned, the matrices have infinite extent due to the fact that the bosonic bond occupation numbers are not limited and in practice one therefore needs to truncate the state space. Since the bond occupation numbers introduce a natural ordering of the states, it is straightforward to choose a cutoff such that the results are not affected. We discuss the technical aspects of this procedure in detail in appendix A. Secondly, the evaluation of the site weights tends to become numerically unstable for large values of the site occupation number. We will deal with this numerical problem in detail in the third paper of our series [5].

2.2 Correlation functions

Next, we extend the concept of transfer matrices to the calculation of correlation functions. Recalling from our first paper how the two-point functions are calculated in the bond language, we realise that the transfer matrix approach provides a perfect tool for the exact calculation of the bosonic as well as the fermionic two-point function. We first consider the bosonic case. To get a contribution to the expectation value of $\langle \phi^j_{x_1} \phi^k_{x_2} \rangle$, we have to add additional bosonic field variables at the sites x_1 and x_2. The transfer matrices at these sites experience a corresponding modification and the graphical representation of the modified transfer matrix with additional bosonic sources is shown in figure 2 where we use the symbol $\bigcirc$ for each additional source. The additional variables affect the weight of the configuration via the occupation number $N(x) \to N(x) + j \cdot \delta_{x,x_1} + k \cdot \delta_{x,x_2}$. Thus, we introduce modified transfer matrices which allow for additional bosonic sources by defining

$$T^F_{\{m^b_i\},\{n^b_i\}}(k) \equiv T^F_{\{m^b_i\},\{n^b_i\}}(\phi^k) = \sqrt{\prod_i \frac{w_i^{m^b_i}}{m^b_i!} \frac{w_i^{n^b_i}}{n^b_i!}}\; Q_F\left(N + k\right) , \tag{15}$$

such that we can calculate the non-normalised expectation value of an arbitrary n-point correlation function by using the transfer matrices $T^F(k)$, i.e.,

$$\langle\!\langle \phi^{p_1}_{x_1} \dots \phi^{p_n}_{x_n} \rangle\!\rangle_F = \mathrm{Tr}\left[\prod_x T^F \left(\sum_i p_i \cdot \delta_{x,x_i} \right) \right] . \tag{16}$$

The originally defined transfer matrices in eq.(12) correspond to transfer matrices with no additional sources, $T^F(0) \equiv T^F$.

As a concrete example we now specify the non-normalised bosonic two-point correlation function $g_F^b(x_2 - x_1) = \langle\!\langle \phi_{x_1} \phi_{x_2} \rangle\!\rangle_F$. Defining $t = (x_2 - x_1) \bmod L_t$ and using translational invariance it reads

$$g_F^b(t) = \begin{cases} \mathrm{Tr}\left[T^F(1)\left(T^F(0)\right)^{t-1} T^F(1)\left(T^F(0)\right)^{L_t-t-1}\right] & \text{if } t \neq 0, \\ \mathrm{Tr}\left[T^F(2)\left(T^F(0)\right)^{L_t-1}\right] & \text{if } t = 0. \end{cases} \tag{17}$$

For the connected part of the bosonic correlation function we also need the expectation value of ϕ. From the previous considerations it is easy to see that the non-normalised expectation value for any moment of ϕ can be calculated as

$$\langle\!\langle \phi^p \rangle\!\rangle_F = \mathrm{Tr}\left[T^F(p)\left(T^F(0)\right)^{L_t-1}\right]. \tag{18}$$

Eventually, the connected part of the bosonic correlation function for each sector is given by

$$C_{0,1}^b(t) = \frac{g_{0,1}^b(t)}{Z_{0,1}} - \left(\frac{\langle\!\langle \phi \rangle\!\rangle_{0,1}}{Z_{0,1}}\right)^2, \tag{19}$$

while for periodic and antiperiodic boundary conditions it is calculated according to the discussion in our first paper [1], i.e.,

$$C_p^b(t) = \frac{g_0^b(t) - g_1^b(t)}{Z_0 - Z_1} - \left(\frac{\langle\!\langle \phi \rangle\!\rangle_0 - \langle\!\langle \phi \rangle\!\rangle_1}{Z_0 - Z_1}\right)^2, \tag{20}$$

$$C_a^b(t) = \frac{g_0^b(t) + g_1^b(t)}{Z_0 + Z_1} - \left(\frac{\langle\!\langle \phi \rangle\!\rangle_0 + \langle\!\langle \phi \rangle\!\rangle_1}{Z_0 + Z_1}\right)^2 \tag{21}$$

for periodic and antiperiodic boundary conditions, respectively.

To construct the fermionic correlation function in the transfer matrix approach, we need to recall the structure of a bond configuration contributing to the fermionic two-point function from our first paper. Similarly to the bosonic case, we introduce new transfer matrices which take into account the additional fields $\overline{\psi}$ and ψ. In particular, we define a transfer matrix representing a site with a fermionic source and sink $\overline{T}(\overline{\psi}\psi)$, one representing a site with a fermionic source, $\overline{T}(\overline{\psi})$, and one with a fermionic sink, $\overline{T}(\psi)$. As usual, single additional fermionic variables have to be paired with a fermionic bond, an outgoing one to the right for a site with a source variable $\overline{\psi}$ and an incoming one from the left for a site with a sink variable ψ. The graphical representation for these transfer matrices is shown in figure 3 where we denote the fermionic source $\overline{\psi}$ by a bold $\times$ and the fermionic sink ψ by a bold $\bigcirc$. Using again $t = (x_1 - x_2) \bmod L_t$ the non-normalised fermionic correlation function $g^f(x_1 - x_2) = \langle\!\langle \psi_{x_1} \overline{\psi}_{x_2} \rangle\!\rangle$ can be composed of these matrices by

$$g^f(t) = \begin{cases} \mathrm{Tr}\left[\overline{T}(\overline{\psi})\left(T^1(0)\right)^{t-1} \overline{T}(\psi)\left(T^0(0)\right)^{L_t-t-1}\right] & \text{if } t \neq 0, \\ \mathrm{Tr}\left[\overline{T}(\overline{\psi}\psi)\left(T^0(0)\right)^{L_t-1}\right] & \text{if } t = 0. \end{cases} \tag{22}$$

Of course this expression can easily be generalised to take into account more complicated fermionic operators such as $\psi\phi^k$ and $\overline{\psi}\phi^k$. The additional presence of the bosonic variable

(a) $\overline{T}(\overline{\psi})$ (b) $\overline{T}(\psi)$ (c) $\overline{T}(\overline{\psi}\psi)$ (d) $T^1(0)$

Figure 3: Graphical representation of the transfer matrices with additional fermionic sources. We use the symbol $\times$ for the fermionic source $\overline{\psi}$ and $\circ$ for the fermionic sink ψ. All examples are for the matrix element $\overline{T}_{2,4}$. The weights for the matrix elements (a-c) are the same and equal to the weight of (d).

ϕ^k simply increases the site occupation number according to the discussion on the bosonic correlation functions.

Since the weight of a site saturated with an additional fermionic source or sink paired with a fermionic bond is the same as the weight of a site saturated with two fermionic bonds or a source and a sink variable, the newly introduced transfer matrices all have the same entries as the transfer matrix $T^1(0)$, i.e.,

$$\overline{T}(\overline{\psi}) = \overline{T}(\psi) = \overline{T}(\overline{\psi}\psi) = T^1(0)\,. \tag{23}$$

Therefore, the definition of new matrices for sites with additional fermionic variables is in fact obsolete in practice and the presence of a fermionic source or sink expresses itself by a change from T^0 to T^1 and vice versa. The non-normalised fermionic two-point function can hence be written in terms of the matrices $T^1(0)$ and $T^0(0)$ as

$$g^f(t) = \mathrm{Tr}\left[\left(T^1(0)\right)^{t+1}\left(T^0(0)\right)^{L_t-t-1}\right]. \tag{24}$$

Yet, the formation of the fermionic correlation function is a little more subtle than the one of the bosonic correlation function. The translation invariance of the two-point function together with the cyclic invariance of the trace amounts to the fact that $g^f(t)$ is a superposition of *all possible* configurations with an open fermionic string where the fermionic source and the sink are separated by the distance t. For a given bosonic bond configuration, there are thus L_t different configurations with an open fermionic string. For t of them, the fermionic string crosses the boundary and for antiperiodic boundary conditions, we have to account for those as they pick up a negative sign. Keeping track of all the signs correctly, the fermionic correlation functions for periodic and antiperiodic boundary conditions, respectively, read

$$C_p^f(t) = \frac{g^f(t)}{Z_0 - Z_1}, \qquad C_a^f(t) = \frac{L_t - 2t}{L_t}\frac{g^f(t)}{Z_0 + Z_1}\,. \tag{25}$$

From our discussion of the fermionic two-point function in our first paper [1] we remember that it is really only defined in the bosonic sector $F = 0$ and we have

$$C_0^f = \frac{g^f(t)}{Z_0}. \tag{26}$$

On the other hand, we can interpret the open fermion string of length t as an open antifermion string of complementary length $L_t - t$ on the background of bond configurations in sector $F = 1$. This interpretation becomes evident when one calculates the energy or mass gaps from the correlation functions in terms of the eigenvalues of the transfer matrices which we are going to do in the next section.

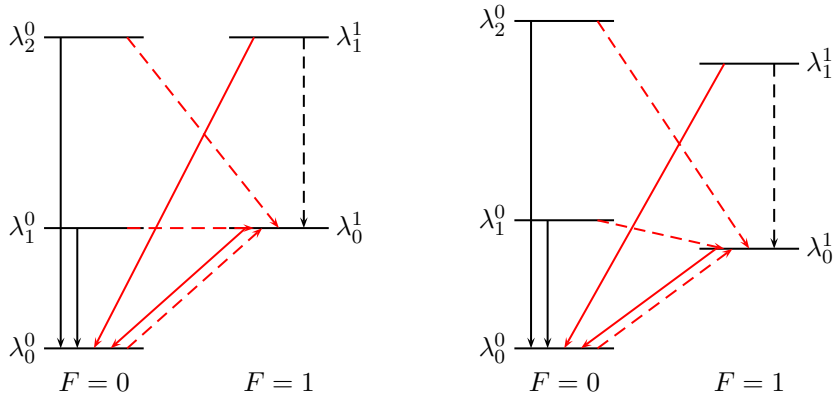

(a) Continuum (b) Finite lattice spacing

Figure 4: Unbroken supersymmetric quantum mechanics. The energy levels and the respective mass gaps in the continuum (a) and for finite lattice spacing (b) where the shifts of the energy levels w.r.t. to the ones in the continuum are due to discretisation artefacts.

2.3 Mass gaps

Observables closely related to the correlation functions are of course the energy or mass gaps. It is well known that in the transfer matrix formalism these mass gaps can be calculated directly from the ratios of eigenvalues of the transfer matrices, cf. [6] for the explicit calculation in our supersymmetric quantum mechanics setup. Ordering the eigenvalues of the transfer matrix T^F according to

$$\lambda_0^F > \lambda_1^F > \dots, \tag{27}$$

the calculation of the i-th fermionic mass gap in the bosonic sector yields

$$m_i^f = -\ln(\lambda_i^1/\lambda_0^0). \tag{28}$$

By interpreting the expectation value $\langle\overline{\psi}_t\psi_0\rangle = C^{\overline{f}}(t)$ as the correlator of the antifermion $\overline{f}$ in the fermionic sector $F = 1$, we can similarly calculate its mass via

$$m_i^{\overline{f}} = -\ln(\lambda_i^0/\lambda_0^1), \tag{29}$$

and we see that the masses of the fermion and antifermion are the same – at least in the continuum – up to a minus sign. Of course, this is in accordance with the standard quantum mechanical interpretation of an antiparticle as a particle with negative energy propagating backward in time, and so this confirms our interpretation of the open fermion string as a propagating fermion in sector $F = 0$ or as a complementary antifermion in sector $F = 1$. The bosonic mass gaps are defined in each sector $F = 0, 1$ individually and are calculated as

$$m_{i,F}^b = -\ln(\lambda_i^F/\lambda_0^F). \tag{30}$$

It is useful to illustrate schematically which mass gap is measured with respect to which vacuum via the ratios of the eigenvalues. In figures 4 and 5 the mass gaps in the bosonic sector, i.e. with respect to the bosonic vacuum, are depicted by full lines while the mass gaps in the fermionic sector, i.e. with respect to the fermionic vacuum, are drawn as dashed lines.

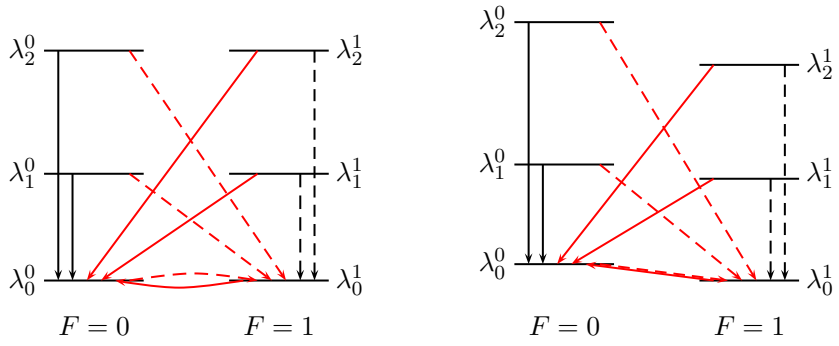

(a) Continuum (b) Finite lattice spacing

Figure 5: Broken supersymmetric quantum mechanics. The energy levels and the respective mass gaps in the continuum (a) and for finite lattice spacing (b) where the shifts of the energy levels w.r.t. to the ones in the continuum are due to discetisation artefacts. Note that the figure (b) illustrates a situation in which the fermionic vacuum is favoured at finite lattice spacing as compared to the bosonic vacuum.

Bosonic mass gaps $m^b_{i,F}$ with bosonic quantum numbers are further differentiated from the fermionic mass gaps $m_i^{f,\overline{f}}$ with fermionic quantum numbers as black versus red lines. Figure 4 illustrates a system with unbroken supersymmetry and a unique bosonic ground state in the continuum (a) and at finite lattice spacing (b), while figure 5 illustrates a system with broken supersymmetry and hence two degenerate bosonic and fermionic ground states, again in the continuum (a) and at finite lattice spacing (b). The shifts in the energy levels w.r.t. to the ones in the continuum are due to discretisation artefacts of $\mathcal{O}(a)$ and are expected to disappear in the continuum. Illustration (b) in figure 5 represents a situation in which the fermionic vacuum is favoured at finite lattice spacing as compared to the bosonic vacuum. Moreover, it is interesting to note that unless the vacua are degenerate, there is always one negative fermionic mass gap, namely the one measured from the energetically lower to the higher vacuum.

2.4 Ward identities

One of the main goals of our efforts in supersymmetric quantum mechanics is to gain a precise understanding of whether and how supersymmetry is restored in the continuum limit. For such investigations Ward identities are most useful and many of our exact results discussed in this paper refer to various Ward identities which can be derived for the different discretisations we consider. A Ward identity can be derived by rewriting the expectation value of an observable $\mathcal{O}(\phi)$ in the path integral formulation for the transformed variable, $\phi \to \phi' = \phi + \delta\phi$, assuming that the measure of the path integral is invariant under this variation, $\mathcal{D}\phi' = \mathcal{D}\phi$. Since the physics cannot depend on the shift of the integration variable, we find to leading order in δ

$$\begin{aligned}
\langle \mathcal{O} \rangle &= \frac{1}{Z} \int \mathcal{D}\phi' \; \mathcal{O}(\phi') \; \mathrm{e}^{-S(\phi')} \\
&= \frac{1}{Z} \int \mathcal{D}\phi \; (\mathcal{O}(\phi) + \delta\mathcal{O}(\phi)) \; \mathrm{e}^{-S(\phi)} (1 - \delta S(\phi)) \\
&= \langle \mathcal{O} \rangle + \langle \delta\mathcal{O} \rangle - \langle \mathcal{O}\delta S \rangle \,,
\end{aligned}$$

and therefore the relation

$$\langle \delta\mathcal{O} \rangle = \langle \mathcal{O}\delta S \rangle \tag{31}$$

must hold for any observable. Now, if the action is invariant under the transformation δ, the r.h.s. of the equation vanishes, yielding

$$\langle \delta\mathcal{O} \rangle = 0 \tag{32}$$

as a condition to test whether supersymmetry is indeed restored in the continuum.

As a first example, we consider the observable $\mathcal{O} = \overline{\psi}$. Its variation under the lattice version of the supersymmetry transformation δ_1 in eq.(2) results in the simple Ward identity

$$W_0 \equiv \langle (\nabla^- \phi + P') \rangle = 0 \,. \tag{33}$$

Thus, the vanishing of the expectation value of the first derivative of the superpotential $\langle P' \rangle$ in the continuum indicates restoration of supersymmetry. Note that the variation of the operator $\mathcal{O} = \overline{\psi}$ under the supersymmetry transformation δ_2 yields $\delta_2 \overline{\psi} = 0$ by definition.

As a second example we consider the observable $\mathcal{O} = \overline{\psi}_x \phi_y$. Its variation under the supersymmetry transformation δ_1 yields Ward identities which connect bosonic and fermionic correlation functions. In particular, we obtain

$$W_1(y-x) \equiv \langle \overline{\psi}_x \psi_y \rangle + \langle (\nabla^- \phi + P')_x \phi_y \rangle = 0 \,, \tag{34}$$

while the variation of the operator under the supersymmetry transformation δ_2 vanishes trivially. Analogously, one can use the observable $\mathcal{O} = \psi_x \phi_y$ which under the supersymmetry transformation δ_2 yields a similar set of Ward identities,

$$W_2(x-y) \equiv \langle \psi_x \overline{\psi}_y \rangle + \langle (\nabla^- \phi - P')_x \phi_y \rangle = 0 \,,$$

while the variation of the operator under the other supersymmetry transformation δ_1 vanishes trivially.

Let us now be more specific and calculate the Ward identities W_0, W_1 and W_2 explicitly for the two superpotentials P_u and P_b employed in our investigation. Using the translational invariance of the lattice, for the superpotential P_u we find the Ward identities

$$W_0 = \langle P_u' \rangle = \mu \langle \phi \rangle + g \langle \phi^3 \rangle \,, \tag{35}$$

$$W_1(t) = -\langle \psi_t \overline{\psi}_0 \rangle + (1+\mu) \langle \phi_t \phi_0 \rangle - \langle \phi_{t+1} \phi_0 \rangle + g \langle \phi_t \phi_0^3 \rangle \,, \tag{36}$$

$$W_2(t) = \langle \psi_t \overline{\psi}_0 \rangle + (1-\mu) \langle \phi_t \phi_0 \rangle - \langle \phi_{t+1} \phi_0 \rangle - g \langle \phi_t^3 \phi_0 \rangle \,, \tag{37}$$

while for the superpotential P_b, we obtain analogously

$$W_0 = \langle P_b' \rangle = -\frac{\mu^2}{4\lambda} + \lambda \langle \phi^2 \rangle \,, \tag{38}$$

$$W_1(t) = -\langle \psi_t \overline{\psi}_0 \rangle + \langle \phi_t \phi_0 \rangle - \langle \phi_{t+1} \phi_0 \rangle - \frac{\mu^2}{4\lambda} \langle \phi \rangle + \lambda \langle \phi_t \phi_0^2 \rangle \,, \tag{39}$$

$$W_2(t) = \langle \psi_t \overline{\psi}_0 \rangle + \langle \phi_t \phi_0 \rangle - \langle \phi_{t+1} \phi_0 \rangle + \frac{\mu^2}{4\lambda} \langle \phi \rangle - \lambda \langle \phi_t^2 \phi_0 \rangle \,. \tag{40}$$

With this we conclude the discussion of the observables which we investigate in the following, and we now proceed to the discussion of the results.

3 Exact results

In this section, we present our exact lattice results for the action with counterterm as well as for the Q-exact action by employing the transfer matrix technique. For the two superpotentials P_u and P_b, the actions are given explicitly in the first paper of our series [1]. For our further discussion it is useful to recall that the continuum limit is taken by fixing the dimensionful parameters μ, g, λ and L while taking the lattice spacing $a \to 0$. In practice, the dimensionless ratios $f_u = g/\mu^2, f_b = \lambda/\mu^{3/2}$ fix the couplings and μL the extent of the system in units of μ, while $a\mu$ and a/L are subsequently sent to zero. We perform our calculations for couplings f_u and f_g which lie well outside of the perturbative regime in order to assess the systematics of the nonperturbative lattice calculations. Finally, we also recall that for antiperiodic fermionic boundary conditions the finite extent μL corresponds to finite inverse temperature in units of μ and the limit $\mu L \to \infty$ is therefore required to recover the system at zero temperature.

3.1 The ratio Z_p/Z_a and the Witten index W

We start by calculating the ratio Z_p/Z_a. At zero temperature this ratio is equal to the Witten index and represents therefore an important indicator for whether supersymmetry is broken or not. In quantum mechanics, whether or not supersymmetry is broken is not a dynamical question, but depends solely on the asymptotic form of the superpotential. For unbroken supersymmetry, the bosonic vacuum lies well below the fermionic one (or vice versa). Thus, in the zero temperature limit $\mu L \to \infty$ only the bosonic sector contributes to the partition function while the fermionic contribution Z_1 vanishes, such that

$$W = \lim_{\mu L \to \infty} \frac{Z_p}{Z_a} = \lim_{\mu L \to \infty} \frac{Z_0 - Z_1}{Z_0 + Z_1} \longrightarrow 1. \tag{41}$$

For finite extent μL (nonzero temperature), there are nonvanishing contributions from the fermionic vacuum, i.e., the partition function Z_1 is no longer zero due to quantum (thermal) fluctuations, resulting in a ratio $Z_p/Z_a < 1$. To leading order in the inverse temperature, the asymptotic dependence is governed by the energy gap m_0^f between the fermionic and bosonic vacuum,

$$\frac{Z_p}{Z_a} \sim \frac{1}{1 + 2e^{-m_0^f L}}\,. \tag{42}$$

For broken supersymmetry on the other hand, both vacua are equally preferable in the continuum and all bosonic and fermionic energy levels are degenerate. Therefore we have $Z_0 = Z_1$ and the Witten index goes to zero,

$$W = \frac{Z_p}{Z_a} = \frac{Z_0 - Z_1}{Z_0 + Z_1} \longrightarrow 0 \tag{43}$$

independent of the extent or temperature of the system. Using our exact lattice calculation we can now investigate how these continuum expectations are modified at finite lattice spacing and how the continuum limit is eventually realised.

First, we consider unbroken supersymmetry. In figure 6, we plot the ratio Z_p/Z_a versus $a\mu$ for different values of fixed μL using the standard discretisation for fixed coupling $f_u = 1$. At nonzero temperature we observe leading order lattice artefacts which are linear in a. In the

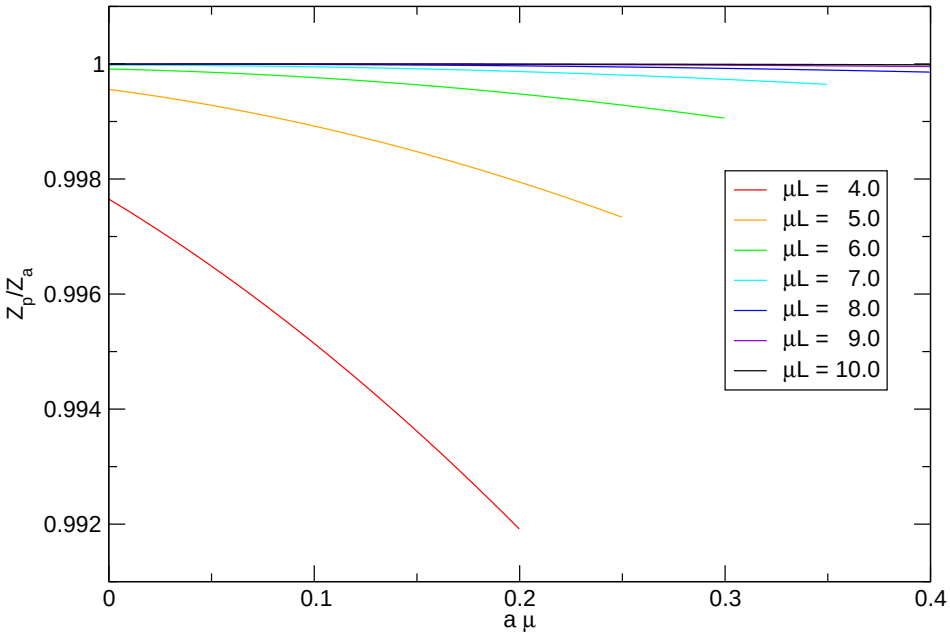

Figure 6: Unbroken supersymmetric quantum mechanics, standard discretisation. Continuum extrapolation of the ratio Z_p/Z_a for different values of μL at fixed coupling $f_u = 1$.

zero temperature limit they are suppressed and the leading artefacts eventually become $\mathcal{O}(a^2)$. Moreover, the artefacts become very small in this limit, simply because at zero temperature only the bosonic groundstate contributes and the nondegeneracies of the excited states at finite a, cf. figure 4, become irrelevant. As the temperature increases, the system gets more sensitive to the excited states since their contributions to the partition function grow larger, and consequently the nondegeneracies between the bosonic and fermionic energy levels crystallise in the growing lattice artefacts. In the continuum limit, we observe the expected deviation of the ratio Z_p/Z_a from one as discussed above. In figure 7, we show the continuum value of the ratio Z_p/Z_a as a function of the inverse temperature μL for two different couplings $f_u = 1$ and $f_u = 2$. The full lines indicate the asymptotic behaviour for $\mu L \to \infty$ according to eq.(42), while the dashed lines include additional higher order contributions. It can be seen that the system reaches the asymptotic zero temperature behaviour already at moderate values of μL. Moreover, contributions from the fermionic vacuum to the partition function are essentially negligible for $\mu L \gtrsim 4$.

For broken supersymmetry we plot the continuum limit of the ratio Z_p/Z_a versus $a\mu$ for different values of μL at fixed coupling $f_b = 1$ using the standard discretisation in figure 8. First we note that the ratio goes to zero towards the continuum limit indicating a vanishing Witten index in that limit independent of the temperature. This is the expected continuum behaviour as argued above in eq.(43) and relies on the fact that all energy levels become degenerate. Since the lattice discretisation breaks this degeneracy explicitly, cf. figure 5, the ratio is nonzero at finite lattice spacing. In a way one can think of the finite lattice spacing as regulating the Goldstino zero mode and the energy difference between the two vacua simply corresponds to the regulated Goldstino mass. As a consequence the associated vanishing Witten index is regulated, too. As explained in detail in the first paper of our series [1] a vanishing Witten index leads to a fermion sign problem for Monte Carlo simulations. Since

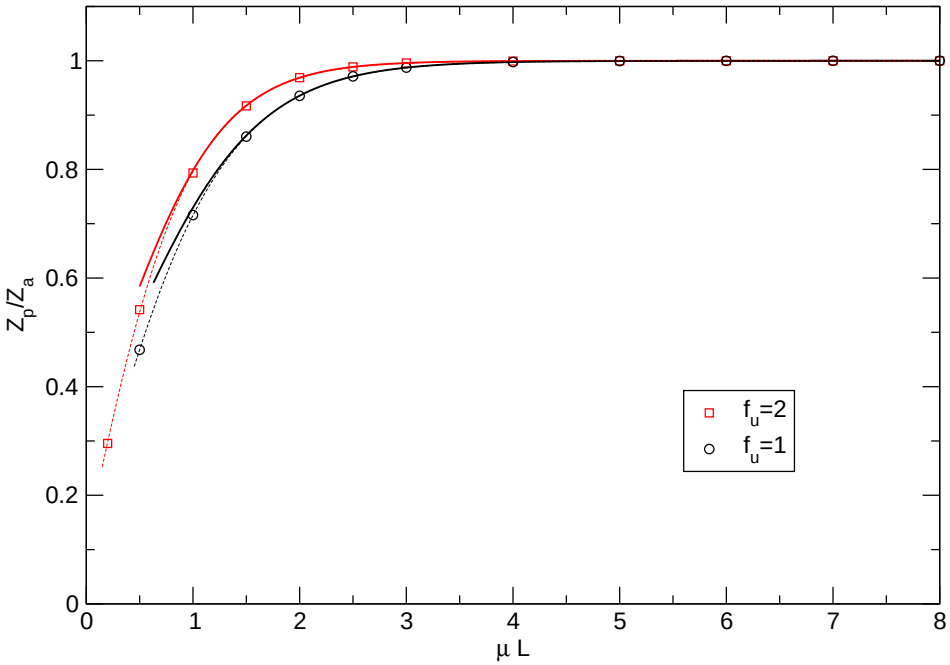

Figure 7: Unbroken supersymmetric quantum mechanics. The continuum values of the ratio Z_p/Z_a versus μL for different couplings $f_u = 1$ (black circles) and $f_u = 2$ (red squares). The full lines describe the asymptotic behaviour according to eq.(42) while the dashed lines include additional higher order contributions.

the finite lattice spacing regulates the index one could argue that the sign problem is avoided in this way, but of course it is not clear whether the lattice artefacts and the statistical fluctuations can be kept under control. In fact it turns out that the lattice artefacts for the ratio Z_p/Z_a can become extremely strong. While the leading artefacts are evidently $\mathcal{O}(a)$, they grow exponentially large as the temperature is lowered, i.e., at low temperature artefacts of all orders in a become relevant such that the finite lattice spacing corrections in the ratio are exponentially enhanced towards low temperatures.

The rather peculiar behaviour of the lattice corrections for small temperatures can be explained as follows. Considering the illustration of the supersymmetry broken spectrum at finite a in figure 5, it is clear that the degeneracy between the bosonic and fermionic vacuum is lifted. For small temperatures (large values of μL) the tunneling from the energetically lower to the higher vacuum are exponentially suppressed with growing μL. On the other hand, exactly these tunnelings are needed in order for the higher vacuum to contribute to the partition function, eventually leading to the vanishing Witten index. Only once the temperature is large enough compared to the energy difference between the two vacua, i.e. the regulated Goldstino mass, the tunneling becomes effective enough to drive the Witten index to zero. Equivalently, at fixed temperature the Goldstino mass, which to leading order is proportional to $a\mu$, needs to become sufficiently small, and from figure 8 it becomes evident when this is the case.

The exponentially enhanced lattice artefacts have a rather dramatic consequence for the Witten index concerning the order of the limits $\mu L \to \infty$ and $a \to 0$. As is evident from our discussion and the data in figure 8, extrapolating the index to $\mu L \to \infty$ always yields $W = -1$ at *any* finite lattice spacing. Therefore the subsequent continuum limit of the index at zero

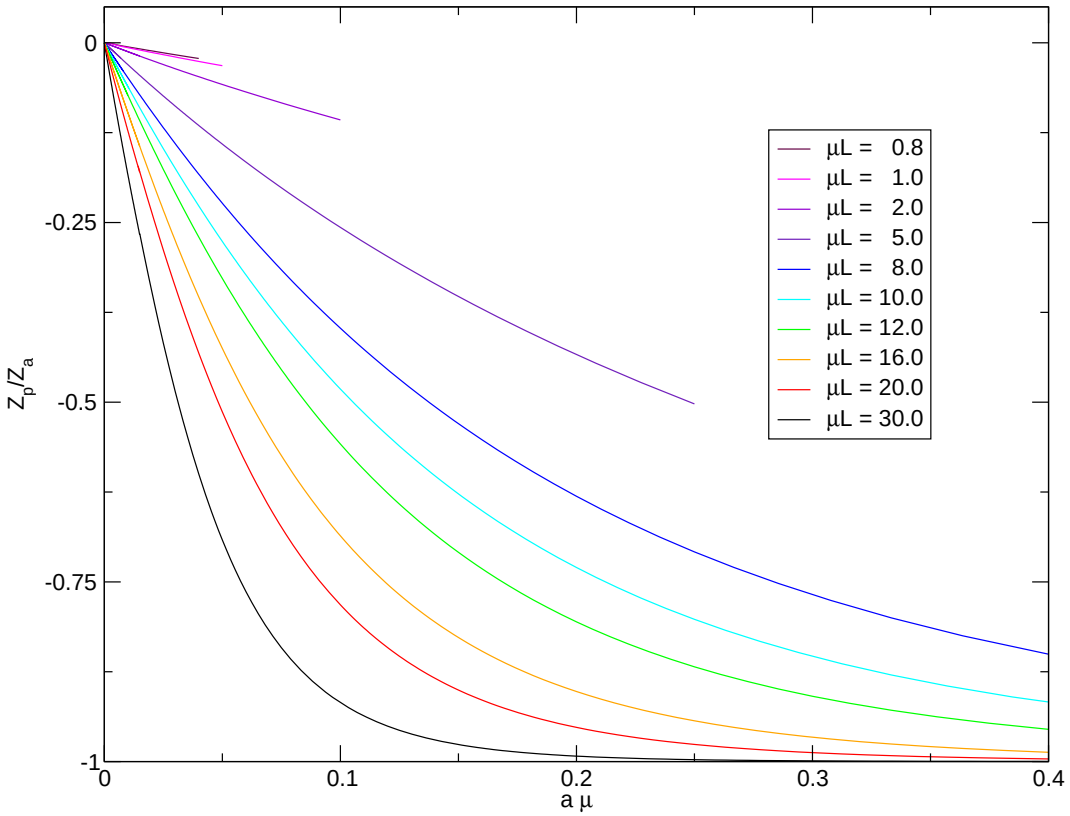

Figure 8: Broken supersymmetric quantum mechanics, standard discretisation. Continuum extrapolation of the ratio Z_p/Z_a for different values of μL at fixed coupling $f_b = 1$.

temperature comes out incorrectly and the expectation in eq.(43) is hence not confirmed. So in contrast to unbroken supersymmetry, here the order of the limits is crucial and has to be taken into account for the correct interpretation of the results. Finally, from the plot we infer that the fermionic vacuum has a lower energy than the bosonic one, hence the Witten index tends to -1 for finite lattice spacing, i.e., the picture at finite a is exactly as depicted in 5.

Next, we consider the results for the Witten index using the Q-exact discretisation. In figure 9 we plot the ratio Z_p/Z_a versus $a\mu$ for different values of μL at fixed coupling $f_u = 1$ for the case when supersymmetry is unbroken. We observe lattice artefacts which are almost identical to the ones found with the standard discretisation. In addition, in the continuum the ratios converge to the same values for any given inverse temperature μL and the temperature dependence in the continuum is therefore given exactly as in figure 7. Of course the agreement is a consequence of the universality of lattice calculations in the continuum which is nicely confirmed by our results. Turning to the case when supersymmetry is broken, the results for the Q-exact discretisation are rather boring. Since the degeneracy between the bosonic and fermionic energy levels is maintained exactly at any value of the lattice spacing a, the contributions from the bosonic and fermionic sector are always exactly equal and cancel precisely, hence the Witten index is zero independent of the temperature. Note however that the exact degeneracy of the energy levels does not exclude lattice artefacts in the spectrum. In fact, they are rather large as we will see in section 3.3, but the Witten index is not sensitive to it as long as the degeneracy between the bosonic and fermionic levels is maintained at finite

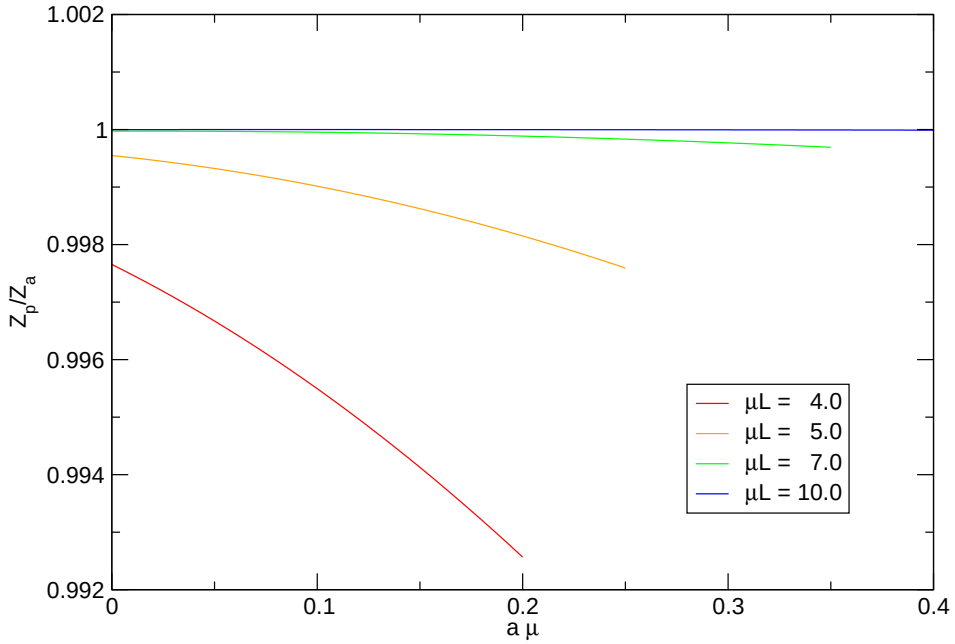

Figure 9: Unbroken supersymmetric quantum mechanics, Q-exact discretisation. Continuum extrapolation of the ratio Z_p/Z_a for different values of μL at fixed coupling $f_u = 1$.

lattice spacing a.

3.2 Correlation functions

In this section, we present some exact results for two-point correlation functions, merely as qualitative illustrations of how they are affected by lattice artefacts. A more quantitative discussion will follow in section 3.3, where we consider the energy gaps, and in section 3.4 where we investigate Ward identities relating fermionic and bosonic correlation functions.

First, we show the bosonic and the fermionic correlation function for unbroken supersymmetry using the standard discretisation. In figure 10(a) we display the bosonic and fermionic two-point correlation functions $C^{b,f}(t)$ for periodic and antiperiodic b.c., respectively, at fixed coupling $f_u = 1$ for $\mu L = 2$ corresponding to a high temperature. In figure 10(b) the same correlation functions are displayed for $\mu L = 10$ corresponding to a low temperature. For $\mu L = 2$, we know from section 3.1 that finite temperature effects are not negligible. In figure 10(a) these effects are reflected by the fact that the correlation functions for periodic and antiperiodic b.c. are clearly distinguishable, i.e. they are sensitive to the boundary conditions. For $\mu L = 10$, we are in a regime where the system behaves as being close to zero temperature where the system is dominated by the bosonic vacuum. Thus, the bosonic correlation functions receive contributions only from the bosonic sector and are hence no longer distinguishable for periodic and antiperiodic b.c. as illustrated in figure 10(b). The fermionic correlation functions on the other hand are different for periodic and antiperiodic b.c. even for this choice of parameters. This difference originates from the specific implementation of the boundary conditions via eq.(25) which takes into account how many times an open fermion string of length t can cross the boundary when the translational invariance of the correlation function is incorporated. To complete our discussion for unbroken supersymmetry, in figure

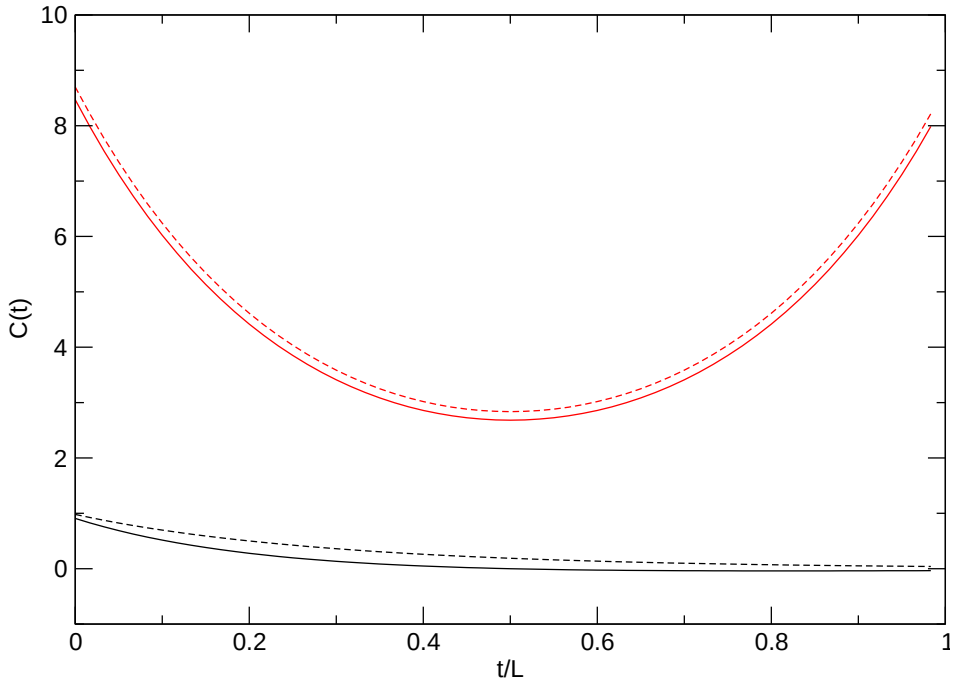

(a) $\mu L = 2$

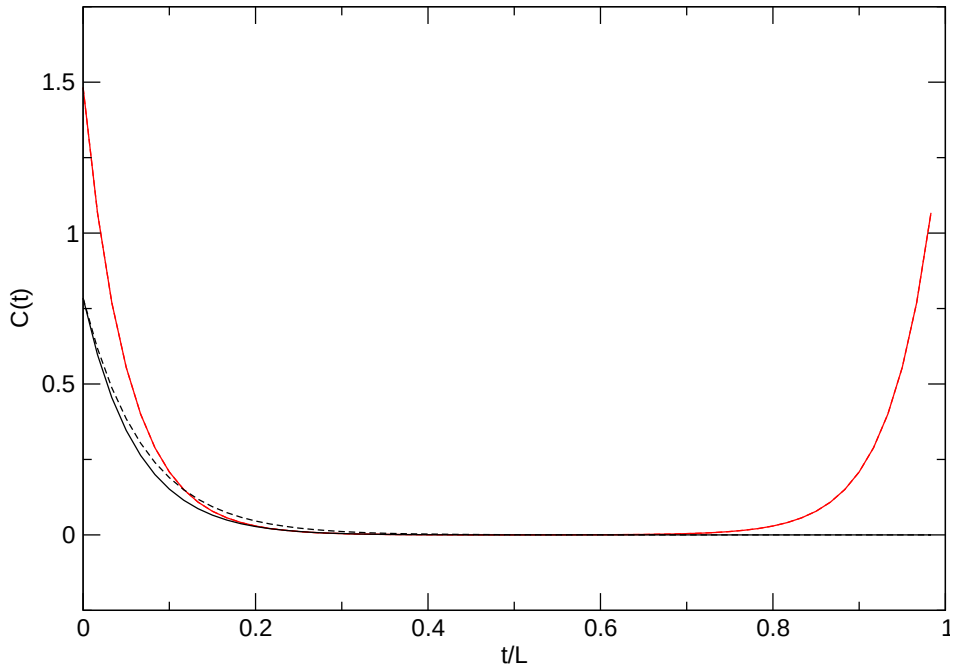

(b) $\mu L = 10$

Figure 10: Unbroken supersymmetric quantum mechanics, standard discretisation. The bosonic (red) and fermionic (black) correlation functions for periodic (dashed) and antiperiodic boundary conditions (solid) at fixed coupling $f_u = 1$. Note that in plot (b) the bosonic correlation functions for periodic and antiperiodic b.c. are indistinguishable.

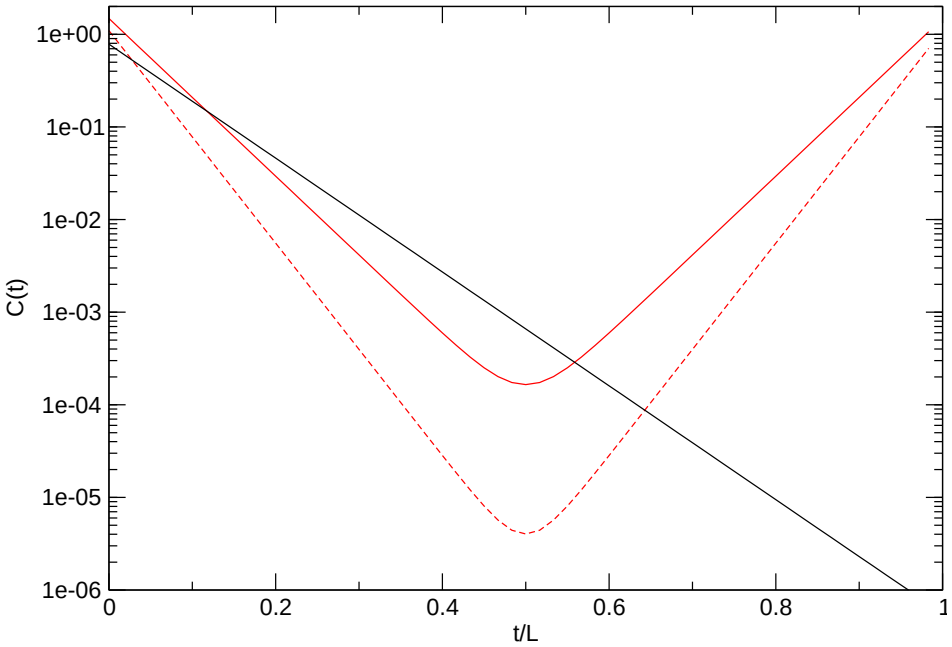

Figure 11: Unbroken supersymmetric quantum mechanics, standard discretisation. The bosonic (red) and fermionic (black) correlation functions in the bosonic sector $F = 0$ (solid) and the bosonic correlation function in the fermionic sector $F = 1$ (dashed) for $\mu L = 10$ and coupling $f_u = 1$.

11 we display the correlation functions for the same calculation as above, but individually for each sector F according to eq.(26). Note that we only plot the fermionic correlation function $C_0^f(t)$ in the bosonic sector $F = 0$, but not the antifermionic correlation function $C_1^{\overline{f}}(t)$ in the fermionic sector $F = 1$, cf. our discussion in [1] and above in section 2.3 and 2.2. The bosonic correlation functions are shown in both the bosonic and fermionic sector. However, in this temperature regime $Z_0 \gg Z_1$ and therefore, the bosonic correlation function in the fermionic sector $C_1^b(t)$ is heavily suppressed with respect to the one in the bosonic sector $C_0^b(t)$ when contributing to the correlation function $C_{p,a}^b(t)$ with fixed fermionic boundary conditions. It is also interesting to note that the correlation functions consist of a single exponential term only, i.e., the overlap of the operators ϕ and ψ with the state corresponding to the lowest mass gap is maximal.

We now turn to the analogous correlation functions for broken supersymmetry. In figure 12, the bosonic and the fermionic correlation functions are displayed for periodic and antiperiodic b.c. for $\mu L = 10$ at fixed coupling $f_b = 1$. In contrast to unbroken supersymmetry, the bosonic correlation functions do not approach zero for $t/L \sim 1/2$. To get an understanding for this, we first need to consider figure 13 where we show the continuum extrapolation for $\langle\phi\rangle$ in the same physical situation, i.e. at $\mu L = 10$ and $f_b = 1$. For each sector the expectation value $\langle\phi\rangle_F$ extrapolates to the same value but with opposite sign. This is expected because of the additional $\mathbb{Z}_2$-symmetry for the superpotential P_b. Furthermore, figure 8 suggests that both sectors Z_0 and Z_1 are weighted equally in the continuum. Therefore, on the one hand, $\langle\phi\rangle_a \to 0$. On the other hand, for periodic b.c., the numerator takes a fixed value while the denominator goes to zero and the expectation value $\langle\phi\rangle_p$ is thus ill-defined in the continuum.

After these considerations concerning the expectation value of ϕ, we are now able to explain the rather strange fact that the bosonic correlation function has a negative offset.

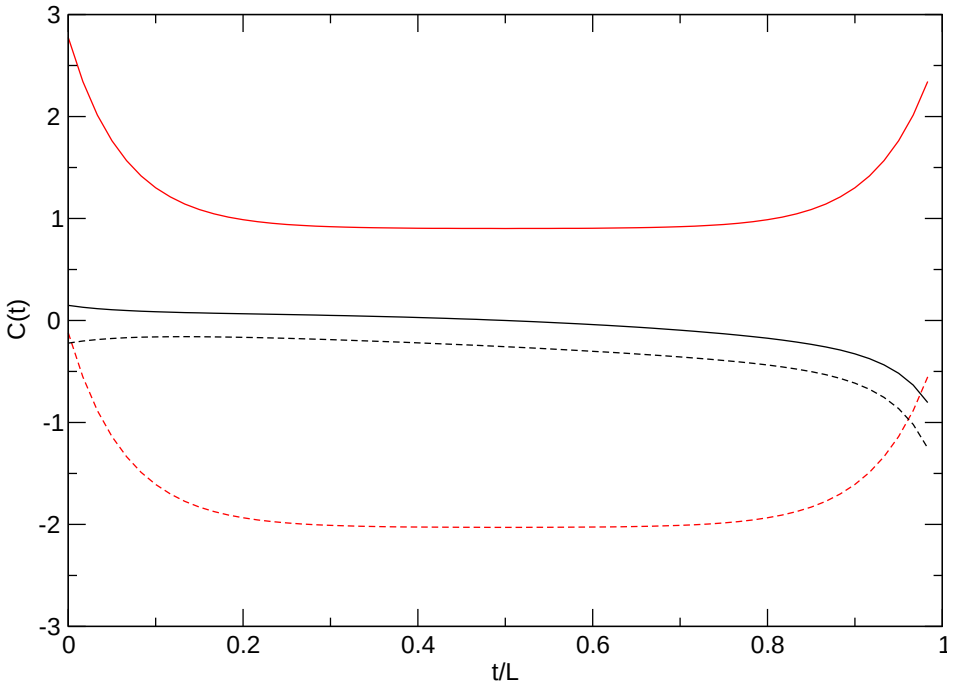

Figure 12: Broken supersymmetric quantum mechanics, standard discretisation. The bosonic (red) and fermionic (black) correlation functions for periodic (dashed) and antiperiodic b.c. (solid) for $\mu L = 10$ and coupling $f_b = 1$.

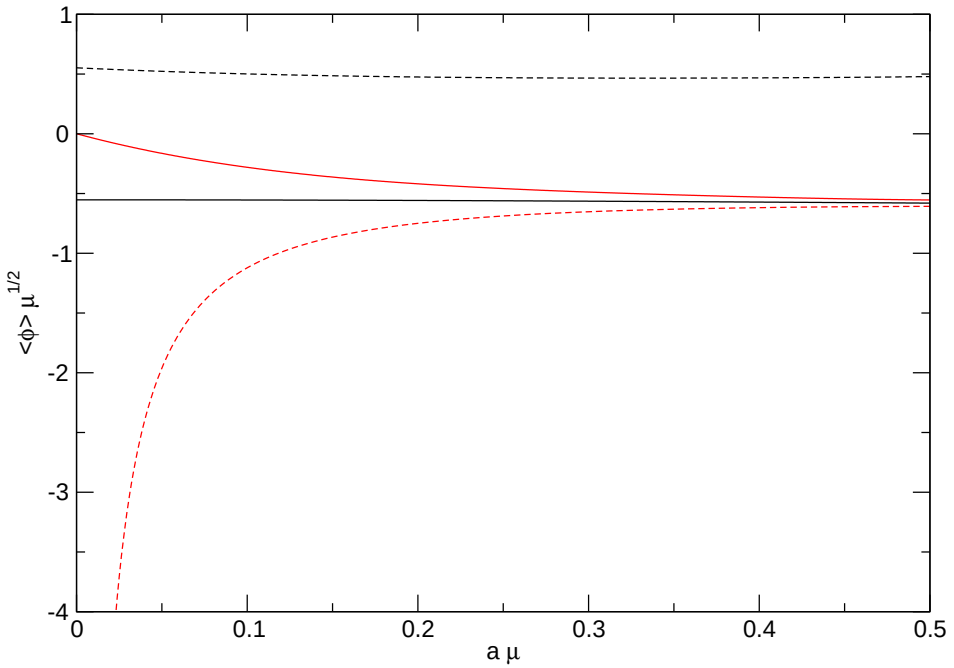

Figure 13: Broken supersymmetric quantum mechanics, standard discretisation. Continuum extrapolation of $\langle\phi\rangle$ in the sectors Z_0 (black dashed line) and Z_1 (black solid line), for antiperiodic (solid red line) and periodic boundary conditions (dashed red line) at $\mu L = 10$ and $f_b = 1$.

Instead of removing a possible constant offset in the connected bosonic two-point function, the term $\langle\phi\rangle_p^2$ shifts the correlation function to negative values. This problem of the shift into the negative worsens closer to the continuum because the term $-\langle\phi\rangle_p^2$ takes larger negative values for smaller lattice spacings. The bosonic correlation function is therefore an ill-defined observable in the continuum for periodic boundary conditions. It is therefore necessary to look at the correlation function in each sector individually and we do so in figure 14. We observe that the bosonic correlation functions are very similar in each sector. Note, that the term $\langle\phi\rangle_F^2$ for the correlation functions measured independently in the bosonic and fermionic sector indeed removes the additional constant shift such that the connected bosonic correlator is close to zero for $t/L \sim 1/2$. It is also worth discussing the rather oddly shaped fermionic correlation function. The figure reveals that there are contributions of four dominant exponentials instead of only one as in the unbroken case. For $t/L \sim 0$ and for $t/L \sim 1$, there are two separate exponentials with large slopes, one in forward direction and one in backward direction. We can interpret these parts as coming from the second mass gap of the fermion yielding an exponential decrease for small t and of the antifermion yielding an exponential increase for large t. In addition, we have two rather flat exponential contributions around $t/L \sim 1/2$. These can be interpreted as the first mass gaps for the fermion and antifermion. As discussed before, for broken supersymmetry the fermionic vacuum has a lower energy than the bosonic one due to lattice artefacts, and therefore the lowest mass gap for the fermion is in fact *negative* and leads to the increase around $t/L \sim 1/2$. The effective masses which are extracted in this region are very small. In fact, these are the first indications for the mass of the Goldstino which appears in the spectrum for broken supersymmetry. We will elaborate further on this when we discuss the exact results for the mass gaps in the following section.

The correlation functions using the Q-exact discretisation do not reveal anything qualitatively different, hence we directly proceed to the discussion of the mass gaps where we can compare the lattice artefacts for the standard and Q-exact discretisation on a more quantitative level.

3.3 Mass gaps

The derivation of the mass gaps using the eigenvalues of the transfer matrices in section 2.3 suggests a calculation the bosonic mass gaps in each sector separately. The fermionic mass gaps are measured via ratios of eigenvalues of T^1 and T^0. This is a reflection of the fermionic correlation function being defined in the bosonic sector, but by reinterpreting the open fermion string in the bosonic sector as describing the antifermion string in the fermionic sector, one can also define the mass of an antifermion. In addition to our exact results at finite lattice spacing we also calculate the spectra directly in the continuum using Numerov's algorithm as a crosscheck and a benchmark for the lattice results. Since the spectrum is a property of the transfer matrix independent of the system size, the results do not depend on μL.

We start as usual with unbroken supersymmetry using the standard discretisation. In figure 15 we plot the bosonic and fermionic masses with respect to the bosonic vacuum at a coupling $f_u = 1$. First, we note that the mass gaps indeed extrapolate to the expected continuum values indicated by the horizontal lines at the left side of the plot. It turns out that the leading lattice artefacts are $\mathcal{O}(a)$ for both the fermion and boson masses but with opposite signs, and are reasonably small even at rather coarse lattice spacings. The mass

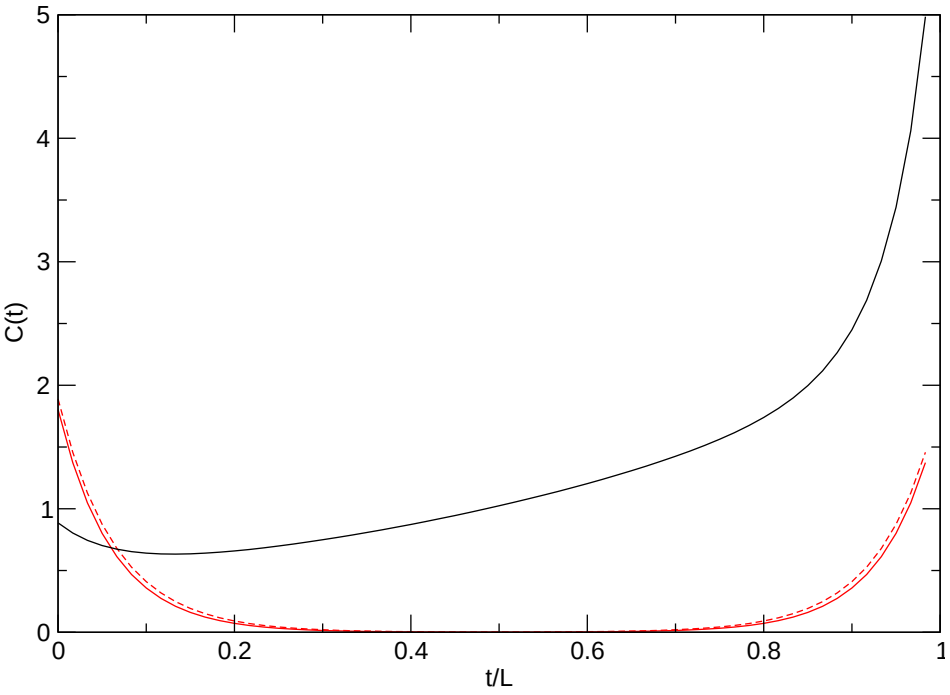

(a) Linear plot

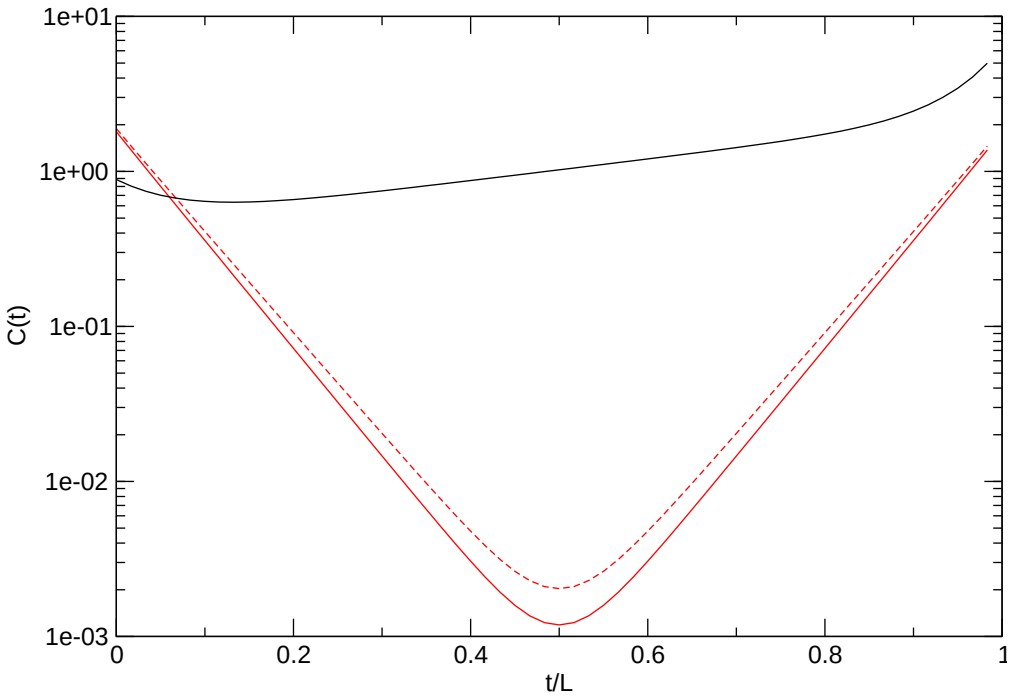

(b) Logarithmic plot

Figure 14: Broken supersymmetric quantum mechanics, standard discretisation. The bosonic (red) and fermionic (black) correlation functions in the sector Z_0 (solid line) and Z_1 (dashed line) at $\mu L = 10$ and $f_b = 1$.

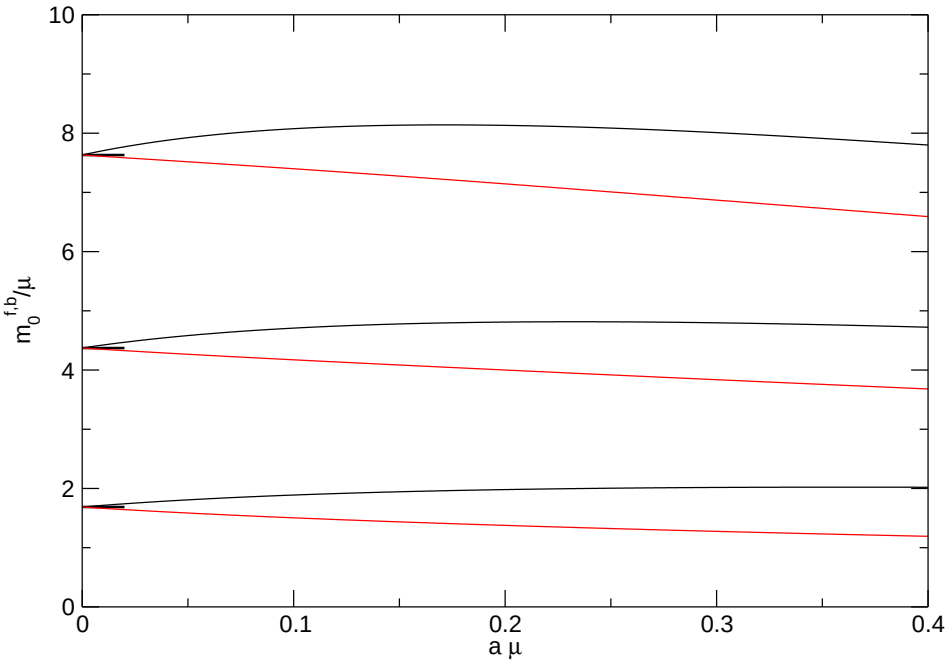

Figure 15: Unbroken supersymmetric quantum mechanics, standard discretisation. Continuum extrapolation of the bosonic (black) and fermionic (red) masses with respect to the bosonic vacuum at $f_u = 1$.

gaps relative to the fermionic vacuum can of course also be calculated, but the information is redundant and we refer to [6] for the detailed results.

Next we discuss our exact results for broken supersymmetry using the standard discretisation. In figure 16, we display the results for the bosonic and the fermionic masses. While the fermionic vacuum is preferred over the bosonic one at finite lattice spacing, cf. figure 8, in the continuum they are on equal footing and contribute equally to the partition functions and observables. Hence in figure 16 we show the result for all the energy gaps, bosonic ones in black and fermionic ones in red, both with respect to the bosonic (solid lines) and fermionic vacuum (dashed lines), despite the fact that the results are partly redundant. In order to distinguish the lines we follow the notation in figure 5 where the energy levels for both sectors are depicted schematically for finite lattice spacing and in the continuum. What is important to note is that also for broken supersymmetry, the bosonic and the fermionic mass gaps extrapolate to the expected continuum values and the supersymmetry in the spectrum, i.e., the degeneracy between the bosonic and fermionic excitations, is restored in the continuum limit. This is in contrast to supersymmetric quantum field theories with spontaneously broken supersymmetry, where the spectrum becomes non-degenerate, see e.g. [7] for a nonperturbative demonstration in the two-dimensional $\mathcal{N} = 1$ Wess-Zumino model.

When supersymmetry is broken, one expects a fermionic zero-energy excitation, the Goldstino mode [8], which is responsible for the tunneling between the bosonic and the fermionic vacuum and hence for the fact that $Z_p = 0$. From figure 16 it becomes clear how the lattice acts as a regulator for the goldstino mode, namely by giving it a small mass of $\mathcal{O}(a)$, hence making it a would-be Goldstino. As a consequence, the Witten index W is regulated. This allows to give meaning to observables even in the system with broken supersymmetry and periodic boundary conditions by defining them at finite lattice spacing, where Z_p is nonzero,

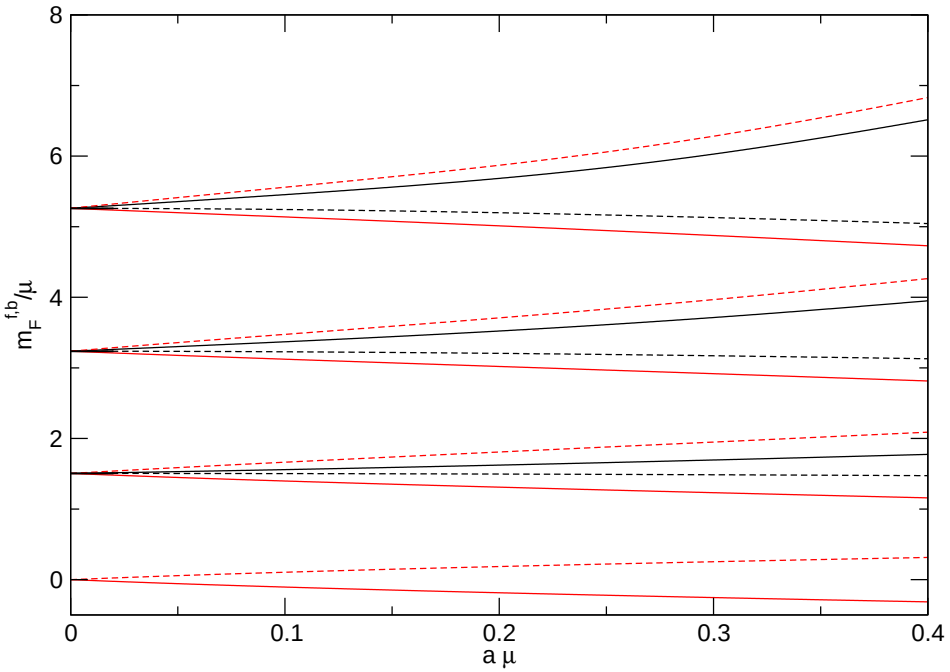

Figure 16: Broken supersymmetric quantum mechanics, standard discretisation. Continuum extrapolation of the bosonic (black) and fermionic (red) masses with respect to the bosonic (solid lines) and the fermionic (dashed lines) vacuum at $f_b = 1$.

and then taking the continuum limit. If the observable couples to the would-be Goldstino mode in the same way as Z_p does, both vanish in the continuum but their ratio is well defined. Note that since the fermionic vacuum has a lower energy than the bosonic one, the would-be Goldstino with positive mass is actually the antifermionic excitation $m_1^{\overline{f}}$ in the fermion sector, while the fermionic excitation m_0^f in the bosonic sector has a negative energy. A posteriori, this explains the rather odd shape of the fermionic correlation function in the bosonic sector displayed in figure 14 where the slope of the slowly increasing correlator corresponds to the small negative mass of the Goldstino fermion.

Finally, we make the observation that the leading lattice artefacts of the spectral mass gaps are all $\mathcal{O}(a)$. This is expected since we use a discretisation of the derivative with $\mathcal{O}(a)$ discretisation errors, both for the bosonic and fermionic degrees of freedom. However, it is intriguing that the linear artefacts of the higher lying bosonic mass gaps $m_{i,1}^b$ in the $F = 1$ sector become very small, and the corrections are eventually dominated by artefacts of $\mathcal{O}(a^2)$, i.e., some interesting conspiration of lattice artefacts appears to cancel the $\mathcal{O}(a)$ artefacts.

Next we consider the spectrum using the Q-exact discretisation. In figure 17 we plot the fermionic (red) and bosonic mass gaps (black) with respect to the bosonic (full lines) and the fermionic vacuum (dashed lines) for unbroken supersymmetry with coupling $f_u = 1$. The characterisation of the lines is as in the previous figures for the mass gaps. From the figure it is clear that the degeneracy between the bosonic and fermionic excitations is maintained for any finite value of the lattice spacing. Apparently, keeping only half of the original symmetries in eq.(2), as realised by the Q-exact discretisation, is sufficient to guarantee the complete degeneracy. However, the lattice artefacts are rather different from the ones observed in the spectrum of the standard discretisation. While the lattice artefacts in the lowest excitation

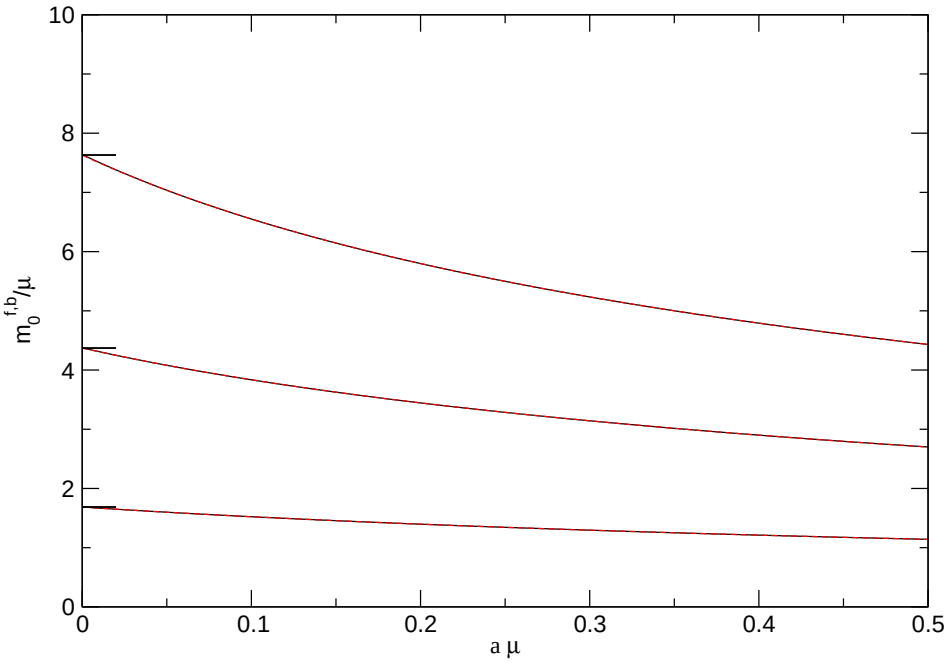

Figure 17: Unbroken supersymmetry, Q-exact discretisation. Continuum extrapolation of the bosonic masses measured with respect to the bosonic (black solid) and the fermionic (black dashed) vacuum and the fermionic masses measured with respect to the bosonic (red dashed) and the fermionic (red dotted) vacuum at $f_u = 1$.

are quantitatively comparable to the ones in the lowest fermionic excitation in the standard scheme, cf. figure 15, they turn out to be much larger for the higher excited states. As an example we find lattice corrections of up to 45% at a lattice spacing of $a\mu = 0.5$ for the third excited state. A possible explanation is that in order to maintain the exact degeneracy between the bosonic and fermionic energies, essentially aligning the lattice artefacts of the bosonic and fermionic states, the eigenvalues have to rearrange in a particular way and push the artefacts into the higher states. So while the Q-exact discretisation is an extremely useful scheme due to its improved symmetry properties, one has to be aware that the lattice artefacts may be dramatically enhanced for certain observables.

The spectrum of the Q-exact action for broken supersymmetry turns out to be very difficult to handle. On the one hand, using the superpotential P_b the transfer matrices T^0 and T^1 come out to be exactly similar for any given cutoff for the bosonic occupation numbers and hence the energy levels are exactly degenerate for any lattice spacing. The similarity transformation relating the two transfer matrices can be understood as the supersymmetry transformation relating the bosonic and the fermionic sector and is exactly maintained at finite lattice spacing. As a consequence of the exact similarity we have an exactly massless Goldstino mode and hence also $Z_p/Z_a = 0$, independently of both the chosen occupation number cutoff and the lattice spacing a. On the other hand, however, we are not able to obtain reliable results which are independent of the cutoff for reasonably large bosonic occupation numbers. Even on very small lattices and for coarse lattice spacings the occupation numbers necessary to produce stable transfer matrix eigenvalues appear to be extremely large. Hence, despite the fact that the properties of the transfer matrices qualitatively yield the correct physics in terms of the spectrum and the Witten index, we have to postpone any further investigation of the system with broken supersymmetry using the Q-exact action.

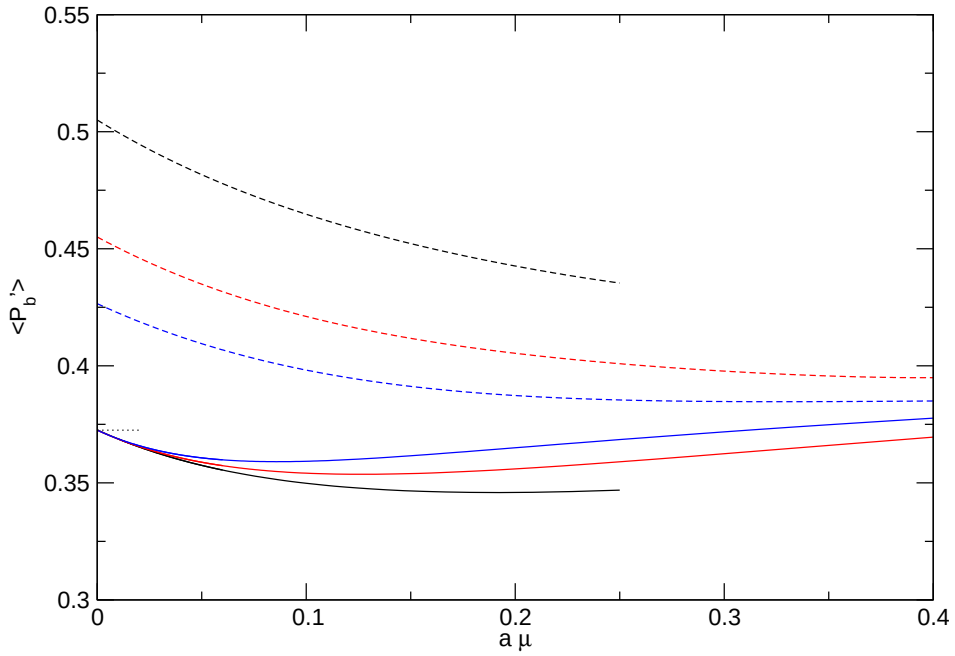

Figure 18: Broken supersymmetric quantum mechanics, standard discretisation. Continuum extrapolation of $\langle P_b' \rangle / \sqrt{\mu}$ for $\mu L = 5$ (black), $\mu L = 8$ (red), and $\mu L = 12$ (blue) using periodic (dashed lines) and antiperiodic b.c. (solid lines) at $f_b = 1$.

3.4 Ward identities

In this section we present our exact results for the Ward identitites which we introduced in section 2.4. We discuss the identitites $W_0, W_1(t)$ and $W_2(t)$ in turn.

As usual we start with the discussion of the system with unbroken supersymmetry using the standard discretisation. In that case, the Ward identity W_0 in eq.(37) is supposed to vanish in the continuum limit. However, it turns out that the expectation value is trivially zero at any value of the lattice spacing, simply because in the bond formulation the $\mathbb{Z}_2$-symmetry $\phi \to -\phi$ is exactly maintained for each bond configuration. This can most easily be seen from the fact that the site weights for this action are zero for an odd site occupation number, $Q_0(2n+1) = Q_1(2n+1) = 0,\ n \in \mathbb{N}_0$, and hence the expectation value of an odd power of ϕ trivially vanishes.

For broken supersymmetry, we need to check whether or not the Ward identity in eq.(40) vanishes. In figure 18, we plot the continuum extrapolation of $\langle P_b' \rangle$ for different values of μL at fixed coupling $f_b = 1$. For antiperiodic b.c., the Ward identity extrapolates to the value $\langle P' \rangle / \sqrt{\mu} = 0.3725\ldots$ independently of the chosen μL. This value is in agreement with a continuum calculation in the operator formalism [9] denoted by the horizontal dotted line at the left side of the plot. The continuum limit for periodic b.c., however, depends on the chosen μL and approaches the continuum value for antiperiodic b.c. only at large μL where the effects from the boundary become smaller and smaller. In figure 19 we show the continuum values of W_0 for periodic b.c. as a function of $(\mu L)^{-1}$, i.e. the temperature in units of μ. The figure reveals that for large μL, the values for periodic b.c. indeed approach the ones for antiperiodic b.c. denoted by the dotted line. Eventually, the values agree in the zero temperature limit, or rather in the limit of infinite extent of the system. Interestingly,

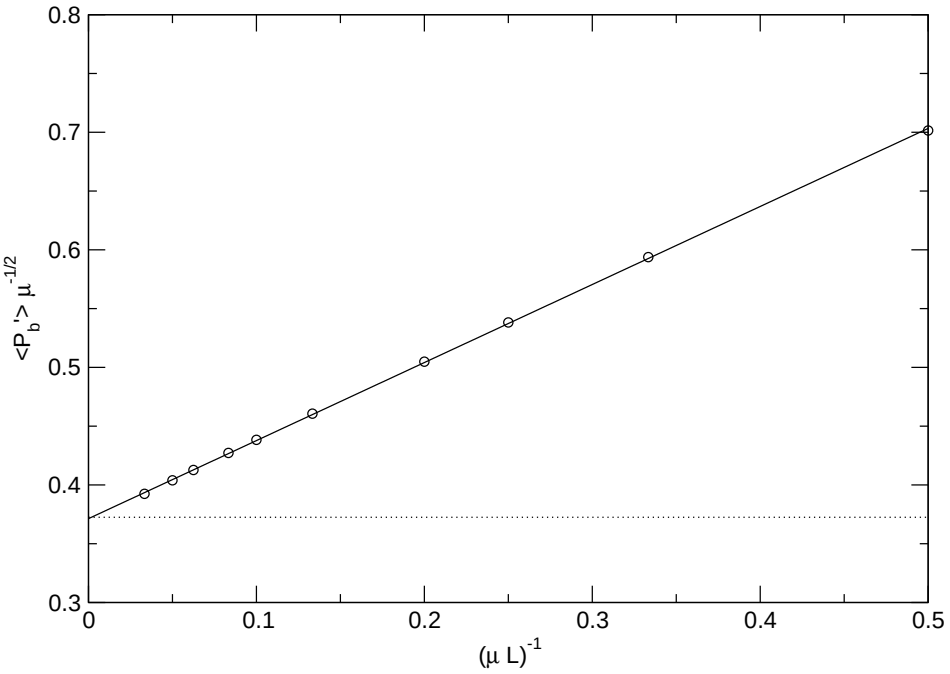

Figure 19: Broken supersymmetric quantum mechanics. The continuum values for $\langle P_b' \rangle / \sqrt{\mu}$ as a function of $1/\mu L$ for periodic b.c. at $f_b = 1$. The continuum value for antiperiodic b.c. is indicated with the black dotted line. The solid black line is a fit linear in $1/\mu L$.

the finite temperature corrections seem to be described by the form $1/\mu L$ up to rather large values of μL. A corresponding fit is shown in figure 19 as the solid line. In conclusion, the Ward identity W_0 serves us indeed to verify that supersymmetry is broken in the continuum for the superpotential P_b.

The results for the Q-exact action do not provide any new interesting insights, because for unbroken supersymmetry W_0 vanishes trivially as for the standard discretisation, while the results for broken supersymmetry are not stable as we discussed at the end of section 3.3.

We now turn to the Ward identity W_1 to verify supersymmetry restoration and breaking for the corresponding superpotentials. We start again with the discussion of the results using the standard discretisation in the system with unbroken supersymmetry. In figure 20, we show the Ward identity $W_1(t)$ for $\mu L = 4$ and $\mu L = 10$ for a range of lattice spacings a/L at fixed coupling $f_u = 1$ for both periodic and antiperiodic boundary conditions. The figure illustrates how the Ward identity $W_1(t)$ is violated for finite lattice spacing. It can be seen that the violation for periodic b.c. becomes less severe as $a \to 0$, whereas for antiperiodic b.c. it does not. In figure 21, we plot the continuum extrapolation of $W_1(t/L = 1/2)$ at the coupling $f_b = 1$ for different values of μL. We find that $W_1(t/L = 1/2)$ extrapolates to zero for periodic b.c., independent of the value of μL. Supersymmetry is therefore restored in the continuum for periodic b.c., even at a finite extent of the quantum mechnical system. For antiperiodic b.c. on the other hand, $W_1(t/L = 1/2)$ does not extrapolate to zero for small μL, i.e., high temperature. However, as the temperature decreases, the violation weakens and for $\mu L \to \infty$ $W_1(t/L = 1/2)$ extrapolates to zero, implying that supersymmetry is restored in the zero temperature limit. On the level of the Ward identities W_1 in the continuum, our results hence confirm all expected features of unbroken supersymmetry at finite as well as at zero

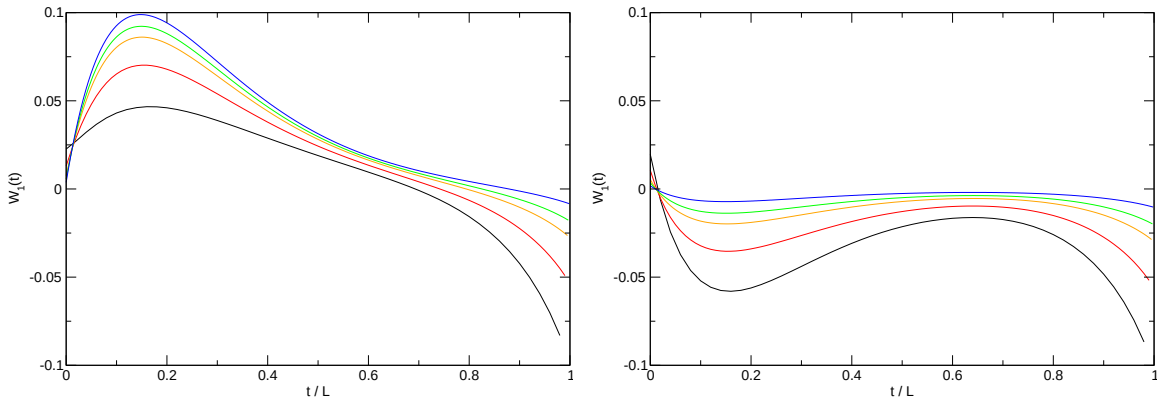

(a) $\mu L = 4, Z_a$ (b) $\mu L = 4, Z_p$

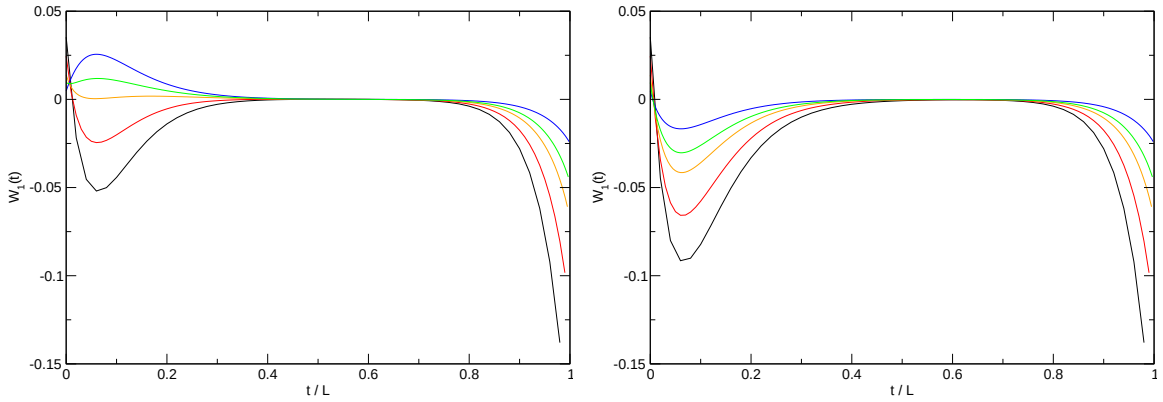

(c) $\mu L = 10, Z_a$ (d) $\mu L = 10, Z_p$

Figure 20: Unbroken supersymmetric quantum mechanics, standard discretization. The Ward identity W_1 for $L/a = 50$ (black), $L/a = 100$ (red), $L/a = 200$ (orange), $L/a = 300$ (green) and $L/a = 600$ (blue) for $\mu L = 4$ and $\mu L = 10$ at fixed coupling $f_u = 1$.

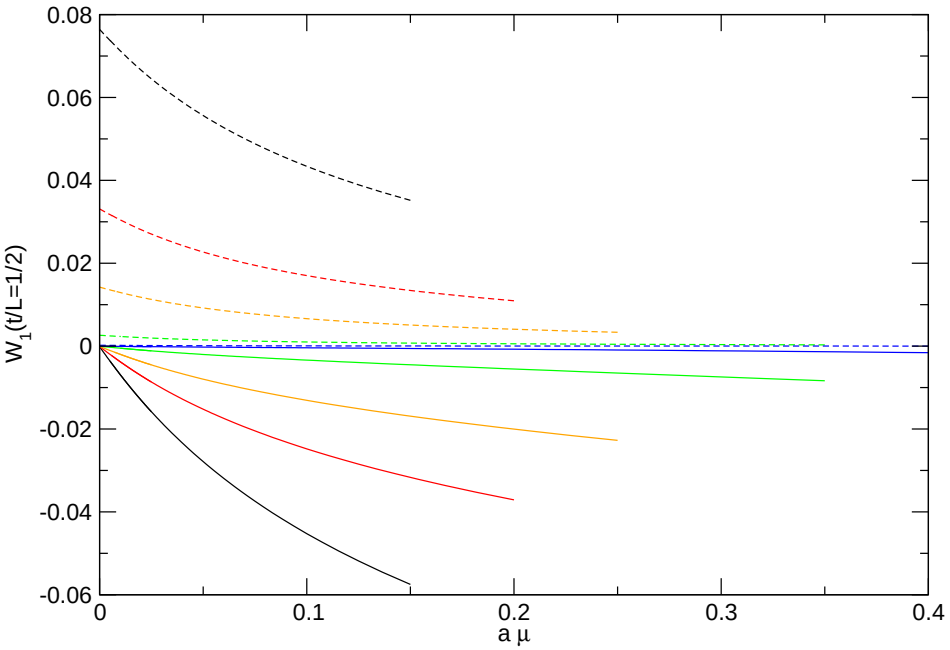

Figure 21: Unbroken supersymmetric quantum mechanics, standard discretisation. Continuum extrapolation of $W_1(t/L = 1/2)$ for $\mu L = 3$ (black), $\mu L = 4$ (red), $\mu L = 5$ (orange), $\mu L = 7$ (green) and $\mu L = 10$ (blue) for periodic (sold lines) and antiperiodic b.c. (dashed lines) at fixed coupling $f_b = 1$.

temperature. Moreover, our results tell us how the system behaves at finite lattice spacing. First we note that at any fixed lattice spacing, W_1 extrapolates to zero in the limit $\mu L \to \infty$ independently of the boundary conditions. This is a reflection of the fact that the violation of the supersymmetry in the action from using the standard discretisation is just a surface term which obviously becomes irrelevant in the limit $\mu L \to \infty$. On the other hand, we note that the decoupling of this artefact seems to happen faster in a system with antiperiodic boundary conditions. In other words, the convergence to $W_1 = 0$ is slower for periodic b.c. as can be seen by comparing the limit $\mu L \to \infty$ for example at fixed $a\mu = 0.15$.

Next, we consider the Ward identity W_1 for broken supersymmetry using the standard discretisation. In figure 22, we show W_1 for $\mu L = 5$ and $\mu L = 10$ for a range of lattice spacings a/L at fixed coupling $f_b = 1$ both for periodic and antiperiodic boundary conditions. This figure illustrates how the Ward identity W_1 is violated for broken supersymmetry at finite lattice spacing. However, unlike in the previous case of unbroken supersymmetry, the violation of the Ward identity W_1 remains finite even when the lattice spacing or the temperature goes to zero. To illustrate this further, we trace the Ward identity $W_1(t/L = 3/4)$ into the continuum for different μL in figure 23. Clearly, the violation remains in the continuum, independently of the boundary conditions and the size or temperature of the system. In this case too, all features of broken supersymmetry are numerically confirmed on the level of the Ward identity W_1.

Next we consider the Ward identity W_1 for unbroken supersymmetry using the Q-exact discretisation. In this case W_1 is of special interest since for this action $\delta_1 S_L^Q = 0$ at finite lattice spacing, and we should hence be able to confirm that $W_1(t) = 0$ exactly $\forall t$ at finite lattice spacing for unbroken supersymmetry and periodic boundary conditions. In figure 24 we show the Ward identity W_1 at different values of the lattice spacing a/L at fixed coupling

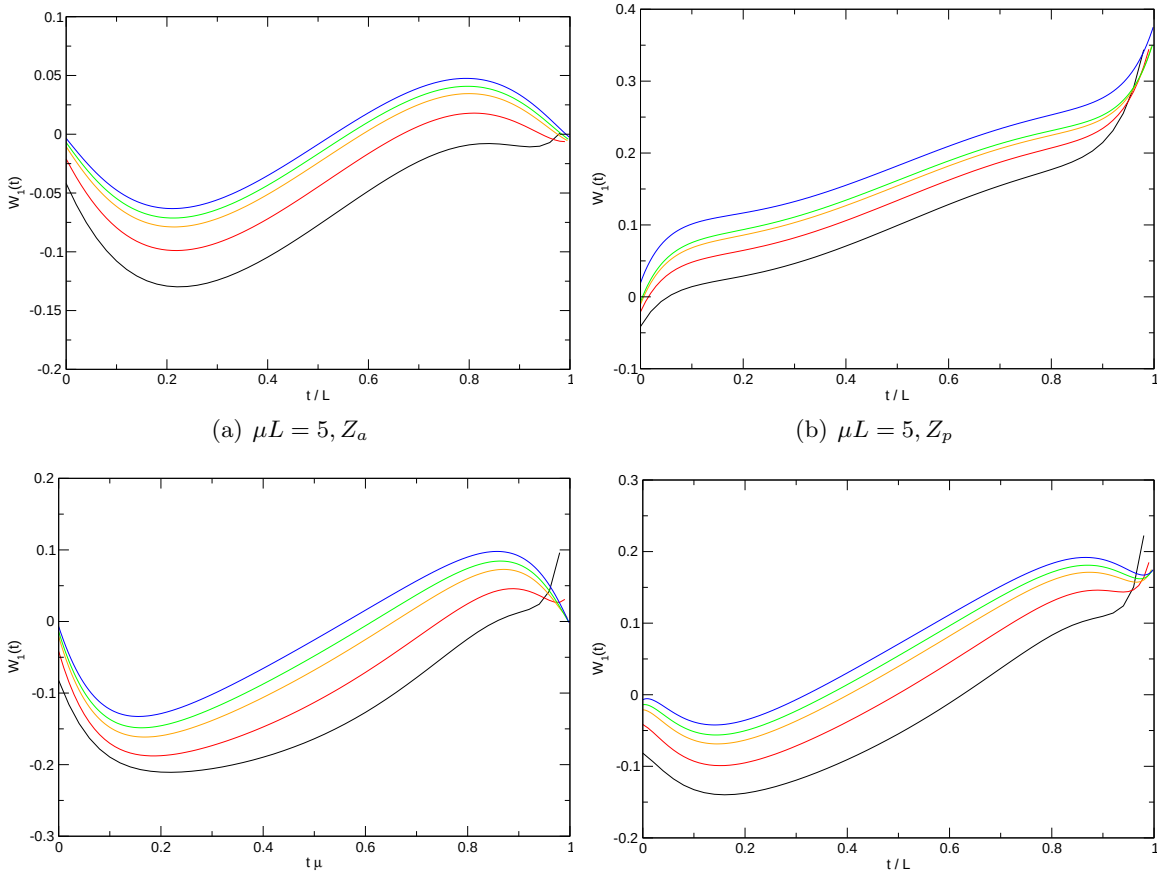

(a) $\mu L = 5, Z_a$ (b) $\mu L = 5, Z_p$

(c) $\mu L = 10, Z_a$ (d) $\mu L = 10, Z_p$

Figure 22: Broken supersymmetric quantum mechanics, standard discretisation. The Ward identity W_1 for $L/a = 50$ (black), $L/a = 100$ (red), $L/a = 200$ (orange), $L/a = 300$ (green) and $L/a = 600$ (blue) for $\mu L = 5$ and $\mu L = 10$ at fixed $f_b = 1$.

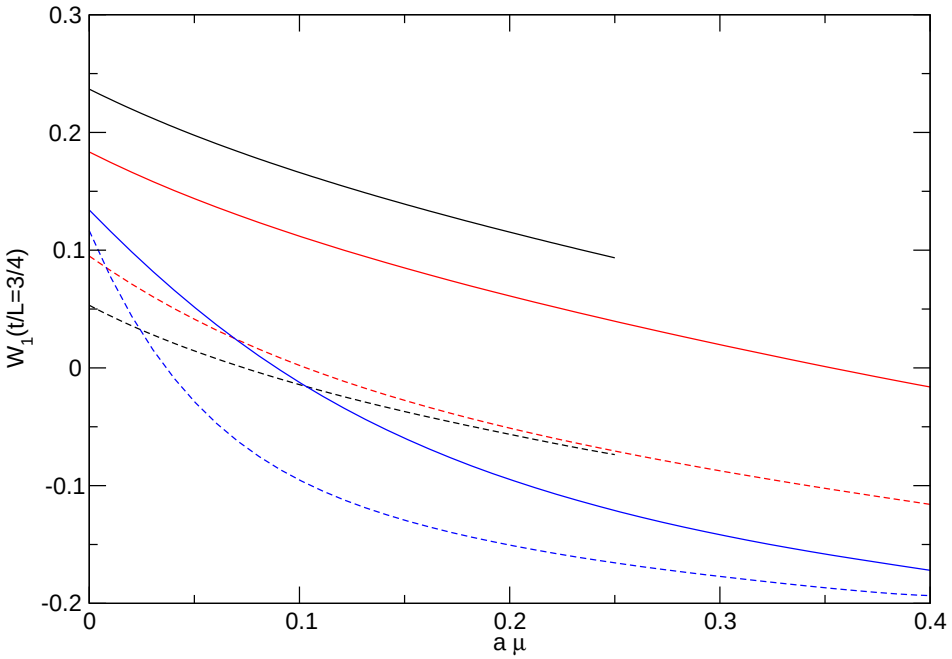

Figure 23: Broken supersymmetric quantum mechanics, standard discretisation. Continuum extrapolation of $W_1(t/L = 3/4)$ for $\mu L = 5$ (black), $\mu L = 10$ (red) and $\mu L = 20$ (blue) for periodic (solid lines) and antiperiodic b.c. (dashed lines) at fixed coupling $f_b = 1$.

$f_u = 1$ and fixed extent $\mu L = 10$ for both periodic and antiperiodic boundary conditions. The plot shows that the Ward identity W_1 represented by the dashed line is indeed zero $\forall t$ using periodic boundary conditions at any finite lattice spacing. Note, that $W_1(t)$ are composed of the bosonic and fermionic correlators as given in eq.(37) and are in fact non-trivially zero. For antiperiodic b.c. on the other hand, the violation of the Ward identity at finite temperature is evident. To observe the behaviour of the Ward identity W_1 in the zero temperature limit, we again trace $W_1(t/L = 1/2)$ into the continuum for different μL. Of course, for periodic b.c. $W_1(t/L = 1/2)$ is zero for any finite $a\mu$ and any value of μL (dashed lines). However, for antiperiodic b.c., the extrapolation of $W_1(t/L = 1/2)$ shows a dependence on μL, but in the limit $\mu L \to \infty$ this violation also vanishes, as expected.

We now perform the same analysis for the Ward identity W_2 given in eq.(2.4). This Ward identity is not expected to vanish for finite lattice spacing, since the action S_L^Q is not invariant under the supersymmetry transformation δ_2. In figure 26 we show $W_2(t)$ for different lattice spacings a/L for $\mu L = 10$ at fixed coupling $f_u = 1$. As expected, this Ward identity is violated for both periodic and antiperiodic b.c. at finite lattice spacing and for finite temperature. To observe the continuum behaviour, we trace $W_2(t/L = 1/2)$ in this case, too. The continuum extrapolation for different μL is shown in figure 27. For periodic b.c., the violation of the Ward identity $W_2(t/L = 1/2)$ vanishes in the continuum independently of the chosen μL. The restoration of supersymmetry in the continuum is thus also confirmed via the Ward identity $W_2(t/L = 1/2)$. For antiperiodic b.c. however, the violation does not vanish for small μL. Again, this is just a reflection of the fact that the finite temperature breaks the supersymmetry, and it is only restored in the zero temperature limit. Hence, on the level of the Ward identities W_1 and W_2, all the features of unbroken supersymmetry formulated with the Q-exact action are numerically confirmed. Analogously to the standard discretisation

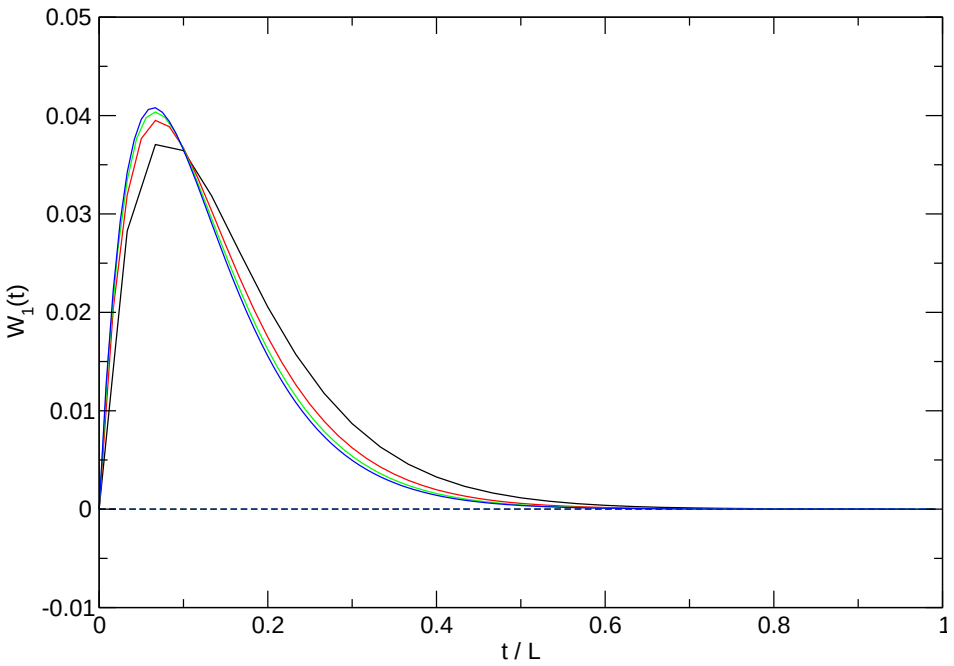

Figure 24: Unbroken supersymmetric quantum mechanics, Q-exact discretisation. The Ward identity $W_1(t)$ for $L/a = 30$ (black), $L/a = 60$ (red), $L/a = 90$ (green) and $L/a = 120$ (blue) for antiperiodic (solid lines) and periodic b.c. (dashed lines) for $\mu L = 10$ at fixed coupling $f_u = 1$.

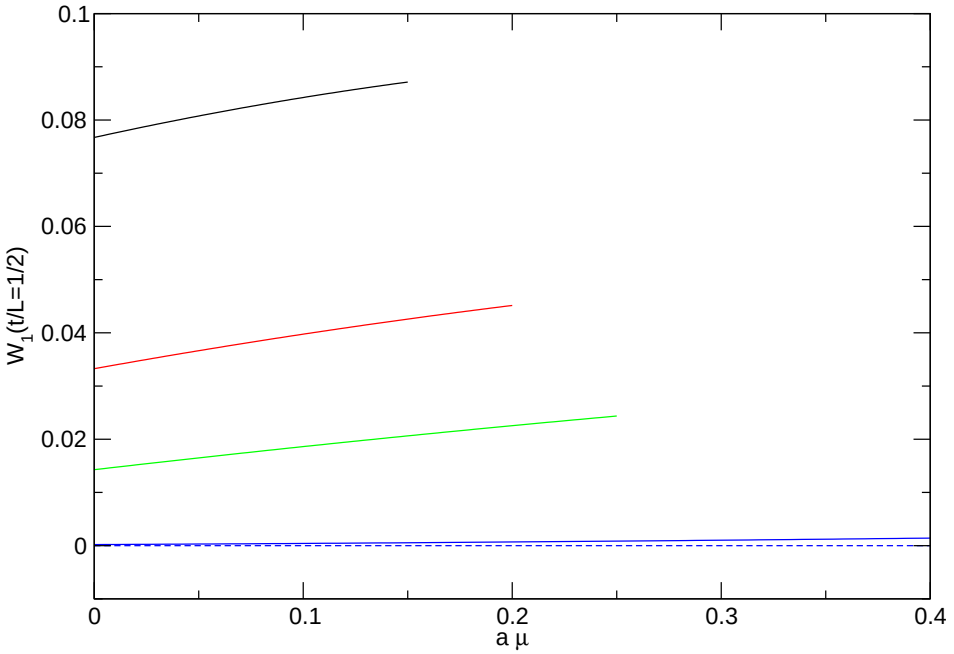

Figure 25: Unbroken supersymmetric quantum mechanics, Q-exact discretisation. Continuum extrapolation of $W_1(t/L = 1/2)$ for $\mu L = 3$ (black), $\mu L = 4$ (red), $\mu L = 5$ (green) and $\mu L = 10$ (blue) for antiperiodic (solid lines) and periodic b.c. (dashed lines) at fixed coupling $f_b = 1$.

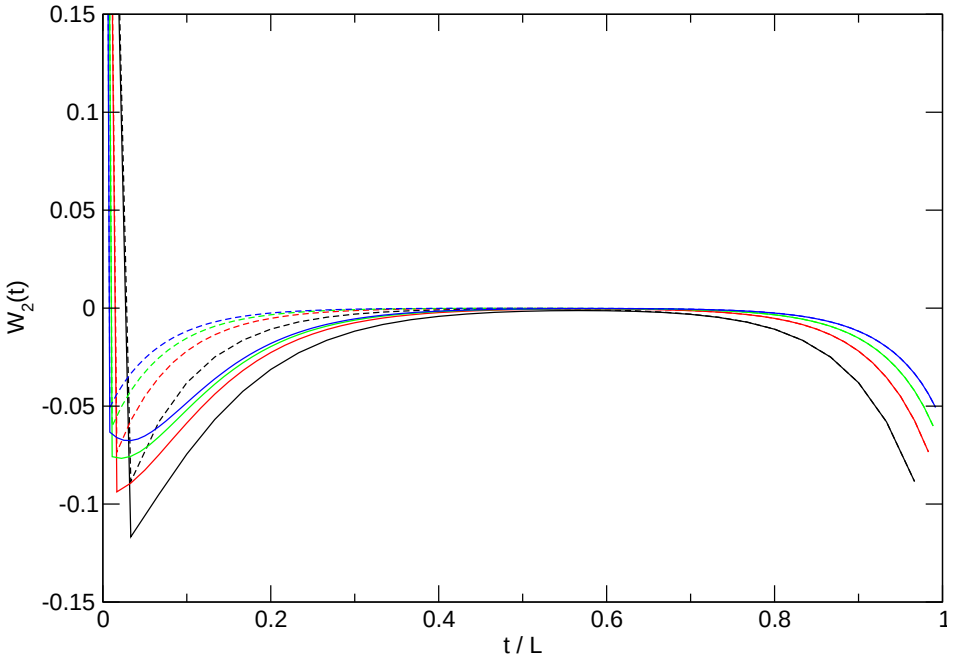

Figure 26: Unbroken supersymmetric quantum mechanics, Q-exact discretisation. The Ward identity W_2 for $L/a = 30$ (black), $L/a = 60$ (red), $L/a = 90$ (green) and $L/a = 120$ (blue) for antiperiodic (solid lines) and periodic b.c. (dashed lines) for $\mu L = 10$ at fixed coupling $f_u = 1$.

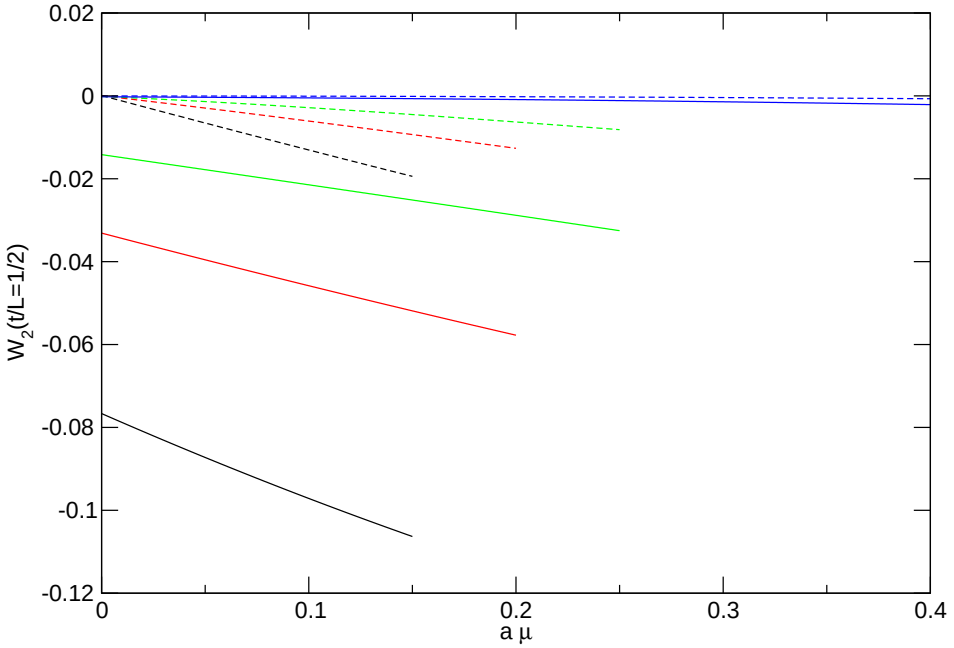

Figure 27: Unbroken supersymmetric quantum mechanics, Q-exact discretisation. Continuum extrapolation of $W_2(t/L = 1/2)$ for $\mu L = 3$ (black), $\mu L = 4$ (red), $\mu L = 5$ (green) and $\mu L = 10$ (blue) for antiperiodic (solid lines) and periodic b.c. (dashed lines) at fixed coupling $f_u = 1$.

$W_2(t/L = 1/2)$ extrapolates to zero at any value of the lattice spacing, independent of the employed boundary conditions. This confirms that the violation of the supersymmetry δ_2 in the Q-exact formulation is just a boundary term which decouples from the system in the limit $\mu L \to \infty$.

3.5 The ground state energy E_0

In this section we follow [10] and measure the ground state energy E_0 for the Q-exact action via the expectation value of an appropriate Hamilton operator H. In a field theory it is a priori not clear how to measure an absolute energy and there are in fact several possible candidate Hamilton operators which differ from each other by constant shifts. However, the authors of [10] argue via the off-shell formulation of the theory, that constructing the Hamilton operator from the Q-exact action leads to the correct mesurement of the ground state energy. In the lattice formulation, it reads

$$H = -\frac{1}{2}(\Delta^- \phi)^2 + \frac{1}{2}\left(P'\right)^2 - \frac{1}{2}\overline{\psi}(\Delta^- - P'')\psi\,. \tag{44}$$

Using the superpotential P_u in eq.(3), the expectation value of this Hamilton operator is explicitly given by

$$\begin{aligned}\langle H\rangle \;\; = \;\; & \frac{1}{2}(\mu^2-2)\langle\phi^2\rangle + \mu g\langle\phi^4\rangle + \frac{1}{2}g^2\langle\phi^6\rangle + \langle\phi_1\phi_0\rangle \\ & + \frac{1}{2}(\mu-1)\langle\overline{\psi}\psi\rangle + \frac{1}{2}\langle\overline{\psi}_1\psi_0\rangle + \frac{3}{2}g^2\langle\overline{\psi}\psi\phi^2\rangle.\end{aligned} \tag{45}$$

In figure 28 we show the continuum values for $\langle H\rangle/\mu$ for different μL for both periodic and antiperiodic b.c. at a coupling $f_u = 1$. For periodic b.c. the operator H yields zero independently of the lattice spacing a/L and μL. here, too, this zero is non-trivial, since it emerges from an exact cancellation of the various expectation values in eq.(45). For antiperiodic b.c. the continuum values show an exponentially decreasing behaviour with μL and the expectation value $\langle H\rangle/\mu$ goes to zero only in the limit $\mu L \to \infty$. The exponential behaviour can easily be inferred from expanding the expectation value in terms of the energy states. Taking only the lowest mass gap into account one obtains

$$\langle H\rangle = \frac{2\, m_1^b\, e^{-m_1^b L}}{1 + 2\, e^{-m_1^b L}}\,. \tag{46}$$

The dotted line in figure 28 corresponds to this expression with $m_1^b/\mu = 1.6865$, in agreement with our results in section 3.3. The full line is a phenomenological fit using m_1^b in eq.(46) as an effective fit parameter which also takes into account additional contributions from higher excitations. In conclusion, our exact results confirm the arguments presented in [10].

4 Conclusions and outlook

In this paper we have presented exact results for $\mathcal{N} = 2$ supersymmetric quantum mechanics discretised on the lattice. Expressing the bosonic and fermionic degrees of freedom in terms of bosonic and fermionic bonds, respectively, allows to completely characterise the system

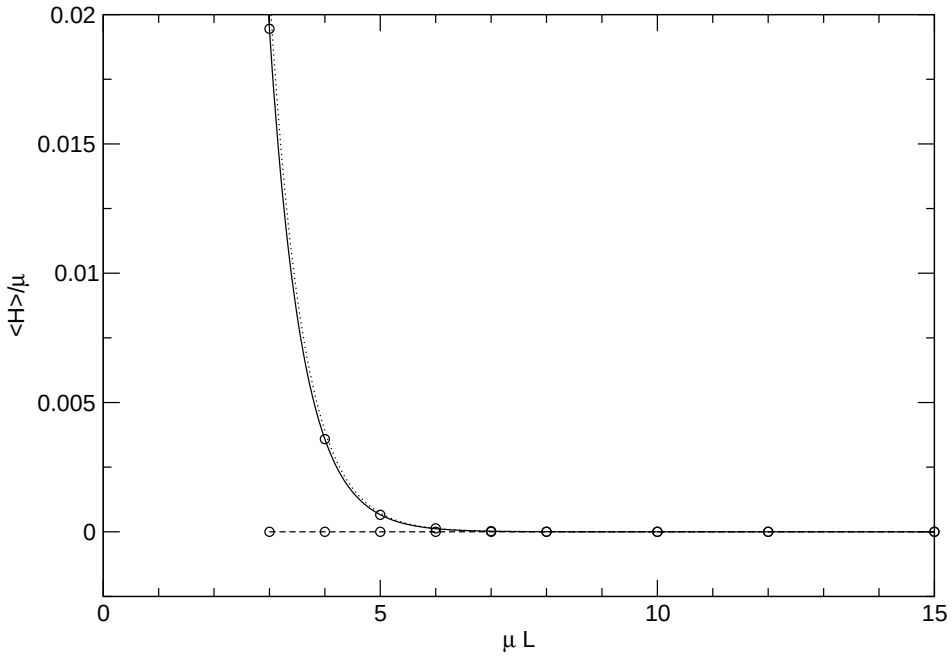

Figure 28: Unbroken supersymmetric quantum mechanics, Q-exact action. Continuum values of $\langle H\rangle/\mu = E_0/\mu$ for periodic (dashed line) and antiperiodic b.c. (solid line) for a range of system sizes μL at fixed coupling $f_u = 1$. The dotted line describes the leading asymptotic behaviour for large μL while the full line is a phenomenological fit.

by means of transfer matrices defined separately in the bosonic and fermionic sector. From the properties of the transfer matrices one can derive exact results for all observables at finite lattice spacing and we present such results for a variety of interesting observables using two different discretisation schemes. The first is the standard discretisation which involves a Wilson term for the fermions and a counterterm which guarantees the restoration of supersymmetry in the continuum. The second discretisation is a Q-exact one which maintains one of the two supersymmetries exactly at finite lattice spacing [4]. The exact calculations allow to study in detail how the continuum limit $a\mu \to 0$ as well as the thermodynamic limit $\mu L \to \infty$ are approached and how the two limits interfere with each other. The latter of the two limits can be interpreted as the zero temperature limit in a system with antiperiodic b.c. for the fermion. Since the supersymmetry of the system can be broken both by the finite lattice spacing and the finite temperature the interplay of the two limits is of particular interest in order to gain a complete understanding of the various lattice discretisation schemes.

For the ratio of partition functions Z_p/Z_a, which is proportional to the Witten index, we find for example the interesting result that in a system with broken supersymmetry, where the Witten index is supposed to vanish, it extrapolates to -1 in the zero temperature limit at any finite lattice spacing. On the other hand, it extrapolates to 0 in the continuum limit for any finite temperature or extent of the system. In fact it turns out that the lattice spacing corrections are exponentially enhanced towards the low temperature limit, so in this case the order of the limits is crucial to describe the correct physics in the continuum. It is also interesting to study the influence of the finite lattice spacing on the fermionic and bosonic two-point correlation functions. In particular, for broken supersymmetry one expects the emergence of a massless Goldstino mode and within our approach we can study in detail

how the mode expresses itself in the fermionic correlation function. Moreover, we study the bosonic and fermionic spectrum of the theory which allows to better quantify the lattice corrections. We demonstrate how the degeneracy between the bosonic and fermionic excitations is restored in the continuum both for broken and unbroken supersymmetry when the standard discretisation scheme is used. For broken supersymmetry we see how the finite lattice spacing regulates the Goldstino mode and hence also the vanishing Witten index. Although the coupling strengths we study are well in the nonperturbative regime, the leading lattice corrections in the spectrum turn out to be reasonably small and follow the usual expectations of being $\mathcal{O}(a)$ to leading order. For the Q-exact dicretisation scheme we find exact degeneracy between the fermionic and bosonic excitations at any finite lattice spacing. It seems that maintaining only one of the supersymmetries on the lattice is sufficient to guarantee the exact degeneracy. In this case, too, the lattice artefacts are $\mathcal{O}(a)$ to leading order, but appear to be enhanced with respect to the standard discretisation, in particular for the higher lying excitations.

Furthermore, we are able to study in detail the behaviour of various Ward identities towards the continuum and thermodynamic limits for both discretisation schemes. Our exact results show that the finite lattice spacing and finite temperature effects can sometimes be rather large, but nevertheless both supersymmetries are completely restored in the appropriate limits without any surprises. The Ward identities W_1 and W_2 play a particularly important role for the Q-exact discretisation. Since in that case half of the supersymmetries is exactly maintained, some of the Ward identities are expected to be fulfilled at finite lattice spacing for periodic boundary conditions. We prove numerically that this is indeed the case. Finally, for the Q-exact discretisation we also demonstrate the correctness of the conjecture in [10, 11] which provides a scheme to calculate the ground state energy.

In conclusion, we now have a rather complete qualitative and quantitative understanding of the interplay between infrared and ultraviolet effects in supersymmetric quantum mechanics regulated on a lattice of finite extent and finite lattice spacing. Moreover, our exact results provide a benchmark for any attempt to deal with supersymmetric field theories using a new discretisation scheme, or in fact even for any new regularisation scheme such as, e.g., the one described in [12]. In addition, new simulation algorithms specific to supersymmetric theories can be tested against our exact results. For example, there exist particular algorithms which are tailored to efficiently simulate bond occupation numbers, be they bosonic [13] or fermionic [14]. In fact, in the third paper of our series [5] we present the practical application of the so called open fermion string algorithm to supersymmetric quantum mechanics in the bond formulation and prove its feasibility to deal numerically with the sign problem associated with broken supersymmetry. Our exact results here provide the necessary background to assess the validity and success of the numerical simulations using the fermion loop approach. Similarly, alternative approaches which attempt or claim to solve fermion sign problems, such as the ones in [15, 16, 17], can be tested in supersymmetric quantum mechanics and gauged against the exact results presented here.

One important question is of course whether the bond formulation and transfer matrix approach outlined here can be extended and applied to more complicated systems. This is indeed possible as we demonstrated in [18] where the fermion loop approach is applied to supersymmetric Yang-Mills quantum mechanics. In that system, transfer matrices describing the fermionic degrees of freedom can also be constructed explicitly in each sector with fixed fermion number and it is shown how they are related to the standard canonical approach

which deals with fermions. What is interesting to note is that the model involves a gauge degree of freedom, and the transfer matrix approach can indeed be extended to handle also this situation. Concerning the extension of the approach to higher dimensions the perspectives are not so bright. Up to a few exceptions, it is in general not possible or practical to construct transfer matrices for systems in higher dimensions. In contrast, the fermion loop formulation can be used on its own and in some cases indeed provides the basis for the solution of the fermion sign problem such as in the $\mathcal{N} = 1$ Wess-Zumino model [7, 19].

A Technical aspects

In this appendix we briefly describe and illustrate our procedure to choose an appropriate cutoff for the bond occupation numbers. The introduction of the cutoff is necessary in order to construct transfer matrices of finite size, such that they can be handled numerically. In the bond formulation the weights involving large bond occupation numbers are suppressed by factors of $1/n_i^b!$, so their contributions become irrelevant as the occupation numbers grow. The truncation of the hopping expansion hence provides a natural and systematic scheme to limit the size of the transfer matrices.

For the standard discretisation we only have one type of bosonic bond $b_{1\to 1}$ and hence the size of the transfer matrix grows linearly with the cutoff $N_{1\to 1}^{cut}$ on the occupation number $n_{1\to 1}^b$. Calculating an observable at different lattice spacings with varying cutoff $N_{1\to 1}^{cut}$, effects from the finite bosonic cutoff manifest themselves as a sudden bend in an otherwise linear curve close to the continuum. In figure 29 we show an example of this effect by means of the expectation value $\langle\phi^2\rangle_a \cdot \mu$ for antiperiodic b.c. and unbroken supersymmetry as a function of the lattice spacing $a\mu$ for different values of μL at fixed coupling $f_u = 1$. The effect of the finite cutoff for the bosonic occupation numbers is illustrated by comparing the observable for two different cutoffs, $N_{1\to 1}^{cut} = 800$ and $N_{1\to 1}^{cut} = 500$ close to the continuum. The curves for the expectation value are indistinguishable for $a\mu \gtrsim 0.075$, but closer to the continuum, the curve for the smaller cutoff suddenly diverges from the curve for the larger cutoff, and the values obtained using the lower cutoff are no longer reliable. For the larger cutoff a similar effect appears at a smaller lattice spacing, but is again clearly visible. So for any given cutoff, the results are reliable only down to a specific lattice spacing, which however is easy to determine since the cutoff effects are so dramatic. It turns out that for the observables considered in this paper, a cutoff $N_{1\to 1}^{cut} = 800$ is sufficient to safely reach a lattice spacing $a\mu \sim 0.005$, well in the regime where the dominating lattice artefacts are of order $\mathcal{O}(a)$ and the corrections of $O(a^2)$ are very small. It is then safe to extrapolate the data to the continuum by fitting a quadratic function

$$f(x) = c_0 + c_1 x + c_2 x^2 \tag{47}$$

to the data with $a\mu \gtrsim 0.005$ while making sure that the data is invariant under a change of the cutoff around $N_{1\to 1}^{cut} = 800$. For almost all observables, these fits can be performed without any difficulties, but in some cases, where the lattice artefacts turn out to be particularly large, higher corrections can be taken into account without any problems and we indicate in the discussion when we do so.

For the Q-exact discretisation, we have two types of bosonic bonds $b_{1\to 1}$ and $b_{1\to\nu}$ and we need to introduce two cutoffs $N_{1\to 1}^{cut}$ and $N_{1\to\nu}^{cut}$ on the corresponding occupation numbers, hence the size of the transfer matrices grows quadratically in the cutoff, i.e. as $N_{1\to 1}^{cut} \cdot N_{1\to\nu}^{cut}$.

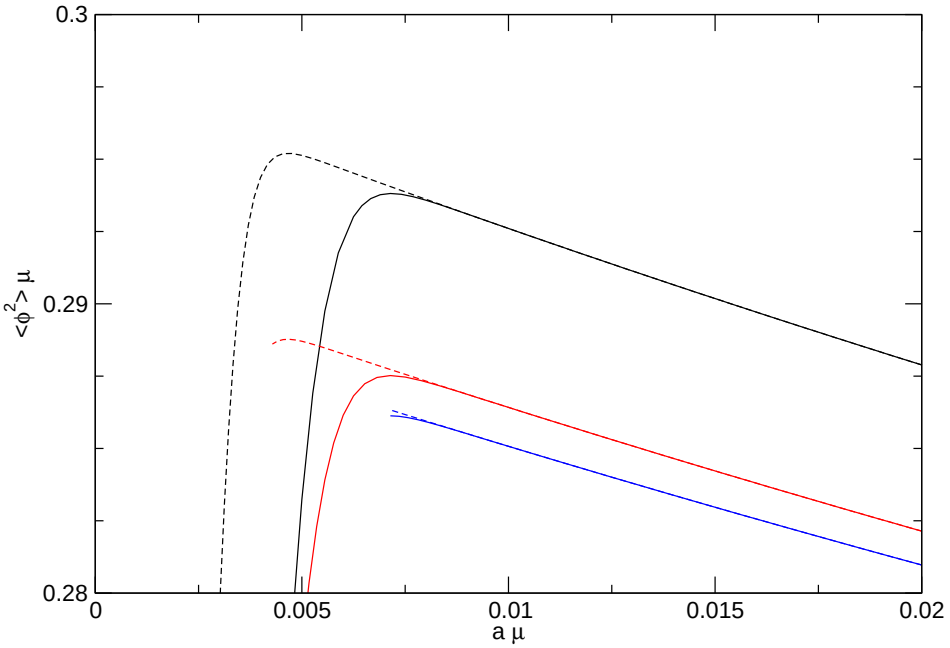

Figure 29: $\langle\phi^2\rangle_a \cdot \mu$ as a function of $a\mu$ at fixed coupling $f_u = 1$ for different $\mu L = 2$ (black), $\mu L = 3$ (red), and $\mu L = 5$ (blue) and $N_{1\to1}^{cut} = 800$ (dashed line) and $N_{1\to1}^{cut} = 500$ (solid line). Effects from the finite cutoff on the bosonic bond occupation numbers near the continuum are clearly visible.

Nevertheless, it turns out that also in this case the onset of cutoff effects in the observables is clearly indicated by a sudden bend away from the linear behaviour expected towards the continuum $a\mu \to 0$. Typically we choose the cutoffs $N_{1\to1}^{cut} = 64$ and $N_{1\to\nu}^{cut} = 16$ for our calculations, yielding transfer matrices of size 1105×1105. For the extrapolations, we proceed analogously to the case with the standard discretisation and we find that extrapolating the exact results with quadratic fits allows for reliable continuum results for the Q-exact discretisation, too.

References

[1] D. Baumgartner and U. Wenger, *Supersymmetric quantum mechanics on the lattice: I. Loop formulation*, .

[2] J. Giedt, R. Koniuk, E. Poppitz, and T. Yavin, *Less naive about supersymmetric lattice quantum mechanics*, *JHEP* **0412** (2004) 033, [hep-lat/0410041].

[3] G. Bergner, T. Kaestner, S. Uhlmann, and A. Wipf, *Low-dimensional Supersymmetric Lattice Models*, *Annals Phys.* **323** (2008) 946–988, [arXiv:0705.2212].

[4] S. Catterall and E. Gregory, *A Lattice path integral for supersymmetric quantum mechanics*, *Phys.Lett.* **B487** (2000) 349–356, [hep-lat/0006013].

[5] D. Baumgartner and U. Wenger, *Supersymmetric quantum mechanics on the lattice: III. Algorithms and simulations*, .

[6] D. Baumgartner, *Supersymmetric Models in Low Dimensions on the Lattice*. PhD thesis, AEC for fundamental physics, University of Bern, 2012.

[7] K. Steinhauer and U. Wenger, *Spontaneous supersymmetry breaking in the two-dimensional N=1 Wess-Zumino model, accepted for publication in PRL* (2014) [arXiv:1410.6665].

[8] A. Salam and J. Strathdee, *On goldstone fermions*, *Physics Letters* **B49** (1974), no. 5 465 – 467.

[9] C. Wozar and A. Wipf, *Supersymmetry breaking in low dimensional models*, *Annals Phys.* **327** (2012) 774–807, [arXiv:1107.3324].

[10] I. Kanamori, F. Sugino, and H. Suzuki, *Observing dynamical supersymmetry breaking with Euclidean lattice simulations*, *Prog.Theor.Phys.* **119** (2008) 797–827, [arXiv:0711.2132].

[11] I. Kanamori, *A Method for Measuring the Witten Index Using Lattice Simulation*, *Nucl.Phys.* **B841** (2010) 426–447, [arXiv:1006.2468].

[12] M. Hanada, J. Nishimura, and S. Takeuchi, *Non-lattice simulation for supersymmetric gauge theories in one dimension*, *Phys.Rev.Lett.* **99** (2007) 161602, [arXiv:0706.1647].

[13] N. V. Prokof'ev and B. V. Svistunov, *Worm algorithms for classical statistical models*, *Phys.Rev.Lett.* **87** (2001) 160601, [cond-mat/0103146].

[14] U. Wenger, *Efficient simulation of relativistic fermions via vertex models*, *Phys.Rev.* **D80** (2009) 071503, [arXiv:0812.3565].

[15] S. Chandrasekharan, *Solutions to sign problems in lattice Yukawa models*, *Phys.Rev.* **D86** (2012) 021701, [arXiv:1205.0084].

[16] S. Chandrasekharan, *Fermion Bag Approach to Fermion Sign Problems*, *Eur.Phys.J.* **A49** (2013) 90, [arXiv:1304.4900].

[17] S. Chandrasekharan, *The Fermion bag approach to lattice field theories*, *Phys.Rev.* **D82** (2010) 025007, [arXiv:0910.5736].

[18] K. Steinhauer and U. Wenger, *Loop formulation of supersymmetric Yang-Mills quantum mechanics, accepted for publication in JHEP* (2014) [arXiv:1410.0235].

[19] D. Baumgartner and U. Wenger, *Simulation of supersymmetric models on the lattice without a sign problem*, *PoS* **LAT2010** (2011) [arXiv:1104.0213].

Paper 8

Supersymmetric quantum mechanics on the lattice: III. Simulations and algorithms

David Baumgartner and Urs Wenger, to be submitted to Nucl. Phys. **B**

Supersymmetric quantum mechanics on the lattice: III. Simulations and algorithms

David Baumgartner and Urs Wenger

Albert Einstein Center for Fundamental Physics,
Institute for Theoretical Physics, University of Bern,
Sidlerstrasse 5, CH–3012 Bern, Switzerland

Abstract

In the fermion loop formulation the contributions to the partition function naturally separate into topological equivalence classes with a definite sign. This separation forms the basis for an efficient fermion update algorithm using a fluctuating open fermion string. It guarantees sufficient tunneling between the topological sectors, and hence provides a solution to the fermion sign problem affecting systems with broken supersymmetry. Moreover, the algorithm shows no critical slowing down even in the massless limit and can hence handle the massless Goldstino mode emerging in the supersymmetry broken phase. In this paper – the third in a series of three – we present the details of the simulation algorithm and demonstrate its efficiency by means of a few examples.

1 Introduction

The reformulation of the system in terms of bosonic and fermionic bonds as derived in the first paper of our series [1] provides a perfect setup for Monte Carlo simulations, since the reduction in complexity by going from continuous to discrete variables is huge. More specifically, expressing the Grassmann fields in terms of fermionic bonds avoids the expensive calculation of the determinant and allows the use of special algorithms for which critical slowing down is essentially absent [2, 3] and simulations are possible even in the massless limit [4]. This is of particular importance for systems with broken supersymmetry, since the physics of those is driven by the massless Goldstino mode. In the present paper – the last in a series of three – we describe in detail such an algorithm and demonstrate its efficiency. Since the model can be solved exactly at finite lattice spacing by means of transfer matrices, as discussed in the second paper of our series [5], there is in principle no need for numerical simulations. So the present paper rather constitutes a feasibility study to test the practicability and efficiency of the proposed simulation algorithm for the quantum mechanical system in the bond formulation. In that sense it also serves as a preparation for the application of the algorithm, in particular the fermionic part, in more complex situations, such as in supersymmetric Yang-Mills quantum mechanics [6], in the $\mathcal{N} = 1$ Wess-Zumino model [7, 8, 9] or in the supersymmetric nonlinear $O(N)$ sigma model [10]. The advantage of the application of the algorithm in the quantum mechanical model presented here is of course the fact that the correctness of the algorithm

can be crosschecked with the exact results from the transfer matrix approach, and that the algorithm can hence be validated in detail.

There is another rather pedagogical reason which motivates to consider a new simulation algorithm for quantum mechanics in the bond formulation. Often, simple quantum mechanical systems such as the harmonic and anharmonic oscillator are used to introduce the path integral approach. Similarly, the systems also provide a pedagogical context in which various Monte Carlo simulation algorithms can be illustrated and discussed, see for example [11] for an early example. However, it turns out that the standard Metropolis algorithms and even more advanced algorithms such as the overrelaxation or heat bath algorithm become extremely inefficient towards the continuum limit. This has to do with the usual critical slowing down of the simulations towards the continuum limit, and for the anharmonic oscillator also with the suppressed tunneling at small lattice spacing. The algorithms presented here do not suffer from these deficiencies, because they eliminate critical slowing down, and in addition, in the bond formulation the $\mathbb{Z}_2$-symmetry $\phi \to -\phi$ is exactly maintained for each bond configuration.

Last but not least, the numerical simulations presented here serve as a test of the practicability of the solution of the fermion sign problem proposed in [4] and discussed further in the first paper of our series [1]. The solution is based on two ingredients. Firstly, the lattice regulates the vanishing Witten index and therefore also the sign problem. Secondly, the fermion loop formulation provides a tool to handle the fluctuating sign, because it naturally separates the contributions into topological equivalence classes possessing a definite sign. Nevertheless, it is a priori not clear whether the lattice artefacts and the statistical fluctuations can be kept under sufficient control in a practical simulation. The statistical fluctuations of the sign are essentially determined by the amount of tunneling between the topological sectors, i.e., between the fermionic and bosonic vacuum. In order for the fermion update algorithm to be a true solution to the sign problem, it must guarantee a sufficiently efficient tunneling rate. The results in this paper demonstrate that this is indeed the case. Not surprinsingly, the open fermion string algorithm discussed here has also been applied in the $\mathcal{N} = 1$ Wess-Zumino model [9], where it has proven to be extremely successful.

Of course, supersymmetric quantum mechanics has already been simulated on the lattice in various setups using standard algorithms, cf. for example [12, 13, 14, 15, 16, 17, 18, 19, 20]. However, the bond formulation together with the simulation algorithm presented here brings the numerical nonperturbative calculations to a new, unprecedented level of accuracy. In that sense, the results presented here and partly in [4] serve as a benchmark against which new formulations or simulation algorithms can be tested.

The present paper is organised as follows. In section 2 we construct in detail an algorithm designed for updating the bosonic and fermionic bond configurations. The discussion includes the explicit update steps and the derivation of the corresponding acceptance ratios. Their evaluation requires the calculation of site weight ratios which turn out to become numerically unstable for large site occupation numbers. Therefore, in section 3 we present a computational strategy which allows to evaluate the ratios for arbitrarily large occupation numbers. In section 4, we then present the results obtained using the proposed algorithm. The simulations are for the same discretisation schemes and superpotentials we used in the previous two papers [1, 5]. Since the section is merely meant as a validation of the algorithm, the discussion of the physics behind the results is kept short and we refer to the exact results in [5] for a more throrough discussion.

2 Simulation algorithm

We start our discussion from the partition function written as a as a sum over all allowed, possibly constrained bond configurations $\mathcal{C} = \{n_i^b(x), n^f(x)\}$ in the configuration space $\mathcal{Z}$,

$$Z = \sum_{\mathcal{C}\subset\mathcal{Z}} W_F(\mathcal{C})\,, \tag{1}$$

where the fermion number $F = 0, 1$ is determined by the fermionic bond configuration $\{n^f(x)\}$ with $n^f(x) = 0, 1$, and the weight $W_F(\mathcal{C})$ of a configuration is given by

$$W_F(\mathcal{C}) = \prod_x \left(\prod_i \frac{w_i^{n_i^b(x)}}{n_i^b(x)!} \right) \prod_x Q_F(N(x))\,. \tag{2}$$

Here, x denotes the sites of the lattice and i labels the various types of bosonic bonds b_i with $i \in \{j \to k \,|\, j, k \in \mathbb{N}\}$. The corresponding bosonic bond weights are denoted by w_i and $n_i^b(x) \in \mathbb{N}_0$ is the occupation number of the bond b_i connecting the sites x and $x+1$. The site weight Q_F depends on the site occupation number, i.e. the total number of bosonic bonds connected to site x,

$$N(x) = \sum_{j,k} \left(j \cdot n^b_{j\to k}(x) + k \cdot n^b_{j\to k}(x-1) \right) \tag{3}$$

and is given by

$$Q_F(N(x)) = \int_{-\infty}^{\infty} d\phi\ \phi^N(x) \mathrm{e}^{-V(\phi)} M(\phi)^{1-F}\,. \tag{4}$$

In section 3 we will discuss in detail the computational strategy necessary to reliably evaluate ratios of these integrals for arbitrary and possibly large site occupation numbers. The type of bonds b_i, the weights w_i as well as the potential $V(\phi)$ and the monomer term $M(\phi)$ in eq.(4) depend on the specifics of the chosen discretisation and the superpotential $P(\phi)$. We refer to the appendix of our first paper [1] for a compilation of the discretisations and superpotentials considered in our series.

As mentioned above, the bond configurations $\mathcal{C} = \{n_i^b(x), n^f(x)\}$ are possibly constrained. In particular we have the local fermionic constraints

$$n^f(x-1) = n^f(x) \tag{5}$$

while the local bosonic constraints

$$N(x) = 0 \mod 2 \tag{6}$$

might be present depending on the bosonic symmetries of the system.

The challenge of updating constrained bond configurations lies precisely in the difficulty to maintain the constraints while moving efficiently through the configuration space $\mathcal{Z}$. In [21] Prokof'ev and Svistunov proposed to extend the constrained bosonic bond configuration space by introducing local sources which explicitly violate the constraints. The so-called worm algorithm then probes the extended configuration space by letting the local violations move around the lattice, thereby sampling directly the bosonic correlation function corresponding to the sources introduced. The contact with the original configuration space $\mathcal{Z}$ is established

when the violations annihilate each other, e.g. when moving to the same site on the lattice, such that the bond configuration fulfills again all constraints.

In [2] the idea has been extended to fermionic systems expressed in terms of fermionic bonds. The fermionic constraint in eq.(5) allows only either an empty or a completely filled fermion bond configuration. The difficulty for the direct application of the worm idea to the fermionic system lies in the fact that the introduction of fermionic source terms $\overline{\psi}_x \psi_x$ is incompatible with the the presence of the fermion loop at site x. A simple solution is to allow the unphysical situation of the site x being occupied by a propagating fermion and two additional sources. Such a configuration violates the Pauli exclusion principle and does not contribute to any physical observable. In the Grassmann path integral such a configurations indeed vanishes trivially.

In order to be more explicit, it is necessary to introduce the bond configuration spaces of bosonic and fermionic two-point correlation functions, $\mathcal{G}_F^b$ and $\mathcal{G}^f$, respectively, following our first paper [1]. Bond configurations in $\mathcal{C}_F^b$ contribute to the non-normalised bosonic two-point function according to

$$g_F^b(x_1 - x_2) \equiv \langle\langle \phi_{x_1} \phi_{x_2} \rangle\rangle_F = \sum_{\mathcal{C} \subset \mathcal{G}_F^b} \left(\prod_x \frac{Q_F(N(x) + \delta_{x,x_1} + \delta_{x,x_2})}{Q_F(N(x))} \right) \cdot W_F(\mathcal{C}) \,, \tag{7}$$

while the configurations in $\mathcal{C}^f$ contribute to the non-normalised fermionic two-point function as

$$g^f(x_1 - x_2) \equiv \langle\langle \psi_{x_1} \overline{\psi}_{x_2} \rangle\rangle = \sum_{\mathcal{C} \subset \mathcal{G}^f} \left[\prod_{x \in \mathcal{F}} \frac{Q_1(N(x))}{Q_0(N(x))} \right] \cdot W_0(\mathcal{C}) \,, \tag{8}$$

where $\mathcal{F}$ denotes the set of lattice sites belonging to the open fermion string associated with the fermionic correlation function. The key point of the bosonic and fermionic updating algorithm is that the bond configurations for $g_F^b(0)$, $g^f(0)$ and Z_F have identical bond elements. As a consequence, statistics for $g^{b,f}$ and Z can be accummulated in the same Monte Carlo process. If the bosonic constraints in eq.(6) are not present, e.g. for superpotentials with broken supersymmetry, the equivalence of bond configurations even extends to $g_F^b(x)$, i.e., $\mathcal{Z}_F = \mathcal{G}_F^b$. The movements from one configuration space to the other are induced by introducing or removing bosonic or fermionic sources according to the scheme given in figure 8 of our first paper [1].

In the following we will now discuss in detail the various updating steps which establish explicitly the connection between the bond configuration spaces $\mathcal{G}^f, \mathcal{Z}_F, \mathcal{G}_F^b$ and in addition move the system within $\mathcal{G}^f$ and $\mathcal{G}_F^b$. The moves are generated by a Monte Carlo process with probabilities given by the weights of the configurations in eq.(2). In particular, we derive the transition probabilities $P_X(\mathcal{C} \to \mathcal{C}')$ for the transition X from bond configuration $\mathcal{C}$ to $\mathcal{C}'$, which is then accepted by the usual Metropolis prescription

$$P_{acc}(\mathcal{C} \to \mathcal{C}') = \min\{1, P_X(\mathcal{C} \to \mathcal{C}')\}. \tag{9}$$

In order to simplify the discussion we select the update from $\mathcal{Z}_F$ to $\mathcal{G}_F^b$ or $\mathcal{G}^f$ with equal probability which is balanced by corresponding proposal probabilities to select between moving in $\mathcal{G}^f$ and $\mathcal{G}_F^b$ or returning to $\mathcal{Z}_F$.

2.1 Updating the fermionic bond configuration

Here we discuss the various update steps which relate the bond configurations spaces $\mathcal{Z}_0$ and $\mathcal{Z}_1$ via $\mathcal{G}^f$.

The step from $\mathcal{Z}_0$ to $\mathcal{G}^f$ and vice versa is induced by introducing or removing a pair of fermionic sources $\overline{\psi}_x\psi_x$ at site x, respectively. It is hence called 'put/remove' update step and is graphically illustrated in figure 1. The removal of the fermionic sources is suggested with

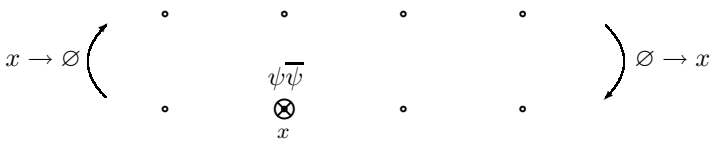

Figure 1: Fermionic bond configuration update algorithm. Graphical representation of the 'put/remove' update step $\varnothing \to x$ and $\varnothing \to x$, respectively. The sources are marked with a $\circ$ for ψ_x and a $\times$ for $\overline{\psi}_x$. The bosonic background bond configuration is not drawn.

probability $p_{\mathrm{rm}} = 1/2$ and is balanced on one side by the probability to add bosonic sources, and on the other by the probability to shift one of the sources and hence move within $\mathcal{C}^f$. Because the update step does not alter the fermionic bond configuration, we have $\mathcal{Z}_0 = \mathcal{G}^f(0)$, but on the other hand it adds or removes a fermionic monomer term $M(\phi)$ at site x. The relative weight of the configurations with or without this term is given by Q_1/Q_0 and the acceptance ratios are hence given by

$$P_{\mathrm{rm}}(x \to \varnothing) = \frac{2}{V}\frac{Q_0(N(x))}{Q_1(N(x))}, \tag{10}$$

$$P_{\mathrm{rm}}(\varnothing \to x) = \frac{V}{2}\frac{Q_1(N(x))}{Q_0(N(x))}. \tag{11}$$

The factor V compensates for the proposition probability to choose lattice site x out of V possibilities when putting the sources, while the factor 2 compensates for the asymmetric shift proposal probability when moving $\overline{\psi}_x$ to $\overline{\psi}_{x-1}$, since the shift of $\overline{\psi}$ from x to $x+1$ is not allowed.

Now let us consider the case where $x \to y$ and $y = x_2$, that is, we propose to shift the head $\overline{\psi}$ to the site where the tail ψ is. To calculate the acceptance ratios for this case, we have to distinguish between the proposition of a shift of the head in the forward direction and a shift in the backward direction. First, let us consider the forward shift, which generates a valid configuration, contributing to $\langle\psi_y\overline{\psi}_y\rangle$. These are the only configurations for which we propose the removal update step with probability $p_{\mathrm{rm}} = 1/2$. The forward shift update step $x \to y$ with $y = x_2 + 1 = x_1$ is balanced with the backward shift update step $y \to x$, where $y = x_2 - 1$. This backward shift, however, is proposed with the probability 1 instead of probability $1/2$ since the shift $y \to x$ for $x = x_2 + 1$ would involve the creation of an open fermion string around the entire lattice. The asymmetry in the proposition probabilities is cured by the choice of the removal probability $p_{\mathrm{rm}} = 1/2$, such that we find the acceptance ratio for a shift in forward direction where $y = x_2$ to be the same as in eq.(14), namely

$$P_{\mathrm{sh}}(x \to y | x_1 \neq x_2 \cap y = x_2 + 1 = x_1) = \frac{Q_1(k(x))}{Q_0(k(x))}. \tag{12}$$

The shift step is balanced with

$$P_{\rm sh}(x \to y | x_1 = x_2) \quad = \quad \begin{cases} \dfrac{Q_0(k(y))}{Q_1(k(y))} & \text{if } y = x_2 - 1, \\ 0 & \text{if } y = x_2 + 1. \end{cases} \tag{13}$$

This latter step belongs to move within $\mathcal{G}^f$ which are induced by shifting $\overline{\psi}$ by one lattice spacing from site x to site $x+1$, and vice versa, while keeping the other source ψ fixed. Such an update step is graphically illustrated in figure 2 and is called 'shift' update step. a

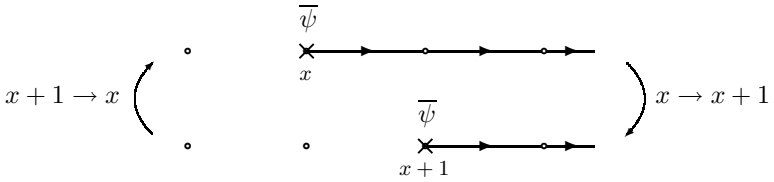

Figure 2: Fermionic bond configuration update algorithm. Graphical representation of the 'shift' update step $x \to x+1$ in forward direction for an open fermion string configuration. It is balanced with the shift update step $x+1 \to x$ in backward direction. The bosonic background bond configuration is not drawn.

shift in forward direction, $x \to y$, where $y = x+1$, automatically involves the removal of the fermionic bond $b^f(y)$, whereas a shift in backward direction, $y \to x$, where $x = y-1$, requires the addition of a new fermionic bond $b^f(x)$. Both directions are proposed with equal probability $1/2$ and are hence balanced against each other as long as the new site does not conicide with the position of the source ψ. The formula in eq.(8) provides us with the acceptance ratios

$$P_{\rm sh}(x+1 \to x) \quad = \quad \frac{Q_1(N(x))}{Q_0(N(x))}\,, \tag{14}$$

$$P_{\rm sh}(x \to x+1) \quad = \quad \frac{Q_0(N(x)}{Q_1(N(x))}\,. \tag{15}$$

Next we consider the shift update step for the case when the source $\overline{\psi}$ at site $x+1$ is shifted backwards to site x which is already occupied by the sink ψ. The step is graphically illustrated in the upper half of figure 3. While the resulting fermion bond configuration is a

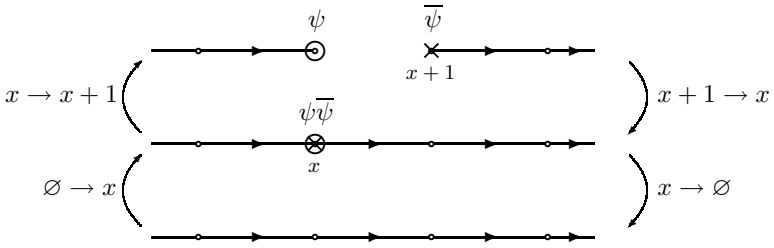

Figure 3: Fermionic bond configuration update algorithm. Graphical representation of the hybrid 'shift/remove' update step $x+1 \to x \to \varnothing$ in backward direction, balanced with the 'put/shift' update step, $\varnothing \to x \to x+1$. The bosonic background bond configuration is not drawn.

valid one (it belongs to $\mathcal{Z}_1$), the whole fermion configuration including the source and the sink

represents an unphysical situation, and in fact does not contribute to any physical observable. Therefore, such a backward shift from $\mathcal{G}^f$ to $\mathcal{Z}_1$, essentially closing the open fermion string, automatically induces the removal of the fermionic source and sink pair $\overline{\psi}\psi$ from site $x-1$ as illustrated in the lower half of the figure. Such a step is called a hybrid 'shift/remove' update step. Of course, the step is balanced with a hybrid 'put/shift' update step when the additional fermionic sink and source variables are put on a closed fermion loop at a site x. As usual, the acceptance ratios for the hybrid update steps can be read off from the weights of the configurations involved and yield

$$P_{\mathrm{sh/rm}}(x+1 \to x \to \varnothing) = \frac{2}{V}, \tag{16}$$

$$P_{\mathrm{sh/rm}}(\varnothing \to x \to x+1) = \frac{V}{2}. \tag{17}$$

The factor V compensates for the proposition probability to choose the same lattice site y when putting back the additional variables on the lattice, whereas the factor 2 compensates for the proposition probability to shift in forward or backward direction when the fermion string is still open. Note that there are no ratios of Q-weights involved, since neither the bosonic bond configuration is changed nor the monomer weight of a site is affected by the hybrid shift/remove update step.

To complete our discussion of the fermionic bond update, we note that the algorithm provides improved estimators for the fermion two-point function $g^f(x)$ and the partition functions Z_F. Because the algorithm samples directly the configuration space $\mathcal{G}^f$, every open fermion string configuration contributes unity to the stochastic Monte Carlo estimator for $g^f(x)$. To be precise we have

$$g^f(x|\mathcal{C} \in \mathcal{G}^f) = \delta_{x,x_1-x_2}\,, \tag{18}$$

where x_1 and x_2 are the end and starting point of the open fermion string, i.e., the positions of the sink ψ and the source $\overline{\psi}$, respectively. Similarly, every bond configuration in $\mathcal{Z}_F$ is generated with its proper weight and hence contributes unity to the stochastic estimator for Z_F, i.e., the Monte Carlo estimators for Z_F is simply

$$Z_F(\mathcal{C} \in \mathcal{Z}_F) = 1\,. \tag{19}$$

Finally we note that the factors of V appearing in the acceptance ratios above may become inconvenient in practice, especially towards the continuum limit when $V \to \infty$. The factors only occur when contact between $\mathcal{Z}_F$ and $\mathcal{G}^f$ is made, i.e., they are responsible for getting the relative normalisation between Z_F and g^f right. However, since we make use of translational invariance in eq.(18) the factors of V are in fact canceled and can hence be omitted.

2.2 Updating the bosonic bond configuration

In this section we now discuss the update steps which relate the bond configuration spaces $\mathcal{Z}_F$ and $\mathcal{G}^b_F$ for a fixed fermionic bond configuration with fermion number $F = 0, 1$.

We point out that for an arbitrary superpotential there are in general no restrictions on the bosonic bond configurations. This is for example the case for the superpotential P_b which we consider in our series of papers. In contrast, the superpotential P_u yields the local constraint $N(x) = 0 \mod 2$ on the site occupation number, due to the parity symmetry

$\phi \to -\phi$. In the following discussion, we always present the generic case first, and then specify the modifications or simplifications due to the constraint. The two elementary update steps we discussed for the fermionic bond update, the 'put/remove' step and the 'shift' step, are also the main steps for updating the bosonic bond configurations. The 'put/remove' step introduces or removes one or two sources ϕ, while the 'shift' step shifts the sources by one lattice spacing. If there are no restrictions on the bond configuration, we are free to decide for each Monte Carlo step whether to proceed by a remove update or a shift update. With probability p_{rm}, we propose to remove the sources from the lattice, while the proposition to continue the worm update with a 'shift' step is chosen with probability $p_1 = 1 - p_{\mathrm{rm}}$.

The step from $\mathcal{Z}_F$ to $\mathcal{G}_F^b$ and vica versa is induced by introducing or removing a bosonic source ϕ at sites x_1 and x_2, with $x_1 = x_2$ not excluded. The step does not alter the bond configuration, but only the site occupation numbers at sites x_1 and x_2. Thus, only the ratios of the site weights Q_F are involved in the acceptance probability

$$P_{\mathrm{rm}}(x_1, x_2 \to \varnothing) = \begin{cases} \dfrac{1}{p_{\mathrm{rm}} V^2} \dfrac{Q_F(N(y)-2)}{Q_F(N(y))} & \text{if } x_1 = x_2 \equiv y, \\ \dfrac{1}{p_{\mathrm{rm}} V^2} \dfrac{Q_F(N(x_1)-1)}{Q_F(N(x_1))} \dfrac{Q_F(N(x_2)-1)}{Q_F(N(x_2))} & \text{if } x_1 \neq x_2. \end{cases} \tag{20}$$

The prefactor $1/(p_{\mathrm{rm}} V^2)$ is motivated as follows. The factor $1/V^2$ balances the probability for the proposition of putting the bosonic sources at the sites x_1 and x_2 when re-entering the configuration space $\mathcal{G}_F^b$, while the factor $1/p_{\mathrm{rm}}$ balances the proposition probability for the choice of proceeding by the shift update instead of the remove update, as discussed above. The acceptance ratios for re-entering the configuration space $\mathcal{G}_F^b$ from $\mathcal{Z}_F$ are given by

$$P_{\mathrm{rm}}(\varnothing \to x_1, x_2) = \begin{cases} p_{\mathrm{rm}} V^2 \dfrac{Q_F(N(y)+2)}{Q_F(N(y))} & \text{if } x_1 = x_2 \equiv y, \\ p_{\mathrm{rm}} V^2 \dfrac{Q_F(N(x_1)+1)}{Q_F(N(x_1))} \dfrac{Q_F(N(x_2)+1)}{Q_F(N(x_2))} & \text{if } x_1 \neq x_2. \end{cases} \tag{21}$$

Two remarks are in order. Firstly, if there are no constraints on the bond configuration, one can in principle introduce just a single source ϕ which subsequently is shifted around. In effect, the algorithm then samples the one-point function which in this situation is indeed not zero. Secondly, we note that if the constraint $N = 0 \mod 2$ is in place, the two sources can only be placed or removed when $x_1 = x_2$. As a consequence, only the first of the two acceptance ratios in eq.(20) and eq.(21) are relevant, while the second ones are zero by definition.

Next, we discuss the 'shift' update. With this step we now change the bosonic bond configuration. Shifting the source from site x to a next neighbouring site y is always associated with an increase or a decrease of the bosonic bond occupation number between the sites x and y by one. Whether or not the occupation number is increased or decreased is decided with probability 1/2. Similarly, the source can move forward or backward, and we propose both directions with equal probability 1/2. In addition, when there are several types of bosonic bonds b_i with $i \in \{j \to k | j, k \in \mathbb{N}\}$, we need to decide in each step which bond is updated. We do so by choosing the proposition probabilities $p_{j\to k}$ with $\sum_{j,k} p_{j\to k} = 1$. However, because

the proposals are completely symmetric, these probabilities do not affect the acceptance ratios. In the following, we will use the shorthand notation

$$n_{xy}^{j\to k} \;=\; \begin{cases} n^b_{j\to k}(x) & \text{if } y = x+1, \\ n^b_{j\to k}(y) & \text{if } y = x-1, \end{cases} \tag{22}$$

for the occupation number of the bosonic bonds $b_{j\to k}$ between the sites x and y. The shifts $x \to y$ and $n_{xy}^{j\to k} \to n_{xy}^{j\to k} + 1$ are balanced with shifts $y \to x$ and $n_{xy}^{j\to k} \to n_{xy}^{j\to k} - 1$, which gives the acceptance ratios

$$\begin{aligned} &P_{\mathrm{sh}}(x \to y, n_{xy}^{j\to k} \to n_{xy}^{j\to k} + 1) \\ &\qquad = \begin{cases} \dfrac{w_{j\to k}}{n_{xy}^{j\to k}+1} \dfrac{Q_F(N(x)+i-1)}{Q_F(N(x))} \cdot \dfrac{Q_F(N(y)+j+1)}{Q_F(N(y))} & \text{if } y = x+1, \\ \dfrac{w_{j\to k}}{n_{xy}^{j\to k}+1} \dfrac{Q_F(N(x)+j-1)}{Q_F(N(x))} \cdot \dfrac{Q_F(N(y)+i+1)}{Q_F(N(y))} & \text{if } y = x-1, \end{cases} \end{aligned} \tag{23}$$

$$\begin{aligned} &P_{\mathrm{sh}}(x \to y, n_{xy}^{j\to k} \to n_{xy}^{j\to k} - 1) \\ &\qquad = \begin{cases} \dfrac{n_{xy}^{j\to k}}{w_{j\to k}} \dfrac{Q_F(N(x)-i-1)}{Q_F(N(x))} \cdot \dfrac{Q_F(N(y)-j+1)}{Q_F(N(y))} & \text{if } y = x+1, \\ \dfrac{n_{xy}^{j\to k}}{w_{j\to k}} \dfrac{Q_F(N(x)-j-1)}{Q_F(N(x))} \cdot \dfrac{Q_F(N(y)-i+1)}{Q_F(N(y))} & \text{if } y = x-1. \end{cases} \end{aligned} \tag{24}$$

Of course, these generic ratios simplify considerably for the specific bonds $b_i, i \in \{1 \to 1, 1 \to 2, 1 \to 3\}$ relevant for the superpotentials considered in our series of papers. For example, the acceptance ratios for updating the bond $b_{1\to 1}$ read

$$P_{\mathrm{sh}}(x \to y, n_{xy}^{1\to 1} \to n_{xy}^{1\to 1} + 1) \;=\; \frac{w_{1\to 1}}{n_{xy}^{1\to 1}+1} \cdot \frac{Q_F(N(y)+2)}{Q_F(N(y))}, \tag{25}$$

$$P_{\mathrm{sh}}(x \to y, n_{xy}^{1\to 1} \to n_{xy}^{1\to 1} - 1) \;=\; \frac{n_{xy}^{1\to 1}}{w_{1\to 1}} \cdot \frac{Q_F(N(x)-2)}{Q_F(N(x))}\,. \tag{26}$$

Because the bond is symmetric, there is no need to distinguish whether $y = x+1$ or $y = x-1$.

To complete the discussion of the bosonic bond update, we again point out that the algorithm provides improved estimators for the bosonic to-point function $g_F^b(x)$ and the partition functions Z_F. As in the fermionic case, the algorithm samples directly the configuration space $\mathcal{G}_F^b$ with the correct weighting when the sources are present. Therefore, every configuration contributes unity to the stochastic Monte Carlo estimator for $g_F^b(x)$, and we have

$$g_F^b(x|\mathcal{G}_F^b) = \delta_{x_1-x_2,x}\,, \tag{27}$$

where x_1 and x_2 are the positions of the two sources. Whenever the bosonic update decides to remove the sources, we have a configuration in $\mathcal{Z}_f$ and hence a contribution of unity to the stochastic estimator for Z_F, that is, we have

$$Z_F(\mathcal{C} \in \mathcal{Z}_F) = 1\,. \tag{28}$$

In complete analogy to the fermionic update we note that the factors of V appearing in the acceptance ratios of the 'put/remove' step can be compensated by adjusting the overall normalisation of the two-point function, e.g. by making use of translational invariance.

3 Calculation of the site weight ratios

In order to calculate the weight of a configuration for supersymmetric quantum mechanics, it is necessary to know the site weights

$$Q_F(n) = \int_{-\infty}^{\infty} d\phi \; \phi^n \mathrm{e}^{-V(\phi)} M(\phi)^{1-F}, \tag{29}$$

where $V(\phi)$ and $M(\phi)$ depend on the superpotential and the discretisation employed, and $F = 0, 1$ is the fermion number, for arbitrary values of n. The values of n required in practice are usually limited to $\mathcal{O}(10^3)$. As we discussed in our second paper [5] this limitation makes the transfer matrix approach practical, because it allows to apply a cutoff on the occupation number without introducing systematic effects. One exception concerns the Q-exact discretisation with broken supersymmetry. There we encountered that the occupation number necessary to obtain reliable results grows beyond what can be handled with reasonable effort. As we will discuss further in section 4, a similar behaviour occurs in the Monte Carlo simulations of systems with broken supersymmetry using the Q-exact action. The following discussion, however, is not affected and applies equally to the calculation of the weights for broken and unbroken supersymmetry using both the standard and Q-exact discretisation.

However, it turns out that even for moderate values of the site occupation number n of order $\mathcal{O}(100)$ the site weights $Q_F(n)$ can quickly grow to values larger than 10^{100} or more. As a consequence, the calculation of the site weights quickly becomes numerically unstable for growing n. In fact, even for simple potentials when the weights can be calculated analytically in terms of confluent hypergeometric functions, the numerical evaluation of these functions is difficult for large n, and even specialised libraries such as the ones available in Wolfram's Mathematica appear not to be accurate enough.

On the other hand, since for the Monte Carlo simulations we only need ratios of the site weights, such as $Q_F(n+2)/Q_F(n), Q_F(n+2)/Q_F(n)$ and $Q_1(n)/Q_0(n)$ the ratios themselves usually do not become larger than $\mathcal{O}(10)$. In addition, also the transfer matrix elements discussed in [5] can be rewritten in terms of these ratios. Therefore, we now present a numerically stable computational strategy to calculate the site weight ratios reliably for arbitrary values of the site occupation numbers.

We start by defining an arbitrary polynomial superpotential

$$P(\phi) = \sum_{i=0}^{p} p_i \phi^i, \tag{30}$$

and the corresponding bosonic self-interaction potential $V(\phi)$ as well as the monomer weight $M(\phi)$,

$$V(\phi) = \sum_{i=0}^{2(p-1)} k_i \phi^i, \qquad M(\phi) = \sum_{i=0}^{p-2} m_i \phi^i. \tag{31}$$

Explicitly, the weights in each sector are then given by

$$Q_0(n) = \int_{-\infty}^{\infty} d\phi \; \phi^n \mathrm{e}^{-V(\phi)} \tag{32}$$

and

$$Q_1(n) = \sum_{i=0}^{p-2} m_i Q_0(n+i). \tag{33}$$

For convenience we also define the ratios of the site weights $Q_F(n)$,

$$R'_F(n) = \frac{Q_F(n+1)}{Q_F(n)}, \tag{34}$$

$$R_F(n) = \frac{Q_F(n+2)}{Q_F(n)}, \tag{35}$$

$$R_m(n) = \frac{Q_1(n)}{Q_0(n)} \tag{36}$$

which are used for the acceptance ratios in the Monte Carlo simulations. In principle, only the ratios $R'_0(n)$ need to be calculated since all other ratios can be derived from those. For example, $R_0(n)$ can be expressed in terms of $R'_0(n)$ as

$$R_0(n) = R'_0(n+1)R'_0(n)\,, \tag{37}$$

but since in some cases $Q_0(n\,\text{odd}) = 0$ the introduction of $R_0(2n)$ is nevertheless necessary. $R_m(n)$ can be expressed via the ratios $R_0(n)$ and $R'_0(n)$ and appropriate products thereof,

$$R_m(n) = m_0 + R'_0(n)\,(m_1 + R_0(n+2)\,(m_3 + \ldots)) + R_0(n)\,(m_2 + R_0(n+2)\,(m_4 + \ldots))\,, \tag{38}$$

and the ratios $R'_1(n)$ and $R_1(n)$ via $R_m(n)$, $R_0(n)$ and $R'_0(n)$ by

$$R_1(n) = \frac{R_m(n+2)}{R_m(n)} R_0(n), \tag{39}$$

$$R'_1(n) = \frac{R_m(n+1)}{R_m(n)} R'_0(n). \tag{40}$$

First, we now discuss how to gain numerical stability for the special case of an even superpotential $P(\phi)$. In a second step we will then adapt the idea to treat the somewhat more subtle case of an arbitrary superpotential.

3.1 Even superpotential

Unbroken supersymmetric quantum mechanics requires a superpotential $P(\phi)$ with $\deg(P(\phi)) = 0 \bmod 2$. In particular, in our series of papers we investigate the superpotential

$$P(\phi) = p_2\phi^2 + p_4\phi^4 \tag{41}$$

symmetric w.r.t. the parity transformation $\phi \to -\phi$. As a consequence of the symmetry, $Q_F(n\,\text{odd}) = 0$ for both $F = 0, 1$ and the ratios $R'_F(n)$ need not be considered – instead, it is sufficient to determine $R_0(2n)$ with $n \in \mathbb{N}_0$ only.

For the the potential $V(\phi)$ we then have the form

$$V(\phi) = k_2\phi^2 + k_4\phi^4 + k_6\phi^6 \tag{42}$$

which is consistent with both the standard discretisation and the Q-exact one. To keep the integrals numerically under control, for fixed n we apply a variable transformation $\phi \to \widetilde{\phi} = \phi/\phi_0$, such that we have rescaled weights $\widetilde{Q}_0(2n)$ as

$$Q_0(2n) = \phi_0^{2n+1} \widetilde{Q}_0(2n). \tag{43}$$

Since we have $Q_0(2n) \geq 0$, we can choose the rescaling factor to be $\phi_0 = Q_0(2n)^{1/(2n+1)}$ and the integral becomes $\widetilde{Q}_0(2n) = 1$. Defining the ratio of rescaled weights as

$$\widetilde{R}_0(2n) = \frac{\widetilde{Q}_0(2n+2)}{\widetilde{Q}_0(2n)} = \widetilde{Q}_0(2n+2), \tag{44}$$

where both integrals $\widetilde{Q}_0(2n+2)$ and $\widetilde{Q}_0(2n)$ are rescaled with the same rescaling factor $\phi_0 = Q_0(2n)^{1/(2n+1)}$, we find that

$$R_0(2n) = \phi_0^2 \widetilde{R}_0(2n)\,. \tag{45}$$

In addition, the rescaled weight $\widetilde{Q}_0(2n+2)$ is now of $\mathcal{O}(1)$ and can be evaluated reliably via numerical integration. So if we start by integrating directly the numerically stable site weights $Q_0(0)$ and $Q_0(2)$, we can recursively generate ratios $R_0(2n)$ with higher and higher n. Note that after each calculation of a ratio $R_0(2n)$, one needs to update the rescaling factor $\phi_0 \to \phi_0'$. This can be achieved most easily via

$$\phi_0' = (\phi_0)^{\frac{2n+1}{2n+3}} R_0(2n)^{\frac{1}{2n+3}}. \tag{46}$$

Our procedure guarantees that all involved quantities are of $\mathcal{O}(1)$. Once all ratios $R_0(2n)$ are known, one can calculate the ratios $R_m(2n)$, noting that for the specific superpotential we consider, eq.(38) simplifies to

$$R_m(2n) = m_0 + m_2 R_0(2n). \tag{47}$$

The calculation of the ratios $R_1(2n)$ as given in eq.(39) is then straightforward.

3.2 Arbitrary Superpotential

In the context of broken supersymmetric quantum mechanics, one encounters superpotentials with $\deg(P(\phi)) = 1 \bmod 2$. Therefore, we now adapt the procedure from above to superpotentials of this form. For simplicity, we restrict ourselves to the odd superpotential we consider as the example in our series of papers,

$$P(\phi) = \sum_{i=1}^{3} p_i \phi^i. \tag{48}$$

If at least one of the coefficients p_1 and p_2 is nonzero, which is always the case for the superpotentials we use, $V(\phi)$ reads

$$V(\phi) = k_1\phi + k_2\phi^2 + k_3\phi^3 + k_4\phi^4, \tag{49}$$

and at least one of the coefficients k_1 and k_3 is nonzero either. This has a two important consequences. Firstly, the moments defined in eq.(32) are nonzero for n odd, from which

follows that the ratios $R'_F(n)$ defined in eq.(36) have to be calculated as well. Secondly, the weights $Q_0(n)$ are no longer necessarily positive, but it turns out that for all pratical purposes it does not affect the simulations. We will discuss this further in section 4.

For the evaluation of the integrals, we apply the same variable transformation $\phi \to \widetilde{\phi} = \phi/\phi_0$ as before, such that we have rescaled weights $\widetilde{Q}_0(n)$ given by

$$Q_0(n) = \phi_0^{n+1} \widetilde{Q}_0(n). \tag{50}$$

We now choose $\phi_0 = |Q_0(n)|^{1/(n+1)} \cdot \mathrm{sgn}(Q_0(n))$. Then, the integral becomes $\widetilde{Q}_0(n) = 1$ again as before. Furthermore, defining the rescaled ratios $\widetilde{R}'_0(n)$ to be

$$\widetilde{R}'_0(n) = \frac{\widetilde{Q}_0(n+1)}{\widetilde{Q}_0(n)} = \widetilde{Q}_0(n+1), \tag{51}$$

where both integrals $\widetilde{Q}_0(n+1)$ and $\widetilde{Q}_0(n)$ are rescaled with the rescaling factor $\phi_0 = |Q_0(n)|^{1/(n+1)} \cdot \mathrm{sgn}(Q_0(n))$, we find $R'_0(n) = \phi_0 \widetilde{R}'_0(n)$. We proceed analogously to the case of the even superpotential by recursive iteration, with the only exception that we generate the ratios $R'_0(n)$ instead of the ratios $R_0(n)$. The update for the rescaling factor $\phi_0 \to \phi'_0$ is done via

$$\phi'_0 = |\phi_0|^{\frac{n+1}{n+2}} |R'_0(n)|^{\frac{1}{n+2}} \cdot \mathrm{sgn}(R'_0(n)). \tag{52}$$

Once all the ratios $R'_0(n)$ are known, one can calculate the ratios $R_0(n)$ via eq.(37), the ratios $R_m(n)$ via eq.(38), and the ratios $R_1(n)$ via eq.(39).

4 Results of the Monte Carlo simulations

The results in this section are merely thought of as a proof of the feasibility of the algorithm and as a test of its efficiency. Comparing the Monte Carlo results with the exact solution of the system at finite lattice spacing provided in our second paper [5] of course also serves as a validation for the algorithm.

For the following Monte Carlo simulations, we will consider the same superpotentials and discretisations as in the previous two papers. In particular, we will simulate the system using the action with counterterm for both unbroken and broken supersymmetry as well as the Q-exact action for unbroken supersymmetry. Details for the various actions can be found in the first paper of our series. Here we only give the details of the superpotentials for unbroken and broken supersymmetry, respectively,

$$P_u(\phi) = \frac{1}{2}\mu\phi^2 + \frac{1}{4}g\phi^4\,, \tag{53}$$

$$P_b(\phi) = -\frac{\mu^2}{4\lambda}\phi + \frac{1}{3}\lambda\phi^3\,, \tag{54}$$

and we recall that the continuum limit is taken by fixing the dimensionful parameters μ, g, λ and L while taking the lattice spacing $a \to 0$. In practice, the dimensionless ratios $f_u = g/\mu^2, f_b = \lambda/\mu^{3/2}$ fix the couplings and μL the extent of the system in units of μ, while $a\mu$ and a/L are subsequently sent to zero. In analogy to the number of sweeps for a standard Monte Carlo simulation, we count the number of times the algorithm is in either one of the

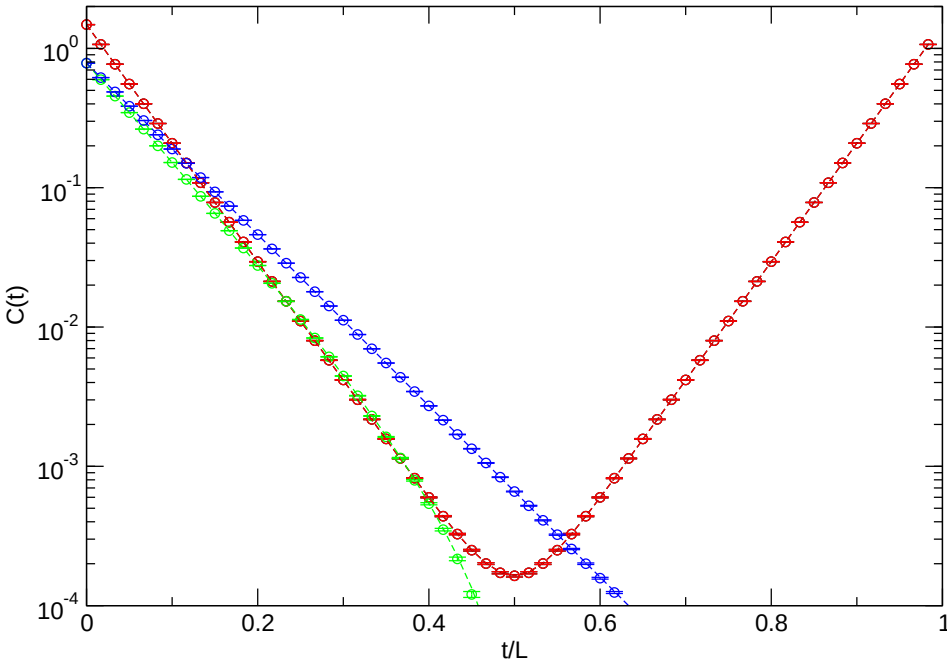

Figure 4: Unbroken supersymmetric quantum mechanics, standard discretisation. Bosonic correlation function for antiperiodic (black) and periodic b.c. (red) (lying on top of each other) and fermionic correlation function for antiperiodic (green) and periodic b.c. (blue) for $\mu L = 10$ at coupling $f_u = 1$. The dashed lines are the exact results from [5].

two configuration spaces $\mathcal{Z}_F, F = 0, 1$. The statistics for a simulation are therefore given by $Z_0 + Z_1 = Z_a$.

First, we consider the standard discretisation with the superpotential P_u such that supersymmetry is unbroken. As a first observable, we show the results for the bosonic and fermionic correlation functions for $\mu L = 10$, $L/a = 60$ and $f_u = 1$ for $Z_a = 10^7$ in figure 4. This is essentially the same plot as figure 10 in our second paper [5], but now with the additional data from the Monte Carlo simulation and plotted on a logarithmic scale. The simulation indeed reproduces the exact result within very small statistical errors which demonstrate the efficiency of the algorithm. The exponential error reduction is due to the use of the improved estimators for the two-point function which are available in the context of the worm algorithms. The improvement is particularly impressive for the fermionic correlator where the error reduction allows to follow the correlator over more than seven orders of magnitude without loss of statistical significance. In fact the relative error for the lowest value of the fermionic correlator is still only 4%.

As a second example, we show the mass gaps for different μL at a coupling $f_u = 1$ with statistics of $Z_a = 10^6$ in figure 5. The μL considered are in the region where thermal effects are negligible and essentially only Z_0 contributes to the total partition function, such that $Z_a \simeq Z_0$. We extract the masses from the asymptotic behaviour of the correlation functon at large t, i.e., we extract the lowest energy gap. Because of the extremely good signal-to-noise ratio the asymptotic behaviour can be truly reached and, in doing so, systematic errors from contributions of excited states are essentially excluded. Of course, we know from our exact results that the overlap of the simple operators we use to construct the two-point function is close to maximal. This is clearly visible in figure 5 where we observe an almost purely

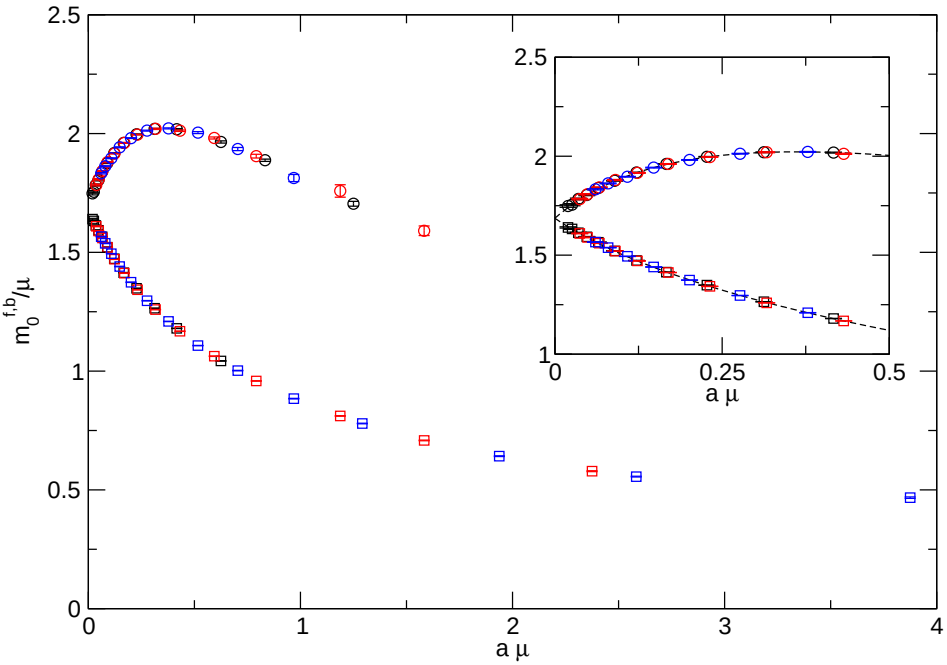

Figure 5: Unbroken supersymmetric quantum mechanics, standard discretisation. Continuum limit of the lowest bosonic (circles) and fermionic (squares) mass gap for $\mu L = 10$ (black), $\mu L = 19$ (red), $\mu L = 31$ (blue) and $f_u = 1$. The inset shows a detailed comparison with the exact results (dashed lines).

exponential decay for all t/L. Because the energy gaps are independent of μL, they are expected to fall on top of each other for all values of μL at fixed lattice spacing $a\mu$. This is indeed the case within our numerical accuracy, and the extracted masses, when expressed in units of μ, indeed extrapolate to the correct zero-temperature continuum limit. The inset of figure 5 shows a detailed comparison of the simulation results with our exact solution from [5] represented by the dashed line and we observe a beautiful agreement even very close to the continuum.

Next, we consider the action with counterterm and the superpotential P_b for which the supersymmetry is broken. In this case we encounter an issue concerning the potential non-positivity of the weights which we already mentioned in section 3.2. This potentially dangerous sign problem is not of fermionic origin, but is instead related to the bond formulation of the bosonic degrees of freedom. As a matter of fact it occurs already in the purely bosonic system, independent of the dimensionality of the system. However, negative weights only occur in a region of parameter space which becomes irrelevant towards the continuum limit. In that sense, the sign problem is a lattice artefact and can be avoided straightforwardly. Nevertheless, in order to eliminate any systematic error we deal with this bosonic sign problem by incorporating the sign of the configuration into the observables, even though it has no practical consequences.

As a first observable in the broken case, we show the bosonic and fermionic two-point functions, $\langle \phi_t \phi_0 \rangle$ and $\langle \psi_t \overline{\psi}_0 \rangle$, for periodic and antiperiodic b.c. for $\mu L = 10$ at fixed coupling $f_b = 1$ in figure 6 for a statistics of $Z_a = 10^8$. The exact results from [5] are shown as dashed lines. The simulation yields results which agree with the exact results within the very small statistical errors on the level of 1‰. Note that the correlators for periodic and antiperiodic

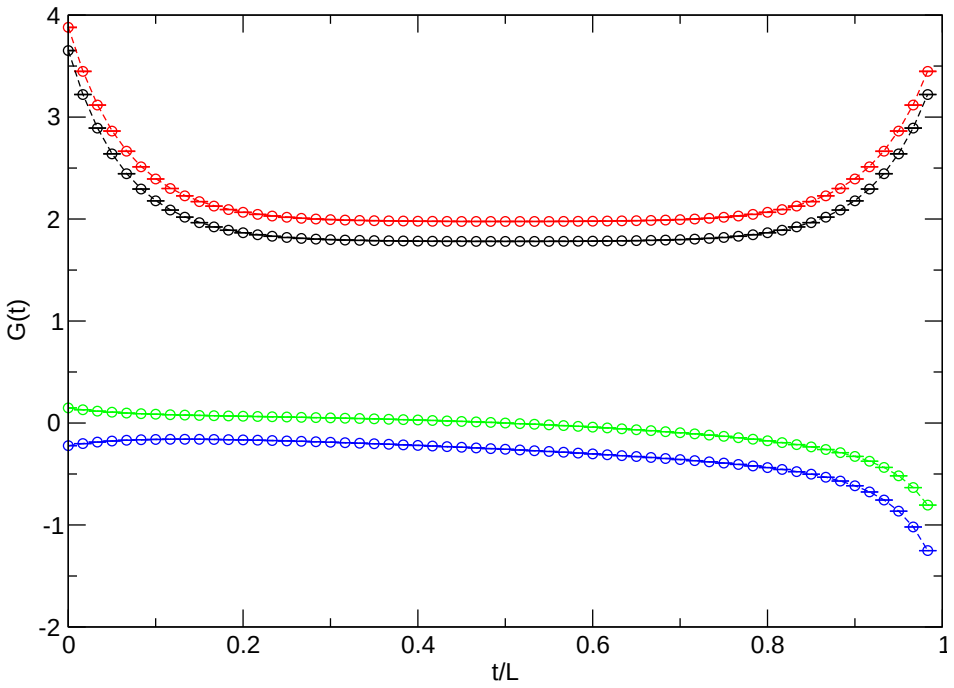

Figure 6: Broken supersymmetric quantum mechanics, standard discretisation. The bosonic two-point function for antiperiodic (black) and periodic b.c. (red) and the fermionic one for antiperiodic (green) and periodic b.c. (blue) for $L/a = 60$, $\mu L = 10$ at coupling $f_b = 1$. The dashed lines are the exact results from [5].

b.c. are constructed a posteriori from the simulation results in the bosonic and fermionic sectors Z_0 and Z_1, respectively, and it is crucial to sample the relative weight between the two sectors correctly in order to the final values right. The relative sampling is solely in the responsibility of the fermion simulation algorithm. Our results in figure 6 show that the open fermion string algorithm indeed transits sufficiently well between the two sectors.

This can be made more quantitative by looking at the ratio Z_p/Z_a which represents the Witten index in our field theoretic setup. From our exact results in [5] we expect a non-zero Witten index at finite lattice spacing which however extrapolates to zero in the continuum limit. So the behaviour of the algorithm towards the continuum limit is particularly interesting, because for vanishing lattice spacing the would-be Goldstino at finite lattice spacing turns into a true, massless Goldstino. In such a situation one usually encounters critical slowing down of the simulation algorithms, such that the errors on the results grow large and the results become unreliable. The massless Goldstino is directly related to the tunneling between the bosonic and the fermionic sector, and the reproduction of a Witten index $W = 0$ in the continuum with small errors is hence a true demonstration of the efficiency of the open fermion string algorithm to transit between the bosonic and fermionic sector. In addition, we know from [5] that the lattice artefacts are exponentially enhanced towards zero temperature and it is interesting to see how the simulation algorithm handles this situation at course lattice spacing.

In figure 7 we show the ratio Z_p/Z_a as a function of the lattice spacing $a\mu$ for different values of μL at fixed coupling $f_b = 1$. For this quantity, too, the simulation yields results which agree with the exact results within the small statistical errors. Moreover, the efficiency of the algorithm does not appear to deteriorate towards the continuum limit or for small

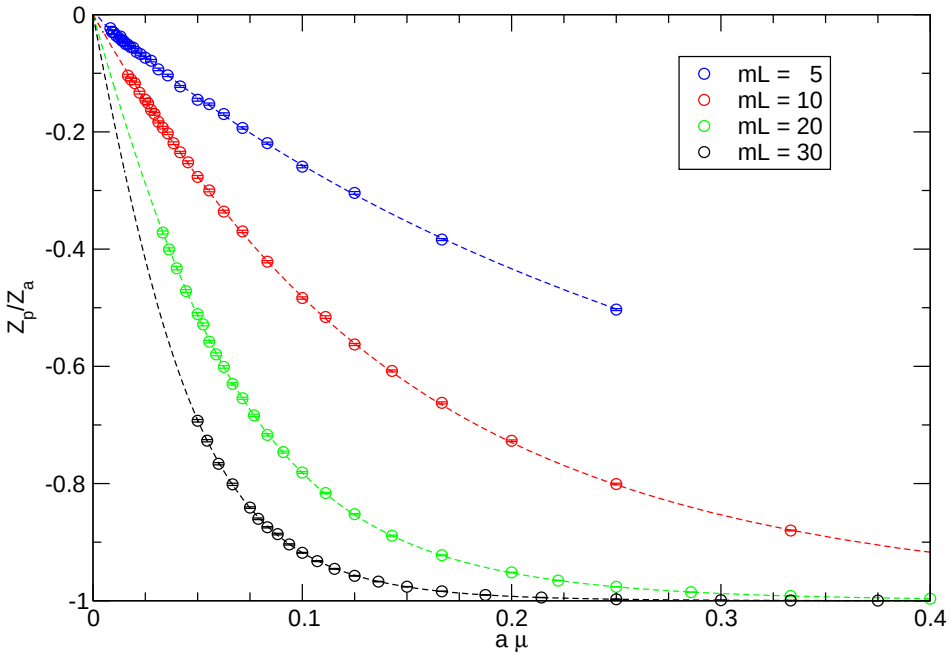

Figure 7: Broken supersymmetric quantum mechanics, standard discretisation. Continuum limit of the partition function ratio Z_p/Z_a, i.e. the Witten index, for $\mu L = 5$ (blue), $\mu L = 10$ (red), $\mu L = 20$ (green), $\mu L = 30$ (black) for $f_b = 1$. The dashed lines are the exact results from [5].

values of μL where the Witten index is very close to zero. This can for example be seen from the fact that the errors obtained with fixed statistics essentially remain constant towards the continuum limit and are also independent of the system size. This nicely demonstrates the efficiency of the algorithm also for a system with broken supersymmetry.

The last system we investigate with the worm algorithm is unbroken supersymmetry formulated with the Q-exact action[1]. We first consider the ratio of partition functions Z_p/Z_a which in the limit of $\mu L \to \infty$ yields the Witten index. From a simulational point of view, the ratio essentially calculates the fraction of configurations in sector $\mathcal{Z}_0$ versus the ones in $\mathcal{Z}_1$. Since for unbroken supersymmetry, the system is almost exclusively in the bosonic sector, the ratio is very close to one except when the size of the system becomes very small, i.e., in the high temperature limit. Moreover, from our exact results in [5] we know that the lattice artefacts in this quantity are very small and the continuum limit is not very interesting. For these reasons, we consider in figure 8 the dependence of the ratio Z_p/Z_a on μL for different values of the lattice spacing a/L with a statistics of $Z_a = 10^8$.

Also for this quantity, we find that the results agree with the exact result within the very small statistical errors. Again, the open fermion string algorithm proves to be very efficient even close to $\mu L \simeq 0$ where the tunneling from the bosonic to the fermionic sector and vice versa becomes important and dominates the behaviour of the system. Thus, even in this somewhat extreme situation of very high temperature, the algorithm does not show any signs of critical slowing down despite the fact that there is a quasi-zero mode in the system. Note,

[1]For Monte Carlo simulations for broken supersymmetry using the Q-exact action, we encounter the very same problems we ran into in the transfer matrix approach. The bond occupation number blows up even for small lattices such that the generation of reliable results turn out to be impossible.

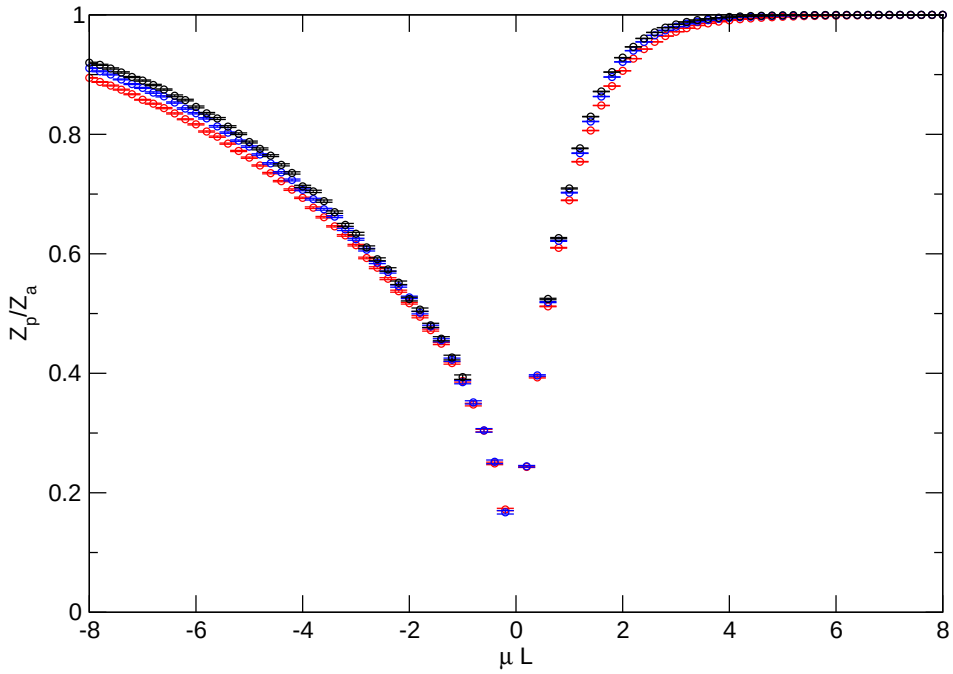

Figure 8: Unbroken supersymmetric quantum mechanics, Q-exact discretisation. Z_p/Z_a as a function of μL for $L/a = 16$ (red), $L/a = 32$ (blue), $L/a = 64$ (black) at fixed coupling $f_u = 1$.

that we also simulate negative bare masses. This is in contrast to the calculations for broken supersymmetry with counterterm in figure 7, where we show only positive μL in the plot.

The last quantity we calculate are the lowest bosonic and fermionic mass gaps for different μL at fixed coupling of $f_u = 1$ from a statistics of $Z_a = 10^6$. The mass gaps are extracted from the two-point correlation functions exactly in the same way as before for the standard action, and in figure 9, we show the results of this analysis. As expected, the masses for the boson and the fermion are indeed indistinguishable within statistical errors. The degeneracy of the masses at finite lattice spacing due to the Q-exactness of the action emerges also for the results via Monte Carlo simulations. Note that the chosen μL lie well within the region where thermal effects are negligible and the masses extrapolate nicely to the correct zero-temperature continuum limit. The inset in figure 9 shows a detailed comparison with our exact results from [5] and we again observe beautiful agreement.

5 Conclusions

In this paper we have presented an algorithm for simulating $\mathcal{N} = 2$ supersymmetric quantum mechanics on the lattice. The algorithm is based on the reformulation of the system in terms of bosonic and fermionic bonds, and in essence represents an efficient Monte Carlo scheme for updating fermionic and bosonic bond configurations. The updating of the fermionic degrees of freedom is of specific interest, because they are the most challenging. This is particularly true for systems with broken supersymmetry, where standard simulation algorithms suffer from critical slowing down due to the massless Goldstino mode. In addition, these systems inevitably also suffer from a sign problem related to the Goldstino and the vanishing Witten

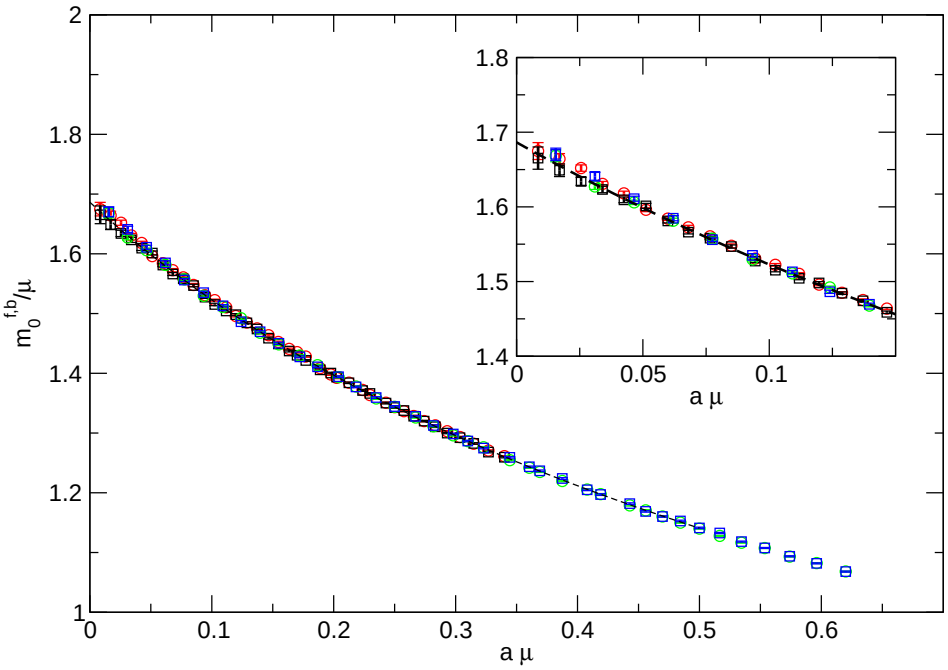

Figure 9: Unbroken supersymmetric quantum mechanics, Q-exact discretisation. Continuum limit of the lowest bosonic (black squares) and fermionic (red circles) mass gaps for $\mu L = 17$, and bosonic (blue squares) and fermionic (green circles) mass gaps for $\mu L = 31$ at fixed coupling is $f_u = 1$. The inset shows a detailed comparison with the exact result (dashed line).

index.

In contrast, the fermion simulation algorithm proposed in [2] eliminates critical slowing down by directly sampling the fermionic two-point correlation function. It is based on introducing a fluctuating open fermion string which efficiently updates the bond configurations on all length scales given by the fermionic correlation function. As a consequence, the fermion string induces frequent tunnelings between the bosonic and fermionic vacuum. Since the two vacua contribute to the partition function with opposite signs, the frequent tunneling guarantees sufficiently small statistical fluctuations for the average sign, and hence a solution to the fermion sign problem. In fact, the more severe the sign problem gets towards the continuum limit, the more efficiently the algorithm tunnels between the bosonic and fermionic sectors. This is of course due to the growing correlation length associated with the vanishing Goldstino mass. The bosonic degrees of freedom can be expressed in terms of bonds as well. Therefore, we also give the details of an updating algorithm for the bosonic bond configurations. Since we consider Q-exact discretisations in addition to the standard one, the algorithm involves updating generic types of bonds.

The simulation algorithm requires the calculation of the site weights $Q_F(N)$. Their numerical evaluation, however, turns out to be numerically unstable for growing site occupation number N. Hence, in section 3, we devise a computational strategy which allows to reliably evaluate the ratios of weights for arbitrarily large occupation numbers. Since this is a generic problem occuring in the bond formulation of field theories with real scalar fields, such an computational scheme is useful also in other situations.

Finally, we present a selection of results obtained using the algorithm. We concentrate

on two specific realisations of supersymmetric quantum mechanics, one with broken and one with unbroken supersymmetry. In addition, we consider both the standard and the Q-exact discretisation. Since exact results are available at finite lattice spacing from our investigation in [5], we can compare our stochastic results and directly validate them. The calculation of the bosonic and fermionic correlation functions shows that they can be determined accurately over several orders of magnitude. This allows for a very precise computation of the boson and fermion masses, the later in many cases with a smaller error than the former. In general, a precision of 1‰ can be reached with a very modest computational effort. In systems with broken supersymmetry it is crucial that the simulation algorithm efficiently samples the relative weights between the bosonic and fermionic sectors. Our results for the partition function ratio Z_p/Z_a, i.e., the Witten index, show that this is indeed the case. For fixed statistics, the errors do not grow towards the continuum limit. In that limit the index gets very close to zero and the sign problem would hence be most severe. Similarly, the error is essentially independent of the system size, which shows that the sign problem is truly solved.

References

[1] D. Baumgartner and U. Wenger, *Supersymmetric quantum mechanics on the lattice: I. Loop formulation*, .

[2] U. Wenger, *Efficient simulation of relativistic fermions via vertex models*, *Phys.Rev.* **D80** (2009) 071503, [arXiv:0812.3565].

[3] U. Wenger, *Simulating Wilson fermions without critical slowing down*, *PoS* **LAT2009** (2009) 022, [arXiv:0911.4099].

[4] D. Baumgartner and U. Wenger, *Simulation of supersymmetric models on the lattice without a sign problem*, *PoS* **LAT2010** (2011) [arXiv:1104.0213].

[5] D. Baumgartner and U. Wenger, *Supersymmetric quantum mechanics on the lattice: II. Exact results*, .

[6] K. Steinhauer and U. Wenger, *Loop formulation of supersymmetric Yang-Mills quantum mechanics*, *accepted for publication in JHEP* (2014) [arXiv:1410.0235].

[7] D. Baumgartner, K. Steinhauer, and U. Wenger, *Supersymmetry breaking on the lattice: the N=1 Wess-Zumino model*, *PoS* **LATTICE2011** (2011) 253, [arXiv:1111.6042].

[8] D. Baumgartner, K. Steinhauer, and U. Wenger, *Spontaneous supersymmetry breaking in the 2d N=1 Wess-Zumino model*, *PoS* **LATTICE2012** (2012) 043, [arXiv:1311.5089].

[9] K. Steinhauer and U. Wenger, *Spontaneous supersymmetry breaking in the two-dimensional N=1 Wess-Zumino model*, *accepted for publication in PRL* (2014) [arXiv:1410.6665].

[10] K. Steinhauer and U. Wenger, *Loop formulation of the supersymmetric nonlinear O(N) sigma model*, *PoS* **LATTICE2013** (2013) 092, [arXiv:1311.5403].

[11] M. Creutz and B. Freedman, *A statistical approach to quantum mechanics*, *Annals of Physics* **132** (1981), no. 2 427 – 462.

[12] S. Catterall and E. Gregory, *A Lattice path integral for supersymmetric quantum mechanics*, *Phys.Lett.* **B487** (2000) 349–356, [hep-lat/0006013].

[13] J. Giedt, R. Koniuk, E. Poppitz, and T. Yavin, *Less naive about supersymmetric lattice quantum mechanics*, *JHEP* **0412** (2004) 033, [hep-lat/0410041].

[14] A. Kirchberg, J. Lange, and A. Wipf, *From the Dirac operator to Wess-Zumino models on spatial lattices*, *Annals Phys.* **316** (2005) 357–392, [hep-th/0407207].

[15] G. Bergner, T. Kaestner, S. Uhlmann, and A. Wipf, *Low-dimensional Supersymmetric Lattice Models*, *Annals Phys.* **323** (2008) 946–988, [arXiv:0705.2212].

[16] T. Kaestner, G. Bergner, S. Uhlmann, A. Wipf, and C. Wozar, *Supersymmetric lattice models in one and two dimensions*, *PoS* **LAT2007** (2007) 265, [arXiv:0709.0822].

[17] C. Wozar and A. Wipf, *Supersymmetry breaking in low dimensional models*, *Annals Phys.* **327** (2012) 774–807, [arXiv:1107.3324].

[18] I. Kanamori, H. Suzuki, and F. Sugino, *Euclidean lattice simulation for dynamical supersymmetry breaking*, *Phys.Rev.* **D77** (2008) 091502, [arXiv:0711.2099].

[19] I. Kanamori, F. Sugino, and H. Suzuki, *Observing dynamical supersymmetry breaking with Euclidean lattice simulations*, *Prog.Theor.Phys.* **119** (2008) 797–827, [arXiv:0711.2132].

[20] I. Kanamori, *A Method for Measuring the Witten Index Using Lattice Simulation*, *Nucl.Phys.* **B841** (2010) 426–447, [arXiv:1006.2468].

[21] N. V. Prokof'ev and B. V. Svistunov, *Worm algorithms for classical statistical models*, *Phys.Rev.Lett.* **87** (2001) 160601, [cond-mat/0103146].

Paper 9

Loop formulation of supersymmetric Yang-Mills quantum mechanics

Kyle Steinhauer and Urs Wenger, Journal of High Energy Physics **12** (2014) 044.

JHEP

Published for SISSA by Springer

Received: October 2, 2014
Accepted: November 17, 2014
Published: December 4, 2014

Loop formulation of supersymmetric Yang-Mills quantum mechanics

Kyle Steinhauer and Urs Wenger

Albert Einstein Center for Fundamental Physics,
Institute for Theoretical Physics, University of Bern,
Sidlerstrasse 5, CH-3012 Bern, Switzerland

E-mail: steinhauer@itp.unibe.ch, wenger@itp.unibe.ch

Abstract: We derive the fermion loop formulation of $\mathcal{N} = 4$ supersymmetric SU(N) Yang-Mills quantum mechanics on the lattice. The loop formulation naturally separates the contributions to the partition function into its bosonic and fermionic parts with fixed fermion number and provides a way to control potential fermion sign problems arising in numerical simulations of the theory. Furthermore, we present a reduced fermion matrix determinant which allows the projection into the canonical sectors of the theory and hence constitutes an alternative approach to simulate the theory on the lattice.

Keywords: Field Theories in Lower Dimensions, Lattice Gauge Field Theories, M(atrix) Theories, Black Holes in String Theory

ArXiv ePrint: 1410.0235

doi:10.1007/JHEP12(2014)044

JHEP12(2014)044

Contents

JHEP12(2014)044

1 Introduction

The conjectured holographic duality between supersymmetric Yang-Mills quantum mechanics and the theory of D0 branes of type IIa string theory in the large-N limit in principle allows to probe the physics of certain supergravity black holes by lattice Monte Carlo simulations. In particular, $\mathcal{N} = 16$ supersymmetric Yang-Mills (SYM) quantum mechanics (QM) stemming from the dimensional reduction of $\mathcal{N} = 1$ SYM in $d = 10$ dimensions is supposed to describe the dynamics of D0 branes which are the degrees of freedom of the underlying M-theory [1]. The connection to so-called black p-branes allows to study the thermodynamics of black holes through the corresponding strongly coupled gauge theory. We refer the reader to the review article [2] for further details. Here we report on our work in this direction on an analogue, but simpler theory, namely $\mathcal{N} = 4$ SYM QM with generic gauge group SU(N). The model stems from dimensionally reducing $\mathcal{N} = 1$ SYM in $d = 4$ dimensions, but is expected to share many qualitative features with the 16 supercharge

model. The aim of this paper is to construct the fermion loop formulation of the strongly coupled gauge theory regularised on the lattice, so as to make it susceptible to numerical simulations.

There have already been a number of nonperturbative investigations of SYM QM using numerical techniques. In [3–7] the Hamiltonian formulation was employed together with the cut Fock space method. This approach also allowed analytic solutions, at least for $d = 2$ dimensional SYM QM [8–12]. On the other hand, in [13] the Wilson lattice discretization was constructed and the $d = 4$ SYM QM was simulated in the quenched approximation [13, 14]. Further discretizations were proposed and investigated by Monte Carlo simulations in [15–17], and it was also shown that the (naive) Wilson discretization does not require any fine tuning to reach the correct continuum limit. A different non-lattice approach has been followed by [18–21] which used a momentum cutoff regularization while completely fixing the gauge.

Our motivation to study the loop formulation of this model is threefold. Apart from the motivation given by the interesting physics related to the thermodynamics of black holes and the possibility to test the gauge/gravity duality outlined above, the loop formulation provides a new approach to simulate fermions on the lattice [22]. In contrast to standard approaches the fermion loop formulation allows for local fermion algorithms [23], i.e., local updates of the fermionic degrees of freedom. The simulation algorithm applicable to the loop formulation works for massless fermions and appears not to suffer from critical slowing down [23, 24]. This is of particular importance in the context of supersymmetric field theories with spontaneously broken supersymmetry, since in such cases one has to deal with a massless fermionic mode, the Goldstino fermion. The third motivation finally stems from the fact that the fermion loop formulation offers the potential to control the fermion sign problem. Again, this is of particular significance in theories with spontaneously broken supersymmery where the partition function for periodic boundary conditions, and hence the fermion determinant (or Pfaffian), averages to zero, since it represents the vanishing Witten index [22, 25–27]. The possibility to control the fermion sign then follows from the fact that in the loop formulation the fermionic contribution to the partition function decomposes into contributions from fixed fermion number sectors, each of which has a definite sign depending only on the specific choice of the fermionic boundary conditions.

The paper is organised as follows. In section 2 we discuss the $d = 4$ dimensional SYM QM in the continuum and describe the lattice regularisation using the Wilson derivative. In section 3 we derive a reduction formula for the determinant of the fermion matrix which separates the dependence of the bosonic degrees of freedom from the chemical potential and which then allows the straightforward discussion of the canonical sectors of the theory. In section 4 the fermion loop formulation is introduced and in section 5 we discuss the various fermion sectors emerging from the transfer matrices in the loop formulation. We close the main part of the paper with our conclusions and an outlook in section 6. Finally, in appendix A we review various ways how to determine the canonical determinants from the reduced fermion matrix and prove in appendix B the algebraic equivalence between the reduced fermion matrix approach and the fermion loop formulation.

JHEP12(2014)044

2 Lattice regularisation

We start from $\mathcal{N} = 1$ SYM in $d = 4$ dimensions with gauge group SU(N) and dimensionally reduce the theory by compactifying the three spatial dimensions. While the temporal component $A(t)$ of the 4-dimensional gauge field remains unchanged, the three spatial components become bosonic fields $X_i(t)$, $i = 1, 2, 3$. The action of the dimensionally reduced theory then reads

$$S = \frac{1}{g^2} \int_0^\beta dt \, \mathrm{Tr} \left\{ (D_t X_i)^2 - \frac{1}{2} [X_i, X_j]^2 + \overline{\psi} D_t \psi - \overline{\psi} \sigma_i [X_i, \psi] \right\} \tag{2.1}$$

where the anticommuting fermion fields $\overline{\psi}(t)$, $\psi(t)$ are complex 2-component spinors, σ_i are the three Pauli matrices and $D_t = \partial_t - i[A(t), \cdot\,]$ denotes the covariant derivative. All fields in the theory are in the adjoint representation of SU(N) and the theory possesses a $\mathcal{N} = 4$ supersymmetry.

Note that the analogue reduction from $\mathcal{N} = 1$ SYM in $d = 10$ dimensions yields a very similar action with the only change that there are 9 bosonic fields $X_i(t)$, $i = 1, \ldots, 9$ corresponding to the 9 compactified gauge degrees of freedom, the σ_i's are the SO(9) γ-matrices and the fermionic Grassmann variables are Majorana, i.e., can be taken to be real. The dimensionally reduced theory then corresponds to $\mathcal{N} = 16$ SYM QM.

Let us now describe the lattice regularised version of the $\mathcal{N} = 4$ SYM QM where the Euclidean time extent is discretised by L_t points. The bosonic part of the action is then given by

$$S_B = \frac{1}{g^2} \sum_{t=0}^{L_t - 1} \mathrm{Tr} \left\{ \hat{D}_t X_i(t) \hat{D}_t X_i(t) - \frac{1}{2} [X_i(t), X_j(t)]^2 \right\} \tag{2.2}$$

where the gauge field is replaced by the gauge link $U(t)$ living in the gauge group SU(N) and the covariant lattice derivative is explicitly given by $\hat{D}_t X_i(t) = U(t) X_i(t+1) U^\dagger(t) - X_i(t)$. For the regularisation of the fermionic part we use the Wilson discretisation to get rid of the fermion doublers. Note that in $d = 1$ dimensions adding a Wilson term with Wilson parameter $r = \pm 1$ to the symmetric derivative yields either a forward or backward derivative,

$$\partial^{\mathcal{W}} = \frac{1}{2}(\nabla^+ + \nabla^-) \pm \frac{1}{2} \nabla^+ \nabla^- = \nabla^\pm \,. \tag{2.3}$$

Hence, the discretised fermion action reads

$$S_F = \frac{1}{g^2} \sum_{t=0}^{L_t - 1} \mathrm{Tr} \left\{ \overline{\psi}(t) \hat{D}_t \psi(t) - \overline{\psi}(t) \sigma_i [X_i(t), \psi(t)] \right\} \tag{2.4}$$

where $\hat{D}_t$ is simply the covariant derviative defined above. Note that the Wilson term breaks the time reversal and hence also the charge conjugation symmetry. However, the symmetries are restored in the continuum limit together with the full supersymmetries without any fine tuning since any further symmetry breaking terms are prohibited by the gauge symmetry [15].

For our further discussion of the fermionic part of the theory, it is convenient to work in uniform gauge $U(t) = U$, although it is not necessary for the derivation of the reduced

JHEP12(2014)044

fermion matrix in the next section. In addition, we also include a finite chemical potential term e^{μ} in the forward fermion derivative [28] in order to facilitate our discussion of the canonical fermion sectors in the next section. To be specific, the fermion action then reads

$$S_F = \frac{1}{2g^2} \sum_{t=0}^{L_t-1} \left[-\overline{\psi}^a_\alpha(t) W^{ab}_{\alpha\beta}\, e^{\mu}\, \psi^b_\beta(t+1) + \overline{\psi}^a_\alpha(t) \Phi^{ab}_{\alpha\beta}(t) \psi^b_\beta(t) \right] \tag{2.5}$$

where the gauge part of the hopping term connecting the nearest neighbour Grassmann fields $\overline{\psi}^a_\alpha(t)$ and $\psi^b_\beta(t+1)$ is given by

$$W^{ab}_{\alpha\beta} = 2\delta_{\alpha\beta} \cdot \mathrm{Tr}\{T^a U T^b U^\dagger\} \tag{2.6}$$

and is independent of t. Here, T^a are the generators of the SU(N) algebra and are normalised such that $\det W = 1$. The Yukawa interaction between the fermionic and bosonic fields is described by a $2(N^2-1) \times 2(N^2-1)$ matrix

$$\Phi^{ab}_{\alpha\beta}(t) = (\sigma_0)_{\alpha\beta} \cdot \delta^{ab} - 2\,(\sigma_i)_{\alpha\beta} \cdot \mathrm{Tr}\{T^a [X_i(t), T^b]\} \tag{2.7}$$

and the fermion action can be compactly written in terms of the fermion Dirac matrix $\mathcal{D}_{p,a}$, i.e.,

$$S_F = \frac{1}{2g^2} \overline{\psi}\, \mathcal{D}_{p,a}[U, X_i; \mu]\, \psi\,. \tag{2.8}$$

where the subscripts $_{p,a}$ specify periodic or antiperiodic temporal boundary conditions for the fermions in time, $\psi(L_t) = \pm\psi(0)$, respectively.

Eventually, the grand canonical partition function reads

$$Z = \int \mathcal{D}U\, \mathcal{D}X_i\, e^{-S_B[U,X_i]} \det \mathcal{D}_{p,a}[U, X_i; \mu] \tag{2.9}$$

where the determinant of the fermion Dirac matrix is the result from integrating out the fermionic degrees of freedom $\overline{\psi}$ and ψ.

3 Fermion matrix reduction and canonical formulation

In $d = 1$ dimensions the fermion matrix is particularly simple and takes a cyclic block bidiagonal form,

$$\mathcal{D}_{p,a} = \begin{pmatrix} \Phi(0) & -We^{\mu} & & & \\ & \Phi(1) & -We^{\mu} & & \\ & & \Phi(2) & \ddots & \\ & & & \ddots & -We^{\mu} \\ \mp We^{\mu} & & & & \Phi(L_t-1) \end{pmatrix}. \tag{3.1}$$

Subsequently, determinant reduction techniques based on Schur complements similar to the ones described in [29] can be applied. As a consequence the grand canonical determinant for the reduced fermion matrix yields

$$\det \mathcal{D}_{p,a}[U, X_i; \mu] = \det \left[\mathcal{T} \mp e^{+\mu L_t} \right] \tag{3.2}$$

where $\mathcal{T}$ is the simple matrix product

$$\mathcal{T} = \prod_{t=0}^{L_t-1} (\Phi(t)W)\,. \tag{3.3}$$

For given background fields U and $X_i(t)$ the formula allows to calculate the determinant for any value of the chemical potential μ by simply diagonalising $\mathcal{T}$ and evaluating the characteristic polynomial of order $2(N^2-1)$ in $e^{\mu L_t}$. The coefficients of the polynomial are then just the fermion contributions to the grand canonical partition functions [29],

$$\det \mathcal{D}_{p,a}[U, X_i; \mu] = \sum_{n_f=0}^{2(N^2-1)} (\mp e^{\mu L_t})^{n_f} \det \mathcal{D}_{n_f}[U, X_i]\,, \tag{3.4}$$

which is the conventional fugacity expansion. Note that the computational effort to evaluate eq. (3.2) grows only linearly with the temporal extent of the lattice (through the number of multiplications in the product), for example as one takes the continuum limit $L_t \to \infty$. One can also work in temporal gauge in which all gauge links are transformed to unity except one denoted by $\widetilde{W}$, e.g., the one connecting time slice $t = L_t - 1$ and $t = 0$. The relation to the uniform gauge is then $\widetilde{W} = W^{L_t}$ and the product becomes $\prod_{t=0}^{L_t-1} \Phi(t) \cdot \widetilde{W}$. Finally we note that for ordinary supersymmetric quantum mechanics the expression for $\mathcal{T}$ reduces to the result given in [30].

Next we turn to the explicit evaluation of the canonical determinants. Denoting the eigenvalues of $\mathcal{T}$ in eq. (3.3) by $\tau_j, j = 1, \ldots, 2(N^2-1)$ we can express the determinants directly in terms of these by comparing the coefficients of the characteristic polynomial

$$\det \mathcal{D}_{p,a}[U, X_i; \mu] = \prod_{j=1}^{2(N^2-1)} \left(\tau_j \mp e^{\mu L_t}\right) \tag{3.5}$$

with eq. (3.4). The canonical determinant in the sector with $n_f = 2(N^2-1) \equiv n_f^{\max}$ fermions is trivial,

$$\det \mathcal{D}_{n_f^{\max}}[U, X_i] = 1\,, \tag{3.6}$$

which simply reflects the fact that the sector with maximally saturated fermion number is quenched. For the sector with $n_f = 0$ we obtain

$$\det \mathcal{D}_{n_f=0}[U, X_i] = \prod_{j=1}^{2(N^2-1)} \tau_j = \det \left[\prod_{t=0}^{L_t-1} (\Phi(t)W)\right] = \det \left[\prod_{t=0}^{L_t-1} \Phi(t)\right] \tag{3.7}$$

where we made use of the fact that $\det W = 1$. The formula shows that the fermion contribution in the $n_f = 0$ sector is nontrivial, even though it is independent of the gauge link U.

The sectors with $n_f = 1$ and $n_f = n_f^{\max} - 1$ fermions are similarly simple,

$$\det \mathcal{D}_{n_f=1} = \sum_{j=1}^{2(N^2-1)} \prod_{k\neq j} \tau_k\,, \tag{3.8}$$

JHEP12(2014)044

$$\det \mathcal{D}_{n_f=n_f^{\max}-1} = \sum_{j=1}^{2(N^2-1)} \tau_j = \mathrm{Tr}(\mathcal{T})\,. \tag{3.9}$$

The generic formula for the canonical determinants in terms of the eigenvalues can be expressed by the elementary symmetric functions S_k of the $n_f^{\max}$ eigenvalues $\tau_1, \ldots, \tau_{n_f^{\max}}$ with $k \leq n_f^{\max}$. The k^{th} elementary symmetric function is defined as

$$S_k(\mathcal{T}) \equiv S_k(\tau_1, \ldots, \tau_{n_f^{\max}}) = \sum_{1 \leq i_1 < \cdots < i_k \leq n_f^{\max}} \prod_{j=1}^{k} \tau_{i_j}\,, \tag{3.10}$$

where the sum has $\binom{n_f^{\max}}{k}$ summands, and the canonical determinant in the sector with n_f fermions eventually reads

$$\det \mathcal{D}_{n_f} = S_{n_f^{\max}-n_f}(\mathcal{T})\,. \tag{3.11}$$

Of course the coefficients of the characteristic polynomial can be obtained in many other ways. In appendix A we present several alternative methods how to calculate the canonical determinants directly from the matrix $\mathcal{T}$. One method makes use of the traces of powers of $\mathcal{T}$ while the other employs the minors of $\mathcal{T}$. The latter turns out to be closely related to the transfer matrices emerging from the fermion loop formulation discussed in the next section.

4 Fermion loop formulation

In the fermion loop formulation the decomposition into the various fermion sectors are recovered in a completely different and independent way. The formulation is based on the exact hopping expansion of the fermion Boltzmann factor involving the action in eq. (2.5). Since the overall prefactor $1/2g^2$ only contributes a trivial factor we suppress it in the following. We apply the expansion not only to the hopping term, but in fact to all terms in the fermion action including the Yukawa term. The expansion is exact because it naturally truncates after the first two terms due to the nilpotency of the Grassmann variables. Such an expansion is most conveniently expressed by

$$e^x = 1 + x = \sum_{m=0}^{1} x^m\,, \tag{4.1}$$

i.e., in terms of occupation numbers m. Applying this equation to each term in the fermion action eq. (2.5) characterised by the colour indices a, b, the Dirac algebra indices α, β and the time coordinate t, the expansion of the fermion Boltzmann factor yields

$$\exp(-S_F) = \prod_{t,a,b,\alpha,\beta} \left[\sum_{m^{ab}_{\alpha\beta}(t)=0}^{1} \left(-\Phi^{ab}_{\alpha\beta}(t) \overline{\psi}^a_\alpha(t) \psi^b_\beta(t) \right)^{m^{ab}_{\alpha\beta}(t)} \right] \times \prod_{t,a,\alpha} \left[\sum_{h^{ab}_{\alpha\beta}(t)=0}^{1} \left(\overline{\psi}^a_\alpha(t) W^{ab}_{\alpha\beta} \psi^b_\beta(t+1) \right)^{h^{ab}_{\alpha\beta}(t)} \right], \tag{4.2}$$

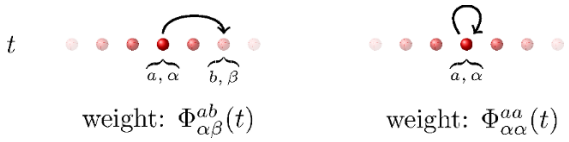

Figure 1. Graphical representation of the Yukawa interaction between the fermionic degree of freedom characterised by (a, α) on time slice t with the one characterised by (b, β) on the same time slice and (a, α) with itself (monomer term). The contributions of the interactions (weights) after the Grassmann integrations are also given.

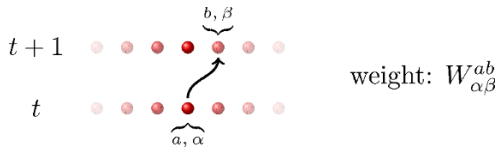

Figure 2. Graphical representation of a gauged temporal hop connecting the fermionic degree of freedom characterised by (a, α) on time slice t with the one characterised by (b, β) on time slice $t + 1$. The contribution of the hop (weight) after the Grassmann integrations is also given.

Here, the terms in the first product follow from the Yukawa interaction while the terms in the second product stem from the hopping terms in which we have put $\mu = 0$ to simplify the discussion. Note that one has a separate expansion for every combination of indices t, a, b, α, β which stops after the first two terms due to the Grassmannian character of the fermionic degrees of freedom. The two terms in each expansion are characterised by the occupation numbers $h^{ab}_{\alpha\beta}(t)$ and $m^{ab}_{\alpha\beta}(t)$ taking the values 0 or 1. The Grassmann integration over the fermion fields requires that every pair $\overline{\psi}^a_\alpha(t)\psi^a_\alpha(t)$ needs to be saturated by the integration measure in order to give a nonvanishing contribution. This condition yields local constraints on the occupation numbers $h^{ab}_{\alpha\beta}(t)$ and $m^{ab}_{\alpha\beta}(t)$ separately at each site t,

$$\sum_{\alpha,a} \left(h^{ab}_{\alpha\beta}(t-1) + m^{ab}_{\alpha\beta}(t) \right) = 1 \quad \forall \beta, b, t\,, \tag{4.3}$$

$$\sum_{\beta,b} \left(h^{ab}_{\alpha\beta}(t) + m^{ab}_{\alpha\beta}(t) \right) = 1 \quad \forall \alpha, a, t\,. \tag{4.4}$$

The integration over the fermion fields is then replaced by a summation over all configurations of occupation numbers satisfying the constraints above.

The various configurations of occupation numbers and the corresponding constraints can most easily be specified graphically by representing each pair $\overline{\psi}^a_\alpha(t)\psi^a_\alpha(t)$ by a point ● and each occupation number $h^{ab}_{\alpha\beta}(t), m^{ab}_{\alpha\beta}(t)$ by an arrow $\longrightarrow$ pointing from point (a, α) to (b, β) saturating $\overline{\psi}^a_\alpha$ and ψ^b_β, respectively. The graphical building blocks are then simply given by the spatial (flavour or colour) hops characterised by $m^{ab}_{\alpha\beta}(t) = 1$, cf. figure 1, and the temporal hops characterised by $h^{ab}_{\alpha\beta}(t) = 1$, cf. figure 2, where the gauge links are reponsible for changing the flavour or colour index from a to b. Due to the breaking of the time inversion symmetry, or equivalently charge conjugation, by the Wilson term

JHEP12(2014)044

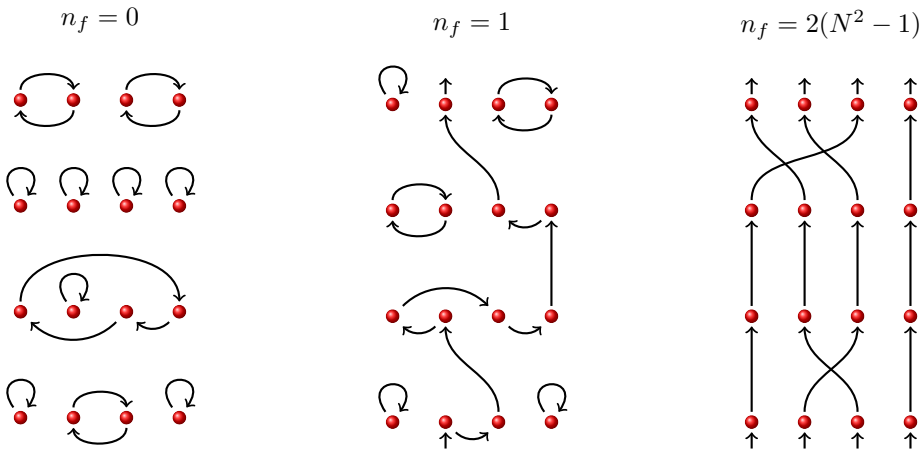

Figure 3. Three sample configurations of closed oriented loops for four fermionic degrees of freedom (representative for the generic $2(N^2-1)$ ones) on a periodic lattice with four time slices.

there exist only temporal hops in forward direction of time. The contribution of each local fermion integration can be read off from eq. (4.2) and are given as the weights in figures 1 and 2. From the contraints in eq. (4.3) and (4.4) it becomes immediately clear that in the graphical representation only closed, oriented fermion loops are allowed. Moreover, each fermion loop picks up the usual factor (-1) from the Grassmann integration. Eventually, the full partition function in the fermion loop formulation reads

$$Z = \int \mathcal{D}U\, \mathcal{D}X\, e^{-S_B[U,X_i]} \sum_{\{h,m\}} \prod_t \left[\left(W^{ab}_{\alpha\beta} \right)^{h^{ab}_{\alpha\beta}(t)} \left(\Phi^{ab}_{\alpha\beta}(t) \right)^{m^{ab}_{\alpha\beta}(t)} \right] \tag{4.5}$$

where the sum is over all combinations of occupation numbers satisfying eq. (4.3) and (4.4).

5 Fermion sectors and transfer matrices

In figure 3 we show three sample configurations consisting of closed oriented fermion loops for four fermionic degrees of freedom (representative for the generic $2(N^2-1)$ ones). One immediately notices that the configurations can be classified according to the number of fermions n_f propagating forward in time. For the three examples depicted in figure 3 the fermion numbers are $n_f = 0, 1$ and 4 (i.e. $n_f = 2(N^2-1)$ for the generic case), respectively. In each sector, the propagation of the n_f fermions can be described by transfer matrices

$$T_{n_f}(t) = T^{\Phi}_{n_f}\left(X_i(t)\right) \cdot T^{W}_{n_f}(U) \tag{5.1}$$

where the first transfer matrix describes the various ways how to connect n_f fermions entering at time t with n_f fermions exiting at t. It depends on the boson field configuration $X_i(t)$ through the Yukawa interactions matrix $\Phi(t)$ and hence depends on t. The second transfer matrix describes how to connect n_f fermions exiting at t and entering at $t+1$, and hence depends on the gauge field U through W in eq. (2.6). In uniform gauge, this transfer matrix has no time dependence. Then, for a given gauge and boson field background

JHEP12(2014)044

$\{U, X_i(t)\}$ the fermion contribution to the partition function in the sector with n_f fermions is simply given by

$$\det \mathcal{D}_{n_f}[U, X_i] = \mathrm{Tr}\left[\prod_{t=0}^{L_t-1} T_{n_f}(t)\right] . \tag{5.2}$$

The full contribution is then obtained by adding up all these terms taking into account a factor $(\mp 1)e^{\mu L_t}$ for each fermion loop winding around the lattice in temporal direction, with the sign depending on whether periodic or antiperiodic boundary conditions are employed. The expression eventually reads

$$\det \mathcal{D}_{p,a}[U, X_i; \mu] = \sum_{n_f=0}^{2(N^2-1)} (\mp e^{\mu L_t})^{n_f} \,\mathrm{Tr}\left[\prod_{t=0}^{L_t-1} T_{n_f}(t)\right] \tag{5.3}$$

and can directly be compared with eq. (3.4).

Let us now look in more detail at the transfer matrices separately in each sector. First we note that the size of T_{n_f} is given by the number of states in sector n_f, i.e.,

$$n \equiv \begin{pmatrix} 2(N^2-1) \\ n_f \end{pmatrix} . \tag{5.4}$$

The sectors with $n_f = 0$ and $n_f = 2(N^2-1)$ are therefore particularly simple since in these cases the transfer matrix is just 1×1. We will hence first discuss these two sectors, followed by the still rather simple sectors with $n_f = 1$ and $n_f = 2(N^2-1)-1$, before presenting the generic case for arbitrary values of n_f.

5.1 Sector $n_f = 0$

For $n_f = 0$ we see by inspection of the corresponding configuration in figure 3 that there is no gauge link dependence, and hence $T_0^W = 1$, while the transfer matrix $T_0^\Phi(t)$ must contain the sum of the weights of all fermion loop configurations on a given time slice t. By doing so, we need to take care that each nontrivial fermion loop picks up the usual factor (-1) from the Grassmann integration. It is not difficult to see that a given time slice configuration can be specified by a permutation σ of the indices $i = 1, \ldots, 2(N^2-1)$ labelling the fermionic degrees of freedom. Each cycle $(ijk\ldots l)$ in the permutation then corresponds to a sequence of indices characterising a specific fermion loop and its weight is given by $\Phi_{ij}\Phi_{jk}\ldots\Phi_{li}$. The total sign of the configuration is given by including a factor (-1) for each nontrivial cycle, i.e., counting whether the number of nontrivial cycles in the permutation is even or odd which corresponds to the parity of the permutation. Finally, the sum over all configurations amounts to summing up all permutations including the corresponding weights and the signs given by the parity of the permutation. This prescription is of course nothing else than the definition for the determinant, so the transfer matrix in the $n_f = 0$ sector is simply given by

$$T_0^\Phi(t) = \det \Phi(t) \tag{5.5}$$

and the total fermion contribution factorises completely,

$$\det \mathcal{D}_{n_f=0}[U, X_i] = \prod_{t=0}^{L_t-1} \det \Phi(t) . \tag{5.6}$$

JHEP12(2014)044

Comparing this with eq. (3.7) we obviously find complete agreement. In the fermion loop approach however it is evident from the beginning that the gauge link U does not contribute in the $n_f = 0$ sector.

5.2 Sector $n_f = n_f^{\max}$

For $n_f = 2(N^2-1) \equiv n_f^{\max}$ the transfer matrix $T_{n_f^{\max}}(t)$ is again 1×1. While there are no contributions from the Yukawa interaction, hence $T^{\Phi}_{n_f^{\max}}(t) = 1$, we need to take into account the nontrivial hopping in colour space. The complication arising here stems from the fact that depending on the number of hoppings in colour space, the total number of fermion loops winding in temporal direction changes, but not the number of winding fermions. For example, if there are only colour diagonal hops, the number of winding loops is $n_f^{\max}$ and the corresponding contribution comes with a positive sign. On the other hand, if there is one single nondiagonal colour hop two loops merge into one, so the number of winding loops becomes $n_f^{\max} - 1$ and the contribution should hence contain a negative sign relative to the contribution with $n_f^{\max}$ loops. So for every nondiagonal colour hop the number of loops is changing by one.

Similarly to the $n_f = 0$ sector we need to take all permutations of the colour indices a, b into account. For each nontrivial permutation of two indices the number of fermion loops winding in temporal direction is reduced by one and we take this into account by including a factor (-1). Summing over all permutations including the sign corresponding to the parity of the permutations again yields the determinant, i.e.,

$$T^{W}_{n_f^{\max}} = \det[W] = 1 \tag{5.7}$$

yielding the total contribution

$$\det \mathcal{D}_{n_f^{\max}}[U, X_i] = \prod_{t=0}^{L_t-1} T_{n_f^{\max}}(t) = 1\,. \tag{5.8}$$

This is in accordance with the result from the determinant reduction, cf. eq. (3.6), and it is obvious that the same result would be obtained without referring to a particular gauge. Since the fermions are completely saturated by the temporal hopping terms and contribute only trivially to the canonical determinant, this sector corresponds to the quenched one as noted before.

5.3 Sector $n_f = 1$

Next, we look at the sector with $n_f = 1$ fermions. The corresponding transfer matrices $T_1(t)$ are of size $2(N^2-1) \times 2(N^2-1)$. Each matrix element $(T_1^{\Phi}(t))_{ij}$ contains the sum of weights of all configurations at fixed t where the fermion degree of freedom $i = (a, \alpha)$ is entering time slice t and $j = (b, \beta)$ is leaving. The corresponding degrees of freedom are then already saturated by the corresponding hops in and out of the time slice and hence the weights Φ_{ki} and $\Phi_{jk}, k = 1, \ldots, 2(N^2-1)$ can not appear in any of the configurations. The remaining time slice configurations can be obtained in analogy to the considerations in the $n_f = 0$ sector, that is by constructing all permutations, i.e., cycles of the remaining degrees

JHEP12(2014)044

of freedom and taking into account factors of (-1) for each nontrivial cycle. Following the arguments from the $n_f = 0$ sector it turns out that this is again equivalent to taking the determinant of $\Phi(t)$, but with row j and column i removed, i.e.,

$$\left(T_1^{\Phi}\right)_{ij} = (-1)^{i+j} \det \Phi|_{\Phi_{ki}=\delta_{kj},\Phi_{jk}=\delta_{ik}} \equiv (-1)^{i+j} \det \Phi^{\not i\not j} \tag{5.9}$$

which is in fact the (j,i)-cofactor of Φ. This will be discussed in more detail in section 5.5. Similarly, in order to include the colour changing hops due to the gauge link between time slices we multiply with the corresponding gauge link transfer matrix T_1^W

$$\left(T_1^{W}\right)_{ij} = (W)_{ij} \tag{5.10}$$

which in uniform gauge is constant in time and is in fact the complementary (i,j)-minor $\det W^{ij}$. Eventually, the full fermion contribution in the $n_f = 1$ sector reads

$$\det \mathcal{D}_{n_f=1}[U, X_i] = \mathrm{Tr} \prod_{t=0}^{L_t-1} \left[T_1^{\Phi}(t) \cdot T_1^{W}\right] \tag{5.11}$$

and comparing this result to the one in eq. (3.8) from the fugacity expansion, we find a nontrivial relationship between the two expressions. We will comment further on this relation in section 5.5 and establish it in detail in appendix B.

5.4 Sector $n_f = n_f^{\max} - 1$

In the sector where all but one, i.e., $n_f^{\max} - 1$ fermions are propagating, the states of the transfer matrices $T_{n_f^{\max}-1}(t)$ are most conveniently labelled by the degree of freedom $i = (a, \alpha)$ not occupied by a temporal hopping term. The transfer matrices are hence of size $2(N^2-1) \times 2(N^2-1) = n_f^{\max} \times n_f^{\max}$. The matrix elements $(T^{\Phi}_{n_f^{\max}-1})_{ij}$ are calculated following the arguments outlined above for the $n_f = 0$ and 1 sector, namely to take the determinant of the Yukawa matrix Φ with all columns and rows deleted except i and j, respectively. The reduced Yukawa matrix is then just a single element and hence we have

$$(T^{\Phi}_{n_f^{\max}-1})_{ij} = (-1)^{i+j} \Phi_{ij} \tag{5.12}$$

which is just the complementary (i,j)-cofactor of Φ up to an overall sign. The transfer matrix describing all the possible configurations within a time slice needs to be complemented by the one inducing the colour changing hops due to the gauge link between the time slices. If fermion i is not hopping out of t and j not into $t+1$ they will not contribute, while the mixing of the remaining degrees of freedom is described as before by taking the determinant of the hop matrix,

$$(T^{W}_{n_f^{\max}-1})_{ij} = \det W^{\not i\not j} \tag{5.13}$$

which is the (i,j)-minor of W. The full fermion contribution in the $n_f = n_f^{\max} - 1$ sector finally yields

$$\det \mathcal{D}_{n_f^{\max}-1}[U, X_i] = \mathrm{Tr} \prod_{t=0}^{L_t-1} \left[T^{\Phi}_{n_f^{\max}-1}(t) \cdot T^{W}_{n_f^{\max}-1}\right] . \tag{5.14}$$

This can be compared to the one in eq. (3.9) from the fugacity expansion and we find again a nontrivial relationship between the two expressions.

JHEP12(2014)044

5.5 Sector with generic n_f

Similar constructions can be worked out in all the other sectors, but the constructions become more involved since the number of states grows rapidly towards the half-filled sector with $n_f = 2(N^2-1)/2$. However, our previous discussion indicates a generic pattern which becomes clear after careful further investigation of all the weights and signs of each configuration. Employing some higher linear algebra one can eventually formulate the following rule. The sector with n_f fermions contains $n = \binom{n_f^{\max}}{n_f}$ states and the elements of the corresponding $n \times n$ transfer matrix $T^{\Phi}_{n_f}$ are given by the cofactors of Φ of order n_f, while the matrix elements of $T^{W}_{n_f}$ are given by the complementary minors of W.

To be more precise, let A and B be two index sets $A, B \subseteq \{1, 2, \ldots, 2(N^2-1)\}$ of size n_f, then the cofactor of Φ of order n_f is the signed determinant of the $(2(N^2-1)-n_f) \times (2(N^2-1)-n_f)$ submatrix $\Phi^{\not B \not A}$ obtained from Φ by deleting the rows indexed by B and the columns indexed by A, so

$$\left(T^{\Phi}_{n_f}\right)_{AB} = (-1)^{p(A,B)} \det \Phi^{\not B \not A} \tag{5.15}$$

where $p(A,B) = \sum_{i \in A} i + \sum_{j \in B} j$, while the complementary minor $\det W^{AB}$ is the determinant of the $n_f \times n_f$ submatrix W^{AB} obtained from W by keeping only the rows indexed by A and the columns indexed by B,

$$\left(T^{W}_{n_f}\right)_{AB} = \det W^{AB} \,. \tag{5.16}$$

If the two sets A and B are equal, the cofactors reduce to minors and the corresponding determinants are called principal minors or principal complementary minors. Note also that in the literature the role of the minor and complementary minor is sometimes exchanged.

In analogy to the discussion before, the cofactor $C_{\not B \not A}(\Phi) = (-1)^{p(A,B)} \det \Phi^{\not B \not A}$ includes all contributions to the transition of n_f fermions indexed by A entering at time t to n_f fermions indexed by B exiting from time t, with all the weights and signs properly accounted for. Similarly, the minor $M_{AB}(W) = \det W^{AB}$ connects n_f fermions indexed by A exiting t in all possible ways with n_f fermions indexed by B entering time $t+1$ with the correct weight and sign for each connection. Hence, the full transfer matrix at time t in the sector with n_f fermions is then $T^{\Phi}_{n_f}(t) \cdot T^{W}_{n_f}$ and the corresponding canonical determinant reads

$$\det \mathcal{D}_{n_f}[U, X_i] = \mathrm{Tr} \prod_{t=0}^{L_t-1} \left[T^{\Phi}_{n_f}(t) \cdot T^{W}_{n_f} \right] \,. \tag{5.17}$$

It is easy to check that this generic definition yields the correct expressions for the transfer matrices and canonical determinants for the cases $n_f = 0, 1, n_f^{\max}-1, n_f^{\max}$ discussed in the previous sections. Note that for the empty sets $A = B = \{\}$ the principal minor, and analogously the complementary principal minor for the full sets $A = B = \{1, \ldots, 2(N^2-1)\}$, is 1 by definition.

Finally, one can show that the canonical determinants obtained in the fermion loop approach are equal to the ones using the fermion matrix reduction, cf. eq. (3.11). Using

JHEP12(2014)044

various relations between matrices of minors and cofactors, one can derive that

$$\left(\prod_{t=0}^{L_t-1}\left[T_{n_f}^{\Phi}(t)\cdot T_{n_f}^{W}\right]\right)_{AB} = (-1)^{p(A,B)}\det \mathcal{T}^{\not A\not B} = C_{\not A\not B}(\mathcal{T})\,. \tag{5.18}$$

The details of this derivation are given in appendix B. The r.h.s. forms the $n \times n$ matrix of cofactors of $\mathcal{T}$ of order n_f and the trace in eq. (5.17) then yields the sum over the n principal minors of $\mathcal{T}$ of order n_f denoted by E_{n_f}, i.e.,

$$\det \mathcal{D}_{n_f} = \sum_B \det \mathcal{T}^{\not B\not B} \equiv E_{n_f}(\mathcal{T})\,. \tag{5.19}$$

Recalling a known relation from linear algebra between the sum of minors of a matrix and its symmetric functions [31] one has

$$E_{n_f}(\mathcal{T}) = S_{n_f^{\max}-n_f}(\mathcal{T}) \tag{5.20}$$

which establishes the equivalence between eq. (3.11) and eq. (5.19).

5.6 Remarks

We close this section with several remarks. Firstly, we note that in contrast to the full determinant $\det[U, X_i]$, which can be proven to be positive [15], the various canonical determinants $\det \mathcal{D}_{n_f}[U, X_i]$ need not necessarily be positive. Obviously, $\det \mathcal{D}_{n_f=2(N^2-1)}[U, X_i]$ is so and it seems that at least $\det \mathcal{D}_{n_f=0}[U, X_i]$ is also positive, although we do not have any proof. It would be interesting to study potential fermion sign problems in the canonical sectors in the present model. Despite its simplicity due to the low dimension, it nevertheless contains all the important features of a gauge theory, and hence conclusions can most likely be generalised to more complicated gauge theories in higher dimensions, such as QCD in the canonical formulation [29].

Secondly, we note that the various sectors, in particular the ones with many fermions, can in principle be simulated by open fermion string (fermion worm) algorithms along the lines described in [23, 24]. This approach has indeed already been applied successfully in ordinary supersymmetric quantum mechanics [22], in the supersymmetric nonlinear O(N) sigma model [32] and in the two dimensional $\mathcal{N} = 1$ Wess-Zumino model [25, 27] where the transfer matrix techniques discussed here and in [26] are out of reach. Furthermore, for the model discussed in this paper, a discrete bond formulation for the bosonic degrees of freedom is available [33]. Such a formulation promises a huge gain in efficiency for numerical simulations, but it is not clear whether the bosonic bond formulation can be put into practice.

Thirdly, from investigations in the Hamiltonian formulation of the theory [3], where time is treated as a continuous variable, it is known that there is a (spectral) symmetry between the sectors with n_f and $2(N^2-1)-n_f$ fermions, due to the exchange symmetry between particles and antiparticles. Our results above indicate that the symmetry is not maintained by our choice of the discretisation in the Lagrangian formalism, but the reason for this is clear. As we mentioned earlier the Wilson term needed to control the doubler

JHEP12(2014)044

fermions explicitly breaks the time reversal and hence the charge conjugation symmetry which of course is crucial for an exact particle/antiparticle exchange symmetry. However, since the symmetries are restored in the continuum limit without fine tuning, the symmetries between the various canonical sectors will also be mended automatically in the continuum, and the difference between the related sectors will provide a good estimate of the remaining systematic lattice artefacts.

6 Conclusions and outlook

In this paper we have investigated in detail the structure of the fermionic part of the $d = 4$ dimensional supersymmetric Yang-Mills quantum mechanics, i.e., $\mathcal{N} = 4$ SYM QM with gauge group SU(N). On the one hand, we derived a reduced fermion matrix whose size is independent of the temporal extent of the lattice. In addition, the dependence on the chemical potential is factored out and this allows the exact projection of the fermion determinant onto the canonical sectors with fixed fermion number, once the eigenvalues of the reduced matrix are calculated. On the other hand, we have presented the fermion loop formulation of the theory in which the grand canonical fermion determinant naturally decomposes into sectors with fixed fermion numbers. The construction of transfer matrices is rather straightforward in the various fermion sectors and the comparison with the fugacity expansion, accessible via the reduced fermion matrix, yields identical results and interesting relations between the transfer matrices and the eigenvalues of the reduced fermion matrix. In fact, we presented a proof which establishes the equivalence of the canonical determinants from the reduced fermion matrix approach and from the fermion loop formulation on the algebraic level.

Our results open various possibilities for a range of nonperturbative investigations of the theory. This can be done for example by numerical simulations using methods different from the usual Hybrid Monte Carlo approach, either using the transfer matrices in the various canonical sectors with fixed fermion numbers, or using the projection to the sectors with the help of the reduced fermion matrix. Another interesting approach could be the application of mean field methods to the spatial gauge degrees of freedom, again either in the transfer matrix approach or using the reduced fermion matrix. It is even conceivable that the methods presented here and the emerged simple structures lead to new analytic results in some interesting limits. All results obtained either way will provide important insights into the conjectured M-theory and will add to our understanding of the corresponding gauge/gravity duality, besides unveiling interesting physics of the model itself.

Another interesting line of research starting from here concerns the investigation of ordinary, non-supersymmetric gauge field theories in higher dimensions at finite fermion density, such as QCD at finite baryon density. It is notoriously difficult to obtain reliable results in these theories using the known numerical approaches, due to the intrinsic fermion sign problem at finite density, and any insight into how the simulations of these theories could be facilitated would be extremely valuable. The explicit fugacity expansion derived in this paper allows to investigate finite density simulations or canonical simulations in a

JHEP12(2014)044

simple setup which nevertheless displays a similar structure, and hence contains all the important features, as the more complicated theories in higher dimensions such as QCD.

Finally, the extension of the loop formulation to $\mathcal{N} = 16$ supersymmetric Yang-Mills quantum mechanics is in principle straightforward but requires special care. This is due to the fact that the corresponding dimensionally reduced model has obviously a different Dirac structure, and it remains to be seen whether the structure is compatible with the requirements for the fermion loop formulation. The fermion matrix reduction on the other hand should be unaffected by the change of the Dirac structure.

Acknowledgments

We thank Dan Boss, Adolpho Guarino, Piotr Korcyl, Andreas Wipf and Jacek Wosiek for useful discussions, and in particular Piotr Korcyl and Dan Boss for sharing their codes for the $d = 4$ dimensional SU(N) SYM QM with $N = 2$ and $N = 2, 3$, respectively.

A Determinations of canonical determinants

In this appendix we review three alternative methods to calculate the canonical determinants from the matrix $\mathcal{T}$ in eq. (3.3). As shown in section 3 the canonical determinants are just the coefficients of the characteristic polynomial of the matrix $\mathcal{T}$. The first method provides recursion relations which yield the coefficients in terms of the eigenvalues τ_i of $\mathcal{T}$. The second method evaluates the coefficients in terms of the traces of powers of $\mathcal{T}$ and the third makes use of the minors of $\mathcal{T}$. The latter method turns out to be closely related to the transfer matrix approach in the fermion loop formulation and hence deserves special emphasis.

In the following we assume the matrix $\mathcal{T}$ to be of size $n \times n$ and for simplicity we consider only the case of antiperiodic b.c., hence the relevant characteristic polynomial is

$$g(x) = \det(\mathcal{T} + x \cdot \mathbb{1}) = \sum_{k=0}^{n} c_k \cdot x^k \tag{A.1}$$

where $\mathbb{1}$ is the $n \times n$ unit matrix and the coefficients c_k are the canonical determinants $\det \mathcal{D}_{n_f=k}$ in sector k.

A.1 Coefficients from recursion relations

The coefficients can be obtained from the eigenvalues τ_i of $\mathcal{T}$ using recursive relations [29]. To this end, we first define the partial products

$$\Pi_r(x) = \prod_{j=1}^{r} (\tau_j + x) = \sum_{k=1}^{r} c_k^{(r)} x^k \tag{A.2}$$

which fulfill $\prod_{r+1}(x) = (\tau_{r+1} + x) \prod_r(x)$. Setting $c_{-1}^{(r)} = 0$ we have the recursion relation

$$c_k^{(r+1)} = \tau_{r+1} c_k^{(r)} + c_{k-1}^{(r)} \tag{A.3}$$

for all $0 \leq k \leq r+1$ which allows to compute $c_k^{(r+1)}$ from $c_k^{(r)}$. After n steps we obtain the coefficients $c_k \equiv c_k^{(n)}$ of $\prod_n(x)$ which are then just the canonical determinants $\det \mathcal{D}_{n_f=k}$. The generalisation of the recursion to include the minus sign from the periodic b.c. is straightforward.

A.2 Coefficients in terms of traces

Here we review the calculation of the coefficients c_k in terms of traces of powers of the matrix $\mathcal{T}$. To do so we introduce the notation

$$t_k = \mathrm{Tr}(\mathcal{T}^k)\,. \tag{A.4}$$

Then, Newton's identities (or the Newton-Girard formulae) provide a set of relations between the traces,

$$t_1 - c_{n-1} = 0, \quad t_k - c_{n-1}t_{k-1} + \ldots - c_{n-k+1}t_1 + k \cdot c_{n-k} = 0, \quad k = 2, 3, \ldots, n\,, \tag{A.5}$$

which can be solved recursively. The solution can conveniently be written down in closed form as

$$c_{n-k} = \frac{1}{k!} \det \begin{pmatrix} t_1 & 1 & 0 & 0 & \cdots & 0 \\ t_2 & t_1 & 2 & 0 & \cdots & 0 \\ t_3 & t_2 & t_1 & 3 & \cdots & 0 \\ \vdots & \vdots & \vdots & \vdots & \ddots & \vdots \\ t_{k-1} & t_{k-2} & t_{k-3} & t_{k-4} & \cdots & k-1 \\ t_k & t_{k-1} & t_{k-2} & t_{k-3} & \cdots & t_1 \end{pmatrix} \tag{A.6}$$

and the generalisation to periodic b.c. is again straighforward.

A.3 Coefficients in terms of minors

Instead of computing the traces of the matrices $\mathcal{T}, \mathcal{T}^2, \mathcal{T}^3, \ldots, \mathcal{T}^n$ we now present an alternative method for determining the coefficients of the characteristic polynomial which is more interesting from the point of view of the transfer matrix construction discussed in section 5. The method involves the expansion of determinants of order 1 to n [34]. In order to determine the coefficients c_k of x^k in $g(x)$ it is useful to separate the occurrences of x by introducing

$$f(x_1, x_2, \ldots, x_n) = \det\left(\mathcal{T} + \mathrm{diag}(x_1, x_2, \ldots\, x_n)\right)\,. \tag{A.7}$$

One then has $g(x) = f(x, x, \ldots, x)$ and c_k is the sum of the coefficients of the terms with total degree k in $f(x_1, x_2, \ldots, x_n)$. Since $f(x_1, x_2, \ldots, x_n)$ is of degree 1 in each x_i, it is straightforward to express the coefficient in terms of derivatives w.r.t. x_i's,

$$c_k = \sum_{1 \leq i_1 < \cdots < i_k \leq n} \frac{\partial^k}{\partial x_{i_1} \partial x_{i_2} \cdots \partial x_{i_k}} f(x_1, x_2, \ldots, x_n) \Big|_{x_1 = x_2 = \ldots = x_n = 0} \tag{A.8}$$

where $0 \leq k \leq n$. As a consequence the coefficients are now expressed explicitly in terms of the matrix elements of $\mathcal{T}$. Denoting them by t_{ij} it turns out that

$$c_k = \sum_{1 \leq i_1 < \cdots < i_k \leq n} \frac{\partial^k}{\partial t_{i_1 i_1} \partial t_{i_2 i_2} \cdots \partial t_{i_k i_k}} \det \mathcal{T}\,. \tag{A.9}$$

This can be seen most easily by suppressing the dependence of $\det \mathcal{T}$ on the off-diagonal elements $t_{ij}, i \neq j$ and define D as a function of the n variables $t_{11}, t_{22}, \ldots, t_{nn}$,

$$D(t_{11}, t_{22}, \ldots, t_{nn}) \equiv \det \mathcal{T}\,, \tag{A.10}$$

and hence

$$f(x_1, x_2, \ldots, x_n) = D(t_{11} + x_1, t_{22} + x_2, \ldots, t_{nn} + x_n)\,. \tag{A.11}$$

It is then immediately clear that

$$\frac{\partial^k f}{\partial x_{i_1} \partial x_{i_2} \ldots \partial x_{i_k}} = \frac{\partial^k D(t_{11} + x_1, t_{22} + x_2, \ldots, t_{nn} + x_n)}{\partial t_{i_1 i_1} \partial t_{i_2 i_2} \cdots \partial t_{i_k i_k}}\,. \tag{A.12}$$

from which eq. (A.9) follows via eq. (A.10).

On the other hand the rules for the Laplace expansion of a determinant by a row or a column indicate that $\partial \det \mathcal{T}/\partial t_{ij}$ is the (i,j)-cofactor of $\mathcal{T}$, or in fact the (i,i)-minor when $i = j$. Therefore, the partial derivatives in eq. (A.9) are simply the subdeterminants of $\mathcal{T}$ resulting from crossing out the rows and columns numbered by $i_1, i_2, \ldots, i_k$, i.e., the principal minors of $\mathcal{T}$ of order k.

Denoting the sum of principal minors of order k of $\mathcal{T}$ by $E_k(\mathcal{T})$ and keeping in mind that $\det \mathcal{D}_k = c_k$ one finds by comparison with eq. (3.11) that

$$S_{n-k}(\mathcal{T}) = E_k(\mathcal{T}) \tag{A.13}$$

for each $k = 1, \ldots, n$, which is a known identity in matrix analysis from linear algebra, see e.g. [31].

Comparing these results with the ones derived in section 5 we immediately notice that the trace over the states of the transfer matrix is represented in eq. (A.9) by the sum $\sum_{i_1<i_2<\ldots<i_k}$. The number of summands here is $\binom{n}{k}$ and indeed equal to the number of states in the sector with $n_f = k$. Furthermore, the principal subdeterminants (minors) in eq. (A.9) correspond to the diagonal elements of the product of transfer matrices in the given sector.

B Equivalence of canonical determinants

Here we show that the canonical determinants obtained in the fermion loop approach, cf. eq. (5.17), are equal to the ones using the fermion matrix reduction, cf. eq. (3.11).

Following the notation introduced in section 5.5, for two index sets A and B of size n_f the transfer matrix $T^{\Phi}_{n_f}$ in eq. (5.15) is the transposed matrix of cofactors of Φ of order n_f and is denoted by

$$\left(T^{\Phi}_{n_f}\right)_{AB} = C_{\bar{B}\bar{A}}(\Phi)\,, \tag{B.1}$$

while the transfer matrix $T^{W}_{n_f}$ in eq. (5.16) is the matrix of complementary minors denoted by

$$\left(T^{W}_{n_f}\right)_{AB} = M_{AB}(W)\,. \tag{B.2}$$

JHEP12(2014)044

Now we note that the complementary minor matrix $M_{AB}(W)$ is related to the minor matrix of the inverse $M_{\bar{A}\bar{B}}(W^{-1})$ by

$$M_{\bar{A}\bar{B}}(W^{-1}) = (-1)^{p(A,B)} \frac{M_{BA}(W)}{\det W} \tag{B.3}$$

where $p(A,B) = \sum_{i\in A} i + \sum_{j\in B} j$. Up to the determinant, the r.h.s. is the higher order generalisation of the adjugate (or classical adjoint) of W, i.e. $\mathrm{Adj}_{AB}(W)$. (To order 1 the adjugate is just the transposed complementary cofactor matrix.) Hence, with $\det W = 1$, $W^{-1} = W^\dagger = W^T$ and $M_{AB}(W) = M_{BA}(W^T)$ we have

$$C_{\bar{B}\bar{A}}(W^\dagger) = C_{\bar{A}\bar{B}}(W) = M_{AB}(W)\,, \tag{B.4}$$

i.e., the transfer matrix $T^W_{n_f}$ can be expressed as a cofactor matrix instead of a complementary minor matrix.

Next, we note that the cofactor matrix C and the corresponding minor matrix M are related by modifying the sign of each element according to $C_{AB} = (-1)^{p(A,B)} M_{AB}$. The sign change can be achieved by a similarity transformation with the matrix $S_{AB} = (-1)^{\sum_{i\in A} i}\,\delta_{AB}$, i.e., $C = S^{-1}\cdot M\cdot S$. Therefore a product of cofactor matrices becomes a product of minor matrices under a trace, and so we can eventually write

$$\det \mathcal{D}_{n_f} = \mathrm{Tr} \prod_{t=0}^{L_t-1} \left[T^\Phi_{n_f}(t)\cdot T^W_{n_f}\right] \tag{B.5}$$

$$= \mathrm{Tr} \prod_{t=0}^{L_t-1} \left[C(\Phi(t))^T \cdot C(W)\right] \tag{B.6}$$

$$= \mathrm{Tr} \prod_{t=0}^{L_t-1} \left[M(\Phi(t))\cdot M(W)\right]\,. \tag{B.7}$$

Note that we have made use of the fact that $C(\Phi)^\dagger = C(\Phi)$ since $\Phi^\dagger = \Phi$.

We can now employ the Cauchy-Binet formula which states in its symmetric form that given the $n\times n$ matrices P, Q with $R = PQ$ and two index sets A, B of size $1 \le k \le n$ the (AB)-minor of R is

$$\det R^{\bar{A}\bar{B}} = \sum_D \det P^{\bar{A}\bar{D}} \det Q^{\bar{D}\bar{B}} \tag{B.8}$$

where the sum is taken over all index sets D of size k. From the formula it follows that for the matrices of minors (and similarly for the matrices of cofactors) one has

$$M(PQ) = M(P)M(Q) \tag{B.9}$$

and consequently from eq. (B.7)

$$\det \mathcal{D}_{n_f} = \mathrm{Tr} \prod_{t=0}^{L_t-1} \left[M(\Phi(t))\cdot M(W)\right] \tag{B.10}$$

$$= \mathrm{Tr}\, M\left(\prod_{t=0}^{L_t-1} \left[\Phi(t) W\right]\right) \tag{B.11}$$

$$= \mathrm{Tr}\, M(\mathcal{T})\,. \tag{B.12}$$

Finally, the trace sums over the $\binom{n_f^{\max}}{n_f}$ diagonal elements of the minor matrix which are just the principal minors,

$$\det \mathcal{D}_{n_f} = \sum_B \det \mathcal{T}^{\not{B}\not{B}} \equiv E_{n_f}(\mathcal{T})\,. \tag{B.13}$$

Recalling from linear algebra [31] the fact that the sum of all principal minors of order n_f of a matrix is equal to the $(n_f^{\max} - n_f)^{th}$ symmetric function of its eigenvalues, i.e. $E_{n_f}(\mathcal{T}) = S_{n_f^{\max}-n_f}(\mathcal{T})$, eventually proves the equivalence between $\det \mathcal{D}_{n_f}$ from the fermion loop formulation in eq. (5.19) and from the fermion matrix reduction in eq. (3.11).

References

[1] T. Banks, W. Fischler, S.H. Shenker and L. Susskind, *M-theory as a matrix model: a conjecture*, *Phys. Rev.* **D 55** (1997) 5112 [hep-th/9610043] [INSPIRE].

[2] W. Taylor, *M(atrix) theory: matrix quantum mechanics as a fundamental theory*, *Rev. Mod. Phys.* **73** (2001) 419 [hep-th/0101126] [INSPIRE].

[3] J. Wosiek, *Spectra of supersymmetric Yang-Mills quantum mechanics*, *Nucl. Phys.* **B 644** (2002) 85 [hep-th/0203116] [INSPIRE].

[4] M. Campostrini and J. Wosiek, *High precision study of the structure of $D = 4$ supersymmetric Yang-Mills quantum mechanics*, *Nucl. Phys.* **B 703** (2004) 454 [hep-th/0407021] [INSPIRE].

[5] G. Veneziano and J. Wosiek, *Planar quantum mechanics: an intriguing supersymmetric example*, *JHEP* **01** (2006) 156 [hep-th/0512301] [INSPIRE].

[6] G. Veneziano and J. Wosiek, *A supersymmetric matrix model. II. Exploring higher-fermion-number sectors*, *JHEP* **10** (2006) 033 [hep-th/0607198] [INSPIRE].

[7] G. Veneziano and J. Wosiek, *A supersymmetric matrix model. III. Hidden SUSY in statistical systems*, *JHEP* **11** (2006) 030 [hep-th/0609210] [INSPIRE].

[8] M. Campostrini and J. Wosiek, *Exact Witten index in $D = 2$ supersymmetric Yang-Mills quantum mechanics*, *Phys. Lett.* **B 550** (2002) 121 [hep-th/0209140] [INSPIRE].

[9] P. Korcyl, *Solutions of $D = 2$ supersymmetric Yang-Mills quantum mechanics with* SU(N) *gauge group*, *J. Math. Phys.* **52** (2011) 052105 [arXiv:1101.0591] [INSPIRE].

[10] P. Korcyl, *Analytic calculation of Witten index in $D = 2$ supersymmetric Yang-Mills quantum mechanics*, *J. Math. Phys.* **53** (2012) 102102 [arXiv:1101.0668] [INSPIRE].

[11] P. Korcyl, *Gauge invariant plane-wave solutions in supersymmetric Yang-Mills quantum mechanics*, *J. Math. Phys.* **52** (2011) 042102 [arXiv:1008.2975] [INSPIRE].

[12] P. Korcyl, *Exact solutions to $D = 2$ supersymmetric Yang-Mills quantum mechanics with* SU(3) *gauge group*, *Acta Phys. Polon. Supp.* **2** (2009) 623 [arXiv:0911.2152] [INSPIRE].

[13] R.A. Janik and J. Wosiek, *Towards the matrix model of M-theory on a lattice*, *Acta Phys. Polon.* **B 32** (2001) 2143 [hep-th/0003121] [INSPIRE].

[14] N. Kawahara, J. Nishimura and S. Takeuchi, *Phase structure of matrix quantum mechanics at finite temperature*, *JHEP* **10** (2007) 097 [arXiv:0706.3517] [INSPIRE].

JHEP12(2014)044

[15] S. Catterall and T. Wiseman, *Towards lattice simulation of the gauge theory duals to black holes and hot strings*, *JHEP* **12** (2007) 104 [arXiv:0706.3518] [INSPIRE].

[16] S. Catterall and T. Wiseman, *Black hole thermodynamics from simulations of lattice Yang-Mills theory*, *Phys. Rev.* **D 78** (2008) 041502 [arXiv:0803.4273] [INSPIRE].

[17] S. Catterall and T. Wiseman, *Extracting black hole physics from the lattice*, *JHEP* **04** (2010) 077 [arXiv:0909.4947] [INSPIRE].

[18] M. Hanada, J. Nishimura and S. Takeuchi, *Non-lattice simulation for supersymmetric gauge theories in one dimension*, *Phys. Rev. Lett.* **99** (2007) 161602 [arXiv:0706.1647] [INSPIRE].

[19] K.N. Anagnostopoulos, M. Hanada, J. Nishimura and S. Takeuchi, *Monte Carlo studies of supersymmetric matrix quantum mechanics with sixteen supercharges at finite temperature*, *Phys. Rev. Lett.* **100** (2008) 021601 [arXiv:0707.4454] [INSPIRE].

[20] M. Hanada, J. Nishimura, Y. Sekino and T. Yoneya, *Direct test of the gauge-gravity correspondence for matrix theory correlation functions*, *JHEP* **12** (2011) 020 [arXiv:1108.5153] [INSPIRE].

[21] M. Honda, G. Ishiki, S.-W. Kim, J. Nishimura and A. Tsuchiya, *Direct test of the AdS/CFT correspondence by Monte Carlo studies of $N = 4$ super Yang-Mills theory*, *JHEP* **11** (2013) 200 [arXiv:1308.3525] [INSPIRE].

[22] D. Baumgartner and U. Wenger, *Simulation of supersymmetric models on the lattice without a sign problem*, PoS(Lattice 2010)245 [arXiv:1104.0213] [INSPIRE].

[23] U. Wenger, *Efficient simulation of relativistic fermions via vertex models*, *Phys. Rev.* **D 80** (2009) 071503 [arXiv:0812.3565] [INSPIRE].

[24] U. Wenger, *Simulating Wilson fermions without critical slowing down*, PoS(LAT2009)022 [arXiv:0911.4099] [INSPIRE].

[25] D. Baumgartner, K. Steinhauer and U. Wenger, *Supersymmetry breaking on the lattice: the $N = 1$ Wess-Zumino model*, PoS(LATTICE 2011)253 [arXiv:1111.6042] [INSPIRE].

[26] D. Baumgartner and U. Wenger, *Exact results for supersymmetric quantum mechanics on the lattice*, PoS(LATTICE 2011)239 [arXiv:1201.1485] [INSPIRE].

[27] D. Baumgartner, K. Steinhauer and U. Wenger, *Spontaneous supersymmetry breaking in the $2d$ $N = 1$ Wess-Zumino model*, PoS(LATTICE 2012)043 [arXiv:1311.5089] [INSPIRE].

[28] P. Hasenfratz and F. Karsch, *Chemical potential on the lattice*, *Phys. Lett.* **B 125** (1983) 308 [INSPIRE].

[29] A. Alexandru and U. Wenger, *QCD at non-zero density and canonical partition functions with Wilson fermions*, *Phys. Rev.* **D 83** (2011) 034502 [arXiv:1009.2197] [INSPIRE].

[30] G. Bergner, T. Kaestner, S. Uhlmann and A. Wipf, *Low-dimensional supersymmetric lattice models*, *Annals Phys.* **323** (2008) 946 [arXiv:0705.2212] [INSPIRE].

[31] R.H. Horn and C.R. Johnson, *Matrix analysis*, second ed., Cambridge University Press, New York U.S.A. (2013).

[32] K. Steinhauer and U. Wenger, *Loop formulation of the supersymmetric nonlinear $O(N)$ σ-model*, PoS(LATTICE 2013)092 [arXiv:1311.5403] [INSPIRE].

[33] K. Steinhauer, *Loop formulation in low dimensional supersymmetric models on the lattice*, Ph.D. thesis, Institute for Theoretical Physics, University of Bern, Bern Switzerland (2014).

[34] L.L. Pennisi, *Coefficients of the characteristic polynomial*, *Math. Mag.* **60** (1987) 31.

JHEP12(2014)044

Part IV

Supersymmetric models in two dimensions

Paper 10

Supersymmetry breaking on the lattice: the $\mathcal{N} = 1$ Wess-Zumino model

David Baumgartner, Kyle Steinhauer and Urs Wenger, Proceedings of Science (Lattice 2011) 253.

PROCEEDINGS OF SCIENCE

Supersymmetry breaking on the lattice: the $\mathcal{N} = 1$ Wess-Zumino model

David Baumgartner, Kyle Steinhauer and Urs Wenger*
Albert Einstein Center for Fundamental Physics
Institute for Theoretical Physics
University of Bern
Sidlerstrasse 5
CH–3012 Bern
Switzerland
E-mail: baumgart@itp.unibe.ch, steinhauer@itp.unibe.ch, wenger@itp.unibe.ch

We discuss spontaneous supersymmetry breaking in the $\mathcal{N} = 1$ Wess-Zumino model in two dimensions on the lattice using Wilson fermions and the fermion loop formulation. In that formulation the fermion sign problem related to the vanishing of the Witten index can be circumvented and the model can be simulated very efficiently using the recently introduced open fermion string algorithm. We present first results for the supersymmetry breaking phase transition and sketch the preliminary determination of a renormalised critical coupling in the continuum limit.

The XXIX International Symposium on Lattice Field Theory - Lattice 2011
July 10-16, 2011
Squaw Valley, Lake Tahoe, California

*Speaker.

PoS(Lattice 2011)253

1. Introduction

Supersymmetry as an extension of the space-time symmetries is an interesting concept which might well be realised in nature in one form or another. Its presence has several intriguing consequences, for example, one expects a vanishing ground state energy, if supersymmetry is exact. Moreover, the particle spectrum contains mass degenerate bosons and fermions which are related by the supersymmetry. However, so far there has not been any experimental sign of such a boson-fermion degeneracy. So, if supersymmetry is indeed realised at some high energy scale, it must be broken at the low energy scales accessible in today's experiments. The scenario of (spontaneously) broken supersymmetry then implies that there is no supersymmetric ground state, the ground state energy is not vanishing, and the particle masses need not be degenerate. In this context, it is interesting to ask how the spontaneous breaking of the supersymmetry is realised. Since spontaneous symmetry breaking is an inherently non-perturbative problem one needs non-perturbative methods in order to approach it meaningfully. One such method is provided by simulating supersymmetric theories on a space-time lattice. However, since the space-time symmetries are explicitly broken by the lattice regularisation and are restored only in the continuum limit, also the supersymmetry is in general not (or not fully) realised on the lattice. As a consequence, there is a subtle and delicate interplay between the various symmetries, and their realisation in the continuum needs to be carefully studied. Here we present preliminary results of such a study for the $\mathcal{N}=1$ Wess-Zumino model in two dimensions. Using the Wilson fermion discretisation one can formulate the model in terms of fermion loops which can be simulated very efficiently using the open fermion string algorithm [1]. In addition, the fermion loop formulation provides a way to circumvent the sign problem related to the vanishing of the Witten index [2].

2. The $\mathcal{N}=1$ Wess-Zumino model

The $\mathcal{N}=1$ Wess-Zumino model in two dimensions is one of the simplest models which may exhibit spontaneous supersymmetry breaking. Its degrees of freedom consist of one real Majorana fermion field ψ and one real bosonic field ϕ, while its dynamics is described by the Lagrangian density

$$\mathscr{L} = \frac{1}{2}\left(\partial_\mu \phi\right)^2 + \frac{1}{2}P'(\phi)^2 + \frac{1}{2}\overline{\psi}\left(\partial\!\!\!/ + P''(\phi)\right)\psi\,. \tag{2.1}$$

Here, $P(\phi)$ denotes a generic superpotential, and P', P'' its first and second derivative with respect to ϕ. In the following we will concentrate on the specific form

$$P(\phi) = \frac{m^2}{4g}\,\phi + \frac{1}{3}g\phi^3 \tag{2.2}$$

which leads to a vanishing Witten index $W=0$ and hence allows for spontaneous supersymmetry breaking [3]. The corresponding action enjoys the following two symmetries. First, there is a single supersymmetry given by the transformations

$$\delta\phi = \overline{\varepsilon}\psi\,, \quad \delta\psi = (\partial\!\!\!/\phi - P')\varepsilon\,, \quad \delta\overline{\psi} = 0\,, \tag{2.3}$$

and second, there is a discrete $\mathbb{Z}(2)$ chiral symmetry given by

$$\phi \to -\phi\,, \quad \psi \to \gamma_5\psi\,, \quad \overline{\psi} \to -\overline{\psi}\gamma_5\,, \tag{2.4}$$

where $\gamma_5 \equiv \sigma_3$ can be chosen to be the third Pauli matrix.

For the chosen superpotential the Witten index turns out to be zero, as can be seen as follows. Integrating out the Majorana fermions yields the (indefinite) Pfaffian PfM of the Majorana Dirac operator M. The corresponding partition function with periodic boundary conditions (b.c.) in all directions is equivalent to the Witten index,

$$\int \mathscr{D}\phi \, e^{-S_\mathrm{b}(\phi)} \, \mathrm{Pf} M_\mathrm{pp}(\phi) \propto W \,,$$

where $S_\mathrm{b}(\phi)$ is the action for the bosonic field. Now, under the $\mathbb{Z}(2)$ symmetry $\phi \to -\phi$ one has

$$S_\mathrm{b} \to S_\mathrm{b}, \quad \mathrm{Pf} M_\mathrm{pp} \to -\mathrm{Pf} M_\mathrm{pp} \,,$$

so for every bosonic field configuration ϕ contributing to the partition function, there exists another one with exactly the same contribution but opposite sign, hence yielding $W = 0$. This constitutes a necessary (but not sufficient) condition for the supersymmetry to be broken spontaneously. In that case, one expects a bosonic and fermionic ground state related to each other by the supersymmetry transformation. On the other hand, if one chooses thermal b.c. (antiperiodic b.c. for the fermions in time direction) the supersymmetry is broken by the finite temperature of the system and one finds

$$S_\mathrm{b} \to S_\mathrm{b}, \quad \mathrm{Pf} M_\mathrm{pa} \to +\mathrm{Pf} M_\mathrm{pa} \,.$$

In order to further understand the supersymmetry breaking pattern, i.e. the relation between the supersymmetry breaking and the $\mathbb{Z}(2)$ symmetry breaking, it is useful to consider the potential for the bosonic field, $\frac{1}{2}P'(\phi)^2 = \frac{1}{2}\frac{m^2}{2}\phi^2 + \frac{1}{2}g^2\phi^4 + \mathrm{const}$. It simply represents a standard ϕ^4-theory in which, depending on the choice of the bare parameters m and g, the $\mathbb{Z}(2)$ symmetry may be broken. Indeed, for large values of m/g the $\mathbb{Z}(2)$ symmetry is spontaneously broken (in infinite volume) and the boson field selects a definite ground state. Denoting with $\overline{\phi}$ the expectation value of the volume averaged boson field, one finds

$$\begin{aligned} \overline{\phi} = +m/2g \quad &\Rightarrow \quad \mathrm{Pf} M_\mathrm{pp} = +\mathrm{Pf} M_\mathrm{pa} \,, \\ \overline{\phi} = -m/2g \quad &\Rightarrow \quad \mathrm{Pf} M_\mathrm{pp} = -\mathrm{Pf} M_\mathrm{pa} \,, \end{aligned}$$

i.e. in the former case the unique ground state is bosonic, while in the latter it is fermionic. In both cases, there is a single, unique ground state tantamount to having unbroken supersymmetry. By contrast, for small values of m/g the $\mathbb{Z}(2)$ symmetry is unbroken, i.e. one has $\overline{\phi} = 0$ which allows both a bosonic and fermionic ground state, tantamount to having broken supersymmetry. Indeed, the tunneling between the two equivalent ground states corresponds to the massless Goldstino mode which comes along with any spontaneous supersymmetry breaking.

2.1 Lattice discretisation and fermion loop formulation

In order to put the Wess-Zumino model on the lattice we follow the approach of Golterman and Petcher [4] where it is shown that using the same lattice derivative for the bosons as for the fermions (and renormalising the mass parameter m accordingly), the supersymmetry is guaranteed to be restored in the continuum limit.

Using the Wilson lattice discretisation for the fermion fields yields the fermion Lagrangian density

$$\mathscr{L} = \frac{1}{2}\xi^T \mathscr{C}(\gamma_\mu \tilde{\partial}_\mu - \frac{1}{2}\partial^*\partial + P''(\phi))\xi\,,$$

where ξ is a real, 2-component Grassmann field, $\mathscr{C} = -\mathscr{C}^T$ is the charge conjugation matrix and ∂^*, ∂ are the backward and forward lattice derivatives, respectively. However, while the Wilson term $\partial^*\partial$ avoids fermion doubling, it spoils the discrete chiral symmetry of the fermion action as well as the $\mathbb{Z}(2)$ symmetry $\phi \to -\phi$ of the boson action[1].

Another problem for simulating the model on the lattice is the fact that the Pfaffian is indefinite. As discussed above, this is due to the vanishing of the Witten index and constitutes a generic problem for any numerical Monte Carlo investigation of spontaneous supersymmetry breaking, independent of the chosen discretisation. The problem stems from the fact that the indefinite Paffian can not be simulated directly by standard Monte Carlo methods. Instead one uses the effective action

$$S_{\text{eff}}(\phi) = S_{\text{b}}(\phi) - \ln|\text{Pf}M(\phi)|$$

for the boson field ϕ and takes the sign of the Pfaffian into account by reweighting. This approach in general leads to severe sign problems [5, 6].

It turns out that the sign problem can be circumvented for Wilson fermions by using an exact reformulation of the lattice model in terms of fermion loops [2] and simulating fluctuating fermionic boundary conditions [1]. In the loop formulation one expands the Boltzmann factor of the fermion action, effectively constructing a hopping expansion. When one subsequently performs the integration over the fermion fields, the nil-potency of the Grassmann elements ensures that only closed, non-oriented and non-intersecting fermion loops survive. The partition function then becomes a sum over all self-avoiding fermion loop configurations ℓ,

$$Z_{\mathscr{L}} = \sum_{\{\ell\}\in\mathscr{L}} \omega[\ell,\phi], \quad \mathscr{L} \in \mathscr{L}_{00}\cup\mathscr{L}_{10}\cup\mathscr{L}_{01}\cup\mathscr{L}_{11}$$

where $\omega[\ell,\phi]$ denotes the weight for a given loop configuration ℓ, and $\mathscr{L}_{ij}$ denotes the equivalence class of loop configurations with an even or odd number of loops winding around the lattice in the spatial and temporal direction, respectively. $Z_{\mathscr{L}}$ represents a system with unspecified fermionic b.c. [7], while the system with periodic b.c. for the fermion, i.e. the Witten index, can be constructed by forming

$$W \equiv Z_{\text{pp}} = Z_{\mathscr{L}_{00}} - Z_{\mathscr{L}_{10}} - Z_{\mathscr{L}_{01}} - Z_{\mathscr{L}_{11}}\,,$$

or the system at finite temperature by forming

$$Z_{\text{pa}} = Z_{\mathscr{L}_{00}} - Z_{\mathscr{L}_{10}} + Z_{\mathscr{L}_{01}} + Z_{\mathscr{L}_{11}}\,.$$

Note that the weight ω does not necessarily need to be positive definite in each of the sectors, but in practice it turns out that it is the case as long as one stays close enough to the continuum limit.

As described in [1] the system can most efficiently be simulated by introducing an open fermion string corresponding to the insertion of a Majorana fermion pair. By letting the ends

[1] In principle this complication can be avoided by using a lattice discretisation which respects the discrete $\mathbb{Z}(2)$ chiral symmetry, e.g. the SLAC derivative [5].

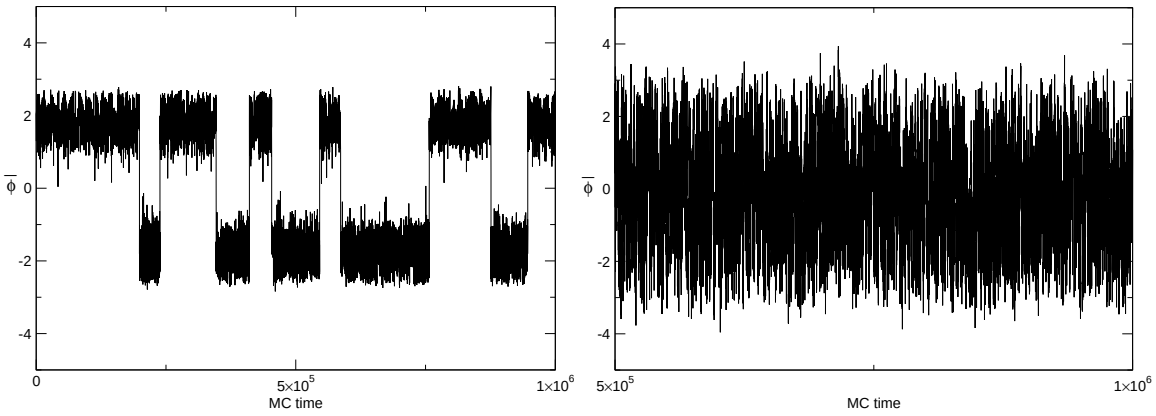

Figure 1: Monte Carlo time history of $\overline{\phi}$ at $m/g = 4$, $ag = 0.125$ (left plot) and $m/g = 0.16$, $ag = 0.03125$ (right plot).

of the string move around the lattice by a standard Metropolis update procedure, one samples the fermion 2-point function as well as the relative weights between $Z_{\mathscr{L}_{00}}, Z_{\mathscr{L}_{10}}, Z_{\mathscr{L}_{01}}$ and $Z_{\mathscr{L}_{11}}$. Finally, the bosonic fields are simulated by standard Monte Carlo methods.

3. Results

By looking at the behaviour of $\overline{\phi}$ for large and small values of m/g one can check for the $\mathbb{Z}(2)$ symmetry breaking[2]. The plots in Fig. 1 show the Monte Carlo time history of $\overline{\phi}$ at $m/g = 4$, $ag = 0.125$ (left plot) and $m/g = 0.16$, $ag = 0.03125$ (right plot). For $m/g = 4$ the system is in the $\mathbb{Z}(2)$ broken phase with $\langle|\overline{\phi}|\rangle \simeq 2$. Since the system is at finite volume it still tunnels between the two vacua with $\langle|\overline{\phi}|\rangle \simeq \pm m/2g$, but the tunnelling will be suppressed in the limit $L \to \infty$ or $m/g \to \infty$. For $m/g = 0.16$ on the other hand, the system is in the $\mathbb{Z}(2)$ symmetric phase with $\langle\overline{\phi}\rangle \simeq 0$.

It is now interesting to see how the partition functions $Z_{\mathscr{L}_{00}}, Z_{\mathscr{L}_{10}}, Z_{\mathscr{L}_{01}}, Z_{\mathscr{L}_{11}}$, or Z_{pp} and Z_{pa}, behave in the two situations. Fig. 2 shows the probability distributions of the various sectors as a function of $\overline{\phi}$, again for $m/g = 4$, $ag = 0.125$ (left plot) and $m/g = 0.16$, $ag = 0.03125$ (right plot). In the first situation where the $\mathbb{Z}(2)$ symmetry is broken, one finds

$$\begin{aligned} \langle\overline{\phi}\rangle \simeq -2: \quad & Z_{00} \simeq Z_{10} \simeq Z_{01} \simeq Z_{11} && \Rightarrow \quad Z_{\mathrm{pp}} \simeq -Z_{\mathrm{pa}}\,, \\ \langle\overline{\phi}\rangle \simeq +2: \quad & Z_{00} \simeq 1,\ Z_{10} \simeq Z_{01} \simeq Z_{11} \simeq 0 && \Rightarrow \quad Z_{\mathrm{pp}} \simeq +Z_{\mathrm{pa}}\,, \end{aligned}$$

so $\langle\overline{\phi}\rangle \simeq -2$ corresponds to the fermionic ground state while $\langle\overline{\phi}\rangle \simeq +2$ corresponds to the bosonic one. In either case, a unique ground state is chosen by the system (up to finite volume tunneling) and hence supersymmetry is unbroken (at least in the thermodynamic and continuum limit).

In the second situation, where the $\mathbb{Z}(2)$-symmetry is unbroken, one finds

$$\langle\overline{\phi}\rangle \simeq 0: \quad Z_{00} \simeq Z_{10} + Z_{01} + Z_{11} \quad \Rightarrow \quad Z_{\mathrm{pp}} \simeq 0\,,$$

so the bosonic and fermionic ground states occur with equal probability (thereby cancelling their contribution in $Z_{\mathrm{pp}} = W$) and hence supersymmetry is spontaneously broken.

As a next step one can now determine the value of m/g at which the transition from the

[2]Note that $\overline{\phi}$ is not a true order parameter for the $\mathbb{Z}(2)$ symmetry since the symmetry is explicitly broken by the lattice discretisation.

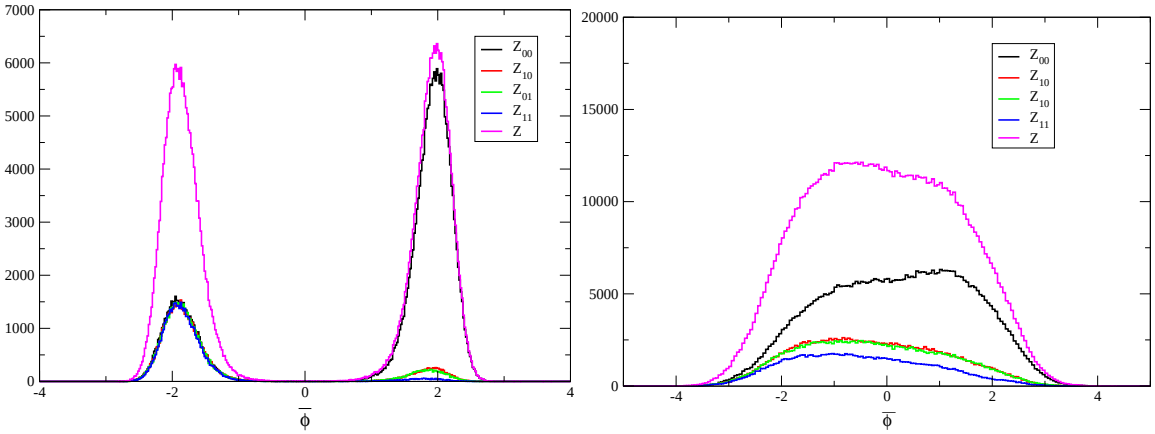

Figure 2: Probability distribution of the partition functions $Z_{\mathscr{L}_{00}}, Z_{\mathscr{L}_{10}}, Z_{\mathscr{L}_{01}}, Z_{\mathscr{L}_{11}}$ and $Z_{\mathscr{L}}$ for $m/g = 4$, $ag = 0.125$ (left plot) and $m/g = 0.16$, $ag = 0.03125$ (right plot) as a function of $\overline{\phi}$.

$\mathbb{Z}(2)$ symmetric and supersymmetry broken phase to the $\mathbb{Z}(2)$ broken and supersymmetric phase occurs. This is most easily done by scanning am at fixed lattice spacing ag for various lattice extents L. The critical value am_c where the phase transition occurs determines the dimensionless critical coupling m_c/g at the given lattice spacing. The procedure is illustrated in Fig. 3 where the left plot shows the ratio $Z_{\rm pp}/Z$ serving as a (pseudo-)order parameter for the supersymmetry breaking phase transition, while the right plot shows $\langle s_\phi \rangle_{\rm pa} = \langle {\rm sign}\overline{\phi} \rangle_{\rm pa}$ as a (pseudo-)order parameter for the $\mathbb{Z}(2)$ symmetry breaking[3], as a function of the bare mass at fixed lattice spacing $ag = 0.03125$ for various lattice extents. We note that the behaviour of s_ϕ seems to suggest a second order phase transition. Setting up the model with the Wilson derivative for bosons and fermions yields a supersymmetric continuum limit [4]. Since the model is superrenomalisable it is

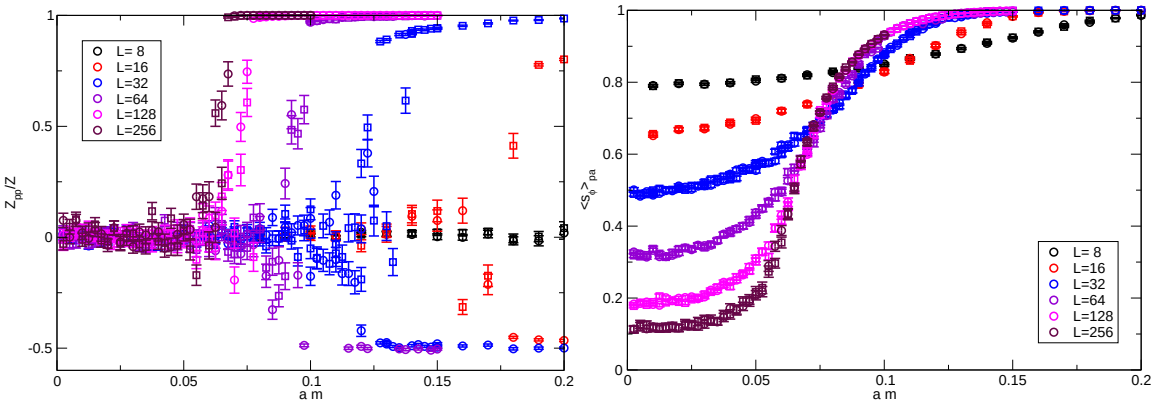

Figure 3: Ratio $Z_{\rm pp}/Z$ (left plot) and $\langle s_\phi \rangle = \langle {\rm sign}\overline{\phi} \rangle$ serving as a (pseudo-)order parameter for the supersymmetry breaking phase transition and the $\mathbb{Z}(2)$-symmetry breaking phase transition, respectively, as a function of am at fixed lattice spacing $ag = 0.03125$ for various lattice extents.

[3]Note that since $Z_{\rm pp} \simeq 0$ in the supersymmetry broken phase, expectation values need to be calculated in the thermal ensemble in order to be under good numerical control.

sufficient to tune only the mass parameter m in order to obtain a renormalised theory. Using the relation $m^2 = m_R^2 + 2g^2/\pi \ln m_R^2$ between the bare mass m and the renormalised one m_R, and setting the scale, i.e. the lattice spacing a, by the dimensionful coupling $g = \hat{g}/a$, one can determine the continuum limit of a dimensionless critical coupling for the supersymmetry breaking transition with

$$f_{\rm crit} = \lim_{\hat{g}\to 0} \frac{g}{m_R}\bigg|_{\rm crit} .$$

The procedure is illustrated in Fig. 4 and it will be interesting to see how this result compares to previous determinations [5, 8].

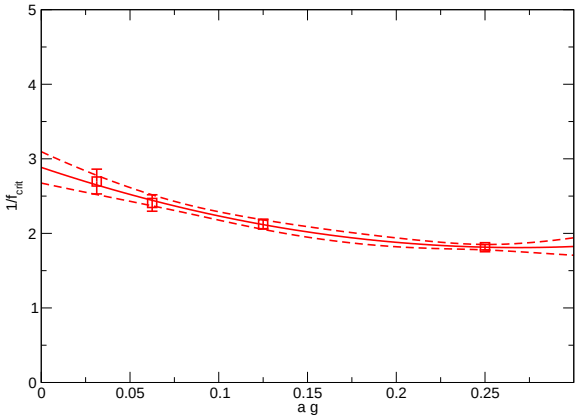

Figure 4: Continuum limit of the renormalised dimensionless critical coupling $f_{\rm crit}$ for the supersymmetry and $\mathbb{Z}(2)$-symmetry breaking phase transition.

4. Outlook

There are a several obvious ways to proceed from this first, preliminary investigation. Firstly, one can use Ward identities as (pseudo-)order parameters to determine the phase transition point. Secondly, one can determine the boson and fermion mass spectra. The latter is particularly simple in the fermion loop formulation. Finally, it would also be interesting to implement the loop formulation of the model with a domain wall or overlap type fermion discretisation for which the discrete $\mathbb{Z}(2)$ chiral symmetry remains exact at finite lattice spacing.

References

[1] U. Wenger, *Efficient simulation of relativistic fermions via vertex models*, *Phys. Rev.* **D80** (2009) 071503, [arXiv:0812.3565].

[2] D. Baumgartner and U. Wenger, *Simulation of supersymmetric models on the lattice without a sign problem*, arXiv:1104.0213.

[3] E. Witten, *Constraints on Supersymmetry Breaking*, *Nucl. Phys.* **B202** (1982) 253.

[4] M. F. L. Golterman and D. N. Petcher, *A local interactive lattice model with supersymmetry*, *Nucl. Phys.* **B319** (1989) 307–341.

[5] C. Wozar and A. Wipf, *Supersymmetry Breaking in Low Dimensional Models*, arXiv:1107.3324.

[6] S. Catterall and S. Karamov, *A lattice study of the two-dimensional Wess Zumino model*, *Phys. Rev.* **D68** (2003) 014503, [hep-lat/0305002].

[7] U. Wolff, *Cluster simulation of relativistic fermions in two space- time dimensions*, *Nucl. Phys.* **B789** (2008) 258–276, [arXiv:0707.2872].

[8] M. Beccaria, G. F. De Angelis, M. Campostrini, and A. Feo, *Phase diagram of the lattice Wess-Zumino model from rigorous lower bounds on the energy*, *Phys. Rev.* **D70** (2004) 035011, [hep-lat/0405016].

Paper 11

Spontaneous supersymmetry breaking in the $2d$ $\mathcal{N} = 1$ Wess-Zumino model

David Baumgartner, Kyle Steinhauer and Urs Wenger, Proceedings of Science (Lattice 2012) 043.

PROCEEDINGS OF SCIENCE

Spontaneous supersymmetry breaking in the $2d$ $\mathcal{N} = 1$ Wess-Zumino model

David Baumgartner, Kyle Steinhauer and Urs Wenger*
Albert Einstein Center for Fundamental Physics
Institute for Theoretical Physics
University of Bern
Sidlerstrasse 5
CH–3012 Bern
Switzerland
E-mail: baumgart@itp.unibe.ch, steinhauer@itp.unibe.ch, wenger@itp.unibe.ch

We study the phase diagram of the two-dimensional $\mathcal{N} = 1$ Wess-Zumino model using Wilson fermions and the fermion loop formulation. We give a complete non-perturbative determination of the ground state structure in the continuum and infinite volume limit. We also present a determination of the particle spectrum in the supersymmetric phase, in the supersymmetry broken phase and across the supersymmetry breaking phase transition. In the supersymmetry broken phase we observe the emergence of the Goldstino particle.

The XXX International Symposium on Lattice Field Theory - Lattice 2012
June 24-29, 2012
Cairns, Australia

*Speaker.

 http://pos.sissa.it/

PoS(Lattice 2012)043

1. Motivation and overview

Despite the fact that the latest results from the Large Hadron Collider make it more and more unlikely that supersymmetry, at least in its variety as a minimal extension to the Standard Model, is accommodated in nature, supersymmetric quantum field theories remain to be interesting in their own right. In particular, spontaneous supersymmetry breaking and the corresponding phase transition is an interesting non-perturbative phenonemon which often evades a quantitative description even in simple models such as the $\mathscr{N}=1$ Wess-Zumino model in two dimension on which we focus in these proceedings. Often, a specific model may or may not undergo a supersymmetry breaking phase transition and it is usually not clear how such a transition is realised in detail. While the lattice regularisation provides a convenient setup to perform detailed non-perturbative numerical investigations, for systems which exhibit spontaneous supersymmetry breaking straightforward Monte Carlo simulations are not possible due to a fermion sign problem related to the vanishing of the Witten index [1]. However, it has been shown that the sign problem can be circumvented by using the fermion loop formulation [1, 2, 3] and simulating the system with the open fermion string algorithm [4, 5].

In these proceedings, we present a quantitative non-perturbative investigation of the $2d$ $\mathscr{N}=1$ Wess-Zumino model as follows. First we give a brief definition of the model and then discuss its formulation in terms of fermion loops. After reviewing its vacuum structure and the symmetry breaking pattern we go on to describe quantitatively its mass spectrum in the supersymmetric and the supersymmetry broken phase as well as across the phase transition.

2. The $\mathscr{N}=1$ Wess-Zumino model on the lattice

The $\mathscr{N}=1$ Wess-Zumino model in two dimensions [6] is one of the simplest models which may exhibit spontaneous supersymmetry breaking. Its degrees of freedom consist of one real Majorana fermion field ψ and one real bosonic field ϕ, while its dynamics is described by the Lagrangian density

$$\mathscr{L} = \frac{1}{2}\left(\partial_\mu \phi\right)^2 + \frac{1}{2}P'(\phi)^2 + \frac{1}{2}\overline{\psi}\left(\partial\!\!\!/ + P''(\phi)\right)\psi\,. \tag{2.1}$$

Here, $P(\phi)$ denotes a generic superpotential, and P', P'' its first and second derivative with respect to ϕ. In the following we will concentrate on the specific form

$$P(\phi) = \frac{m^2}{4g}\,\phi + \frac{1}{3}g\phi^3 \tag{2.2}$$

which leads to a vanishing Witten index $W=0$ and hence allows for spontaneous supersymmetry breaking [7]. The corresponding action enjoys the following two symmetries. First, there is a single supersymmetry given by the transformations

$$\delta\phi = \overline{\varepsilon}\psi\,, \quad \delta\psi = (\partial\!\!\!/\phi - P')\varepsilon\,, \quad \delta\overline{\psi} = 0\,, \tag{2.3}$$

and secondly, there is a discrete $\mathbb{Z}(2)$ chiral symmetry given by

$$\phi \to -\phi\,, \quad \psi \to \gamma_5\psi\,, \quad \overline{\psi} \to -\overline{\psi}\gamma_5\,, \tag{2.4}$$

where $\gamma_5 \equiv \sigma_3$ can be chosen to be the third Pauli matrix. The fact that the Witten index is zero for the chosen superpotential can be derived from the transformation properties of the Pfaffian of the Dirac operator under the $\mathbb{Z}(2)$ symmetry $\phi \to -\phi$ [3].

Let us now move on to describe the regularisation of the model on the lattice. For the fermionic fields we use the Wilson lattice discretisation yielding the fermion Lagrangian density

$$\mathscr{L} = \frac{1}{2}\xi^T \mathscr{C}(\gamma_\mu \tilde{\partial}_\mu - \frac{1}{2}\partial^* \partial + P''(\phi))\xi \,,$$

where ξ is a real, 2-component Grassmann field, $\mathscr{C} = -\mathscr{C}^T$ is the charge conjugation matrix and ∂^*, ∂ are the backward and forward lattice derivatives, respectively. In order to guarantee the full supersymmetry in the continuum limit, one needs to introduce the same derivative, in particular the Wilson term, also for the bosonic fields [8]. As a consequence, in addition to the supersymmetry also the $\mathbb{Z}(2)$ chiral symmetry is broken by the lattice regularisation both in the bosonic and the fermionic sector.

Nevertheless we can now use the exact reformulation of the fermionic degrees of freedom in term of closed fermion loops (cf. [1] for further details). Together with the fermion string algorithm [4, 5] this allows simulations with unspecified fermionic boundary conditions which do not suffer from the fermion sign problem [3] and for which critical slowing down is essentially absent even in the presence of a massless fermionic mode such as the Goldstino.

3. Supersymmetry breaking pattern

It is useful to briefly review the (super-)symmetry breaking pattern. The potential for the bosonic field is a standard ϕ^2-theory which may trigger a $\mathbb{Z}(2)$ symmetry breaking phase transition. In particular, for large m/g one expects that the $\mathbb{Z}(2)$ symmetry is broken. In that case, the vacuum expectation value of the boson field $\langle\overline{\phi}\rangle = \pm m/2g$ is expected to select a definite ground state for the system, either bosonic or fermionic. On the other hand, for small m/g one expects the $\mathbb{Z}(2)$ symmetry to be restored with $\langle\overline{\phi}\rangle = 0$ in which case no unique ground state is selected and hence supersymmetry is broken. In fact, the associated tunneling between the two allowed bosonic and fermionic vacua corresponds to the infamous massless Goldstino mode.

In [3] it was indeed demonstrated, using the Witten index

$$W \equiv Z_{\text{pp}} = Z_{\mathscr{L}_{00}} - Z_{\mathscr{L}_{10}} - Z_{\mathscr{L}_{01}} - Z_{\mathscr{L}_{11}} \,,$$

as an order parameter, that a supersymmetry breaking phase transition occurs for specific couplings $\hat{g}/\hat{m}$ depending on the lattice spacing set by ag. Here, Z_{pp} denotes the partition function with periodic boundary conditions in both directions while $Z_{\mathscr{L}_{ij}}$ denote partition functions with fixed topological boundary conditions [2]. The expected symmetry breaking pattern and the corresponding vacuum structure follow exactly the expectations described above. In particular, for large m/g one is in a $\mathbb{Z}(2)$ broken phase where supersymmetry is unbroken, while for small m/g the $\mathbb{Z}(2)$ symmetry is restored and the supersymmetry is broken. Note that this situation only holds in the infinite volume limit: at any finite volume the $\mathbb{Z}(2)$ symmetry is always restored (and hence the supersymmetry broken) by soliton solutions which mediate transitions between boson field configurations with $\langle\overline{\phi}\rangle = \pm m/2g$ [9]. We have now further confirmed this scenario using the Ward identity $\langle P'\rangle$.

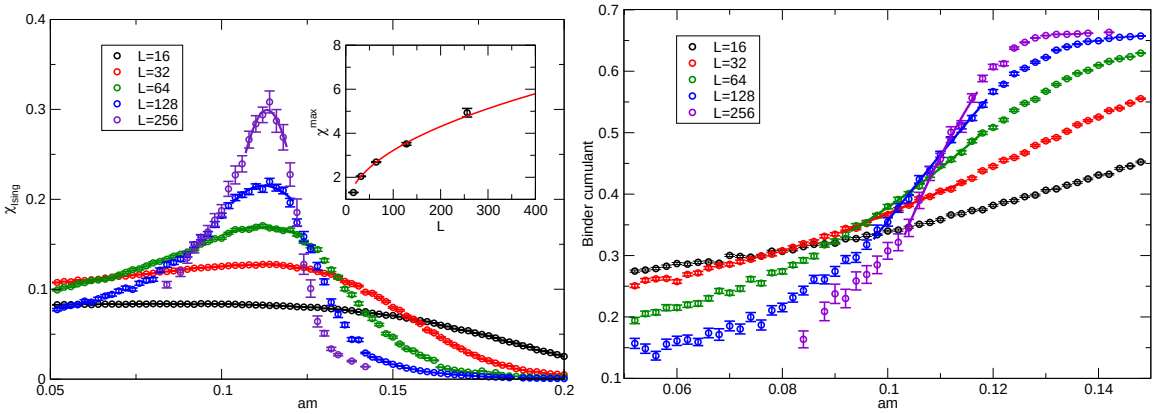

Figure 1: Susceptibility of the volume averaged Ising projected boson field (left plot) and the Binder cumulant of the boson field (right plot) for several volumes at $ag = 0.0625$.

3.1 $\mathbb{Z}(2)$ phase transition

In order to further quantify the phase transition we investigated in detail several order parameters sensitive to the $\mathbb{Z}(2)$ phase transition. It should be noted that there exists no real order parameter for the $\mathbb{Z}(2)$ transition, since the Wilson lattice discretisation breaks not just the supersymmetry, but also the $\mathbb{Z}(2)$ chiral symmetry in the bosonic sector. However, it turns out that at the lattice spacings $ag \leq 0.25$ which we simulated, the system behaves sufficiently continuum-like, so that accurate determinations of the phase transition are possible without problems. This is exemplified in figure 1. In the left plot we show the susceptibility χ_{Ising} of the volume averaged Ising projected boson field $\overline{\phi}_{\mathrm{Ising}} = 1/V \sum_x \mathrm{sign}[\phi_x]$. The susceptibility shows a nice finite volume scaling and the scaling of the susceptibility peak indicates a second order phase transition, presumably in the universality class of the $2d$ Ising model. The right plot of figure 1 shows the Binder cumulant of the boson field for various volumes, all at fixed lattice spacing $ag = 0.0625$. From the position of the susceptibility peak and the crossing of the Binder cumulant one can infer the critical bare mass am_c at which the phase transition occurs.

In general, different order parameters consistently indicate a phase transition only in the thermodynamic limit when the finite volume pseudo-phase transition becomes a true one. In the left plot of figure 2 we show the critical bare mass am_c as a function of the inverse volume expressed in units of g, as obtained from the two (pseudo-)order parameters discussed above. We find that the determination from the Binder cumulant shows rather large finite size effects, in contrast to the one from the susceptibility. However, in the thermodynamic limit they both agree and this is sustained for all lattice spacings (right plot). The inset finally shows the continuum extrapolation of the critical coupling $f_c = g/m_c$ using the bare mass am_c and the one renormalised using 1-loop continuum perturbation theory, am_c^{R}. The renormalised critical coupling in the continuum can now be compared to the one obtained in [10] using a different discretisation and algorithm.

4. Mass spectrum

We determine the mass spectrum from the temporal behaviour of correlators projected to zero spatial momentum, $C(t) \sim \langle \mathscr{O}(0)\mathscr{O}^{(T)}(t)\rangle$. For the boson masses we use the $\mathbb{Z}(2)$-odd and -even

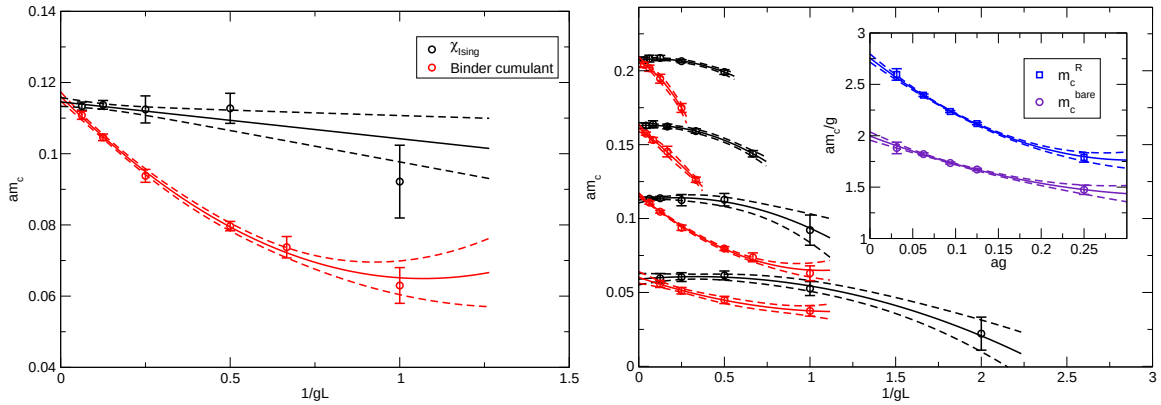

Figure 2: Thermodynamic limit of the critical mass am_c from the Binder cumulant and the peak of the susceptibility at $ag = 0.0625$ (left plot) and for a range of other couplings $ag = 0.25 - 0.03125$ (right plot). The inset shows the continuum limit of the bare and the renormalised critical coupling $f_c = g/m_c^{\text{bare,R}}$.

operators $\mathcal{O} = \phi$ and ϕ^2, respectively, while for the fermion masses we use $\mathcal{O} = \xi$ and $\xi\phi$. We note that in the supersymmetric/$\mathbb{Z}(2)$-broken phase the vacuum can not distinguish between the even and odd states and hence we extract the same mass using the two operators, while in the supersymmetry (SUSY) broken/$\mathbb{Z}(2)$ restored phase, the vacuum respects the $\mathbb{Z}(2)$ symmetry and distinguishes between states with different $\mathbb{Z}(2)$ quantum numbers. Furthermore, in the SUSY broken phase we can measure excitations both in the bosonic vacuum, i.e. in $Z_{\mathscr{L}_{00}}$, and in the fermionic one, i.e. $Z_{\mathscr{L}_{10}} + Z_{\mathscr{L}_{01}} + Z_{\mathscr{L}_{11}}$. We emphasise that simulations in the SUSY broken phase are only feasible due to the fact that the fermion loop algorithm essentially eliminates critical slowing down [4, 5], despite the emergence of the (would-be) Goldstino.

In figure 3 we show examples of boson mass extractions in the SUSY broken/$\mathbb{Z}(2)$-symmetric (left plot) and in the supersymmetric/$\mathbb{Z}(2)$ broken phase (right plot), both in the bosonic vacuum. The top panel shows the full correlator, the middle one the connected part and the lowest one the corresponding effective masses. In the SUSY broken phase we can fit double exponentials (plus a small shift due to the residual $\mathbb{Z}(2)$ breaking), while in the $\mathbb{Z}(2)$ broken phase only one exponential can be fitted, since the signal is quickly dominated by the fluctuations stemming from the large disconnected contribution.

In figure 4 we show examples of fermion mass extractions in both phases. In the left plot (SUSY broken phase) the top panel shows the correlator of the $\mathbb{Z}(2)$-even state which can be well fitted with a double exponential with the lowest mass corresponding to the Goldstino mass. The middle panel shows the $\mathbb{Z}(2)$-odd state fitted with a single exponential. The right plot shows the fermion correlator in the supersymmetric phase (top panel), on a log scale (middle panel) and the corresponding effective masses (bottom panel). It is remarkable that the signal of the fermion correlator can be followed over more than six orders of magnitude. Of course this just reflects the efficiency of the employed fermion loop algorithm [4].

Finally, in figure 5 we show the full boson and fermion mass spectrum in the left and right plot, respectively, as a function of the bare mass am across the supersymmetry breaking phase transition occurring at around $am_c \sim 0.042$. We see how the mass spectrum in the SUSY broken/$\mathbb{Z}(2)$-symmetric phase fans out into the $\mathbb{Z}(2)$-even and -odd states, with bosonic and fermionic masses non-degenerate, while in the supersymmetric/$\mathbb{Z}(2)$-broken phase the states collapse onto a degen-

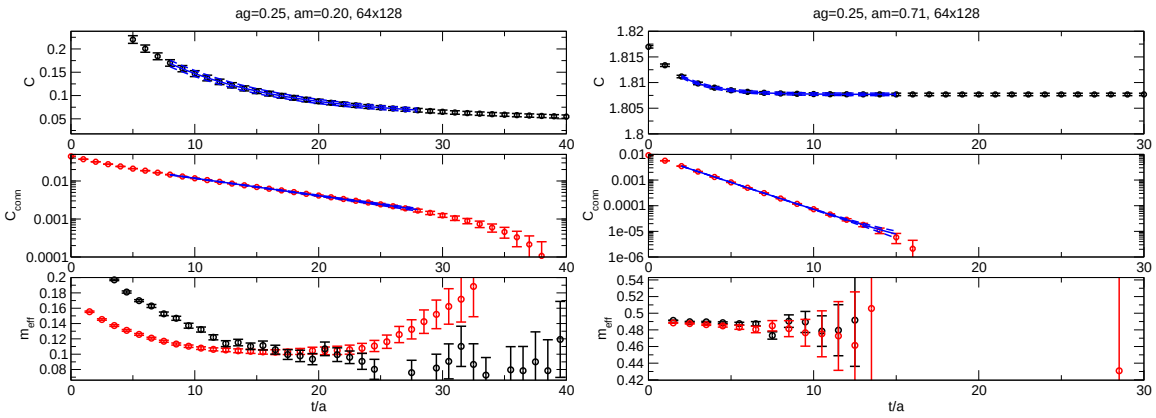

Figure 3: Boson mass extraction in the SUSY broken/$\mathbb{Z}(2)$-symmetric (left plot) and in the supersymmetric/$\mathbb{Z}(2)$ broken phase (right plot).

erate mass, in addition to the boson and fermion masses being equal. In the SUSY broken phase we can crosscheck the mass determination in the bosonic sector with the one in the fermionic sector and we find very convincing consistency. This agreement in the SUSY broken phase and the degeneracy of the boson and fermion masses in the supersymmetric phase is rather surprising, given the fact that the simulations are at finite and rather coarse lattice spacing $ag = 0.25$. Moreover, it should be kept in mind, that in the SUSY broken phase it is rather difficult to keep the systematic effects from mixing with higher excited states under control.

A first preliminary investigation of the effects of the finite volume on the spectrum reveals that they are essentially negligible for the volume $L/a = 64$ that we are using here. This is not quite the case for the boson mass spectrum in the SUSY broken phase. In fact, the investigation in [11] suggests a distinct finite volume scaling of the boson masses with the lowest boson mass vanishing towards the thermodynamic limit.

An interesting feature of the spectrum of a theory with spontaneously broken supersymmetry is of course the occurrence of the massless Goldstino. Since in our regularisation the supersymmetry is broken explicitely at any finite lattice spacing, the Goldstino is only approximately massless as

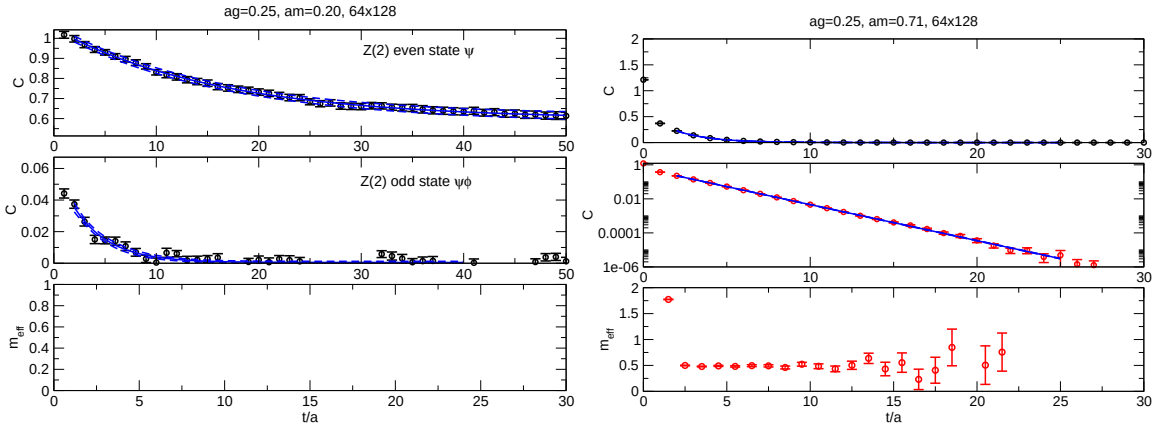

Figure 4: Fermion mass extraction in the SUSY broken/$\mathbb{Z}(2)$-symmetric (left plot) and in the supersymmetric/$\mathbb{Z}(2)$ broken phase (right plot).

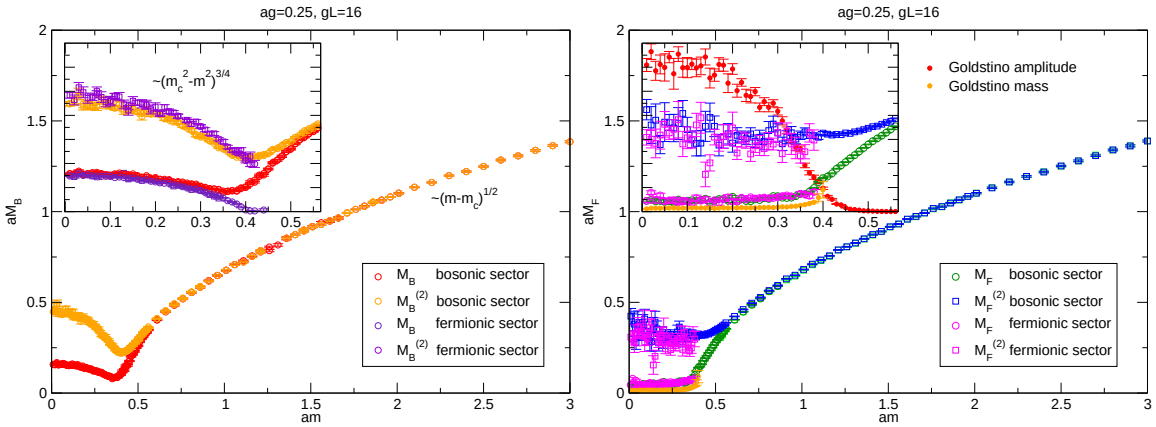

Figure 5: Mass spectrum for bosonic (left plot) and fermionic excitations (right plot). The superscript $^{(2)}$ denotes the excited state.

can be seen in figure 5. To corroborate the identification of this low mass state as the Goldstino, we plot in the inset of the right plot also the contribution (amplitude) of that state to the full fermion correlator. It turns out that the amplitude decreases as we increase the bare mass and vanishes at the transition to the supersymmetric phase, i.e. the Goldstino decouples from the system at the supersymmetry restoring phase transition.

References

[1] D. Baumgartner and U. Wenger, *Simulation of supersymmetric models on the lattice without a sign problem*, *PoS* **Lattice2010** (2010) 245, [arXiv:1104.0213].

[2] D. Baumgartner, K. Steinhauer, and U. Wenger, *Supersymmetry breaking on the lattice: the N=1 Wess-Zumino model*, *PoS* **LATTICE2011** (2011) 253, [arXiv:1111.6042].

[3] D. Baumgartner and U. Wenger, *Exact results for supersymmetric quantum mechanics on the lattice*, *PoS* **LATTICE2011** (2011) 239, [arXiv:1201.1485].

[4] U. Wenger, *Efficient simulation of relativistic fermions via vertex models*, *Phys. Rev.* **D80** (2009) 071503, [arXiv:0812.3565].

[5] U. Wenger, *Simulating Wilson fermions without critical slowing down*, *PoS* **LAT2009** (2009) 022, [arXiv:0911.4099].

[6] S. Ferrara, *Supersymmetric Gauge Theories in Two-Dimensions*, *Lett.Nuovo Cim.* **13** (1975) 629.

[7] E. Witten, *Constraints on Supersymmetry Breaking*, *Nucl. Phys.* **B202** (1982) 253.

[8] M. F. L. Golterman and D. N. Petcher, *A local interactive lattice model with supersymmetry*, *Nucl. Phys.* **B319** (1989) 307–341.

[9] S. Catterall and S. Karamov, *A lattice study of the two-dimensional Wess Zumino model*, *Phys. Rev.* **D68** (2003) 014503, [hep-lat/0305002].

[10] C. Wozar and A. Wipf, *Supersymmetry Breaking in Low Dimensional Models*, *Annals Phys.* **327** (2012) 774–807, [arXiv:1107.3324].

[11] F. Synatschke, H. Gies, and A. Wipf, *Phase Diagram and Fixed-Point Structure of two dimensional N=1 Wess-Zumino Models*, *Phys.Rev.* **D80** (2009) 085007, [arXiv:0907.4229].

Paper 12

Spontaneous supersymmetry breaking in the $2d$ $\mathcal{N} = 1$ Wess-Zumino model

Kyle Steinhauer and Urs Wenger, Physical Review Letters **113**, 231601 (2014).

Spontaneous Supersymmetry Breaking in the 2D $\mathcal{N} = 1$ Wess-Zumino Model

Kyle Steinhauer and Urs Wenger*
Albert Einstein Center for Fundamental Physics, University of Bern, Sidlerstrasse 5, 3012 Bern, Switzerland
(Received 21 August 2014; published 2 December 2014)

We study the phase diagram of the two-dimensional $\mathcal{N} = 1$ Wess-Zumino model on the lattice using Wilson fermions and the fermion loop formulation. We give a complete nonperturbative determination of the ground state structure in the continuum and infinite volume limit. We also present a determination of the particle spectrum in the supersymmetric phase, in the supersymmetry broken phase and across the supersymmetry breaking phase transition. In the supersymmetry broken phase, we observe the emergence of the Goldstino particle.

DOI: 10.1103/PhysRevLett.113.231601 PACS numbers: 11.30.Pb, 05.50.+q, 11.30.Qc, 12.60.Jv

Introduction.—Understanding the spontaneous breakdown of supersymmetry is a generic nonperturbative problem which is relevant not only for particle physics, but in fact, for many physical systems beyond quantum field theories. The $\mathcal{N} = 1$ Wess-Zumino model [1,2] in two dimensions is one of the simplest supersymmetric quantum field theories which allows for spontaneous supersymmetry breaking since it enjoys the necessary, but not sufficient, condition of a vanishing Witten index [3]. The model has been analyzed employing various approaches such as Monte Carlo methods [4,5], Hamiltonian techniques [6–8], or exact renormalization group methods [9]. Wilson derivatives for fermions and bosons, guaranteeing a supersymmetric continuum limit [10], were used in [11] and a numerical analysis of the phase diagram using the SLAC derivative has been conducted in [12]. All approaches use various regulators which are more or less difficult to control. In this Letter, we report on our results for the two-dimensional $\mathcal{N} = 1$ Wess-Zumino model regularized on a Euclidean spacetime lattice. The discretization using Wilson derivatives for the fermions and bosons [10] together with the fermion loop formulation and a novel algorithm [13] allows us to systematically remove all effects from the IR and UV regulators by explicitly taking the necessary limits in a completely controlled way. One reason why this has not been achieved so far with other methods is the fact that all supersymmetric systems with spontaneously broken supersymmetry suffer from a fermion sign problem related to the vanishing of the Witten index [14]. However, that sign problem can be circumvented in our approach by using the exact reformulation of the lattice model in terms of fermion loops [14]. In this formulation, the partition function is obtained as a sum over closed fermion loop configurations and separates naturally into its bosonic and fermionic parts for which the sign is perfectly under control. Efficient simulations with an open fermion string (or fermionic worm) algorithm [13] are then possible even in the phase with spontaneously broken supersymmetry where the massless Goldstino mode is present.

The two-dimensional $\mathcal{N} = 1$ Wess-Zumino model [1,2] contains a real two component Majorana spinor ψ and a real bosonic field ϕ and is described in Euclidean spacetime by the on-shell continuum action

$$S = \int d^2x \left\{ \frac{1}{2}(\partial_\mu \phi)^2 + \frac{1}{2}\bar{\psi} D \psi + \frac{[P'(\phi)]^2}{2} \right\}, \quad (1)$$

where $D = [\not{\partial} + P''(\phi)]$ is the Majorana Dirac operator. Here, $P(\phi)$ denotes a generic superpotential and P' and P'' its first and second derivative with respect to ϕ, respectively. The action is invariant under a supersymmetry transformation δ which transforms ϕ, ψ, and $\bar{\psi}$ as

$$\delta\phi = \bar{\epsilon}\psi, \qquad \delta\psi = (\not{\partial}\phi - P')\epsilon, \qquad \delta\bar{\psi} = 0, \quad (2)$$

where ϵ is a constant Majorana spinor. In the following, we will concentrate on the specific superpotential

$$P(\phi) = \frac{1}{3} g \phi^3 - \frac{m^2}{4g}\phi. \quad (3)$$

With this potential, the action is also invariant under a discrete $\mathbb{Z}_2$/chiral symmetry transformation

$$\phi \to -\phi, \qquad \psi \to \sigma_3 \psi, \qquad \bar{\psi} \to -\bar{\psi}\sigma_3, \quad (4)$$

which, in the following, we denote by $\mathbb{Z}_2^\chi$ symmetry. The potential yields a vanishing Witten index $W = 0$ and, hence, allows for spontaneous supersymmetry breaking [3]. This can be derived, for example, from the transformation properties of the Pfaffian $\mathrm{Pf}(D)$ under the $\mathbb{Z}_2$ symmetry $\phi \to -\phi$ [15].

Fermion loop formulation.—When the model is regularized on a discrete spacetime lattice, both the $\mathbb{Z}_2^\chi$ and the supersymmetry are broken explicitly, but the discretization can be chosen such that the restoration of the symmetries is guaranteed in the continuum limit [10]. This can be achieved because the model is super-renormalizable, and

only one counterterm is necessary to renormalize the bare mass m, while the coupling g is not renormalized and, hence, can be used to define the continuum limit $ag \to 0$ where a is the lattice spacing. The loop formulation is obtained by constructing an exact hopping expansion of the fermion action to all orders. When expanding the Boltzmann factor and subsequently performing the integration over the fermion fields, the nilpotency of the Grassmann elements ensures that only closed, nonoriented, and self-avoiding fermion loops survive. The partition function then becomes a sum over all fermion loop configurations $l \in \mathcal{L}$,

$$Z_{\mathcal{L}} = \sum_{l \in \mathcal{L}} \prod_{x} w_l(x), \tag{5}$$

where the weight for a given loop configuration is a product over site weights $w_l(x)$ which depend only on the local geometry of the loop at the lattice site x, if a fermion loop is present, or on an integral over an ultralocal function of the bosonic field ϕ. The configuration space of all loop configurations $\mathcal{L}$ naturally separates into equivalence classes $\mathcal{L}_{ij}$ characterized by the even or odd number of loops winding around the lattice in the spatial and temporal direction, respectively. The loop configurations in each equivalence class pick up a definite sign depending on the chosen boundary conditions (BC) for the Majorana fermion [16], so the partition function in Eq. (5) represents a system with unspecified (or fluctuating) BC, while the one with periodic BC,

$$W \propto Z_{pp} = Z_{\mathcal{L}_{00}} - Z_{\mathcal{L}_{10}} - Z_{\mathcal{L}_{01}} - Z_{\mathcal{L}_{11}}, \tag{6}$$

is proportional to the Witten index and the one with antiperiodic BC in time,

$$Z_{ap} = Z_{\mathcal{L}_{00}} + Z_{\mathcal{L}_{10}} - Z_{\mathcal{L}_{01}} + Z_{\mathcal{L}_{11}}, \tag{7}$$

describes the system at finite temperature. Note that the weight is not necessarily positive definite in each of the sectors, but sufficiently close to the continuum limit, it turns out to be so. As described in [13], the system can most efficiently be simulated, essentially without critical slowing down, by introducing an open fermion string corresponding to the insertion of a Majorana fermion pair. By letting the ends of the string move around the lattice by a standard Metropolis update procedure, one samples the fermion two-point function as well as the relative weights between $Z_{\mathcal{L}_{00}}$, $Z_{\mathcal{L}_{10}}$, $Z_{\mathcal{L}_{01}}$, and $Z_{\mathcal{L}_{11}}$ which allows precise determinations of Eqs. (6) and (7) *a posteriori*. Finally, the bosonic fields are integrated over by standard Monte Carlo methods using a Metropolis algorithm.

Vacuum structure.—The vacuum structure of the system depends on the two bare parameters m and g and, hence, is a function of the dimensionless ratio $f \equiv g/m$. The expected symmetry breaking pattern in the continuum [3] is characterized by a supersymmetric phase with spontaneously broken $\mathbb{Z}_2^\chi$ symmetry and a unique (bosonic or fermionic) vacuum (ground state) at small f, and a $\mathbb{Z}_2^\chi$ symmetric phase at large f with spontaneously broken supersymmetry accompanied by tunneling between the bosonic or fermionic vacua (ground states). The two phases are separated by a phase transition at $f_c = g/m_c$.

In Fig. 1, we show histograms of the partition functions $Z_{\mathcal{L}_{ij}}$ as a function of the vacuum expectation value $\langle\phi\rangle$ of the bosonic field in both phases. The top panel shows data for $f < f_c$ ($\mathbb{Z}_2^\chi$ broken and supersymmetric) where $\langle\phi\rangle = \pm m/(2g)$ corresponds to the two classical minima of the potential with $Z_{pp}/Z_{ap} = \pm 1$ in the continuum. From the plots, we infer that the ground state at $+m/2g$, where $Z \simeq Z_{\mathcal{L}_{00}}$ and $Z_{\mathcal{L}_{10}} \simeq Z_{\mathcal{L}_{01}} \simeq Z_{\mathcal{L}_{11}} \simeq 0$, and hence, $Z_{pp}/Z_{ap} \simeq +1$, corresponds to the bosonic vacuum while the ground state at $-m/2g$, where $Z_{\mathcal{L}_{00}} \simeq Z_{\mathcal{L}_{10}} \simeq Z_{\mathcal{L}_{01}} \simeq Z_{\mathcal{L}_{11}} \simeq Z/4$, and hence, $Z_{pp} \simeq -Z_{ap}$, corresponds to the fermionic one [17]. In the infinite volume limit, either the bosonic or fermionic ground state is selected, and consequently, supersymmetry is intact (but the $\mathbb{Z}_2^\chi$ symmetry is spontaneously broken). For increasing f, the tunneling between the ground states is enhanced and eventually triggers the restoration of the $\mathbb{Z}_2^\chi$ symmetry accompanied by the spontaneous breakdown of the supersymmetry at f_c. This is illustrated in the lower panel of Fig. 1 where the data for $f > f_c$ clearly display $\langle\phi\rangle \simeq 0$ and $Z_{pp}/Z_{ap} \simeq 0$, both of which become exactly zero in the continuum limit [17]. Note that the skewness of the distribution is due to the residual $\mathbb{Z}_2^\chi$ symmetry breaking at finite lattice spacing. Whether the spontaneous phase transition survives the continuum and infinite volume limit, i.e., whether f_c remains finite and nonzero, needs to be investigated by quantitatively determining f_c at various lattice spacings and volumes and carefully taking, first, the infinite volume limit followed by the continuum one.

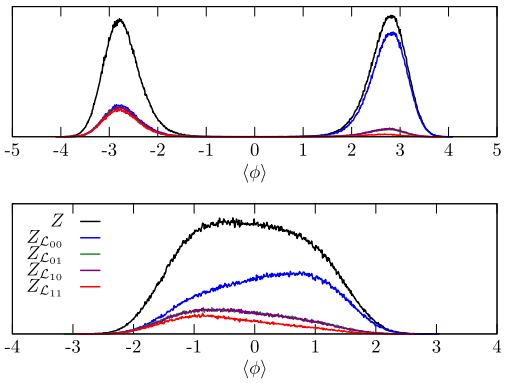

FIG. 1 (color online). Histograms of partition functions $Z_{\mathcal{L}_{ij}}$ on an 8×8 lattice at fixed lattice spacing $ag = 0.0625$ for two different couplings $f < f_c$ (top) and $f > f_c$ (bottom).

The (pseudo)critical point am_c of the spontaneous $\mathbb{Z}_2^\chi$ symmetry breaking phase transition is determined at fixed lattice spacing ag by considering the intersection point of the Binder cumulant $U = 1 - \langle\phi^4\rangle/3\langle\phi^2\rangle^2$ obtained from different volumes using Z_{ap} [17]. This can be compared with the determination from the peak of the susceptibility χ of the average sign of the bosonic field. In the inset of Fig. 2, we show data exemplarily for $ag = 0.125$ extrapolated to the infinite volume limit $gL \to \infty$ using linear and quadratic terms in $1/gL$. Both observables yield values which agree in the thermodynamic limit. Similarly, the (pseudo)critical point of the spontaneous supersymmetry breaking phase transition can be determined from the supersymmetric Ward identity $\langle P'/m\rangle$ yielding results which, in the infinite volume limit, are in agreement with the determinations from the $\mathbb{Z}_2^\chi$ transition already at finite lattice spacing. In order to take the continuum limit, this procedure is repeated for a range of lattice spacings, and the resulting bare critical couplings $f_c = g/m_c(ag)$ are renormalized by subtracting the logarithmically divergent one-loop self-energy from the bare mass m^2 and computing the renormalized critical coupling $f_c^R = g/m_c^R(ag)$. In Fig. 2, we show $1/f_c^R$ in the infinite volume limit as a function of the lattice spacing together with an extrapolation to the continuum using corrections linear plus quadratic in a. The average of this extrapolation with one using only a linear correction yields

$$1/f_c^R = 2.286(28)(36), \tag{8}$$

where the first error is statistical, and the second comes from the difference of the two extrapolations. The result demonstrates that the supersymmetry breaking phase transition coinciding with the $\mathbb{Z}_2^\chi$ symmetry restoration survives the infinite volume and the continuum limit, and it provides a precise nonperturbative determination of the perturbatively renormalized critical coupling. Finally, we note that the determination in [12], using SLAC fermions, is fully compatible with our result once the exact same renormalization procedure is applied.

Mass spectrum.—Next, we consider the mass spectrum of the system below, above, and across the phase transition. The lowest masses are obtained from the exponential temporal decay of two-point correlation functions $\langle\mathcal{O}(t)\mathcal{O}(0)\rangle$ of appropriate fermionic or bosonic operators $\mathcal{O}$ projected to zero spatial momentum [18]. Because of the open fermion string algorithm, the correlation functions can be determined to very high accuracy even in the massless phase or when the signal falls off by many orders of magnitude [13]. In Fig. 3, we show the lowest boson and fermion masses $m_\phi^{(0)}$, $m_\phi^{(1)}$ and $m_\psi^{(0)}$, $m_\psi^{(1)}$, respectively, in the bosonic sector $Z_{\mathcal{L}_{00}}$ at $ag = 0.25$ on a lattice with extent 128×48. For bare masses $m > m_c$, the system is in the supersymmetric phase, and we observe perfect mass degeneracy between the lowest fermion and boson mass already at finite lattice spacing. In the supersymmetry broken phase $m < m_c$, the masses split up and the degeneracy is lifted. In this phase, the masses can also be determined in the fermionic sector $Z_{\mathcal{L}_{01}} + Z_{\mathcal{L}_{10}} + Z_{\mathcal{L}_{11}}$, and we find the same values within our numerical accuracy. Further excited states can be obtained by employing the operators $\mathcal{O} = \psi\phi$ and ϕ^2 which, in the $\mathbb{Z}_2^\chi$ symmetric phase, do not mix with the above operators $\mathcal{O} = \psi$ and ϕ, respectively. The result for $\mathcal{O} = \phi^2$ is also displayed in Fig. 3. In the inset, we show a zoom of the mass $m_\psi^{(0)}$ and the amplitude $A_\psi^{(0)}$ of the lowest fermionic state. When approaching the phase transition in the supersymmetry broken phase, the amplitude decreases and vanishes at the critical point m_c; i.e., the particle decouples from the system when entering the supersymmetric phase. The mass is by an order of magnitude smaller than the next-to-lowest

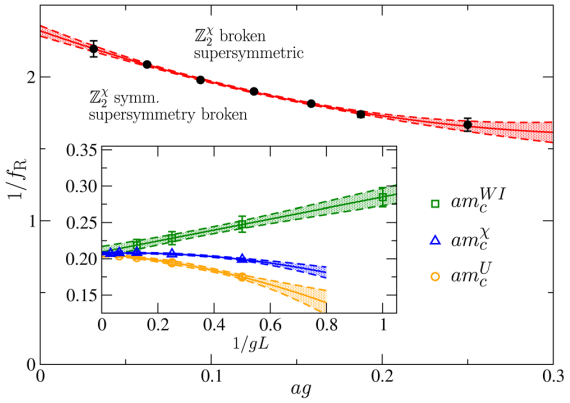

FIG. 2 (color online). Continuum limit of the inverse critical coupling $1/f_c^R$. The inset shows the infinite volume extrapolations of m_c from various definitions at $ag = 0.125$.

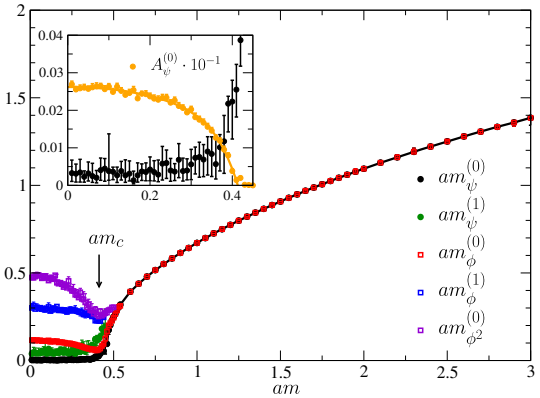

FIG. 3 (color online). The lowest boson and fermion masses at $ag = 0.25$ in the bosonic sector $Z_{\mathcal{L}_{00}}$. The inset shows a zoom of the Goldstino mass $m_\psi^{(0)}$ and its amplitude $A_\psi^{(0)}$.

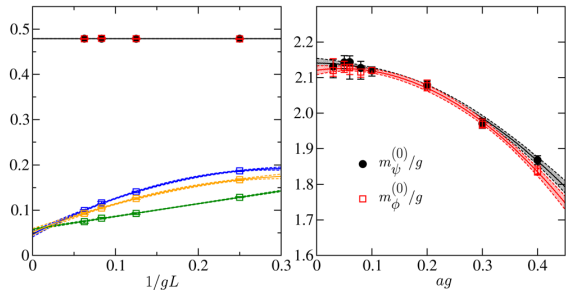

FIG. 4 (color online). Left: Infinite volume extrapolation of $m_\phi^{(0)}$ at fixed lattice spacing $ag = 0.25$ for three bare masses $am = 0.30, 0.18$, and 0.02 (from bottom up) in the supersymmetry broken phase and $m_\phi^{(0)}$, $m_\psi^{(0)}$ for one bare mass $am = 0.70$ in the supersymmetric phase (top). Right: Continuum extrapolation of $m_\phi^{(0)}/g$ and $m_\psi^{(0)}/g$ at fixed volume $gL = 8$ and renormalized coupling $1/f^R = 3$ in the supersymmetric phase.

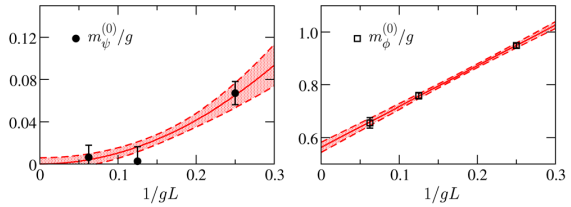

FIG. 5 (color online). Infinite volume extrapolation of $m_\psi^{(0)}$ and $m_\phi^{(0)}$ in the supersymmetry broken phase at $1/f^R = 1.2$.

mass, and the investigation of the finite volume corrections shows that the data for $m_\psi^{(0)}$ is compatible with zero in the infinite volume limit, even at finite lattice spacing. Therefore, the massless fermionic mode can be identified with the Goldstino particle [19] which mediates the tunneling between the fermionic and bosonic vacua and is expected to emerge in the phase with spontaneously broken supersymmetry. It is quite astonishing, though, that the Goldstino mode materializes so clearly already at rather coarse lattice spacing. Finally, from the behavior of the lowest fermion mass in the supersymmetric phase, we can determine the critical exponent ν related to the divergence of the fermionic correlation length. Using $m_\psi^0 \propto (m - m_c)^\nu$, we obtain $\nu = 0.45 \pm 0.03$ indicating a universality class different from the Ising one.

Next, we consider the infinite volume extrapolation of the lowest boson mass $m_\phi^{(0)}$ in the supersymmetry broken phase for three different bare masses $am = 0.02, 0.18$, and 0.30 at fixed lattice spacing in the left panel of Fig. 4. The data clearly indicate a finite boson mass which in the infinite volume limit is independent of m. For comparison, we also show the extrapolation of $m_\phi^{(0)}$ and $m_\psi^{(0)}$ at a bare mass $am = 0.70$ in the supersymmetric phase where we observe negligible finite volume effects. Hence, in this phase, the continuum extrapolation of the lowest fermion and boson mass can be done at fixed physical volume gL and constant renormalized coupling f^R. This is done in the right panel of Fig. 4 where we show the data for $gL = 8$ and $1/f_R = 3$ at different lattice spacings ag. A quadratic plus linear function of ag allows for a good parametrization of the finite lattice spacing effects. It is surprising to see that the mass degeneracy holds up even at coarse lattice spacings where the lattice artifacts are rather strong, e.g., ~14% at $ag = 0.4$.

Finally, going back to the supersymmetry broken phase, we consider the infinite volume limit of $m_\phi^{(0)}$ and $m_\psi^{(0)}$ in the continuum at fixed $1/f^R = 1.2$ in Fig. 5. We find a finite boson mass accompanied by the vanishing fermion mass of the Goldstino.

Conclusion.—We have established the fermion loop formulation for the two-dimensional $\mathcal{N} = 1$ Wess-Zumino model which allows efficient simulations with a worm algorithm by avoiding the fermion sign problem generically appearing in the phase with spontaneously broken supersymmetry due to the vanishing Witten index. We clearly observe a $\mathbb{Z}_2^\chi$ symmetric, supersymmetry broken phase where the bosonic and fermionic vacua (ground states) are degenerate and a $\mathbb{Z}_2^\chi$ broken, supersymmetric phase where one of the two ground states is spontaneously selected in the infinite volume limit. This confirms the expected symmetry breaking pattern and the corresponding vacuum structure. The phase transition separating those two phases can be analyzed using different observables in the infinite volume limit, and our calculations at several lattice spacings provide a precise nonperturbative determination of the renormalized critical coupling in the continuum limit.

Concerning the mass spectrum, we observe degenerate boson and fermion masses in the supersymmetric $\mathbb{Z}_2^\chi$ broken phase, surprisingly, even at finite and rather coarse lattice spacing. In the $\mathbb{Z}_2^\chi$ symmetric, supersymmetry broken phase, the nondegeneracy of the lowest few bosonic and fermionic masses can also be accurately resolved due to the efficient algorithm employed. The mass of the lowest fermionic state is compatible with zero in the thermodynamic and continuum limit, allowing us to identify it with the expected massless Goldstino mode.

*wenger@itp.unibe.ch

[1] J. Wess and B. Zumino, Phys. Lett. **49B**, 52 (1974).
[2] S. Ferrara, Lett. Nuovo Cimento Soc. Ital. Fis. **13**, 629 (1975).
[3] E. Witten, Nucl. Phys. **B202**, 253 (1982).
[4] J. Bartels and J. B. Bronzan, Phys. Rev. D **28**, 818 (1983).
[5] J. Ranft and A. Schiller, Phys. Lett. **138B**, 166 (1984).
[6] M. Beccaria, M. Campostrini, and A. Feo, Phys. Rev. D **69**, 095010 (2004).

[7] M. Beccaria, G. F. De Angelis, M. Campostrini, and A. Feo, Phys. Rev. D **70**, 035011 (2004).
[8] S. Elitzur, E. Rabinovici, and A. Schwimmer, Phys. Lett. **119B**, 165 (1982).
[9] F. Synatschke, H. Gies, and A. Wipf, Phys. Rev. D **80**, 085007 (2009).
[10] M. Golterman and D. Petcher, Nucl. Phys. **B319**, 307 (1989).
[11] S. Catterall and S. Karamov, Phys. Rev. D **68**, 014503 (2003).
[12] C. Wozar and A. Wipf, Ann. Phys. (Amsterdam) **327**, 774 (2012).
[13] U. Wenger, Phys. Rev. D **80**, 071503 (2009).
[14] D. Baumgartner and U. Wenger, *Proc. Sci.*, LATTICE2010 (2010) 245 [arXiv:1104.0213].
[15] D. Baumgartner and U. Wenger, *Proc. Sci.*, LATTICE2011 (2011) 239 [arXiv:1201.1485].
[16] U. Wolff, Nucl. Phys. **B789**, 258 (2008).
[17] D. Baumgartner, K. Steinhauer, and U. Wenger, *Proc. Sci.*, LATTICE2011 (2011) 253 [arXiv:1111.6042].
[18] D. Baumgartner, K. Steinhauer, and U. Wenger, *Proc. Sci.*, LATTICE2012 (2012) 043 [arXiv:1311.5089].
[19] A. Salam and J. A. Strathdee, Phys. Lett. **49B**, 465 (1974).

Paper 13

Loop formulation of the supersymmetric nonlinear O(N) sigma model

Kyle Steinhauer and Urs Wenger, Proceedings of Science (Lattice 2013) 092.

PROCEEDINGS OF SCIENCE

Loop formulation of the supersymmetric nonlinear O(N) sigma model

Kyle Steinhauer* **and Urs Wenger**
Albert Einstein Center for Fundamental Physics
Institute for Theoretical Physics
University of Bern
Sidlerstrasse 5
CH–3012 Bern
Switzerland
E-mail: steinhauer@itp.unibe.ch, wenger@itp.unibe.ch

We derive the fermion loop formulation for the supersymmetric nonlinear O(N) sigma model by performing a hopping expansion using Wilson fermions. In this formulation the fermionic contribution to the partition function becomes a sum over all possible closed non-oriented fermion loop configurations. The interaction between the bosonic and fermionic degrees of freedom is encoded in the constraints arising from the supersymmetry and induces flavour changing fermion loops. For $N \geq 3$ this leads to fermion loops which are no longer self-avoiding and hence to a potential sign problem. Since we use Wilson fermions the bare mass needs to be tuned to the chiral point. For $N = 2$ we determine the critical point and present boson and fermion masses in the critical regime.

31st International Symposium on Lattice Field Theory - LATTICE 2013
July 29 - August 3, 2013
Mainz, Germany

*Speaker.

 http://pos.sissa.it/

PoS(LATTICE 2013)092

1. Motivation

Despite the fact that nature has so far not revealed any trace of supersymmetry in its elementary particle spectrum, supersymmetric quantum field theories remain to be fascinating objects to study *per se*. It is for example most interesting to examine various discretisation schemes for supersymmetric field theories regularised on the lattice, e.g. using twisted supersymmetry or orbifolding techniques, in order to understand how the supersymmetry is realised in the continuum limit. Moreover, recent developments in simulating supersymmetric field theories in low dimensions efficiently and without critical slowing down [1, 2] brings the non-perturbative study of these theories to a new, unprecedented level of accuracy, allowing for example precise investigations of spontaneous supersymmetry breaking phase transitions [3, 4]. In these proceedings we report on our ongoing study to apply such a programme to the supersymmetric nonlinear O(N) sigma model regularised on the lattice. This model has already been investigated numerically using a variety of different discretisations [5, 6, 7]. Here we concentrate on reformulating the model in terms of fermion loops in order to make use of the efficient simulation algorithms and related methods to control the fermion sign problem accompanying any spontaneous supersymmetry breaking [8].

2. Continuum model

The Lagrangian density of the supersymmetric nonlinear O(N) sigma model in two-dimensional Euclidean spacetime, originally derived in [9, 10], can be written as

$$\mathscr{L} = \frac{1}{2g^2}\left(\partial_\mu\phi\partial^\mu\phi + i\overline{\psi}\partial\!\!\!/\psi + \frac{1}{4}(\overline{\psi}\psi)^2\right) \tag{2.1}$$

where ϕ is a N-tuple of real scalar fields, ψ a N-tuple of real Majorana fields with $\overline{\psi} = \psi^T\mathscr{C}$ and $\mathscr{C}$ the charge conjugation matrix. For the action to be O(N)-invariant and supersymmetric the fields must fulfill the constraints

$$\phi^2 = 1 \qquad \text{and} \qquad \phi\psi = 0\,. \tag{2.2}$$

The model described in eq.(2.1) and the constraints in eq.(2.2) are both invariant under the $\mathscr{N} = 1$ supersymmetry transformations

$$\delta\phi = i\overline{\varepsilon}\psi \quad \text{and} \quad \delta\psi = (\partial\!\!\!/ + \frac{i}{2}\overline{\psi}\psi)\phi\varepsilon$$

where ε is a constant Majorana spinor. There is an additional $\mathbb{Z}_2$ chiral symmetry realised by $\psi \to i\gamma_5\psi$ with $\gamma_5 = i\gamma_0\gamma_1$. As shown in [11] the one-loop β-function coincides with the one calculated for the model without SUSY, so it is asymptotically free for $N \geq 3$. As pointed out in [12] there exists an $\mathscr{N} = 2$ extension for supersymmetric nonlinear sigma models which have a Kähler target manifold. This is the case for $N = 3$ and hence an additional SUSY can be worked out [7]. The constraints in eq.(2.2) are implemented in the partition function by inserting adequate Dirac delta functions in the integration measure,

$$\begin{aligned} Z &= \int \mathscr{D}\phi\,\delta(\phi^2-1)\int \mathscr{D}\psi\,\delta(\phi\psi)e^{-S(\phi,\psi)} \\ &= \int \mathscr{D}\phi\,\delta(\phi^2-1)e^{-S_B(\phi)}\int \mathscr{D}\psi\left(\sum_{i\leq j}^{N}\phi_i\phi_j\overline{\psi}_i\psi_j\right)e^{-S_F(\psi)}\,, \end{aligned}$$

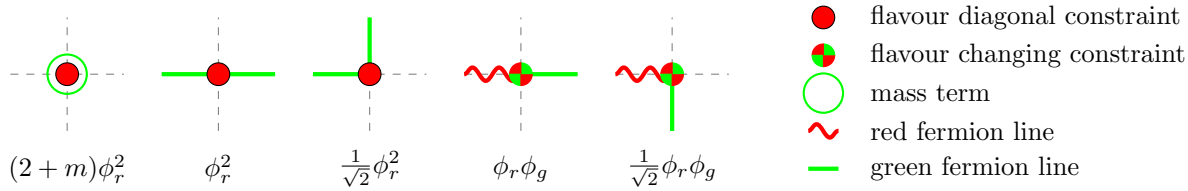

Figure 1: All possible vertices for $N = 2$ up to rotations and exchange of the two flavours denoted as r (red) and g (green) with the corresponding weights.

where the fermionic measure is rewritten in the second line using the Grassmann integration rules for Dirac delta functions. In this form it is explicit that the fermionic constraint $\phi\psi = 0$ induces flavour-diagonal ($i = j$) and flavour-changing ($i \neq j$) interactions between the bosonic and fermionic degrees of freedom.

3. Loop formulation and sign problem

When regularising the model on a discrete space-time lattice we follow the strategy in [7] and use the Wilson derivative for both the fermionic and the bosonic action. This strategy is well supported by various theoretical and numerical arguments [3, 4, 8, 13, 14, 15, 16, 17, 18]. We can then perform a hopping expansion to all orders for the fermionic and the bosonic variables in order to obtain an exact reformulation of the partition function in terms of non-oriented, closed fermion loops and constrained bosonic bond configurations (boson loops) [8]. These loops can in principle be simulated effectively by enlarging the configuration space by an open fermionic string [1, 2] and bosonic worms [19], respectively. The fermion loop formulation in particular solves the fermion sign problem since it naturally decomposes the contributions to the partition function into bosonic and fermionic ones, each with a definite sign depending on the employed boundary conditions [8]. The control of these signs is particularly important in the context of spontaneous supersymmetry breaking when the partition function for periodic boundary conditions, i.e. the Witten index, vanishes due to the exact cancellation of the bosonic and fermionic contributions.

Unfortunately, the model as discretised above nevertheless suffers from a sign problem. Firstly, the fermionic constraint $\phi\psi = 0$ requires on each lattice site exactly one term of the form $\phi_i\phi_j\overline{\psi}_i\psi_j$ inducing the interactions between fermions and bosons. Since the flavour-nondiagonal constraint with $i \neq j$ changes the flavour content within a fermion loop, a loop can be self-intersecting for $N \geq 3$ and hence looses the crucial property of having a definite sign depending only on its winding topology. Secondly, the Wilson term introduced in the bosonic sector generates a next-to-nearest neighbour diagonal hopping term with the wrong sign leading to an overall sign which fluctuates under local changes of the bosonic bond configuration. In order to avoid these complications we restrict ourselves in the following to $N = 2$ for which the fermion loops remain self-avoiding and in addition treat the bosonic degrees of freedom in the standard way, i.e., without employing a hopping expansion. The partition function for a system with V lattice sites can then be written as

$$Z = \left(\frac{1}{g^2}\right)^V \int \mathscr{D}\phi\, \delta(\phi^2 - 1)\, e^{-S_B(\phi)} \sum_{\{l\}} w(l,\phi)$$

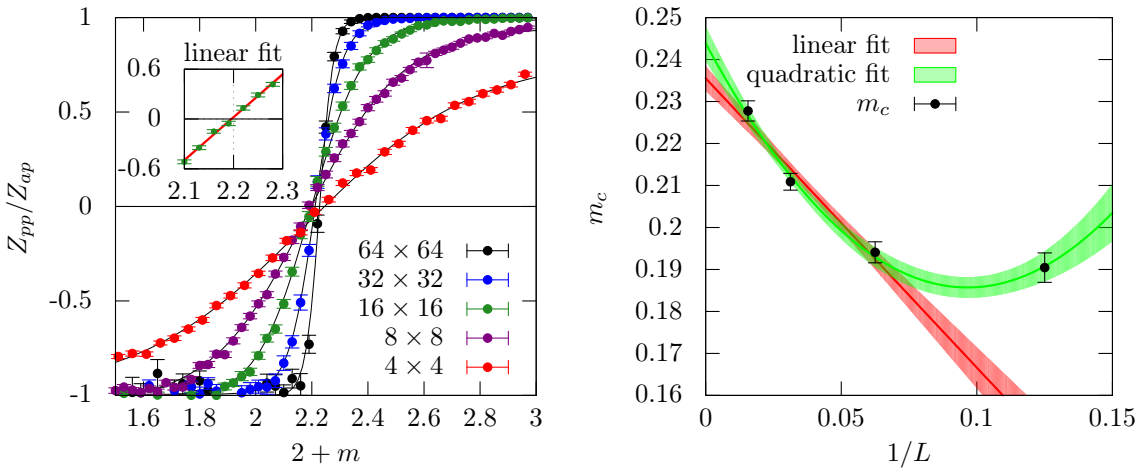

Figure 2: *Left plot*: Z_{pp}/Z_{ap} as a function of the bare mass m at $g = 0.5$ for various lattice extents. The small inset shows a linear fit used to obtain the critical mass defined by $Z_{pp}(m_c) = 0$. *Right plot*: Critical masses $m_c(L)$ at $g = 0.5$ for various lattice extents together with an extrapolation to the thermodynamic limit.

where the weight $w(l,\phi)$ for a given loop configuration l is determined solely by the geometry of the loops and, through the constraints in eq.(2.2), depends on the bosonic field ϕ. As an interesting side remark we note that the coupling g has no influence on the fermion loops except indirectly through the bosonic fields. In Figure 1 we show all allowed vertices up to rotations and exchange of the two flavours denoted as r (red) and g (green). The additional factors are $1/\sqrt{2}$ from the Dirac algebra structure for each corner in the loop [20] and $(2+m)$ from the fermionic monomer term (with m being the bare fermion mass). Note that the weights corresponding to the flavour changing constraints are still not guaranteed to be positive definite since the bosonic field components appear linearly in those. For certain values of the parameters m and g this leads to a sign fluctuating under local changes of the bosonic field and this is why we consider the phase quenched model with $w(l,\phi) \to |w(l,\phi)|$ in the following. The correct model can then be recovered by reweighting with the sign $\sigma(w)$ and this seems to work well in some of the interesting parameter regimes.

4. Results for $N = 2$

The supersymmetric nonlinear O(N) sigma model is defined in the chiral limit where both the fermions and bosons are massless. However, since the Wilson term explicitly breaks chiral symmetry even at zero bare fermion mass, the chiral limit of the regularised theory is not defined simply by the vanishing of that mass. Instead, it needs to be tuned to the critical value m_c where the correlation length of the fermion diverges and the fermion develops a zero mode yielding $Z_{pp}(m_c) = 0$ for the partition function with periodic boundary conditions in both directions [20, 21].

The behaviour of Z_{pp}/Z_{ap} when varying the bare mass is illustrated in the left panel of fig. 2 for various lattice extents L at $g = 0.5$. The inset illustrates for the 16×16 lattice how the values of $m_c(L)$ are extracted by performing linear fits to Z_{pp}/Z_{ap} in the region close to zero. It is evident that this definition of the critical mass allows rather accurate determinations of m_c and hence leads to precise extrapolations to the thermodynamic limit. In the right panel of fig. 2 we show such an

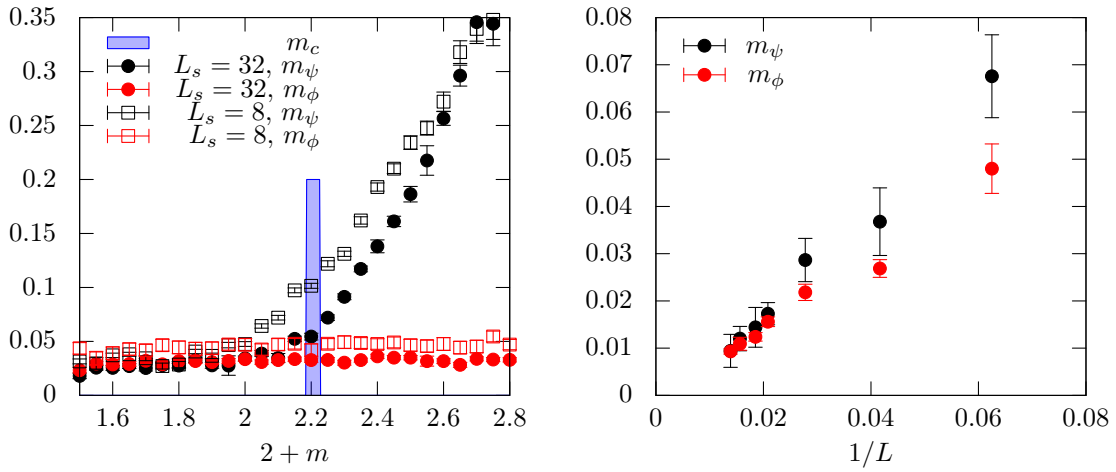

Figure 3: *Left plot*: Boson and fermion masses at coupling $g = 0.5$ as a function of the bare mass for two different lattice volumes. *Right plot*: Boson and fermion masses for $g = 0.5$ at the critical mass m_c versus the inverse lattice extent.

extrapolation at fixed coupling $g = 0.5$. Eventually, this procedure can be repeated for a range of couplings in order to obtain $m_c(g)$ in the thermodynamic limit. We note however that the behaviour of the system changes significantly for $g \gtrsim 0.8$ where we expect the occurrence of a Kosterlitz-Thouless phase transition.

Next we investigate the boson and fermion mass spectrum of the theory. The fermion correlator can be measured with high accuracy using the open fermionic string update introduced in [1]. In the left panel of fig. 3 we show the observed masses at fixed coupling $g = 0.5$ for the two volumes with spatial extent $L_s = 8$ and 32 and temporal extent $L_t = 32$. The boson mass m_ϕ depends noticeably on the volume, but is essentially independent of the bare fermion mass and remains constant across the phase transition. The fermion mass m_ψ on the other hand drops when the bare mass is decreased towards its critical value and becomes degenerate with the boson mass in the regime close to the critical point m_c (denoted by the blue bar). The mass degeneracy is further examined in the right panel of fig. 3 where the two masses m_ϕ and m_ψ at the critical mass m_c for $g = 0.5$ are plotted versus the inverse lattice extent. The data indicate that the mass degeneracy between the boson and fermion mass at the critical point survives the continuum limit where the model becomes chirally invariant.

We emphasise again that the above calculations are made in the phase quenched model. The only sources of negative contributions are the flavour changing constraints $\phi_r \phi_g \overline{\psi}_r \psi_g$. We are investigating their occurrence in the left panel of fig. 4 where the flavour changing constraint density is plotted versus the bare mass for various couplings g on a lattice of size 8×8. For large g the number of flavour changing interactions grows for decreasing $m < m_c$ while for smaller couplings the number remains rather small. On the other hand, for large values of $m > m_c$ the density of flavour changing interactions vanishes for any coupling. In this region there are predominantly flavour diagonal constraints contributing positively with ϕ_r^2 or ϕ_g^2. As a consequence the average sign $\langle \sigma \rangle$ plotted in the right panel of fig. 4 appears to behave reasonably well and this suggests that approaching the chiral limit from $m > m_c$ is under good control.

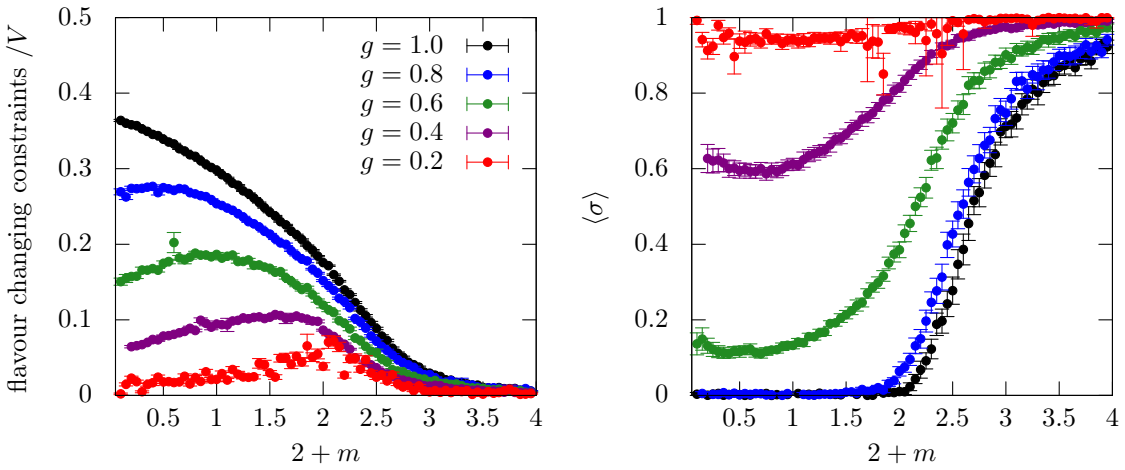

Figure 4: *Left plot*: Density of flavour changing constraints as a function of the bare mass for a range of couplings. *Right plot*: Same but for the average sign $\langle\sigma\rangle$.

5. Summary and outlook

We constructed a fermion loop formulation of the supersymmetric nonlinear O(N) sigma model on an Euclidean space-time lattice using the Wilson derivative for both the bosonic and fermionic fields. This formulation maintains both the O(N) symmetry and the constraints arising from the supersymmetry and in principle allows a straightforward simulation of the model. For $N = 2$ we determined the critical mass, defining the massless model in the continuum limit, for a range of couplings and showed how the fermion and boson masses become degenerate at this point. A careful analysis of Ward identities is necessary in order to clarify whether or not the supersymmetry is fully restored in the continuum limit, but in principle it is now possible to determine the full phase diagram of the model, i.e., the range of parameters for which the supersymmetry is spontaneously broken, if at all.

One obstacle towards this goal is the fluctuating sign stemming from the bosonic degrees of freedom entering in the constraints $\phi\psi = 0$. However, it is not clear whether this sign problem survives the continuum limit since it is a pure artefact of the particular regularisation chosen. In fact, the sign problem can be completely avoided by introducing the Wilson term only in the fermionic sector and performing the hopping expansion also for the bosonic degrees of freedom as outlined in section 3, but of course it remains to be seen whether supersymmetry is restored in the continuum also for such a regularisation.

References

[1] U. Wenger, *Efficient simulation of relativistic fermions via vertex models*, *Phys.Rev.* **D80** (2009) 071503, [arXiv:0812.3565].

[2] U. Wenger, *Simulating Wilson fermions without critical slowing down*, *PoS* **LAT2009** (2009) 022, [arXiv:0911.4099].

[3] D. Baumgartner, K. Steinhauer, and U. Wenger, *Supersymmetry breaking on the lattice: the N=1 Wess-Zumino model*, *PoS* **LATTICE2011** (2011) 253, [arXiv:1111.6042].

[4] U. Wenger, K. Steinhauer, and D. Baumgartner, *Spontaneous supersymmetry breaking in the 2d N=1 Wess-Zumino model*, *PoS* **LATTICE2012** (2012) 043, [arXiv:1311.5089].

[5] S. Catterall and S. Ghadab, *Lattice sigma models with exact supersymmetry*, *JHEP* **0405** (2004) 044, [hep-lat/0311042].

[6] S. Catterall and S. Ghadab, *Twisted supersymmetric sigma model on the lattice*, *JHEP* **0610** (2006) 063, [hep-lat/0607010].

[7] R. Flore, D. Körner, A. Wipf, and C. Wozar, *Supersymmetric Nonlinear O(3) Sigma Model on the Lattice*, *JHEP* **1211** (2012) 159, [arXiv:1207.6947].

[8] D. Baumgartner and U. Wenger, *Simulation of supersymmetric models on the lattice without a sign problem*, *PoS* **LATTICE2010** (2010) 245, [arXiv:1104.0213].

[9] E. Witten, *A Supersymmetric Form of the Nonlinear Sigma Model in Two-Dimensions*, *Phys.Rev.* **D16** (1977) 2991.

[10] P. Di Vecchia and S. Ferrara, *Classical Solutions in Two-Dimensional Supersymmetric Field Theories*, *Nucl.Phys.* **B130** (1977) 93.

[11] A. M. Polyakov, *Interaction of Goldstone Particles in Two-Dimensions. Applications to Ferromagnets and Massive Yang-Mills Fields*, *Phys.Lett.* **B59** (1975) 79–81.

[12] B. Zumino, *Supersymmetry and Kähler Manifolds*, *Phys.Lett.* **B87** (1979) 203.

[13] M. F. Golterman and D. N. Petcher, *A Local Interactive Lattice Model With Supersymmetry*, *Nucl.Phys.* **B319** (1989) 307–341.

[14] S. Catterall and S. Karamov, *A Lattice study of the two-dimensional Wess-Zumino model*, *Phys.Rev.* **D68** (2003) 014503, [hep-lat/0305002].

[15] G. Bergner, T. Kästner, S. Uhlmann, and A. Wipf, *Low-dimensional Supersymmetric Lattice Models*, *Annals Phys.* **323** (2008) 946–988, [arXiv:0705.2212].

[16] T. Kästner, G. Bergner, S. Uhlmann, A. Wipf, and C. Wozar, *Two-Dimensional Wess-Zumino Models at Intermediate Couplings*, *Phys.Rev.* **D78** (2008) 095001, [arXiv:0807.1905].

[17] C. Wozar and A. Wipf, *Supersymmetry Breaking in Low Dimensional Models*, *Annals Phys.* **327** (2012) 774–807, [arXiv:1107.3324].

[18] D. Baumgartner and U. Wenger, *Exact results for supersymmetric quantum mechanics on the lattice*, *PoS* **LATTICE2011** (2011) 239, [arXiv:1201.1485].

[19] N. Prokof'ev and B. Svistunov, *Worm Algorithms for Classical Statistical Models*, *Phys.Rev.Lett.* **87** (2001) 160601.

[20] U. Wolff, *Cluster simulation of relativistic fermions in two space-time dimensions*, *Nucl.Phys.* **B789** (2008) 258–276, [arXiv:0707.2872].

[21] O. Bär, W. Rath, and U. Wolff, *Anomalous discrete chiral symmetry in the Gross-Neveu model and loop gas simulations*, *Nucl.Phys.* **B822** (2009) 408–423, [arXiv:0905.4417].

Part V

Appendix

Paper 14

QCD at non-zero density and canonical partition functions with Wilson fermions

Andrei Alexandru and Urs Wenger, Physical Review D **83**, 034502 (2011).

PHYSICAL REVIEW D **83,** 034502 (2011)

QCD at nonzero density and canonical partition functions with Wilson fermions

Andrei Alexandru[1] and Urs Wenger[2]

[1]*Physics Department, The George Washington University Washington, D.C. 20052, USA*

[2]*Albert Einstein Center for Fundamental Physics, Institute for Theoretical Physics, Sidlerstrasse 5, CH–3012 Bern, Switzerland*

(Received 23 September 2010; published 11 February 2011)

We present a reduction method for Wilson-Dirac fermions with nonzero chemical potential which generates a dimensionally reduced fermion matrix. The size of the reduced fermion matrix is independent of the temporal lattice extent and the dependence on the chemical potential is factored out. As a consequence the reduced matrix allows a simple evaluation of the Wilson fermion determinant for any value of the chemical potential and hence the exact projection to the canonical partition functions.

DOI: 10.1103/PhysRevD.83.034502 PACS numbers: 11.15.Ha, 12.38.Gc, 12.38.Mh, 21.65.Qr

I. INTRODUCTION

Nonperturbative lattice calculations of Quantum Chromodynamics (QCD) at zero density have seen remarkable progress in recent years. However, simulations at nonzero quark or baryon density remain a challenge due to the occurrence of a complex phase in the fermion determinant at nonzero chemical potential. The fluctuation of this phase is the source of the notorious fermionic sign problem and obstructs the straightforward simulation of the theory using Monte Carlo importance sampling. This problem limits the reliability of present-day lattice QCD calculations at finite baryon density and makes it difficult to explore the QCD phase diagram in parameter regimes which are particularly interesting, e.g. for the identification of different phases of matter, the determination of phase transition lines and the location of possible critical endpoints. However, credible nonperturbative results at nonzero quark density would provide important phenomenological information, e.g. for understanding the structure of neutron stars or the dynamics of relativistic heavy-ion collisions.

One approach to QCD at finite density makes use of the canonical formulation where the net quark (or baryon) number is held constant. This can be achieved by separating the grand-canonical partition function Z_{GC} into a sum of canonical partition functions $Z_C(k)$ with a fixed net number k of quarks and antiquarks. Quantities at fixed chemical potential, i.e. in the standard grand-canonical formulation of QCD, can then be obtained by averaging over the canonical partition functions. It turns out that the projection to the canonical sectors can be done exactly, gauge field by gauge field, however it requires the integration of the fermion determinant over the whole range of imaginary chemical potential $\phi = i\mu/T \in [0, 2\pi]$.

In the past, this approach could only be made practical in connection with staggered fermions. For those, clever fermion matrix reduction methods were developed [1–3] that allow the evaluation of the determinant for any value of the chemical potential once the eigenvalues of the reduced fermion matrix are known. We refer to [4] for an extended overview of studies following this approach. The reduction of the fermion matrix in size by a factor half the temporal lattice extent is the crucial ingredient since it reduces the complexity of the eigenvalue computation by the corresponding factor cubed. Unfortunately, however, for Wilson fermions so far no such reduction method was known despite various attempts [5,6].

In this paper, we present such a reduction method for Wilson fermions, i.e. we derive a dimensionally reduced Wilson fermion matrix whose size is independent of the temporal lattice extent and for which the dependence on the chemical potential is factored out. It therefore allows easy and exact evaluation of the determinants at any value of the chemical potential and hence the straightforward projection to the various canonical sectors. Applications which are facilitated by the reduction method for Wilson fermions presented here include the reweighting of ensembles to different values of the chemical potential and calculations based on canonical ensembles [7–10].

The reduction of the four-dimensional Wilson-Dirac operator to the three-dimensional reduced fermion matrix is very similar to the construction of the four-dimensional overlap operator from the five-dimensional domain wall fermion operator [11–13]. A similar reduction method for the Wilson fermion matrix has also been proposed in [14] in the context of reweighting with stochastic determinants. Finally, while preparing the paper we were informed by Nakamura and Nagata about their development of similar reduction techniques for the Wilson fermion matrix [15].

The paper is organized as follows. In Sec. II, we briefly review the separation of the grand-canonical partition function of QCD into a sum of canonical partition functions with fixed quark or baryon number. In Sec. III, we present the reduction method for Wilson fermions which renders the computational complexity of the determinant independent of the temporal lattice extent and factorizes the dependence on the chemical potential. In Secs. IV and V we discuss spectral properties of the reduced matrix and some properties of the projected determinants, respectively. While the results from these sections so far do not have a direct physical application, we would like to

emphasize their potential importance for the development of new canonical simulation algorithms, or for the optimization of reweighting strategies. Finally, in Sec. VI we present some results from a reweighting of canonical ensembles, merely as a demonstration of the potential of the reduced fermion matrix approach.

II. CANONICAL FORMULATION OF QCD AT FIXED BARYON NUMBER

The grand-canonical partition function at temperature T and chemical potential μ_q for a single quark flavor can be defined as

$$Z_{GC}(\mu_q) = \int \mathcal{D}U e^{-S_g(U)} \det M(U, \mu_q), \tag{1}$$

where $M(U, \mu_q)$ denotes the Dirac operator, U collects the gauge field degrees of freedom from the color gauge group $\mathrm{SU}(N_c)$ and $S_g(U)$ is the gauge field action. This is the commonly used partition function for simulating QCD thermodynamics on the lattice [16–19], which in general, however, suffers from a strong fermionic sign problem. The same thermodynamic physics can also be extracted using the canonical partition function [7,8,20–22], although one should keep in mind that the physics of the two systems strictly coincide only in the thermodynamic limit, i.e. in the limit of infinite spatial volume. The partition function in the canonical approach, for a system with a net number of k quarks, can be written as

$$Z_C(k) = \int \mathcal{D}U e^{-S_g(U)} \det{}_k M(U), \tag{2}$$

where the fermionic contribution is now included in the projected determinant

$$\det{}_k M(U) \equiv \frac{1}{2\pi} \int_0^{2\pi} d\phi e^{-ik\phi} \det M(U, \mu_q = i\phi T), \tag{3}$$

and one has made use of the fact that $\det M(U, \mu_q = i\phi T)$ enjoys a $\frac{2\pi}{N_c}$-periodicity in ϕ [23,24]. The periodicity stems from the fact that a shift in the imaginary chemical potential $\phi \to \phi + \frac{2\pi}{N_c}$ can be exactly compensated by a corresponding $\mathbb{Z}(N_c)$-transformation of the underlying gauge field. From this periodicity, it also follows that $Z_C(k) = 0$ for $k \neq 0 \bmod N_c$, i.e. it vanishes for noninteger baryon numbers $n_B \notin \mathbb{Z}$, while $Z_C(k) = Z_C^*(-k)$ follows from the evenness $Z_{GC}(\mu_q) = Z_{GC}(-\mu_q)$ due to time-reversal symmetry.

Finally, one can relate the canonical partition functions back to the grand-canonical ones using the fugacity expansion

$$Z_{GC}(\mu_q) = \sum_{k=-\infty}^{+\infty} e^{k\mu_q/T} Z_C(k), \tag{4}$$

where the sum can in principle be restricted to $k = 0 \bmod N_c$, i.e. integer baryon numbers, following the discussion above. Furthermore, the equation also motivates the determination of the baryon chemical potential in the canonical approach by a definition based on the free energy. Essentially, the baryon chemical potential is the response of the system when introducing one more baryon to the system, i.e.

$$\mu_B(n_B) \equiv F(N_c \cdot (n_B + 1)) - F(N_c \cdot n_B), \tag{5}$$

where $F(k) = -T \log Z_C(k)$ is the Helmholtz free energy of the canonical partition function. In a finite volume V, this definition is ambiguous due to the discreteness of the baryon number, however, in the thermodynamic limit it yields $\mu_B(\rho_B) = df/d\rho_B$, where $\rho_B = n_B/V$ and $f = F/V$ are the baryon and free energy densities. Note that the baryon chemical potential μ_B is different from the quark chemical potential μ_q used above. The quark chemical potential cannot be defined as the increase of the free energy when introducing a quark in the system since the free energy is infinite for systems that have fractional baryon numbers. If we need to compare the chemical potential used in the grand-canonical approach to the chemical potential measured in the canonical approach, we use $\mu_q \simeq \mu_B/N_c$.

III. REDUCTION TECHNIQUE FOR THE WILSON FERMION MATRIX

In the following, we consider QCD with Wilson fermions on a periodic lattice with temporal and spatial extent L_t and L_s, respectively. The quark chemical potential is $\mu \equiv a\mu_q$ where a is the lattice spacing.[1] The massive Wilson-Dirac operator can be written as

$$M = \frac{1}{2}\Gamma_\nu(\nabla_\nu + \nabla_\nu^*) - \frac{1}{2}\nabla_\nu^*\nabla_\nu + m, \tag{6}$$

where ∇_ν, ∇_ν^* denote the covariant forward and backward lattice derivative, Γ_ν are the Euclidean Dirac matrices and m is the bare quark mass. The chemical potential μ couples to the fermion number operator and is introduced on the lattice [25] by furnishing the forward and backward temporal hopping terms by factors of $e^{\pm\mu}$, respectively. More explicitly, we have

$$\begin{aligned} M_{x,y} = (m+4)\cdot\delta_{x,y} - \sum_{k=1}^{3}\{&P(+k)U_k(x)\delta_{y,x+\hat{k}} \\ &+ P(-k)U_k^\dagger(y)\delta_{y,x-\hat{k}}\} - \{e^{+\mu}P(+4)U_4(x)\delta_{y,x+\hat{4}} \\ &+ e^{-\mu}P(-4)U_4^\dagger(y)\delta_{y,x-\hat{4}}\}, \end{aligned} \tag{7}$$

where $U_\nu(x) \in \mathrm{SU}(N_c)$ are the gauge field links and $P(\pm\nu) = \frac{1}{2}(1 \mp \Gamma_\nu)$, $\nu = 1, \ldots, 4$. Further, for convenience

[1] From now on we set $a = 1$.

we introduce $P_\pm \equiv P(\pm 4)$ for the projectors in temporal direction and will use this notation in the following. Choosing the spatial Euclidean Dirac matrices as

$$\Gamma_k = \begin{pmatrix} 0 & \sigma_k \\ \sigma_k^\dagger & 0 \end{pmatrix} \tag{8}$$

and hence Hermitian, we note that the spatial part of the Wilson-Dirac operator, i.e. the first line of Eq. (7), can be written in the form

$$B = \begin{pmatrix} B_{++} & C \\ -C^\dagger & B_{--} \end{pmatrix}, \tag{9}$$

where $B_{++} = B_{--}$ is Hermitian and trivial in Dirac space,

$$(B_{++})_{x,y} = (m+4)\cdot\delta_{x,y} - \frac{1}{2}\sum_{k=1}^{3}\{\delta_{y,x+\hat{k}}U_k(x) + \delta_{x,y+\hat{k}}U_k^\dagger(y)\}, \tag{10}$$

while

$$C_{x,y} = \frac{1}{2}\sum_{k=1}^{3}\sigma_k\{\delta_{y,x+\hat{k}}U_k(x) - \delta_{x,y+\hat{k}}U_k^\dagger(y)\} \tag{11}$$

is Hermitian if the Heisenberg matrices σ_k in Eq. (8) are chosen to be Hermitian. The derivations presented below focus on the unimproved version of the Wilson-Dirac operator. However, the addition of the clover term can be easily accommodated: it only changes the spatial hopping matrix B in a way that is consistent with the structure in Eq. (9), which is all that is needed for some of the more specific derivations in Secs. III B and IV A. In fact, the numerical experiments presented later in the paper use the clover-improved version of the Dirac operator.

A. Reduction of $\det M$

The Wilson fermion matrix (6) in temporal gauge with (anti-)periodic boundary conditions in space (time) direction for a single quark flavor with chemical potential μ can be represented by

$$M = \begin{pmatrix} B_0 & P_+ & & & -P_-\cdot\mathcal{U}^\dagger\cdot e^{-\mu L_t} \\ P_- & B_1 & P_+ & & \\ & P_- & B_2 & \ddots & \\ & & \ddots & \ddots & P_+ \\ -P_+\cdot\mathcal{U}\cdot e^{+\mu L_t} & & & P_- & B_{L_t-1} \end{pmatrix}, \tag{12}$$

where the B_t's are $(4\cdot N_c\cdot L_s \times 4\cdot N_c\cdot L_s)$-matrices and represent the (spatial) Wilson-Dirac operator on time-slice t and where we have rescaled the fermion fields such that the dependence on the chemical potential resides on the links connecting the last and the first time slice. The temporal gauge links also reside only on those links and are collected in the matrix $\mathcal{U}$ so that $P_+\cdot\mathcal{U}$ is of the same size as B_t. For convenience, we abbreviate in the following $A^- \equiv -\mathcal{U}^\dagger\cdot e^{-\mu L_t}$ and $A^+ \equiv -\mathcal{U}\cdot e^{+\mu L_t}$ and note that the matrix can be written in the form

$$M = \begin{pmatrix} B_0 & & & A^- \\ 1 & B_1 & & \\ & \ddots & \ddots & \\ & & 1 & B_{L_t-1} \end{pmatrix}P_- + \begin{pmatrix} B_0 & 1 & & \\ & B_1 & \ddots & \\ & & \ddots & 1 \\ A^+ & & & B_{L_t-1} \end{pmatrix}P_+, \tag{13}$$

using the fact that $P_+ + P_- = 1$. Essentially, this splits the matrix into two parts, describing the components of the Dirac particle moving forward and backward in time. Next, we define the shift-projection matrix

$$\mathcal{P} = \begin{pmatrix} P_+ & P_- & & & \\ & P_+ & P_- & & \\ & & P_+ & \ddots & \\ & & & \ddots & P_- \\ P_- & & & & P_+ \end{pmatrix}, \tag{14}$$

which leaves the forward moving part invariant and shifts the backward moving part by on time slice. We further note that $\det\mathcal{P} = 1$. Multiplying M with $\mathcal{P}$ from the right, we find

$$M\cdot\mathcal{P} = \begin{pmatrix} Q_0^-(P_-A^- + P_+) & Q_0^+ & & & \\ & Q_1^- & Q_1^+ & & \\ & & Q_2^- & \ddots & \\ & & & \ddots & Q_{L_t-2}^+ \\ Q_{L_t-1}^+(P_+A^+ + P_-) & & & & Q_{L_t-1}^- \end{pmatrix}, \tag{15}$$

where we defined

$$Q_i^\pm = B_i P_\mp + P_\pm \tag{16}$$

and used the fact that

$$P_- A^- + B_0 P_+ = Q_0^- (P_- A^- + P_+), \tag{17}$$

$$P_+ A^+ + B_{L_t-1} P_- = Q_{L_t-1}^+ (P_+ A^+ + P_-). \tag{18}$$

Now, we define the block diagonal matrix

$$\mathcal{Q} = \begin{pmatrix} Q_0^- & & & \\ & Q_1^- & & \\ & & \ddots & \\ & & & Q_{L_t-1}^- \end{pmatrix} \tag{19}$$

and find

$$\tilde{M} \equiv \mathcal{Q}^{-1} \cdot M \cdot \mathcal{P} = \begin{pmatrix} (P_- A^- + P_+) & T_0 & & & \\ & 1 & T_1 & & \\ & & 1 & \ddots & \\ & & & \ddots & T_{L_t-2} \\ T_{L_t-1}(P_+ A^+ + P_-) & & & & 1 \end{pmatrix}, \tag{20}$$

where

$$T_i = (Q_i^-)^{-1} \cdot Q_i^+. \tag{21}$$

Note that the matrix $\tilde{M}$ is essentially a transfer matrix describing fermions hopping forward and backward between time slices. We discuss this further in Sec. III C.

We can now easily calculate the determinant of the transfer matrix $\tilde{M}$ using Schur complement techniques [13]. Defining

$$T \equiv T_0 \cdot T_1 \cdot \ldots \cdot T_{L_t-1}, \tag{22}$$

we find =

$$\det[\mathcal{Q}^{-1} \cdot M \cdot \mathcal{P}] = \det[(P_- A^- + P_+) - (-1)^{L_t} T \cdot (P_+ A^+ + P_-)], \tag{23}$$

and hence

$$\det[M] = \left(\prod_{i=0}^{L_t-1} \det Q_i^- \right) \cdot \det[\mathcal{Q}^{-1} \cdot M \cdot \mathcal{P}]. \tag{24}$$

Note that the first factor $\det[\mathcal{Q}]$ from canceling the effect of multiplication with $\mathcal{Q}^{-1}$ is independent of μ and cancels when we take the ratio of two determinants, e.g. with two different chemical potentials. Furthermore, from now on we assume L_t to be even in order to get rid of the inconvenient factor $(-1)^{L_t}$.

In order to separate the dependence on the chemical potential μ from the gauge field dependence, we first note that for arbitrary matrices A, B, C, D diagonal in Dirac space, i.e. commuting with $P_\pm$, we have

$$(P_\pm A + P_\mp B)(P_\pm C + P_\mp D) = P_\pm AC + P_\mp BD. \tag{25}$$

So, multiplying Eq. (23) by $\det[P_+ A + P_- B]$ with $A = e^{-\mu L_t}$ and $B = -\mathcal{U}$, we obtain

$$\det[\mathcal{Q}^{-1} \cdot M \cdot \mathcal{P}] \det[P_+ e^{-\mu L_t} - P_- \mathcal{U}] = \det[e^{-\mu L_t} + T \cdot \mathcal{U}]. \tag{26}$$

This is the determinant of the reduced Wilson fermion matrix. Note that the gauge field dependence resides in $T \cdot \mathcal{U}$ only and is completely separated from the dependence on μ. This allows now for an efficient calculation of the determinant as a function of μ for a fixed gauge field background. Denoting the eigenvalues of $T \cdot \mathcal{U}$ by λ_i, $i = 1, \ldots, 4N_c L_s^3$, we have

$$\det[e^{-\mu L_t} + T \cdot \mathcal{U}] = \prod_{i=1}^{4N_c L_s^3} (e^{-\mu L_t} + \lambda_i). \tag{27}$$

In order to establish the equivalence between $\det[M]$ and Eq. (27), we need to cancel the contribution from multiplying with $\det[P_+ e^{-\mu L_t} - P_- \mathcal{U}]$. First we note that the matrix has an inverse,

$$(P_+ e^{+\mu L_t} - P_- \mathcal{U}^\dagger) \cdot (P_+ e^{-\mu L_t} - P_- \mathcal{U}) = 1, \tag{28}$$

hence the canceling is always possible. In fact, we can calculate the determinant explicitly, since the matrix splits into the two orthogonal blocks $\propto P_\pm$ (this is due to the fact that $\mathcal{U}$ and $e^{-\mu L_t}$ are trivial in Dirac space) and the determinant is just the product of the determinants of the two subblocks,

$$\det[P_+ e^{-\mu L_t} - P_- \mathcal{U}] = \det[e^{-\mu L_t}] \cdot \det[-\mathcal{U}] = e^{-\mu L_t \cdot 2N_c L_s^3}, \tag{29}$$

where the factor of 2 in the exponent comes from the fact that the subblock matrix spans over only half the Dirac indices.

B. Calculation of T

A drawback of the matrix reduction is that we need to explicitly calculate T, which contains the inverses of Q_i^- of size $(4N_c L_s^3) \times (4N_c L_s^3)$. It turns out, however, that the size of the matrix to be inverted can be halved. To see this, consider the following explicit form of Q_i^-. The spatial Wilson-Dirac operator B_i on time slice i inherits the structure of the full spatial Wilson-Dirac operator B according to Eq. (9). When the σ_k in Γ_k are chosen to be Hermitian, it can be written as

$$B_i = \begin{pmatrix} D_i & C_i \\ -C_i & D_i \end{pmatrix}, \tag{30}$$

with $D_i^\dagger = D_i$ and $C_i^\dagger = C_i$.[2] Then, in a basis where Γ_4 is block diagonal, one has

[2]Note that a similar argument goes through for the choice of anti-Hermitian Dirac matrices, in which case one has $C_i^\dagger = -C_i$.

$$Q_i^- = P_- + B_i P_+ = \begin{pmatrix} D_i & 0 \\ -C_i & 1 \end{pmatrix}. \quad (31)$$

We then find for the inverse of Q_i^-

$$(Q_i^-)^{-1} = \begin{pmatrix} D_i^{-1} & 0 \\ C_i \cdot D_i^{-1} & 1 \end{pmatrix}, \quad (32)$$

so B_i needs to be inverted only in the subspace proportional to P_+, i.e. only D_i^{-1} is needed. Further, we also need to calculate $\det[Q_i^-]$, although these factors cancel exactly in the ratio of determinants, e.g. for different chemical potentials. From Eq. (31), we read off $\det[Q_i^-] = \det[D_i]$. Finally, for later use we also note the explicit form of Q_i^+,

$$Q_i^+ = P_+ + B_i P_- = \begin{pmatrix} 1 & C_i \\ 0 & D_i \end{pmatrix}. \quad (33)$$

C. Physical interpretation of the reduced matrix

It is straightforward to give a physical interpretation of the dimensionally reduced Wilson-Dirac fermion matrix. The equivalence of the determinants

$$\det M = \det \mathcal{Q} \cdot \det[e^{-\mu L_t/2} + T \cdot \mathcal{U} \cdot e^{+\mu L_t/2}] \quad (34)$$

establishes an equivalence (up to the bulk term $\det \mathcal{Q}$) between the four-dimensional Wilson-Dirac operator M and the effective three-dimensional operator $e^{-\mu L_t/2} + T \cdot \mathcal{U} \cdot e^{+\mu L_t/2}$, similar to the equivalence between the five-dimensional domain wall fermion operator and the four-dimensional overlap Dirac operator [11–13]. The analogy becomes even more transparent at $\mu = 0$ when the reduced operator becomes $1 + T \cdot \mathcal{U}$, similar to the massless overlap Dirac operator. The factors $e^{\pm \mu L_t/2}$ can then be understood as mass terms for the fermions and antifermions propagating forward and backward in time.

This picture is corroborated by the matrix $\tilde{M}$ in Eq. (20) which is essentially a transfer matrix describing fermions and (anti-)fermions hopping forward and backward between time slices, respectively. The dynamics of these hoppings are described by the transfer matrices T_i which, however, are independent of μ. Fermions winding around the time direction in forward direction will eventually pick up a factor $e^{+\mu L_t}$ (residing in A^+) for each winding while the antifermions winding around the time direction in backward direction will pick up corresponding factors of $e^{-\mu L_t}$ (residing in A^-). In addition, the winding fermion modes are then weighted by $\mathcal{U}$ which contains the temporal gauge field dynamics. In that sense, the reduced matrix is equivalent to a fermion winding number expansion.

To complement this interpretation, it is worthwhile to consider alternative forms of the reduced matrix. In the present form, the reduced matrix $e^{-\mu L_t/2} + T \cdot \mathcal{U} \cdot e^{+\mu L_t/2}$ makes the propagation of the fermion forward in time explicit. One can equally well emphasize the propagation of the antifermion backwards in time. This can, for example, be achieved by considering, instead of $\mathcal{Q}^{-1} \cdot M \cdot \mathcal{P}$, the dimensional reduction of $\mathcal{P} \cdot M \cdot \tilde{\mathcal{Q}}^{-1}$ where $\tilde{\mathcal{Q}}$ is the block diagonal matrix containing Q_i^+ along the diagonal. The reduced matrix then becomes

$$e^{+\mu L_t/2} + \mathcal{U}^\dagger \cdot \tilde{T} \cdot e^{-\mu L_t/2}, \quad (35)$$

where

$$\tilde{T} = \tilde{T}_{L_t-1} \cdot \ldots \cdot \tilde{T}_1 \cdot \tilde{T}_0 \quad \text{with} \quad \tilde{T}_i = T_i^{-1}, \quad (36)$$

so making the backward propagation of the antifermions (and their weighting with $-\mu$ instead of $+\mu$) explicit.[3]

Finally, the construction of the reduced matrix presented in Sec. III A is done for gauge field configurations fixed to temporal gauge. However, the construction can easily be extended to the generic case without gauge fixing, leading to a reduced matrix where the structure $T \cdot \mathcal{U}$ becomes

$$T_0 \cdot \mathcal{U}_0 \cdot T_1 \cdot \mathcal{U}_1 \cdot \ldots \cdot T_{L_t-1} \cdot \mathcal{U}_{L_t-1} = \prod_{i=0}^{L_t-1} T_i \cdot \mathcal{U}_i. \quad (37)$$

Here, the matrices $\mathcal{U}_t$ now collect all the temporal gauge links at fixed time coordinate t, so the matrix $\mathcal{U}_{L_t-1}$ is just $\mathcal{U}$ from before. The factors in the product of Eq. (37) can be cyclically permuted without changing the physical content, i.e. the spectrum of the reduced matrix. This is due to the fact that all the cyclic permutations are related to each other by similarity transformations (involving the matrices $\mathcal{U}_i$ and T_i which have determinant one, cf. Sec. IV A), while the first term in the reduced matrix is trivial in Dirac and color space.

IV. SPECTRAL PROPERTIES OF THE REDUCED MATRIX

A. Symmetry of $T \cdot \mathcal{U}$

In the construction of the reduced Wilson fermion matrix, the crucial object is the matrix $T \cdot \mathcal{U}$. It turns out that this matrix has interesting properties which express themselves in peculiar symmetry properties of the eigenvalue spectrum.

The first thing to note is that

$$\det T \cdot \mathcal{U} = 1. \quad (38)$$

This can easily be seen from Eq. (32) and (33) where we read off $\det(Q_i^-)^{-1} = \det D_i^{-1}$ and $\det Q_i^+ = \det D_i$, respectively, and hence $\det T_i = \det[(Q_i^-)^{-1} \cdot Q_i^+] = 1$.

Second, we note that the eigenvalues of $T \cdot \mathcal{U}$ come in pairs: for every eigenvalue of λ, there is an eigenvalue $\lambda' = 1/\lambda^*$. This can be seen as follows. The product

[3] We note that further equivalent variants of the reduced matrix can be obtained. By considering projection of M with $\mathcal{P}^\dagger$ instead of $\mathcal{P}$ from the left or right, one is led to reduced matrices with modified T' or $\tilde{T}' = T'^{-1}$ related to the original T by $T' = \tilde{T}^\dagger$.

$T_i = (Q_i^-)^{-1} \cdot Q_i^+$ can be LDU-decomposed with the help of Eq. (32) and (33)

$$(Q_i^-)^{-1} \cdot Q_i^+ = \begin{pmatrix} 1 & 0 \\ C_i & 1 \end{pmatrix} \begin{pmatrix} D_i^{-1} & 0 \\ 0 & D_i \end{pmatrix} \begin{pmatrix} 1 & C_i \\ 0 & 1 \end{pmatrix}. \quad (39)$$

In this form, it is easy to calculate its Hermitian conjugated inverse, i.e.

$$[((Q_i^-)^{-1} \cdot Q_i^+)^{-1}]^\dagger = \begin{pmatrix} 1 & -C_i \\ 0 & 1 \end{pmatrix} \begin{pmatrix} D_i & 0 \\ 0 & D_i^{-1} \end{pmatrix} \times \begin{pmatrix} 1 & 0 \\ -C_i & 1 \end{pmatrix}. \quad (40)$$

Comparing this with Eq. (39), we find that

$$[((Q_i^-)^{-1} \cdot Q_i^+)^{-1}]^\dagger = S \cdot ((Q_i^-)^{-1} \cdot Q_i^+) \cdot S^{-1}$$

$$\text{with} \quad S = \begin{pmatrix} 0 & 1 \\ -1 & 0 \end{pmatrix}, \quad (41)$$

and hence

$$[(T \cdot \mathcal{U})^{-1}]^\dagger = S \cdot (T \cdot \mathcal{U}) \cdot S^{-1}. \quad (42)$$

As a consequence, the matrix $T \cdot \mathcal{U}$ shares the eigenvalue spectrum with its Hermitian conjugated inverse, that is, for each eigenvalue $\lambda \in \mathrm{spec}(T \cdot \mathcal{U})$ there is another eigenvalue $1/\lambda^* \in \mathrm{spec}(T \cdot \mathcal{U})$. The spectral symmetry hints at the possibility that the reduced matrix could be further compressed in size by a factor of two without losing any spectral information. In principle, this can be achieved by the projection of $T \cdot \mathcal{U}$ to a suitable subspace, but so far we have not been able to construct such a projection, essentially due to the fact that $T \cdot \mathcal{U}$ is non-normal.

B. Eigenvalue distribution of the reduced matrix

So far we have been concerned with purely algebraic properties of the Wilson-Dirac matrix M and the corresponding reduced matrix $T \cdot \mathcal{U}$. In practice, what is needed are all the eigenvalues λ_i of the latter matrix, such that the determinant of $M(\mu)$ can be evaluated for any arbitrary value of the chemical potential according to

$$\det M(\mu) = \det \mathcal{Q} \cdot e^{+\mu L_t \cdot 2N_c L_s^3} \prod_{i=1}^{4N_c L_s^3} (e^{-\mu L_t} + \lambda_i). \quad (43)$$

Apart from the symmetry property $\lambda \leftrightarrow 1/\lambda^*$ discussed in Sec. IV A, the eigenvalue spectrum has additional interesting features. To illustrate these, we will use configurations generated for a previous study of nonzero baryon density systems using the canonical partition function [26]. These $6^3 \times 4$ configurations are picked from $N_f = 4$ ensembles at a temperature close to the deconfining transition: $T \approx 0.95 T_c$. The parameters for the fermionic matrix will be set to the values used to generate the ensembles: $\kappa = 0.1371$ and $c_{\mathrm{sw}} = 1.96551$ corresponding to a pion mass of about 700–800 MeV.

In Fig. 1, we plot the eigenvalue distribution of the matrix $T \cdot \mathcal{U}$ for a random selection of gauge field configurations drawn from canonical ensembles with baryon number $n_B = 4$ (top two rows) and $n_B = 11$ (bottom two rows), respectively. The plots represent the eigenvalue distribution in the complex plane and the scale is from $\mathrm{Re}, \mathrm{Im}\lambda \in [-600, 600]$. Only the large magnitude eigenvalues are visible (the low magnitude members are also plotted, but they are not visible on this scale). Note that there is a cone empty for each configuration and that the distributions exhibit a three lob structure which, from configuration to configuration, is related by $\mathbb{Z}(3)$-rotations in the complex plane. An interesting observation is the fact that, for each configuration, the structure is correlated with the value of the spatially averaged Polyakov loop, which in the temporal gauge is given by

$$P(U) = \frac{1}{4N_c L_s^3} \mathrm{tr}\mathcal{U}. \quad (44)$$

In Fig. 1, we make this correlation explicit for each configuration by imposing the corresponding (rescaled) value of $P(U)$ onto the eigenvalue spectrum. Of course this correlation is no surprise, since from the structure $T \cdot \mathcal{U}$ it is immediately clear that under a $\mathbb{Z}(3)$-transformation of the temporal gauge fields $\mathcal{U}$, the eigenvalues are simply rotated by the corresponding $\mathbb{Z}(3)$ factor. On the other hand, one should also keep in mind that some of the correlations we observe between the determinant and the Polyakov loop might be due to the rather heavy quark mass [27] and the correlations might become less pronounced as we move toward lower quark masses.

In order to further expose the influence of the $\mathbb{Z}(3)$ phase of $P(U)$ (or rather $\mathcal{U}$) on the spectrum, we perform the following exercise. Instead of computing the eigenvalues of the original reduced matrix $T \cdot \mathcal{U}$, we calculate the spectrum of a modified reduced matrix where we set the temporal gauge fields $\mathcal{U}$ to the $\mathbb{Z}(3)$ phase as given by the Polyakov loop $P(U)$. We show the result of this calculation for a configuration with $\arg P(U) \simeq 0$ in Fig. 2 in the leftmost plot. The only gauge field dependence is now through the spatial gauge links in T, and we see that this dependence is responsible for the eigenvalues' variation in magnitude, while the phase of the eigenvalues fluctuates very weakly around zero. (Note that the spectrum of the reduced free Wilson-Dirac operator is real and the eigenvalues $\lambda > 1$ span the range between roughly 6 and 2000.) Of course, we can also turn the argument around and put all the spatial links to unity, so that the gauge field dependence resides in $\mathcal{U}$ alone. The spectrum of the reduced matrix modified in this way is shown in the rightmost plot in Fig. 2. Comparing this with the original spectrum shown in the middle plot, we conclude that the phase variation of the eigenvalues is determined almost solely by the temporal gauge fields $\mathcal{U}$ while the spatial gauge fields only add small fluctuations to the phase. In

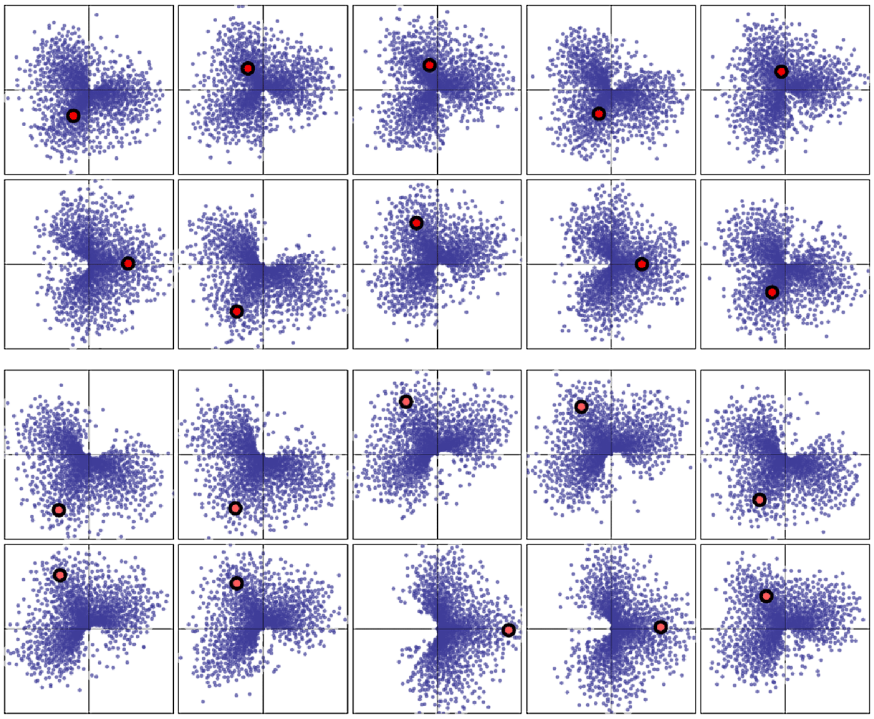

FIG. 1 (color online). The eigenvalue distribution for 10 arbitrary configurations drawn from canonical ensembles with $n_B = 4$ (top) and $n_B = 11$ (bottom). The red point indicates a scaled value of the spatially averaged Polyakov loop to show its correlation with the eigenvalue distribution.

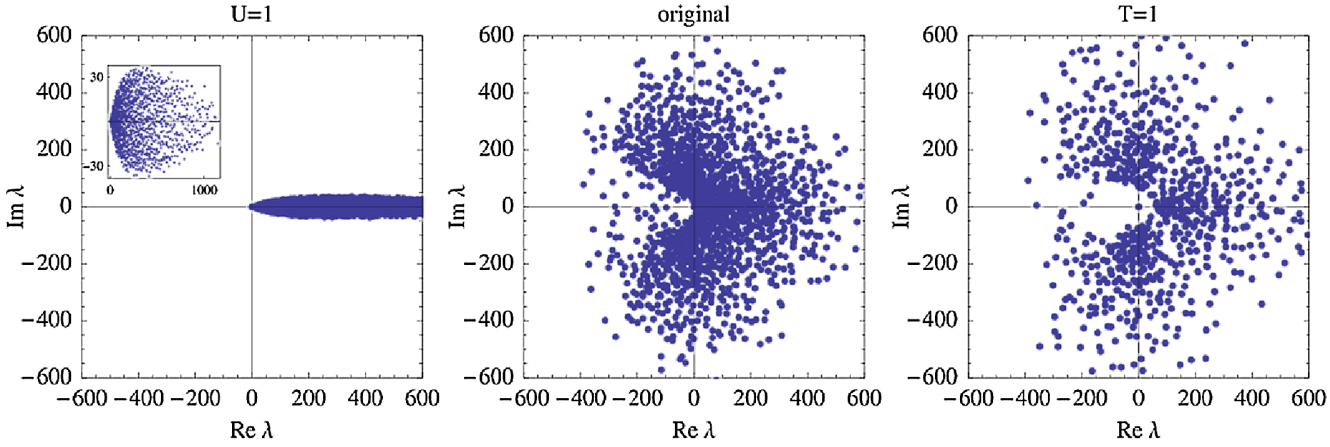

FIG. 2 (color online). The eigenvalue spectrum of $T \cdot \mathcal{U}$ for an arbitrary configuration with $\arg P(U) \approx 0$ (middle plot), in the case when $\mathcal{U} = 1$ is put by hand (left plot), or when all spatial links are set to one (right plot).

Fig. 11, we repeat this exercise for configurations with $\arg P(U) \simeq \pm 2\pi/3$. As discussed above, in this case the spectra are simply rotated by the corresponding $\mathbb{Z}(3)$ factors, and the conclusion remains the same.

V. PROJECTED DETERMINANT OF THE CANONICAL PARTITION FUNCTION

After having discussed the properties of the reduced matrix and its spectrum, the next interesting quantity to study is the determinant as a function of the (real or imaginary) chemical potential, and eventually also the projected determinant which subsumes the dynamics of the fermions in the canonical partition function.

A. The determinant at nonzero chemical potential

Having the eigenvalues λ_i of $T \cdot \mathcal{U}$ at hand, it is now easy to evaluate the determinant of the Wilson-Dirac operator for arbitrary chemical potential according to

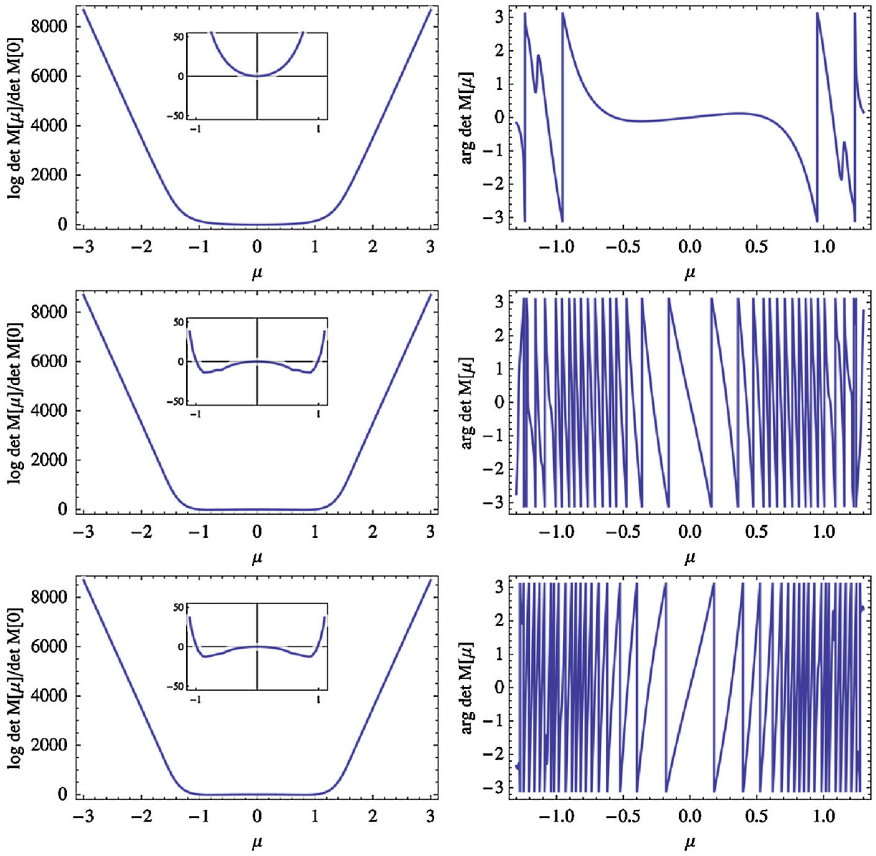

FIG. 3 (color online). The logarithm of the determinant $|\det M(\mu)|$ normalized to $\det M(\mu = 0)$ (left row) and the argument of $\det M(\mu)$ (right row) for three configurations from a canonical ensemble with $n_B = 4$. From top to bottom, the configurations have $\arg P(U) \approx 0$, $+2\pi/3$ and $-2\pi/3$.

Eq. (43). In Fig. 3, we show the logarithm of the determinant $\det M(\mu)$ for three configurations from a canonical ensemble with $n_B = 4$. From top to bottom the configurations have $\arg P(U) \approx 0$, $+2\pi/3$ and $-2\pi/3$. The first row shows the logarithm of $|\det M(\mu)|$ normalized to $\det M(\mu = 0)$, i.e. $|\log\det M(\mu)|/\det M(\mu = 0)$, while the second row shows the argument $\arg\det M(\mu)$ modulo 2π. We note significant differences between the results for configurations in the various triality sectors. First, while in all sectors the size of the determinant ratio starts to grow exponentially with $|\mu|$ beyond $|\mu| \gtrsim 1$, configurations in the nontrivial $\mathbb{Z}(3)$-sectors show a local minimum just below $|\mu| \sim 1$ in contrast to configurations in the trivial sector, which show a monotonic increase with $|\mu|$. Second, the derivative of the phase with respect to μ stays roughly constant for $|\mu| \lesssim 0.5$, but depends strongly on the $\mathbb{Z}(3)$-sector.

In Fig. 4, we show the same kind of plots for three typical configurations (with $\arg P(U) \approx 0$, $+2\pi/3$ and $-2\pi/3$ from top to bottom) from a canonical ensemble with $n_B = 11$. The picture qualitatively remains the same except that the features described before are accentuated. For configurations in the nontrivial $\mathbb{Z}(3)$-sectors, the minima of $|\det M(\mu)|$ become slightly deeper and move to slightly larger values of $|\mu|$. Furthermore, for those configurations the phase of $\det M(\mu)$ changes more rapidly while the change of the phase in the trivial $\mathbb{Z}(3)$-sector becomes smoother and stretches further into larger values of $|\mu|$, possibly allowing reweighting to larger chemical potential.

Note that the wild phase fluctuations observed for configurations with nontrivial Polyakov loop are due to the contributions from the fractional baryon number sectors. To illustrate this point, following the ideas presented in [24], we define a modified determinant that only includes the integral baryon number sectors:

$$\det\hat{M}(U, \mu) \equiv \sum_{n_B} e^{3n_B\mu/T} \det{}_{3n_B} M(U). \qquad (45)$$

This definition is equivalent to the fugacity expansion for the determinant where we only sum over the sectors that have a net number of quarks divisible by 3. In Fig. 5, we plot the absolute value and phase of this modified determinant for a configuration with $\arg P(U) \approx 2\pi/3$ (the same one used in the middle panel of Fig. 4). We see that the magnitude now increases monotonically and that the

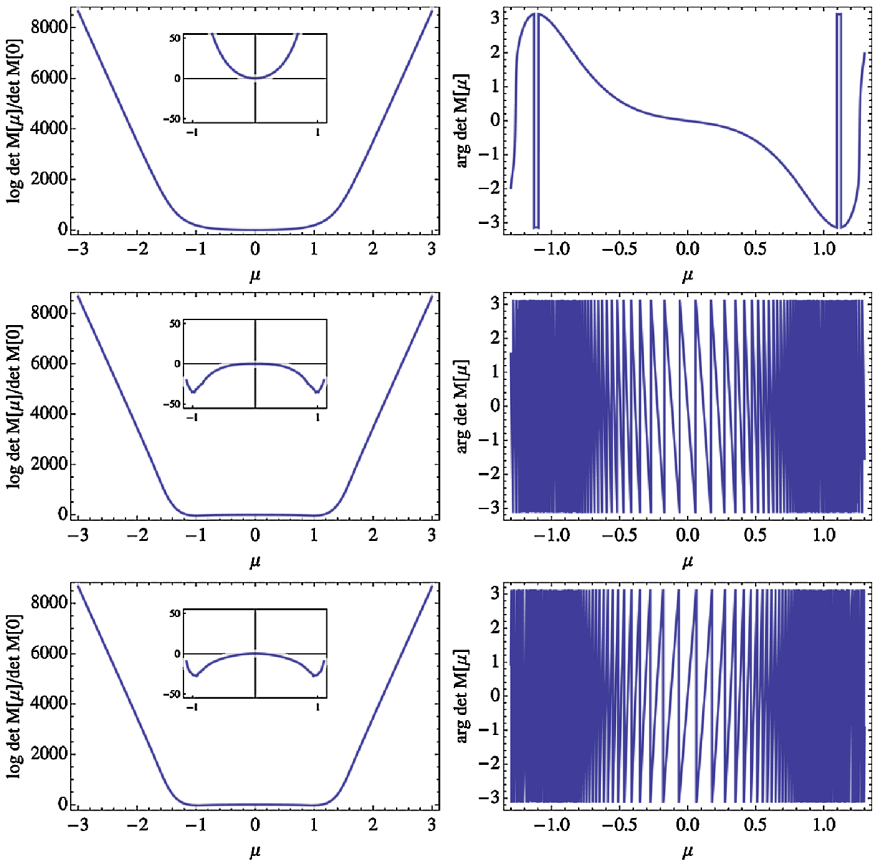

FIG. 4 (color online). Same as Fig. 3, but for three configurations from a canonical ensemble with $n_B = 11$.

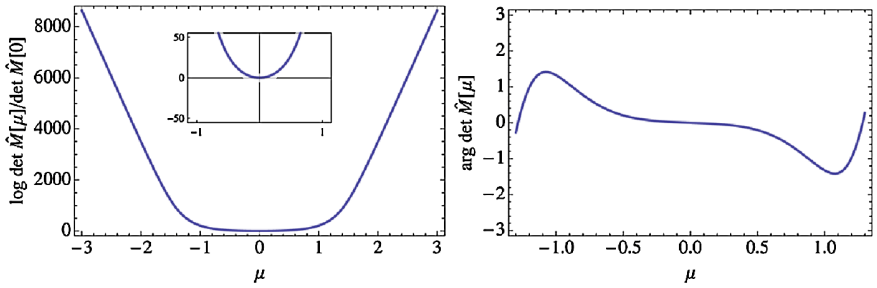

FIG. 5 (color online). Same as the middle panel of Fig. 4 but for the modified determinant Eq. (45).

phase changes much slower with μ—this is exactly the behavior of configurations that have $\arg P(U) \approx 0$.

As we emphasized in the Introduction, these observations are hard to interpret physically, but we believe that they might play an important role for the optimization of reweighting strategies, or for the development of new canonical simulation algorithms.

B. Calculation of the projected determinants

Using Eq. (43), we can show that the projected determinants $\det_k M$ defined in Eq. (3), up to a multiplication with $\det \mathcal{Q}$, are the coefficients $c_{k+k_{\max}}$ of the polynomial

$$\Pi(x) = \prod_{i=1}^{2k_{\max}} (x + \lambda_i) = \sum_{k=0}^{2k_{\max}} c_k x^k, \tag{46}$$

where $k_{\max} = 2N_c N_s^3$. A couple of coefficients can be computed easily: $c_{2k_{\max}} = 1$ and $c_0 = \prod_i \lambda_i = \det T \cdot \mathcal{U} = 1$, as discussed before. All other coefficients can be calculated recursively. To show this, we first define the partial product:

$$\Pi_n(x) = \prod_{i \le n} (x + \lambda_i) = \sum_{k \le n} c_k^{(n)} x^k. \tag{47}$$

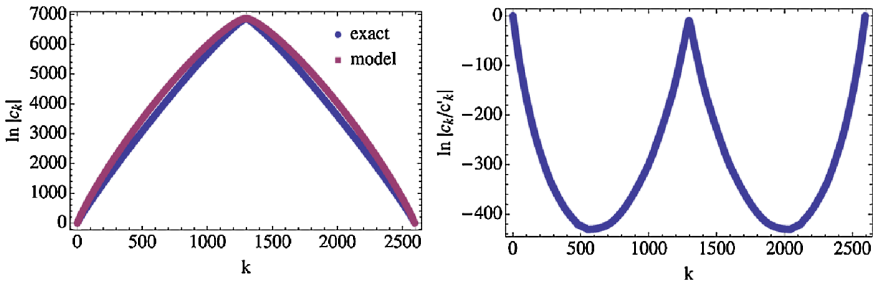

FIG. 6 (color online). Simple model calculation: on the left, the exact values and the model values are shown. In the right panel, the ratio between the exact and model values are shown.

Clearly, $\Pi_{n+1}(x) = (x + \lambda_{n+1})\Pi_n(x)$, and hence we have

$$c_k^{(n+1)} = \lambda_{n+1} c_k^{(n)} + c_{k-1}^{(n)}, \tag{48}$$

for all $0 \le k \le n+1$ (we set $c_{-1}^{(n)} = 0$). For Π_0 all coefficients are zero except for $c_0^{(0)} = 1$. Using Eq. (48) to compute $c^{(n+1)}$ from $c^{(n)}$, after $2k_{\max}$ steps we obtain the coefficients of $\Pi_{2k_{\max}} \equiv \Pi$.

The recursive steps of the iteration have to be carried out using a high-precision library. The reason for this is that the magnitude of the coefficients vary over thousands of orders of magnitude. We used GNU Multi-Precision library, which can easily handle numbers of this magnitude. While the calculation takes significantly longer than when using the standard floating point arithmetic, the total time is small compared to the time it takes to compute the eigenvalues of the reduced matrix. One possible issue when using a high-precision library is that the results look deceptively precise since the inputs are treated as high-precision numbers, when their real precision is at the level of machine precision or less. To check the robustness of our calculation, we performed the following tests: In the first test, we added random numbers of the order of 10^{-15} (double precision level) to the links and recomputed the projected determinants; the relative change in the projected determinants was at the level of 10^{-10}. Next, we randomly reordered the eigenvalues of the reduced matrix and repeated the recursive step. We find that the relative change in the coefficients is of the order of 10^{-9}. We conclude that our procedure is robust and it produces accurate results.

Before we conclude this section, we want to point out that the $\lambda \leftrightarrow 1/\lambda^*$ symmetry of the reduced matrix, together with the fact that $\det T \cdot \mathcal{U} = 1$, can be used to show that $c_{k_{\max}+k} = c^*_{k_{\max}-k}$. Since $\det \mathcal{Q}$ is real, this ensures that $\det_k M = (\det_{-k} M)^*$, a fact easily derived from the definition of the projected determinant and the reality of $\det M(\phi)$.

C. Size distribution of the projected determinant

One of the interesting aspects of this calculation is the fact that the magnitude of the projected determinants varies over many orders of magnitude as we change the quark number sector. In this section, we will show that the bulk of this variance can be captured by a simple combinatorial argument. However, this only captures part of the variance; in order to describe the variance accurately, we need to take into account the complex phase of the eigenvalues of the reduced matrix.

In the main, the bulk of the magnitude is given by the average magnitude of the eigenvalues and combinatorics. To illustrate this point, in Fig. 6 we compare the value of the coefficients of the polynomial $\Pi(x)$ for a given configuration with the coefficients of the polynomial $\Pi'(x) = (x + \bar{\lambda})^{k_{\max}}(x + 1/\bar{\lambda})^{k_{\max}}$, where $\bar{\lambda}$ is the geometric mean of the magnitude of the large eigenvalues $\bar{\lambda} = (\prod_{|\lambda|>1} |\lambda_i|)^{1/k_{\max}}$.

For any given configuration, the eigenvalues vary both in phase and magnitude; in the comparison above, we quenched both fluctuations. While this approximation captures a good part of the variation of magnitude, there is still quite a discrepancy left. To trace the source of discrepancy, we compare the coefficients of $\Pi(x)$ with a polynomial where each eigenvalue is replaced with its magnitude: $\Pi''(x) = \prod_i (x + |\lambda_i|)$. The results of this comparison are presented in Fig. 7: we see that the discrepancy is similar to the one above. This shows that the source of discrepancy is the complex phase fluctuation that is disregarded here. This conclusion is also supported by the fact that the coefficients of $\Pi''(x)$ are larger in magnitude than the coefficients of $\Pi(x)$; this is due to cancellations produced by phase fluctuations.

To prove that phase fluctuations are responsible for the discrepancy, we model the rough features of the phase distribution. The phase distribution is illustrated in Fig. 1. One obvious feature is that the eigenvalues are concentrated around the $\mathbb{Z}(3)$ axes. This makes sense; if the eigenvalues were exactly along the $\mathbb{Z}(3)$ axes, the projected determinants that have zero triality ($k = 3n_B$) will be real, whereas the ones with nonzero triality will have a fluctuating phase and they will vanish when averaged over gauge configurations, as expected.

To check that phase fluctuations are responsible for reducing the magnitude of the coefficients, we compare

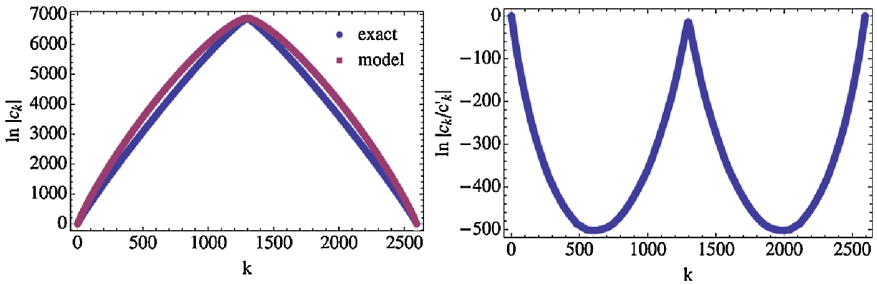

FIG. 7 (color online). Comparison between true polynomial coefficients and the ones where the eigenvalue phase is quenched.

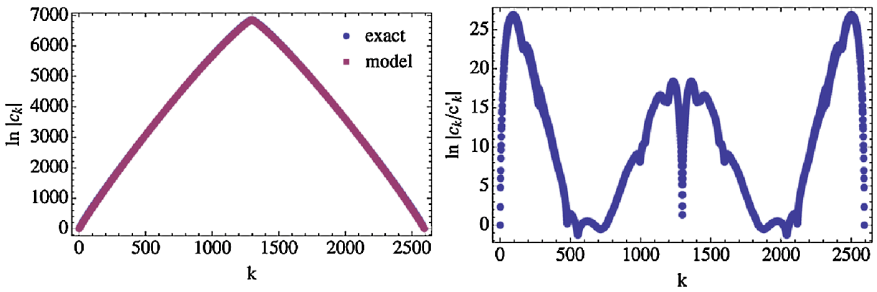

FIG. 8 (color online). Comparison between true polynomial coefficients and the ones where the eigenvalue phase is drawn from a random $\mathbb{Z}(3)$ distribution. Note the difference in scale in the right plot as compared to Figs. 7 and 6.

the coefficients of $\Pi(x)$ with $\Pi'''(x) = \prod_i (x + z_i|\lambda_i|)$, where z_i is a random $\mathbb{Z}(3)$ phase with one constraint: we enforce the $(\lambda, 1/\lambda^*)$ pairing. The results are presented in Fig. 8: we see that the results agree much better now. It is clear that the phase fluctuations play an important role in determining the coefficients. Phase fluctuations reduce the value of the coefficients significantly. From Fig. 7 we see that for intermediate k values they reduce the magnitude by about 200 orders of magnitude. From Fig. 8 we see that this is mostly due to the $\mathbb{Z}(3)$ nature of the fluctuations (we also tested random $\mathbb{Z}(n)$ phases with $n \in \{2, 4, 5, 6\}$, but they fail to produce the same agreement).

VI. PHASE FLUCTUATIONS IN CANONICAL ENSEMBLES

The reduced Wilson fermion matrix constructed and discussed in the previous sections allows for several intriguing applications. Presumably among the most interesting are the direct simulation of canonical ensembles and the reweighting to different fermion numbers, or values of the chemical potential. In the following, we briefly discuss these two applications and present some results on the phase fluctuations encountered in direct simulations of canonical ensembles, merely to illustrate the capabilities of the reduced fermion matrix approach.

In order to simulate the canonical partition function Eq. (2) by Monte Carlo techniques, one needs the integrand to be real and positive. Since in general this is not guaranteed, the approach so far [8] has been to ensure positivity by fiat, i.e. to generate an ensemble using the weight $W_{|k|}(U) \propto |\mathrm{Redet}_k M(U)|$, while the phase

$$\alpha(U) \equiv \frac{\det_k M(U)}{W_{|k|}(U)} \tag{49}$$

is introduced when computing the observable

$$\langle O(U) \rangle_k = \frac{\langle O(U)\alpha(U) \rangle_{|k|}}{\langle \alpha(U) \rangle_{|k|}}, \tag{50}$$

where $\langle \cdot \rangle_{|k|}$ denotes the average with regard to the generated ensemble based on the $W_{|k|}$ measure. In practice, to evaluate the partition function numerically, the continuous Fourier transform in Eq. (3) has so far either been replaced by a discrete Fourier transform [8] or by a more sophisticated approximation [26,28] and the so-introduced bias needs a careful treatment. With the reduced Wilson fermion matrix, these approximations have become obsolete, simply because the Fourier transform can now be evaluated exactly.

Still, the quenching of the phase of the integration measure, $\det_k M(U) \to W_{|k|}$, introduces a systematic error which one needs to control. A measure of how severe the fluctuations of the phase are is provided by the expectation value of $\alpha(U)$ in Eq. (49) in a given ensemble. It turns out that the sign fluctuations for the canonical ensembles seem to be under good control and one might wonder how generic this feature is. One way to estimate the reliability of the simulations is to reweigh results generated at one

TABLE I. The real part of the average reweighting factor Eq. (51). The imaginary part vanishes by symmetry. This factor is computed based on the ensemble generated with $n_B = 4$ (marked with a star above).

n_B	$\langle\alpha\rangle$	$\sigma_{\langle\alpha\rangle}$	$\sigma_{\langle\alpha\rangle}/\langle\alpha\rangle$
00	$7.63 \times 10^{+2}$	$3.93 \times 10^{+2}$	0.515
04*	4.87×10^{-1}	3.09×10^{-2}	0.064
08	1.60×10^{-4}	1.21×10^{-5}	0.076
12	7.78×10^{-9}	1.11×10^{-9}	0.143
16	1.82×10^{-14}	9.81×10^{-15}	0.540

value of k to other values k' and to check consistency between the reweighted results and the ones obtained from direct simulations. For the reweighting from one canonical ensemble $Z_C(k)$ to another $Z_C(k')$, the relevant quantity is

$$\alpha_{|k|\to k'}(U) = \frac{\det_{k'} M(U)}{W_{|k|}(U)}. \tag{51}$$

For this definition of the reweighting factor, we see from the second column of Table I that its magnitude changes very fast as we move away from the original ensemble, in this case the one with $n_B = 4$. However, the value of the factor changes for all configurations in a similar manner and the average is still comfortably away from zero in terms of its standard deviation (cf. third and fourth column) even though its magnitude is dramatically changed. (Note that this dramatic change is related to the variation of $\det_k M$ with k over many orders of magnitude.) What we mean by that is that its magnitude, as compared with its standard deviation, is larger than 2 or more. In principle, it is when this ratio becomes close to 1 that the reweighting in the equation above will run into numerical difficulties. We see from Table I that for baryon numbers as large as $n'_B = 16$, the average is still twice the standard deviation.

In Fig. 9, we plot the ratio between the standard deviation of the mean and the average of the real phase factor reweighted from the canonical ensembles with $n_B = 4$ and 11, as a function of the reweighted baryon number. Note that in both cases the average reweighting factor is well behaved over a large range of reweighted baryon numbers.

Encouraged by this result, one might also try to reweight the chemical potential as a function of the baryon number following the definition in Eq. (5). The chemical potential, as defined there, can be shown to be

$$\mu_B(n_B)/T = -\log\frac{Z_C(3(n_B+1))}{Z_C(3n_B)} = -\log\left\langle\frac{\det_{3(n_B+1)} M}{\det_{3n_B} M}\right\rangle_{3n_B} \tag{52}$$

$$= -\log\frac{\langle\det_{3(n_B+1)} M/W_{|3n_B|}\rangle_{|3n_B|}}{\langle\det_{3n_B} M/W_{|3n_B|}\rangle_{|3B|}}. \tag{53}$$

In Fig. 10, we show the reweighted chemical potential as defined by Eq. (5), for the same ensembles as before, $n_B = 4$ (left plot) and $n_B = 11$ (right plot). Despite the absence of a sign problem in the reweighting factor, it is evident that the reweighting fails. The ensemble $n_B = 4$ in the confined phase misses to describe even the neighboring ensemble with only slightly different baryon number $n_B = 5$. The ensemble $n_B = 11$, on the other hand, is in the deconfined phase and seems to be able to describe other deconfined phases with different baryon numbers. Not surprisingly, however, it completely fails to describe ensembles with $n_B \leq 8$, and hence the phase transition, simply because it does not contain any information about the confined phase.

The next interesting question would now be to reweight an ensemble in the mixed phase, e.g. with $n_B = 7$. However, the reweighted results turn out to be too noisy, indicating that the information gathered in the canonical ensembles is simply not enough to allow for a reliable reweighting. One has to keep in mind that the canonical ensembles used here only contain about 1500 configurations each. The next obvious step is then to employ a multiensemble reweighting, combining the information from all the ensembles into the reweighting. What we find is that for $n'_B = 4$ the most important contributions indeed come from the ensembles with small n_B and that, as we move towards larger n'_B, higher ensembles come into play as expected. However, even the multiensemble reweighting does not seem capable to reproduce the

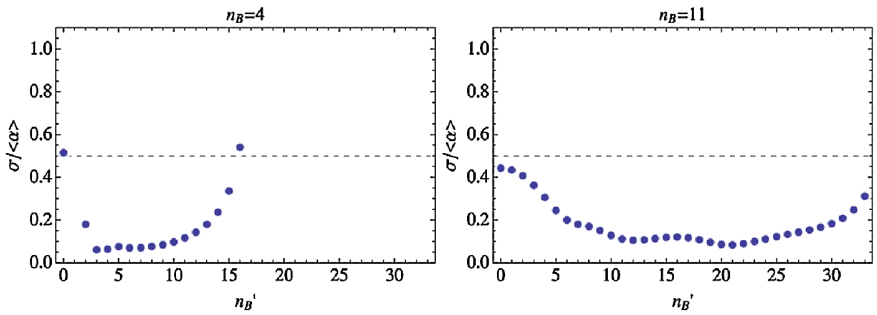

FIG. 9 (color online). The real part of the average phase factor: the ratio between the standard deviation of the mean and the average.

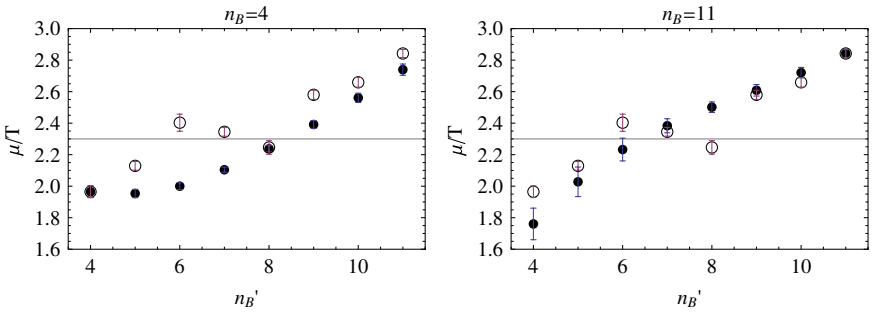

FIG. 10 (color online). The baryon chemical potential reweighted from the ensemble with $n_B = 4$ (left plot) and $n_B = 11$ (right plot). Empty circles are the results of the direct calculation.

S-shape behavior typical for a first order phase transition, and we conclude that the reweighting suffers from a severe overlap problem. Nevertheless, the example impressively demonstrates the ease with which such calculations can be achieved using the reduced Wilson fermion matrix.

VII. CONCLUSIONS

We have presented a reduction method for Wilson-Dirac fermions which generates a dimensionally reduced fermion matrix. The size of the reduced matrix is independent of the temporal lattice extent. Moreover, the dependence of the matrix on the chemical potential factors out and reduces to a simple multiplicative factor. This allows to evaluate the Wilson fermion determinant for any value of the chemical potential, once the eigenvalues of the reduced matrix are calculated, and hence allows to perform the exact projection of the determinant to the canonical sectors with fixed fermion number.

The reduced fermion matrix presented here facilitates various interesting applications, for example, the reweighting of ensembles to arbitrary values of the chemical

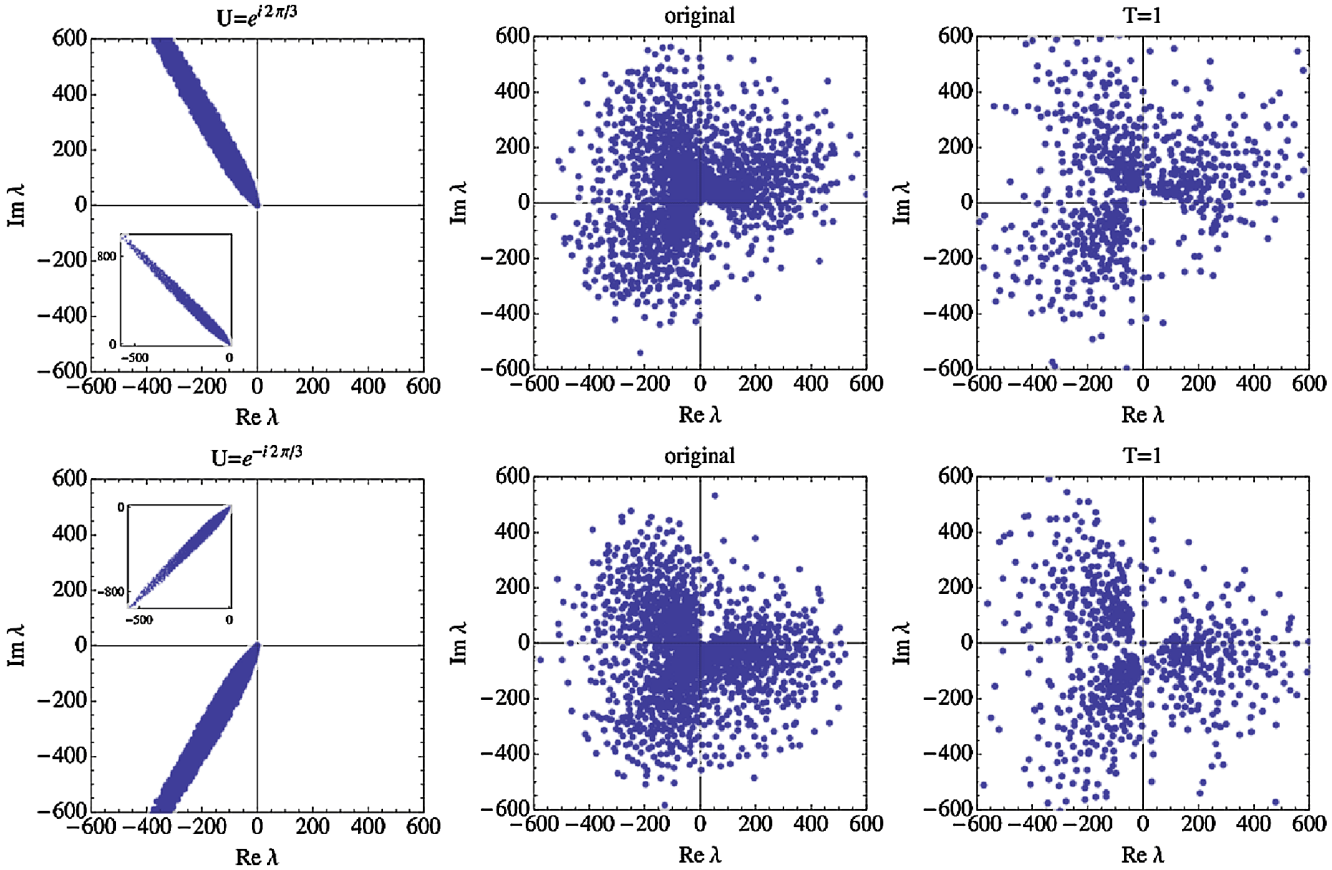

FIG. 11 (color online). Same as Fig. 2, but for a configuration with $\arg P(U) \approx +2\pi/3$ (top row) and one with $\arg P(U) \approx -2\pi/3$.

potential or the fermion number. So far, this has only been possible for staggered fermions. Another application is the direct simulation of canonical ensembles and this is now possible without any bias from inexact projections to the canonical sectors. Since the size of the reduced matrix is independent of the temporal lattice extent, such calculations can, in principle, be done at arbitrarily low temperatures, barring possible sign problems.

The reduced fermion matrix has some interesting properties like the spectral symmetry $\lambda \leftrightarrow 1/\lambda^*$, a simple behavior of the spectrum under $\mathbb{Z}(N_c)$-transformations and the correlation of the spectrum with the Polyakov loop. We believe that such properties may be important for the development of more efficient canonical simulation algorithms, or for the optimization of reweighting strategies.

As a first test, we applied the reduction method to a set of canonical ensembles and determined the phase fluctuations of the Wilson fermion determinant at nonzero chemical potential, or nonzero fermion number, using standard reweighting techniques. It turns out that for the ensembles considered here, the overlap problem inherent in all reweighting methods introduces a systematic bias that forbids reliable calculations, e.g. using multiensemble reweighting. On the other hand, the phase fluctuations seem to be rather well controlled and it will be interesting to see whether this is a generic feature of canonical partition functions.

ACKNOWLEDGMENTS

We would like to thank Philippe de Forcrand for discussions, and Atsushi Nakamura and Keitaro Nagata for correspondence on their related work. Andrei Alexandru is supported in part by the U.S. Department of Energy under Grant No. DE-FG02-95ER-40907. The computational resources for this project were provided by the George Washington University IMPACT initiative. We would like to thank Anyi Li for providing us with the configurations needed for this study.

[1] P. E. Gibbs, Phys. Lett. B **172**, 53 (1986).
[2] I. M. Barbour, C. T. H. Davies, and Z. Sabeur, Phys. Lett. B **215**, 567 (1988).
[3] A. Hasenfratz and D. Toussaint, Nucl. Phys. **B371**, 539 (1992).
[4] O. Philipsen, arXiv:1009.4089.
[5] J. Danzer and C. Gattringer, Phys. Rev. D **78**, 114506 (2008).
[6] C. Gattringer and L. Liptak, arXiv:0906.1088.
[7] S. Kratochvila and P. de Forcrand, Proc. Sci., LAT2005 (2006) 167 [arXiv:hep-lat/0509143].
[8] A. Alexandru, M. Faber, I. Horvath, and K.-F. Liu, Phys. Rev. D **72**, 114513 (2005).
[9] Z. Fodor, K. K. Szabo, and B. C. Toth, J. High Energy Phys. 08 (2007) 092.
[10] P. de Forcrand, M. A. Stephanov, and U. Wenger, Proc. Sci., LAT2007 (2007) 237, [arXiv:0711.0023].
[11] A. Borici, arXiv:hep-lat/0402035.
[12] R. G. Edwards, B. Joo, A. D. Kennedy, K. Orginos, and U. Wenger, Proc. Sci., LAT2005 (2006) 146 [arXiv:hep-lat/0510086].
[13] R. G. Edwards, B. Joo, A. D. Kennedy, K. Orginos, and U. Wenger, "Five dimensional variants of overlap fermions" (unpublished).
[14] A. Borici, Prog. Theor. Phys. Suppl. **153**, 335 (2004).
[15] K. Nagata and A. Nakamura, Phys. Rev. D **82**, 094027 (2010).
[16] Z. Fodor and S. D. Katz, Phys. Lett. B **534**, 87 (2002).
[17] C. R. Allton *et al.*, Phys. Rev. D **66**, 074507 (2002).
[18] P. de Forcrand and O. Philipsen, Nucl. Phys. **B642**, 290 (2002).
[19] M. D'Elia and M.-P. Lombardo, Phys. Rev. D **67**, 014505 (2003).
[20] S. Kratochvila and P. de Forcrand, Nucl. Phys. B, Proc. Suppl. **140**, 514 (2005).
[21] A. Alexandru, M. Faber, I. Horvath, and K.-F. Liu, Nucl. Phys. B, Proc. Suppl. **140**, 517 (2005).
[22] S. Ejiri, Phys. Rev. D **78**, 074507 (2008).
[23] A. Roberge and N. Weiss, Nucl. Phys. **B275**, 734 (1986).
[24] S. Kratochvila and P. de Forcrand, Phys. Rev. D **73**, 114512 (2006).
[25] P. Hasenfratz and F. Karsch, Phys. Lett. B **125**, 308 (1983).
[26] A. Li, A. Alexandru, K.-F. Liu, and X. Meng, Phys. Rev. D **82**, 054502 (2010).
[27] P. de Forcrand and V. Laliena, Phys. Rev. D **61**, 034502 (2000).
[28] X.-f. Meng, A. Li, A. Alexandru, and K.-F. Liu, Proc. Sci., LATTICE2008 (2008) 032 [arXiv:0811.2112].